STUDY OF ELECTRODEPOSITION METHOD TO PRODUCE CARBON NANOTUBES

AHMAD ATIF FIKRI

Doctor of Philosophy

ASTON UNIVERSITY

December 2021

Abstract

Since its first observation, Carbon Nanotubes (CNT) has drawn considerable research interest. Numerous investigations revealed outstanding properties for this unique form of carbon. Its remarkable characteristics include its electronic properties, thermal conductivity, and mechanical properties offer tremendous new opportunities and applications, often described as technological marvels. Nevertheless, like other new materials, CNT faces the transfer phenomenon from marvel material to market driven by its profitability or marketability.

From the market perspective, the need for carbon nanotubes increases each year, while in the manufacturing view, production is plateauing. Therefore the gap between supply and demand exists, and the commercial viability of CNTs seems assured. However, the market's growth will depend on the efficiency in tackling dominant factors such as price to be competitive. No matter how excellent new materials are, the requirement of cheap to produce, consistent quality, easy handle and toxicity tolerance were always the rule.

This study presents the Electrodeposition method as an alternative method to producing Multiwalled Carbon Nanotubes (MWCNT) utilising CO2 as carbon feedstock. Four approaches are discussed in this thesis: Literature review, Molecular dynamics, and experiments using Taguchi and OFAT (One Factor at a Time).

Electrodeposition is a method that utilises molten salt, atmospheric CO_2, and electrodes that can perform without catalyst preparations. At the same time, the requirements of well-established methods such as Arc Discharge, Laser Ablation, and Chemical Vapour Deposition result in a less cost-effective product and are challenging to scale up. In arc discharge, pure

graphitic carbon soot can be utilised to synthesise CNT, but the addition of catalysts and preparation is required to produce a large amount of CNT. However, the electrode size and high current proportion are limited even with the extra preparation process. Laser ablation produces high-quality CNT with the limitation of its laser power requirement, while preparing catalyst in CVD also adds time or labour cost. The literature review in this study concludes that Electrodeposition can produce carbon nanotubes in an uncomplex way due to preparation ease.

Electrodeposition does not have the limitation of the previous process and is arguably easier to scale up. However, this method has some challenges that need to be addressed, most related to synthesis parameters. In the previous research, the study is conducted partially and comparing the result is sometimes unusable since each investigator weighs in some value over another. For example, yield is measured in the purity or weight of the end product, and other research considers the CNT growth area or catalyst-CNT ratio in the system.

In this research, Molecular dynamics, Taguchi and OFAT (One Factor at a Time) methods counter the challenges by providing a thorough study. Molecular dynamics determine the base behaviour expected from variables, focusing only on parameter changes that affect the carbon bonds formed in the electrodeposition system. Furthermore, Taguchi and OFAT are used to optimise variables and examine the end-product properties of each variable on an experiment basis.

From molecular dynamics, it is found that the carbon bond created is affected by the total energy in the system, while total energy depends on variable value. Under the theoretical models used in the simulation, increasing parameters value which includes temperature, external potential, Carbon number in the system, and synthesis time, increases the carbon

bond created in the system. Furthermore, changing the cathode from Ni to Cu decreases the carbon bond formed.

Using the Taguchi method L25 design with five parameters, optimisation was conducted. The optimisation result is not as linear as the expectations of the Molecular dynamic and revealed that other factors, such as the Expansion of molten salt, conductivity gain, current instability, and excessive carbon debris, play roles in the system. The use of metal alloys was essential to promote CNT, as suggested in the previous investigation, which is supported in this thesis. Further evidence of better performance electrode metal alloys is found in Taguchi and OFAT, in which Zn alloys dominated early research. The OFAT also present the end-product characterisation under parameter changes utilising XRD, FTIR, Raman SEM, and EDX analysis.

In the Experiment result, increasing the Temperature parameter is only applicable to improve carbon growth rate and MWCNT yield to a certain degree, but higher Temperature generally decreases the Electrodeposition performance. In terms of external potentials, the general trend is higher Voltage resulting in better carbon growth and MWCNT yield until current instability occurs. The higher value CO2 flowrates parameter positively affects the performance; however, this research's highest CO2 flow rate negatively impacts the current efficiency. Higher value synthesis Time parameters result in lower carbon growth rate and MWCNT yield despite producing a more considerable amount of soot. The Cathodes used in this research produce MWCNT with different sizes, purity and overall performance.

Keywords: Electrodeposition, Carbon nanotubes, CO_2 Utilisation

Acknowledgements

First and foremost, I would like to thank my supervisor, Prof Yuchun Xu and Dr Alex Rozhin for their encouragement, guidance and supervision throughout this project. I am grateful for the invaluable assistance from Aston University staff, the research fellow, friends and colleagues, especially from the Mechanical, Biomedical, and Design Engineering Department. I would also like to acknowledge incredible support from Universitas Negeri Malang staff, friends and colleagues. I would also like to express gratitude to IDB 3 in 1 project committee for making this project possible. Finally, I wish to thank my family for their support and encouragement during and throughout this PhD project.

Table of Contents

Table of Figures

List of Tables

Chapter 1 – Introduction

This thesis focuses on the Electrodeposition method to produce valuable products, mainly carbon nanotubes (CNT), from carbon dioxide conversion. Before the further study of Electrodeposition, the stimulus of the research will be discussed first as well as general CO_2 conversion. Furthermore, CNT production issues will be disclosed first. From the subjects, it

will be elucidated the advantage and disadvantages of the Electrodeposition method. A brief discussion of crucial points to improve this method also will be divulged.

1.1 Background

Carbon nanotubes (CNT) are tube-like materials made of carbon with a diameter calculated on the nanometer scale. They are derived from graphite sheets, and these layers of graphite appear similar to an unbroken hexagonal-like rolled mesh structure. Since its first discovery by Sumio Iijima in 1991[1], Carbon nanotubes (CNT) have been studied extensively to fullerenes, this material has opened a new science and technology. Advance research on this material was conducted because of its appealing potential. These potentials are based on their electronic structures[2][3], chemical reactivity[5][6], optical activity[6][7], mechanical strength[8][9], hardness[10], wave absorption[11], and thermal properties[12][13], which are helpful in advanced technology applications. Therefore, the interest in this material causes the carbon nanotube studies to expand and address issues from the preparation, structure, properties, and application. Furthermore, some considerations of biodegradation and toxicity need to be addressed in certain areas, such as the medical field[14][15].

Market estimation of CNT can be divided by its application, mainly as polymers. The increasing trend is noticeable each year (Figure 1). Prediction of the market size of CNT in North America also supports this data (Figure 2). The estimation graph shows an increasing market trend each year, with most of the market being MWCNT. Therefore, demand from the market is increasing (Figure 4). On the other hand, manufacturing data shows plateau production since 2014 (Figure 3). CNT production decreased significantly when Bayer Material science shut down its production in 2013. From the market data, a significant gap between supply and demand exists, and without another stimulus from the research side, the gap resulting in CNT's high price and

further CNT application research will be negatively affected from price to performance perspectives.

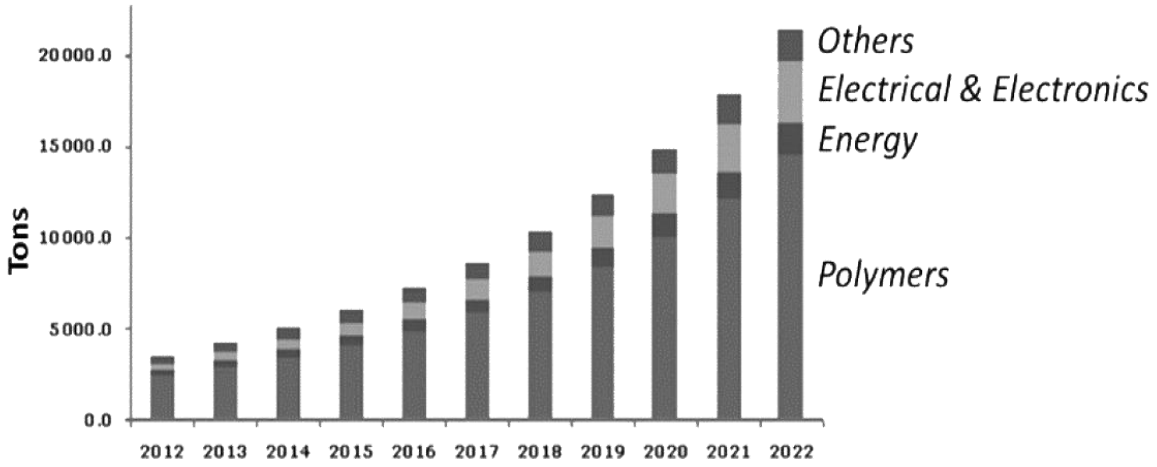

Figure 1 Market estimates for CNT per area of application [16]

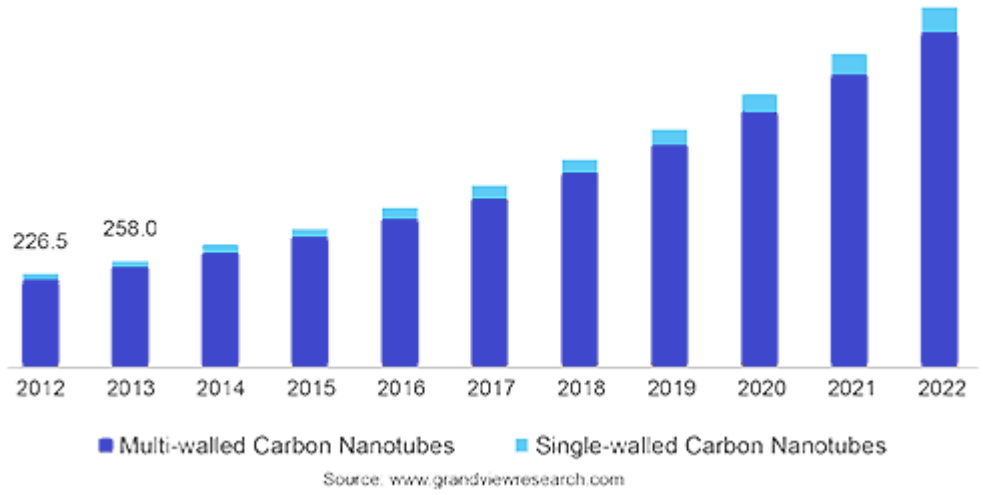

Figure 2 North America carbon nanotubes market size estimation (adapted from https://www.grandviewresearch.com/industry-analysis/carbon-nanotubes-cnt-market. Accessed 23 July 2018)

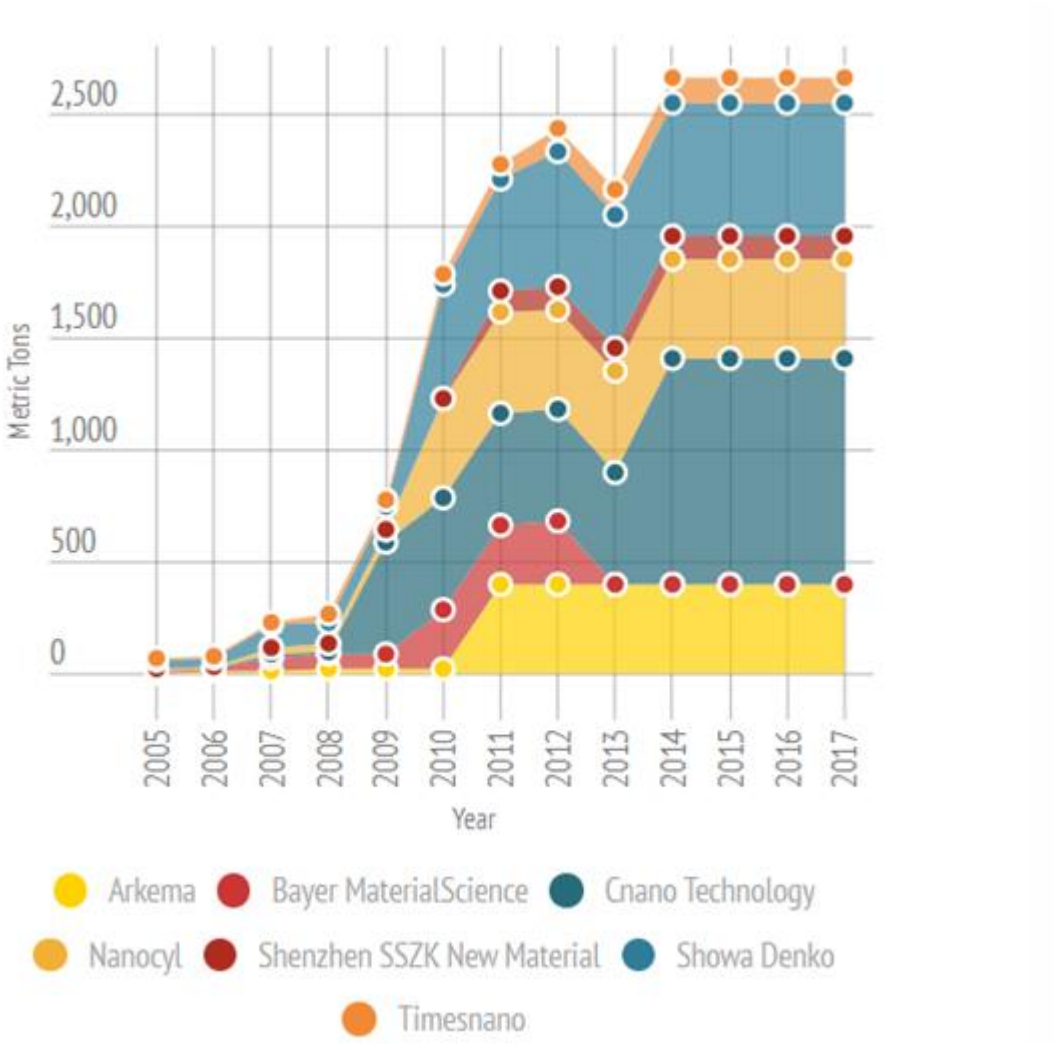

Figure 3 CNT manufacturer and capacity (Adapted from: http://cenm.ag/nanotubes2015. Accessed 15 July 2018.)

Visibility fluctuation of new technology is also applied in carbon nanotubes (Figure 5). From 1995 to 2005, the visibility of CNT was raised due to the insufficient investigation of CNT characteristics and their application. However, in 2004, graphene's entrance as a CNT competitor slowed down the CNT hype. In 2010 CNT surplus was built up and might be the cause of Bayer material science shutting down its CNT production. However, further research and application raise the CNT visibility[17][18]. Although the rise of the hype is promoting new research, the plateau of CNT production still occurs and combining the increasing demand each year results in a high price of CNT and impacts CNT justification to be applied or utilised despite its potential. Therefore, a new approach to producing CNT still needs to be studied.

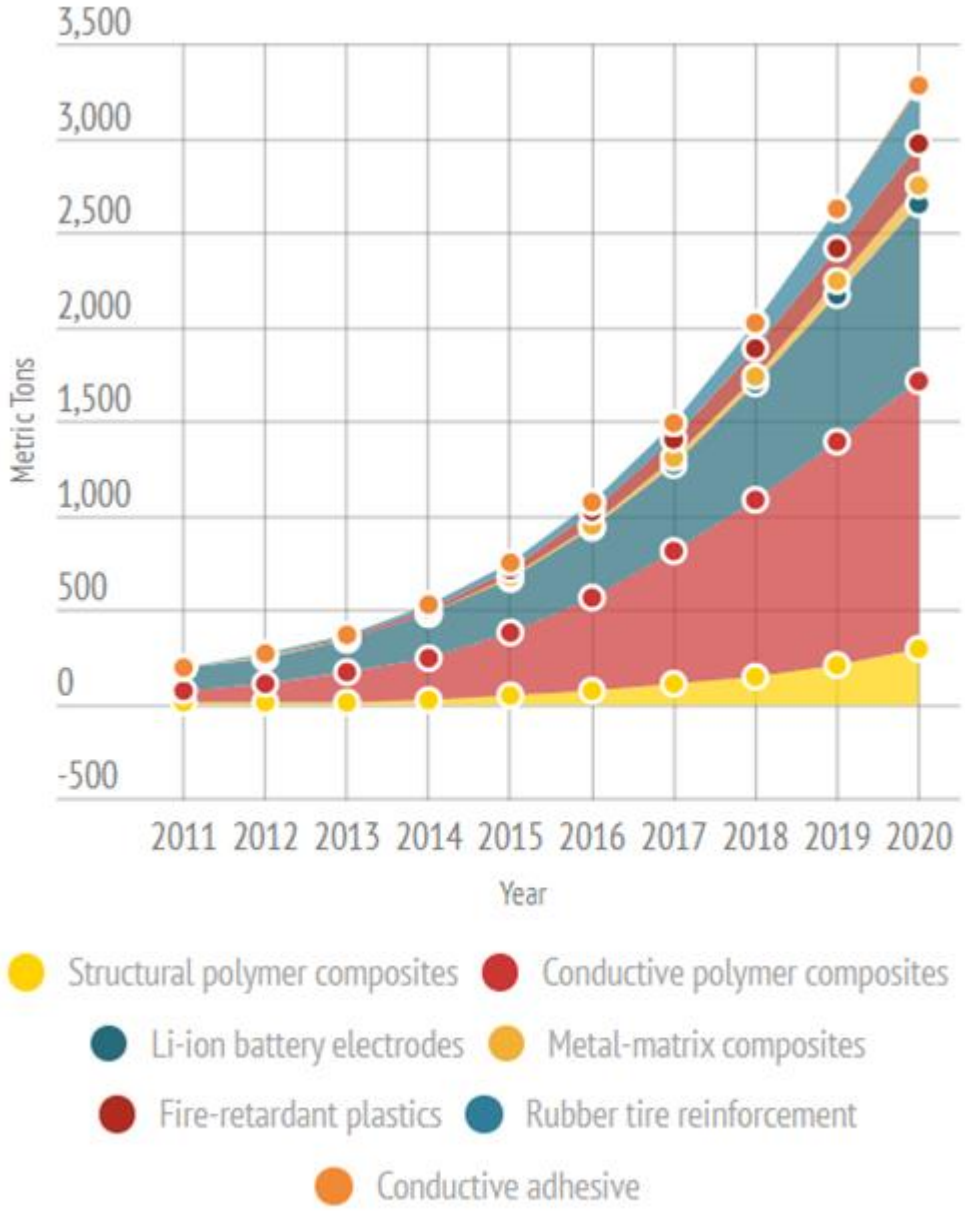

Figure 4 CNT Demand estimation based on application (Adapted from: http://cenm.ag/nanotubes2015. Accessed 15 July 2018.)

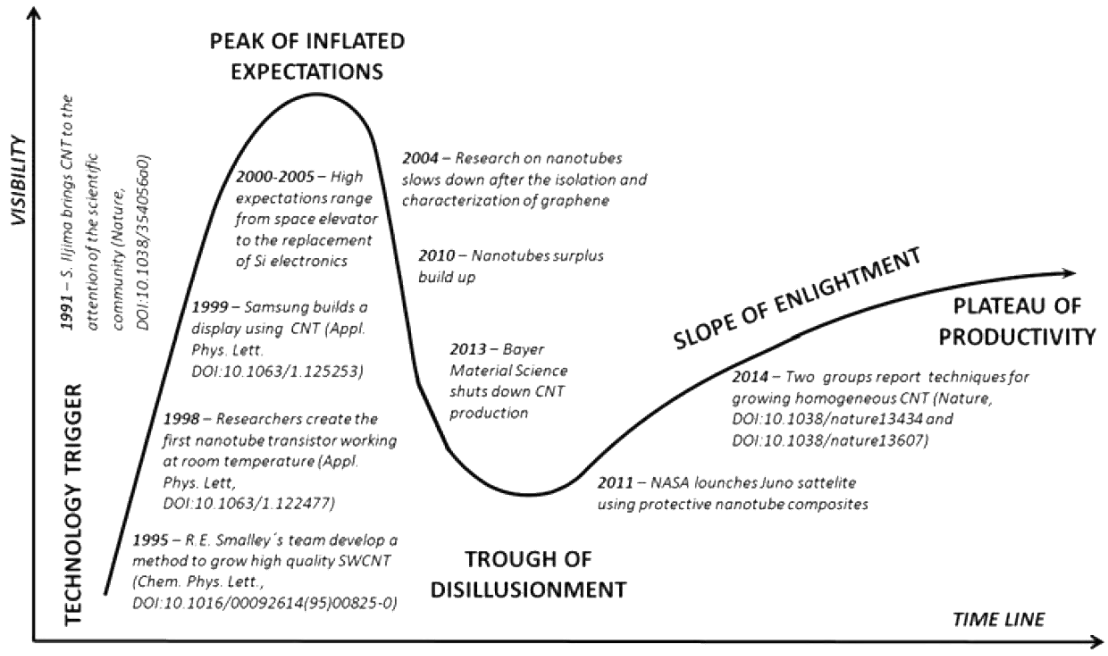

Figure 5 The hype cycle of carbon nanotubes [19]

Carbon capture and storage technology can be developed to convert CO_2 gas into high-value materials. One method which utilised this technology is Electrodeposition. The main advantages of the Electrodeposition method are the ease of preparation of the catalyst, electrolyte, and other supporting materials and equipment, which are crucial to developing an inexpensive method to produce valuable materials such as Carbon Nano Fiber (CNF) and Carbon nanotubes (CNT). Another advantage of this method is that the availability of CO_2 leads to lower-cost production. Furthermore, the Electrodeposition method potentially reduces the amount of CO_2 in the atmosphere to overcome emissions of greenhouse gases and lead to addressing climate change challenges[20]. However, further LCA analysis needs to be developed to fully understand the environmental impact of the Electrodeposition method[21]. Nonetheless, Electrodeposition is a promising approach to producing CNT with uncomplex preparation.

1.2 Knowledge gaps

Critical knowledge gaps concerning the Electrodeposition method are related to known parameters and optimisation. First, while well-established methods such as Arc Discharge, Laser ablation, and Chemical vapour Deposition are regarded as reliable methods, the limitation due to their complex preparation still occur. The arc discharge is the earliest method of CNT production; it produces both SWCNT and MWCNT with 1nm to 30 nm diameter. The yield for this method is ~10 g for each synthesis. Utilising 100-200 A current with 20 V voltage in Argon/Helium typically, the synthesis is 1 hour long. Although arc discharge protocol is simple, it is challenging to scale up outside a laboratory. The laser ablation method produces up to 90% purity SWCNT with a 1g/day yield. Although it has more scalability than arc discharge, Laser ablation is not as simple as arc discharge because of catalyst preparation requirements. CVD catalyst preparation requirement is the most complicated. However, it is the most scalable method due to its extensive research. From arc discharge, laser ablation and CVD, CNT production method scalability and complexity is inversely proportional; therefore, an alternative method that reduces the complexity but has moderate scalability is still desired. The prime method for this is Electrodeposition which provides uncomplex protocol and good yield.

Second, regarding the Electrodeposition method as an alternative, more work is needed to optimise the parameters to improve the end product quantity and quality. Third, there are still questionable effects on the end product due to partial research and in conjunction with the parameters. Research on Electrodeposition is not as mature as other methods, and most of them are done separately with a wide variety of parameters value. Therefore, combining the previous research to reach optimation is challenging.

Forth, little is known about the parameter's effect on other parameters. Utilising more than five parameters, the effect of the unavoidable parameters on other parameters occurs. For

example, extensive CO_2 will affect the external current reported[22], and other possible parameter effects might also occur.

Fifth, much of the research does not provide complete data on the effect of every parameter. The incomplete data also occurs since the research was done in a partial fashion and with a wide variety of parameters. Finally, using the Molecular Dynamics Simulation approach is desirable to understand the behaviour of the parameters from numerical and theoretical points of view. Molecular dynamics describes natural motion from a molecular structure driven by energy procedure; therefore, it can be a tool to set a base understanding behaviour of Electrodeposition parameters.

1.3 Research aim and objectives

Although several researchers examined Electrodeposition to produce CNT, product consistency issues occur. Limited studies were conducted without comprehensive optimization of parameters to improve the quality and quantity of CNT. From the issues raised, this study aims to optimise the Electrodeposition parameters to produce high-quality MWCNT efficiently while maintaining the uncomplex nature of the method. There are four objectives to achieve this goal.

1. Conducted a literature study to compose the state-of-the-art CNT production and a research gap.
2. Determining essential variables expectation behaviour in the Electrodeposition method.
3. Variables optimisation to improve the end product quantity and quality.
4. Conduct an Unpartial study by examining the dynamics of CNT properties for each parameters changes.

1.4 Methodology overview

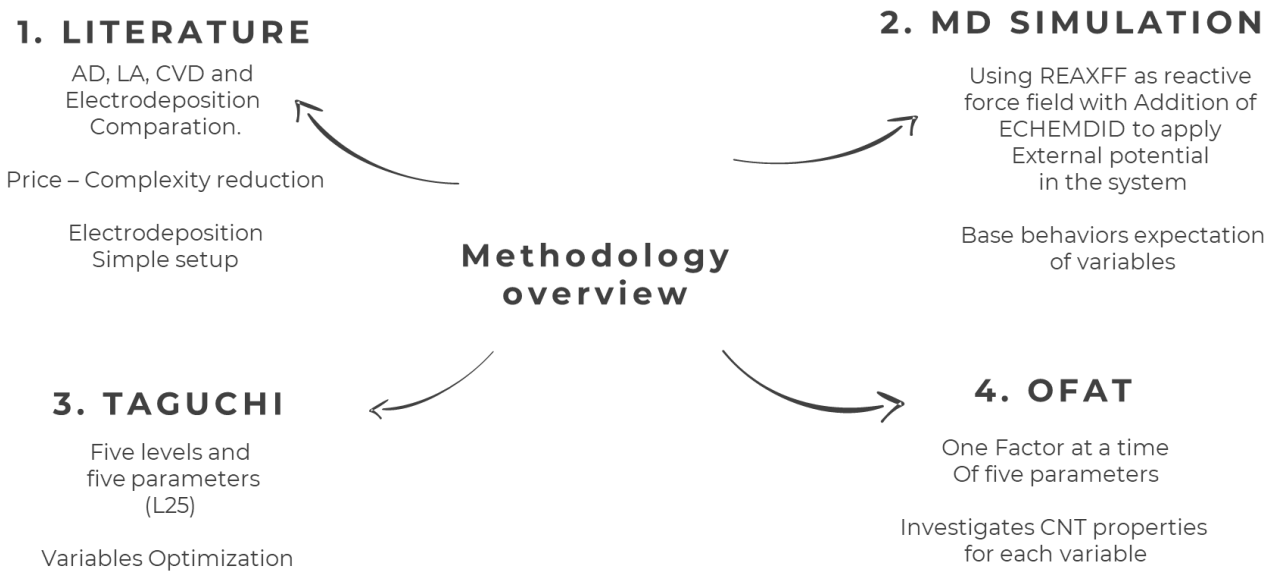

The literature review concludes that Electrodeposition can produce carbon nanotubes in an uncomplex way due to a lack of catalyst preparation. However, this method has some challenges that need to be addressed, most related to synthesis variables. Molecular dynamics simulation and experimental study utilised Taguchi and OFAT methods to counter the challenges. Molecular dynamics determine the base behaviour expected from variables. Furthermore, Taguchi and OFAT are used to optimise variables and examine the end-product properties of each variable.

From molecular dynamics, base expectations of the behaviour of the parameters were presented, and it is found that the carbon bond created is affected by the total energy in the system, while total energy depends on variable value. Using the Taguchi method, optimisation was conducted. It revealed that other factors such as the Expansion of molten salt, conductivity gain, current instability, excessive carbon deposit, and diffusion rates might play roles in the

system. OFAT provides XRD, FTIR, Raman SEM, and EDX analysis will reveal the end-product properties.

1.5 Structure of the thesis

This thesis contains five chapters that will explore the study of Electrodeposition to improve this method of producing carbon products, mainly CNT. The first chapter gives the Introduction of the thesis. It includes the background of the thesis to describe the motivation of the research, followed by knowledge gaps, research aim and objectives, and methodology overview used in this thesis. The second chapter predominantly explores the Electrodeposition discernibly from literature. Although the literature study mainly CNT related products, it does not mean attenuating the discussion of the synthesis process itself. The third chapter explores Molecular dynamics simulation. Chapter four focuses on the experimental study of Electrodeposition. Chapter five discusses the thesis as a whole and gives conclusions.

Chapter 2 – Literature review

The literature on CNT products and their production methods is presented to give profound knowledge and correctly manage research to improve the Electrodeposition method. This chapter is not limited to but mainly describes characterization, synthesis, and feasible ways to improve CNT quality and quantity.

Several widely used CNT synthesis methods, arc discharge, laser ablation, and CVD, have advantages and disadvantages. The arc discharge and laser ablation are based on the carbon evaporation method. This simple method produces low cost with wide diameter distribution, bundle accumulation, and low control over the CNT alignment. On the other hand, a chemical process such as CVD is considered more promising with a high yield of CNT products and the controllable effect of CNT alignment[22]. The chemical method also utilized catalysts which play a crucial role in determining the final product type. One chemical method considered a novel method is the Electrodeposition method. This method uses an electric current and chemical reaction to control the synthesis process and maintain the superficial aspect of the carbon evaporation method. The Electrodeposition method can be conducted without any catalyst preparation, which simplifies this method.

Electrodeposition can be a reliable method to produce CNT, which is an uncomplex method and produce a high yield of CNT. However, the Electrodeposition method requires deeper study, especially in the synthesis factors or variables affecting the final product. Besides a catalyst and electric current, several factors, such as synthesis temperature, carbon source, and synthesis time, can affect the Electrodeposition method. The advanced knowledge of these factors will improve the reliability of the Electrodeposition method.

2.1 Carbon nanotubes types, properties and characterisation

Carbon nanotubes (CNT) are classified as single-walled carbon nanotubes (SWCNT) and multiple-walled carbon nanotubes (MWCNT) based on the carbon layer. Another classification is based on carbon structures: armchair, zigzag, and chiral. SWCNT is a single layer of graphene. In most cases, SWCNT is challenging to synthesise because it demands proper growth control.

In contrast, multiple rolled graphene layers are easier to synthesize in bulk compared to SWCNT. SWCNT also tend to be produced in bundled form and dispersed condition, opposite to MWCNT, which in most cases is homogeneously dispersed with minimum bundled formed. In terms of purity, SWCNT is achieved higher using the arc discharge method than CVD. The high purity of MWCNT can achieve CVD, up to 90%[23].

The chirality of CNT can determine its types. Figure 6 describes the chirality of carbon nanotubes. Carbon nanotubes can be imaged as rolled over graphene sheets, and the chirality depends on how the sheet is rolled. For example, if the origin point (0,0) meets (7,7), then the CNT has (7,7) chirality. The red dot in Figure 6 represents the metallic. Its chirality defines the electronics and optical properties of CNT. Therefore, exploiting its practical applications in controlling CNT chirality is needed.

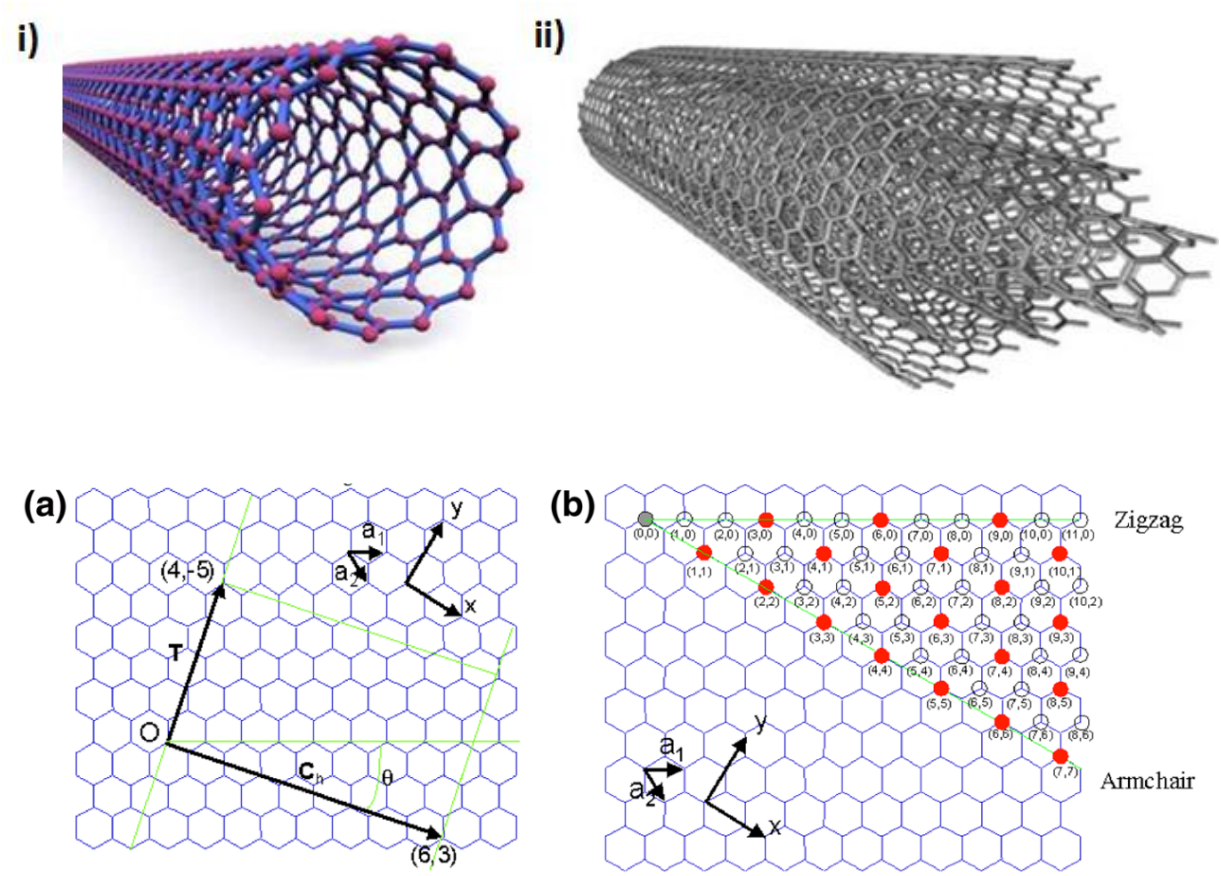

Figure 6 Carbon nanotubes types i) Single-wall carbon nanotubes. ii) multiwall carbon nanotubes. a) Chiral vectors of carbon nanotubes. b) CNT chirality (n,m), the electronics form is metallic if the value of (n-m)/3 integers. the red dots represent metallic CNT [24]

There are four characterisation methods commonly used in CNT characterisation: Fourier Transform Infrared (FTIR), X-Rays Diffraction (XRD), Raman spectroscopy, and Scanning Electron Microscopy. FTIR has three primary functions: knowing the presence of a molecule in a sample, comparing the composition of one substance to another, and the last function is to determining the concentration of molecules in the sample. The first and second functions are analyzed using qualitative methods, while the third function is an analysis using quantitative approaches with Beer's Law. The basic description of FTIR can be found in Appendix 3.

Carbon nanotubes have different infrared mode activities depending on the type of carbon nanotubes (SWCNT, MWCNT, chirality), but the primary mode is A_{2u} and E_{1u} [25]–[28]. These modes' values are 850 and 1590 cm^{-1} in SWCNT and 868 and 1575 cm^{-1} in MWCNT. Two

things can be obtained from the CNT FTIR analysis results: knowing the presence of carbon nanotubes in the sample and the number of molecules in the sample.

However, because the deviation value from graphite wavelength is 5-8 cm^{-1}, FTIR is commonly used to determine impurities and molecules capped on the CNT surface. These impurities and the capped molecule are associated with the defect. The defect is also widely considered functionalization, associated with O-H, COOH and CHx. O-H presented with 1600 cm^{-1}, 3450 cm^{-1} and 1445 in MWCNT cases. [29].

The acid treatment also plays a role in opening the end cap of MWCNT, which changes the functionalization of CNT. A previous study analyzed that OH and C=O responses at 3440 cm^{-1} and 1711 cm^{-1} have low intensity in pure MWCNT. The appearance of two additional peaks, 2923 cm^{-1} and 2853 cm^{-1}, is noticeable after MWCNT is treated with acid. These different peaks belong to the CH_2 group on the surface of MWCNT (Figure 7). Furthermore, the addition of 1719 cm^{-1} also arises due to C=O stretching[30].

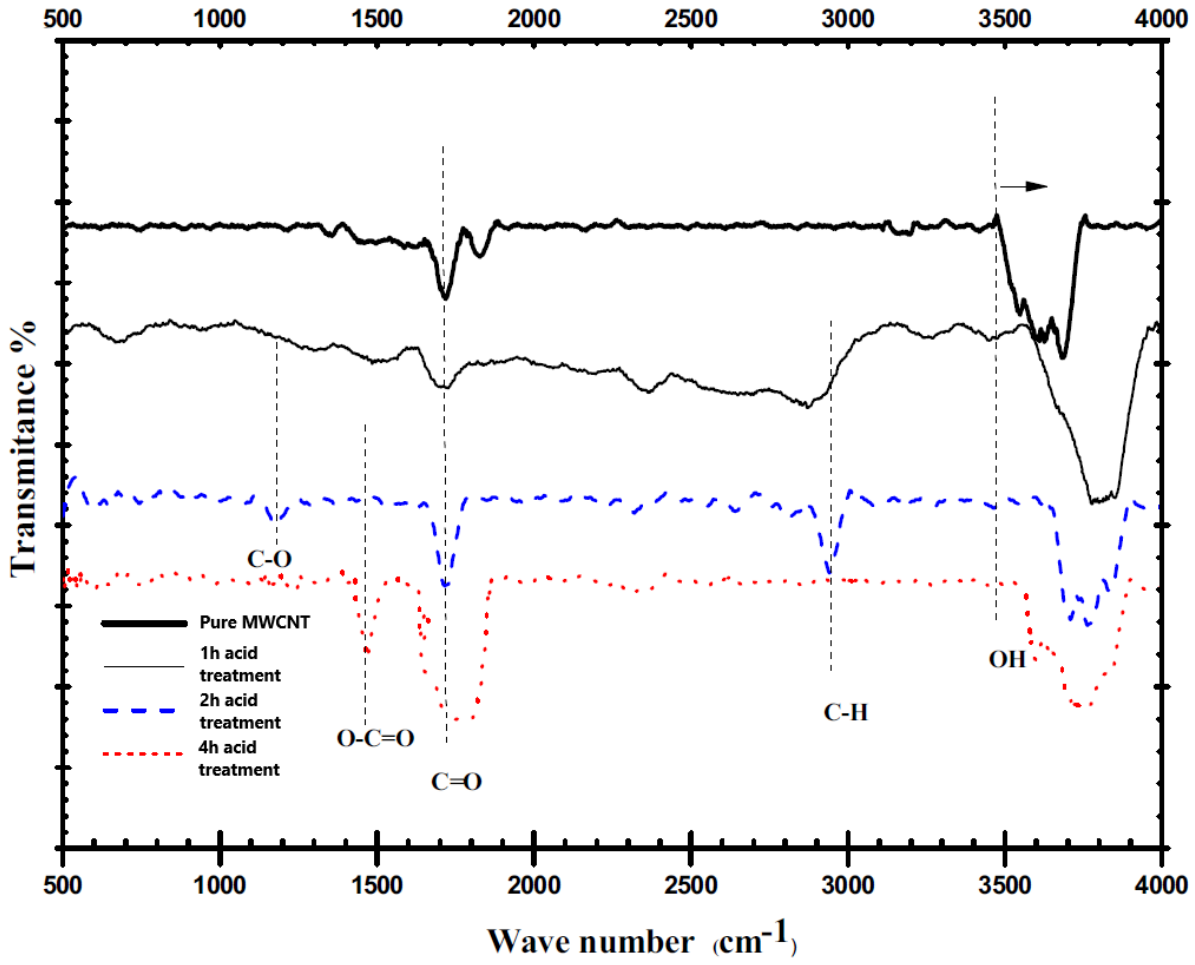

Figure 7 FTIR analysis on CNT functionalization [30]

XRD analysis method was used to describe the morphology and structure of CNTs at different angles. The basic information on XRD can be found in Appendix 4. The periodic structure of the XRD results will produce specific peaks. The peaks are almost similar to the pattern of XRD analysis on graphite. The difference in peaks can be used to identify the type of CNT. Moreover, this identification can determine the layer of MWCNT and the carbon amorph that follows it (Figure 8).

The dominant peaks in the CNT XRD pattern are (002), (100), and (101) miller indices. Due to graphene's different sizes and shapes, the XRD CNT pattern will experience shifts and expansion of peaks. Broader peaks can indicate CNTs with fewer impurities. The peak height

(002) indicates the thickness of the CNT wall; the higher the peak, the thicker the CNT wall. A higher peak value is because the constructive interference in Bragg's law will be higher in thicker CNT walls [31]. Peaks (100) and (101) (Figure 8) indicate crystalline or amorphous properties. Increasing peak width and decreasing intensity refer to the amorphous crystal form. The intensity shows the layer identification from the CNT, as the high-intensity value indicates more layers[32].

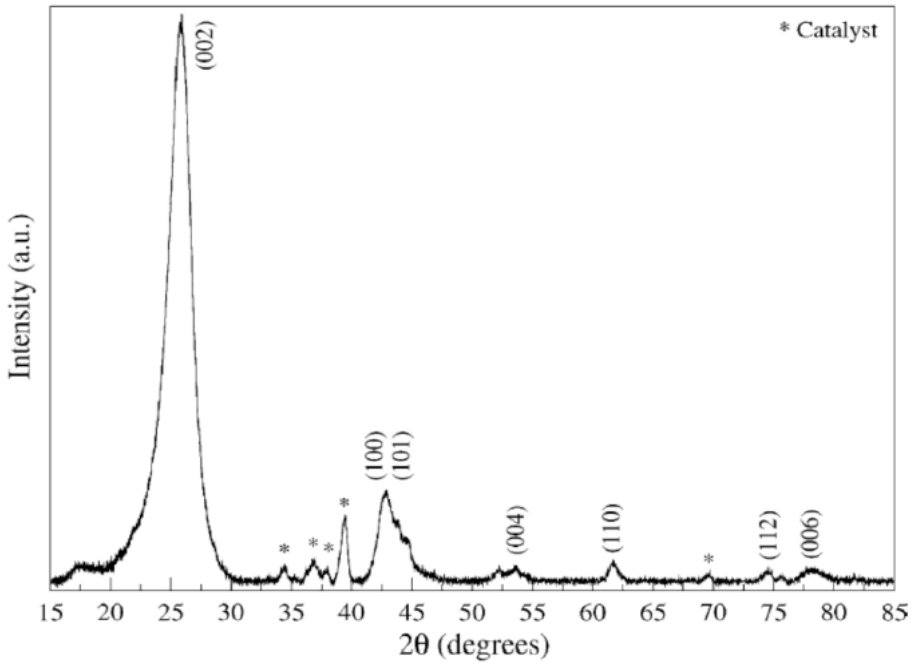

Figure 8 XRD result of CNT [33]

Raman spectroscopy is a fast and non-destructive analysis to characterize carbon nanotubes with relatively few sample preparation. It utilizes the shift in wavelength of the inelastically scattered radiation. There are four primary features in CNT characterization in Raman spectroscopy as follows:

1) RBM (radial breathing mode), which low-frequency peak (120-250 cm^{-1})
2) D band (~1350 cm^{-1})
3) G band (1500 - 1600 cm^{-1})

4) G' band, which D band overtone (2450 - 2650 cm^{-1})

RBM corresponds to the tube's radial vibration (A1g), which depends on the geometry and environment of nanotubes. RBM's relation with nanotube diameter can be found in Appendix 5. However, RBM peaks are hard to detect if the diameter of the nanotubes is larger than 2 nm.

D band is activated because of defects in sp^2 carbon materials, which will appear differently on each type of graphite-based structure. Therefore, this Raman D band feature helps determine carbon types based on their value and position. Smaller linewidth (10-30 cm^{-1}) in 1285 – 1300 cm^{-1} is the characteristic of SWCNT, while broader linewidth (>100 cm^{-1}) is related to amorphous carbon. MWCNT can be identified with the position of the D band in 1305 – 1330 cm^{-1} with a width of 30-60 cm^{-1} [33]. D band intensity can be used to quantify disorder. However, because absolute intensity measurement is complex, the I_D/I_G ratio (normalized intensity) is widely used as disorder measurement. It is also necessary to mention that this ratio depends on excitation laser energy.

The G band feature in Raman spectroscopy is related to the C-C bond stretching, the primary signature of all sp^2 carbons. It can be observed as a peak or multiple peaks ~ 1585 cm^{-1}. Rolled graphene sheets such as SWCNT will split the G band into ω_{G^-} and ω_{G^+}, which are parallel (LO modes) and perpendicular (TO modes) to the tube folding axis in semiconducting tubes. For metallic tubes, the mode is opposites. Several quantum confinements generate G band peaks associated with LO and TO, namely A1, E1, and E2. However, due to resonance and depolarisation conditions, A1 modes dominate G band spectra [34].

The G' band is the second order of Raman's signature in sp^2. The G' band intensity will be changing based on $E_{laser,}$ which can be observed in the range of 2450-2800 cm^{-1} as a peak or multiple peaks. In CNT, the G' band number of peaks and frequency depends on the chirality due to vibrational structures and quantum confinement [34]. Overall, D, G and G' band is often

used to measure the purity of CNT. The combination of I_D/I_G, $I_{G'}/I_G$ and $I_{G'}/I_D$ is demonstrated as viable means of purity assessment [35].

The purity assessment of CNT was described in Figure 9 by calculating the Raman spectroscopy features ratios. However, some research suggests that the intensity and frequency of Raman features are affected by E_{laser} [28][29]; therefore, using different E_{laser} will result in different ratios. In the later research, R. Dileo et al. at 2007 revealed that although different E_{laser} resulting different Raman intensity and frequency values, the $I_{G'}/I_D$ ratios profile remains identical with different E_{laser}[36]. A similar profile is primarily because the ID is E_{laser}-independent when measured in the 1.9-2.7 eV range[34].

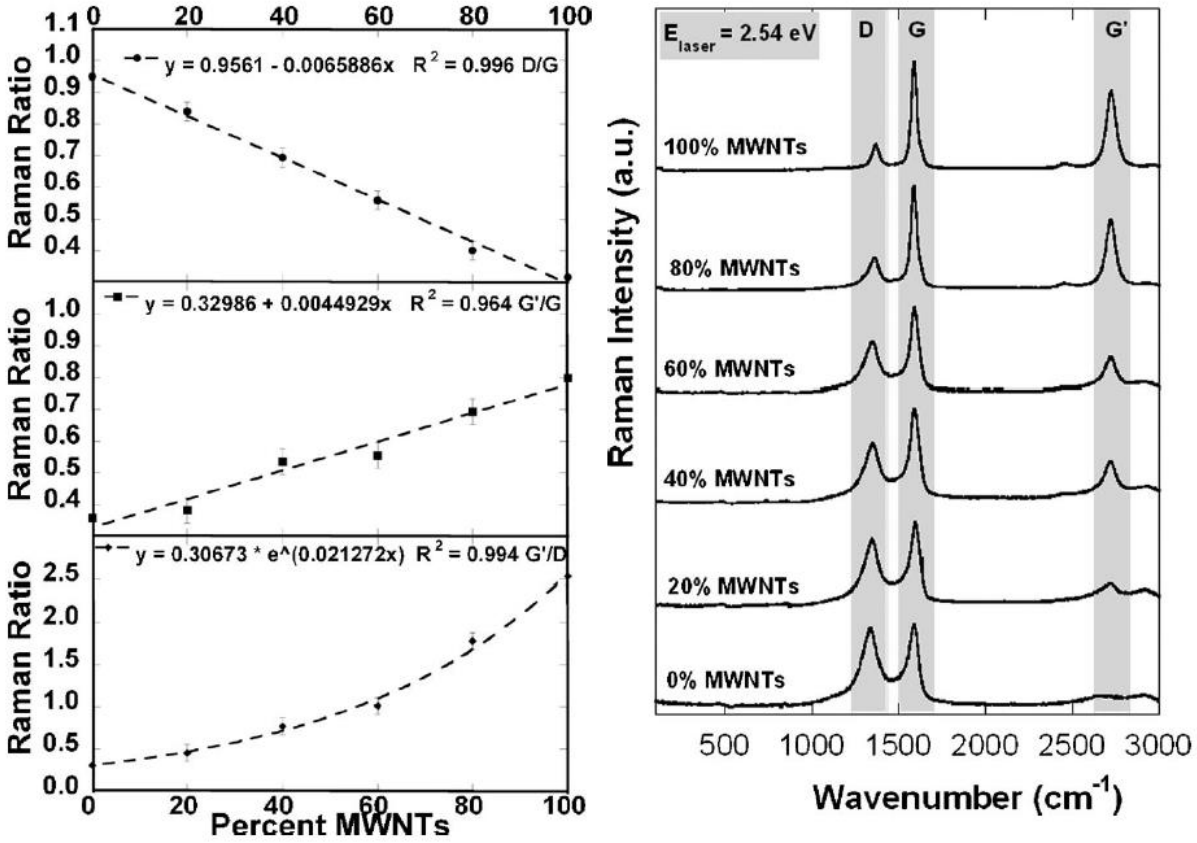

Figure 9 Examining MWCNT Raman Spectroscopy features related to its purity based on the ID/IG, IG'/IG and IG'/ID ratios. Adapted from [35]

The Notable I_D/I_G ratio might not be helpful to measure purity in all ranges of E_{laser}, but it is still widely used to measure the amount of disorder that leads to the quality of CNT. I_D/I_G ratio represents the normalized intensity for disorder measurement since the absolute intensity measurement is a challenging task in Raman spectroscopy[34]. One of the examples of utilizing ID/IG is in the pharmaceutical field, which compares eighteen different CNT materials and suggests that lower ID/IG represents a better quality or less defective CNT [37].

Lastly, SEM is one of the most commonly used methods to measure its outer diameter and length in carbon nanotube characterization. A basic description of this method can be found in Appendix 6. Size distribution measurement is also one of the strengths of this technique. Raul H. Basurto, in 2015, reported MWCNT SEM analysis, which was evaluated by Raman and proven this method is adequate to measure its diameter and diameter distribution. Furthermore, this study employed ionic liquids to enhance carbon nanotube dispersion[38].

2.2 Carbon nanotubes application

2.3.1 Medical

There are currently two primary purposes for the medical application of CNT: diagnostics and therapeutics. The diagnostic application includes biosensors, which are used to detect substances using biological and physicochemical detectors. This method allows in vitro and in vivo diagnostics monitoring. For example, Carbon nanotubes nanoelectrode ensembles' use improves the fabrication of glucose biosensors to detect hydrogen peroxide. These improvements simplify the design and increase blood sugar detection accuracy because CNT can detect cholesterol, alcohol, lactate, xanthine, choline, hypoxanthine, and acetylcholine. The characteristic of CNT used in this study was bulk SWCNT and MWCNT, high electrocatalytic, and fast electron-transfer rate [39].

Other applications of CNT in biosensors, due to its physical/chemical transduction and high surface area to volume ratio, are developing enzyme biosensors. Vicentini et al. used MWCNT, which characterised 20-30 nm in diameter, 1-2nm wall thickness, and 0.5 2μm in length and 95% purity for Tyrosinase detection. This study shows that MWCNT-based biosensors are easy to prepare, have lower cost, better stability and have a longer lifespan [40].

Biocompatibility is one of the challenges in the CNT application in medic. Toxicity is needed to be managed to achieve biocompatibility. The factors influencing the toxicity of CNT are metal impurities, CNT type, and surface properties[41]. The CNT synthesis process typically uses a metal catalyst which becomes impurities and potentially harmful. The lower impurities lead to a lower toxicity level. The relation between impurities and toxicities is supported in the previous research by Pietroiusti et al. in 2011[42]. This research compares three types of SWCNTs: pristine, oxidized, and ultra oxidized, with diameter specifications of 2.37 $\pm$ 0.40 nm, 1.58 $\pm$ 0.20 nm, and 1.80 $\pm$ 0.40 nm, respectively. This research is in line with other research by Yang et al. in 2007, which shows that pristine CNT is more biocompatible and pro-carcinogenic will increase toxicity [43]. Metal impurities can be solved with the purification process and better growth control. The purification process can be done using a physical, such as a sonic bath and a chemical, such as acid treatment.

Second, CNT biocompatibility is a type of CNT because some CNT types are reactive and cause toxicity. An example is 0.9-1.7 nm SWCNT indicates preventing DNA repair. The growth control and purification process, similar to metal impurities, is key to resolving this issue. The third factor affecting biocompatibility is the surface properties of CNT. Because it is directly linked to physicochemical characteristics that affect the reactivity level of CNT, this challenge can be solved with the addition of substances such as oxidative enzymes.

2.3.2 Photovoltaics

CNT has gained interest in photovoltaics because of its optical and electronic properties[44]. One of the CNT roles in the photovoltaic is used as a p-n Junction diode, resulting in the

photovoltaic effect. Furthermore, CNT is effective as a light harvester and charge transporter in photoactive layers [24]. For example, in the previous study, SWCNT was mixed with Poly(3-hexylthiophene) or P3HT and poly(3-octylthiophene) or P3OT in the solar cell. The result is better to charge separation and efficient charge collection [45].

One challenge in using CNT in photovoltaics is the Schottky barrier on the surface of CNT and metal electrodes, resulting in the current loss. Preceding research attempts to resolve these with the addition of metal oxide. Metal oxide options that are relatively affordable and have good results are MoO_2 and ZnO. The utilization of these metal oxides by layering them into solar cells resolves the Schottky barrier and improves photovoltaic or power conversion efficiency (PCE) up to 17% [46].

The bandgap in the CNT will affect the use of this material in the photovoltaic. The bandgap in semiconductors will determine the wave spectrum that absorbs by photovoltaic. CNT bandgap can be adjusted into different bandgaps. A study by C. W. Chen shows a bandgap modification on Carbon and Boron nitride nanotubes using Single-Walled Carbon Nanotubes (SWCNT) with chirality (10,0). This study successfully modified the semiconductor CNT bandgap with a zigzag profile Using an external electric field[47].

CNT could also be used in the Dye-Sanitized Cell (DSSC) method, potentially improving PCE. Research conducted by Colin et al. used CNT as a dye which resulting PCE improvement using semiconductor CNT. The thin film contains 90% semiconductor and 10% metallic CNT[48].

2.3 CNT Synthesis method

In general, it is not easy to directly compare the production methods of CNTs objectively. Each technique has its process steps, variables and requirement, resulting in unique advantages and disadvantages. The number of CNTs research also continued growth and pushed the limitations of the methods. Therefore, The primary consideration in the technique selections comes down to the availability of the resources as it will be different in each location and

condition. The summary of several previous research is presented in Table 1 as general guidance.

Table 1 Comparison of CNT fabrication methods [49][50][51][52][53][54][55][56][57]

Properties component	Synthesis method			
	Arc Discharge	Laser Ablation	Chemical Vapor Deposition	Electrodeposition
Advantages	Inexpensive. SWCNTs have limited structural defects. Simple protocol. high-quality nanotubes	Scalable production of SWCNTs. Produces long nanotubes. High purity. Controllable diameter. Relatively high purity, room-temperature synthesis	Uniform SWCNTs. High purity. low temperature, high purity, large-scale production, aligned growth possible	Inexpensive, uncomplicated set-up, abundant raw material availability, Flexible method to produce SWCNT and MWCNT. relatively low temperature, large-scale production
Disadvantages	Short nanotubes. Inconsistent size of SWCNTs. A heterogeneous reaction product requires purification. High temperature, purification required, tangled nanotubes	Cost and labour-intensive technique Method limited to the lab scale, crude product purification required	Best fit for producing MWCNTs. Synthesized CNTs are usually MWNTs, defects	SWCNT production will sacrifice the setup simplicity and add catalyst preparation. Under ongoing investigation, research is not as established as other methods.

The four methods can also be compared by comparing Appendixes 8, 9 and 10. The arc discharge method is typically synthesised in Argon, Hydrogen and Helium environments, and a few are in methane. Most of them used pressure below atmospheric and relatively low voltage ~20V with up to 200 A of current. The CNT quality of this method ranges from SWCNT (1- 20 nm) and MWCNT (5-20 nm), with a growth rate up to 115 mg/min. Laser ablation is synthesised using inert argon gas, resulting in up to 90% purity SWCNT with a 1g/day yield. The laser used in this method typically is Nd: YAG with various wavelengths and pulses. The laser used in laser ablation is notorious for being high power, up to 12000 watts. The environment temperature is ~1000 ºC and up to 1200 ºC. Various metal catalysts are also used; the common

one is Ni. The CVD method uses hydrocarbon gasses as the prime carbon source. The working temperature of CVD is 550 ºC up to 1200 ºC. Catalyst research for CVD is the prime topic, but Ni, Co, and Fe are the most common use. The CVD can produce SWCNT with a 450 mg/h yield. The Electrodeposition method uses molten salt to synthesise CNT; the molten salt uses Li_2CO_3 typically. This method does not require catalyst preparation because the electrode used in the synthesis enables metal nuclei growth mechanism with supporting metal initiation from molten salt[56]. The working temperature of the Electrodeposition depends on the melting point of the salt (in Li_2CO_3 723 ºC) up to 1200 ºC. The electrode used in the synthesis is typically metals and alloys with a 90% yield[55].

2.3.1 Arc discharge

Iijima first used the arc discharge method to produce a carbon nanotube in 1991 from pure graphitic carbon soot [1]. He reported that needle-like tubes of carbon could be synthesized by this method; CNT was produced at the cathode ranging from 4 to 30 nm in diameter, up to 1μ single wall and multi-wall. After discovering these novel materials, many researchers suggest different environments and settings improve the final result.

Arc discharge deposition is a method that places positive and negative electrodes a few millimetres apart. A high current is used to form a spark or plasma, decomposing the source of carbon and forming CNT. The arc discharge method can be classified into carbon and metal electrodes based on the electrode and carbon source (Figure 10). The first method uses metal electrodes submerged in toluene, and after arc discharge is initiated, it will decompose the toluene, which acts as a CNT source. T. Okada et al. and M.V. Antasari et al. studies are examples of this method[58][59]. The second method, which uses carbon electrodes, is similar to the first method in utilizing arc discharge to decompose carbon sources and produce CNT. However, in this method, the carbon anode sublimes and evaporates at high temperatures giving a carbon source for CNT. Thermal energy in plasma disintegrates carbon vapour into

carbon ions, moves to a relatively lower temperature cathode, and forms rod-shaped deposition.

A catalyst affects CNT growth in the arc discharge process, and the favourable use of catalysis was using a graphite anode rod with a drilled channel and filling it with catalyst. The catalyst preparation can be varied but generally contains Ni, Co and Fe. Due to the wide range of catalyst types and mixtures, the effect of catalyst is vastly varied, and the mechanism of the catalyst effect is followed. For example, X. Lin (1994) proposes that copper's presence will enhance the smaller and single-layer form of CNT. The hypothesis was that copper's existence changed the arc produced in the system by altering temperature distribution and halting the growth of multilayer CNT[60].

Other factors, such as temperature, pressure, electrode shape, and size, affect CNT growth and the overall complexing process. However, the effects were tracked down into the critical points of the arc discharge method, producing a high-temperature arc to dissolve the carbon source, followed by plasma generation and later deposits as CNT.

The most significant parameter in this method is the amount of current because it directly relates to the energy used in this synthesis. Also, the direct current type is used more than the alternating current. Alternating current is not favourable because the carbon ion will likely be detached from the carbon deposit and inhibit the CNT growth process. Other variables that significantly influence energy consumption are temperature and catalyst. These two variables determine the nucleation process and the quality of the CNT.

Based on Appendix 8, the synthesis uses 40-200 A arc current, 18-20 V potential difference, 30-120 minutes synthesis time, and produces 10-3-6.8 g/ minute. As mentioned, the cost reduction of CNT can be linked to energy and time consumed in the process. The main point here is to reduce arc current at least stay in the 40 A and produce as many as possible CNT in the shortest time. However, the catalyst also has a significant effect on the synthesis. Shi et al.

use Ni–Y catalyst that is placed in the small hole at anode rod carbon [61]. This modification method not only produces MWNT but also SWNT type armchair (n, n) type tubes with n = 8, 9, 10 and 11. This production is rapid progress because it lowers arc current yet keeps the quality of CNT.

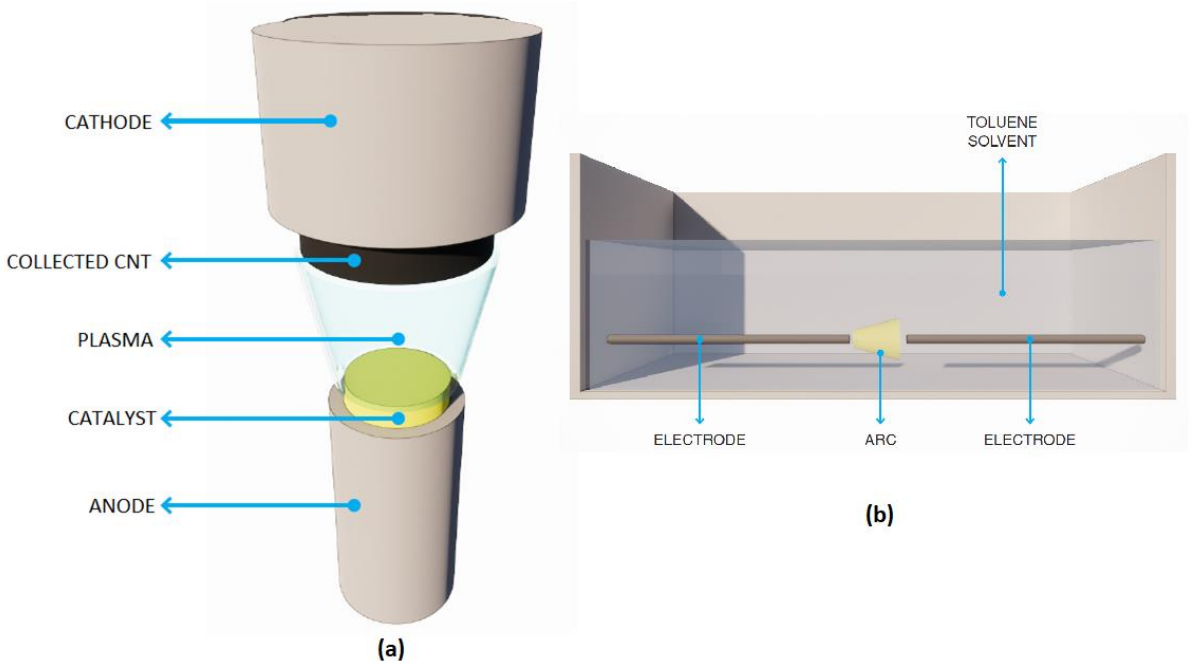

Figure 10 Arc discharge method types a) Arc discharge using carbon electrode b) arc discharge using a metal electrode

2.3.2 Laser ablation

Laser ablation uses metal graphite composite as the primary feedstock of carbon (Figure 11). The composite can be varied. In the first introduction of this method in 1995 mixed of high purity metal/metal oxide and graphite powder was used[62]. In the study, Ni and Co were used to learn the behaviour of metals in the laser ablation process[63]. The graphite composite is hit by pulses laser in the high-temperature reactor, and then inert gas carries vapours to the cooled

reactor, which collects the CNT. Single-wall carbon nanotubes are produced without the presence of multi-walled nanotubes. Combined metals as graphite mixture improved yields further in these studies. The addition method in laser utilization can also improve the outcome by using a continuous-wave laser[64].

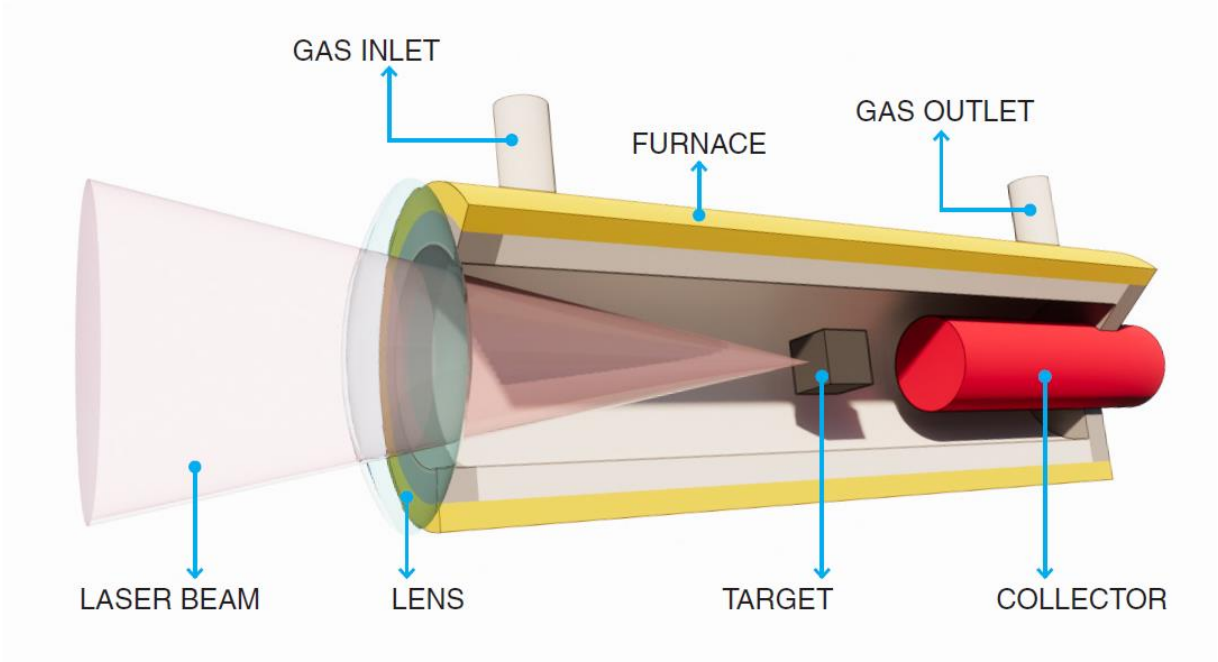

Figure 11 Laser ablation setup

There are several keynotes drawn by analyzing previous research. Firstly, both pure graphite and catalyst mixed graphite can obtain CNT. MWCNT with 4-24 layers can be acquired by hitting a 1.25 cm pure carbon rod with 3mm and 6mm laser beam spot (Nd: YAG with 532 nm wavelength) in a 1200 °C/ 500 torr quartz chamber[65]. Because of the limitation of graphite targets, the quality of CNT can be improved by changing other parameters. The utilization of metal catalysts in graphite affects the yield, types and quality of CNT. Comparing the result using different metal catalysts, Ni had the most significant yield, followed by Co and Pt. In contrast, Cu and Nb do not produce any nanotubes. The bi-metal graphite mixture is superior to the mono-metal, with the most significant yield achieved by Co/Ni and followed by Co/Pt, Ni/Pt and Co/Cu, respectively[62][64].

Secondly, the adequate pressure of the laser ablation is ~500 torr if lower pressure is used, resulting in high amorphous carbon and while using higher pressure, lean to a large quantity of MWCNT with fine structure[66]. Thirdly, high temperature (>1000 ^{o}C) results in an increased yield and less defect CNT[65][67]. However, high temperature also raises CNT diameters[68]. Fourth, argon is frequently used in laser ablation, but research suggests that hydrogen reduces amorphous carbon[69].

2.3.3 CVD

CVD, generally used to produce thin film and substrate similar to PVD, is a reliable method to produce CNT. In 1996, Hongjie Dai reported that SWNT synthesis was possible using the CVD method [70]. The process involves two steps: (1) the preparation of the catalyst on a surface and (2) the growth by the decomposition of reactant gases. The catalyst metals commonly used for nanotube growth are Fe, Ni and Co [71]. Decomposed hydrocarbon vapour or volatile carbon will grow on the prepared metal catalyst, which acts as the CNT's nucleation site.

On the catalyst preparation side, previous research attempts to increase the amount of product, increase the quality, and homogenize distribution by tweaking, adjusting, changing, and using different approaches to prepare the catalyst. Furthermore, changing the pressure, carbon feedstock flow rate, and temperature can improve the growth process.

The bulk synthesis can be achieved by utilizing the sol-gel technique based on Al_2O_3 and Mo nanoparticles on catalyst preparation[72]. This method allows the growth of SWCNT on a more significant amount while maintaining CNT quality.

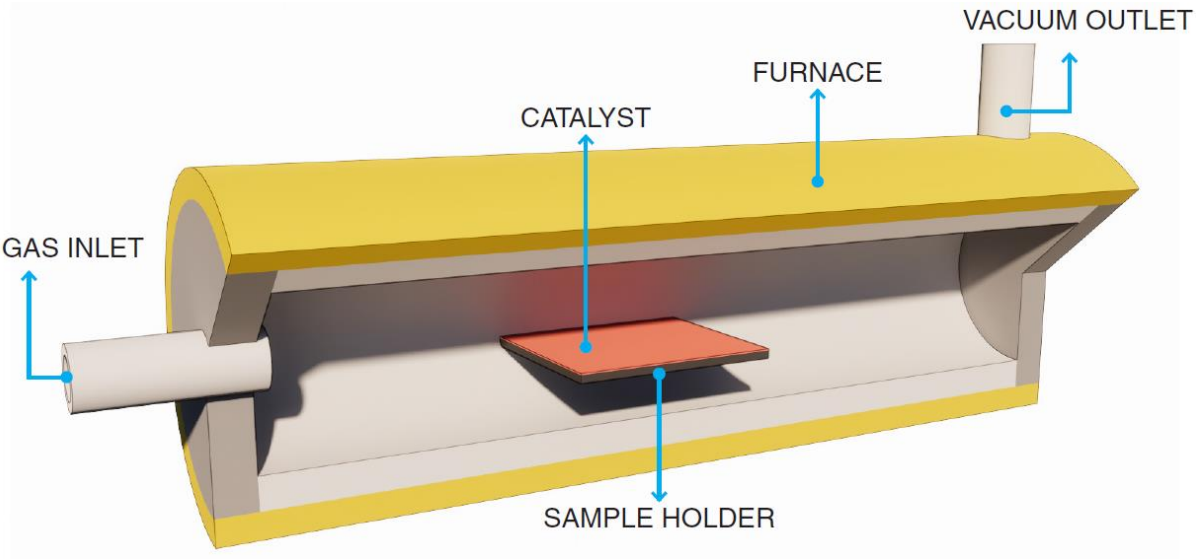

Figure 12 CVD method setup to synthesise CNT

Carbon monoxide is an alternative carbon feedstock rather than hydrocarbon, such as methane. Both can be mixed to achieve good emission properties[73]. Combining carbon monoxide and iron pentacarbonyl as a catalyst in gas form reduces amorphous carbon as a side product, which will need to eliminate in the purification process.

Controlling the pressure of feedstock and the overall synthesis process also affects the size and diameter distribution of CNT. Combining higher pressure with a gas-phase catalyst produces CNT in a smaller diameter and better distribution. This characteristic can be explained because the pressure in the carbon source causes a faster disproportionation reaction and supplies the C atom earlier to the catalyst particle before forming a more extensive particle. This reaction leads to a smaller diameter CNT and gas-phase catalyst, ensuring the catalyst is well distributed and has better diameter distribution [74].

2.3.4 Electrodeposition method

The Electrodeposition method was used in 1966 as the carbon capture technique. In the previous research, Ingram et al. used a gold electrode with a 20% mixture of palladium, platinum, gold and stainless steel. Electrolyte used was Li_2CO_3, Na_2CO_3, K_2CO_3 with

temperature and potential external variation of 600 °C, 773 °C and 2-2.6 V, respectively. The result was a deposited amorphous carbon. This deposit was only 3% solid carbon; the rest was an electrolyte mixture [75].

The Electrodeposition technique could utilize atmospheric CO_2 as a carbon source. This method can decrease CO_2 in the atmosphere, considered a greenhouse gas and one main factor of global warming. This hypothesis was proposed in the previous study [56][76][77][78]. Future life cycle analyses of these processes might be needed to make this hypothesis more admissible. The most feasible advantage of the Electrodeposition in current progress is relatively uncomplex equipment and source (Figure 13). Therefore, allowing the Electrodeposition method to be conducted everywhere. Furthermore, the end product of the Electrodeposition technique might have a high value.

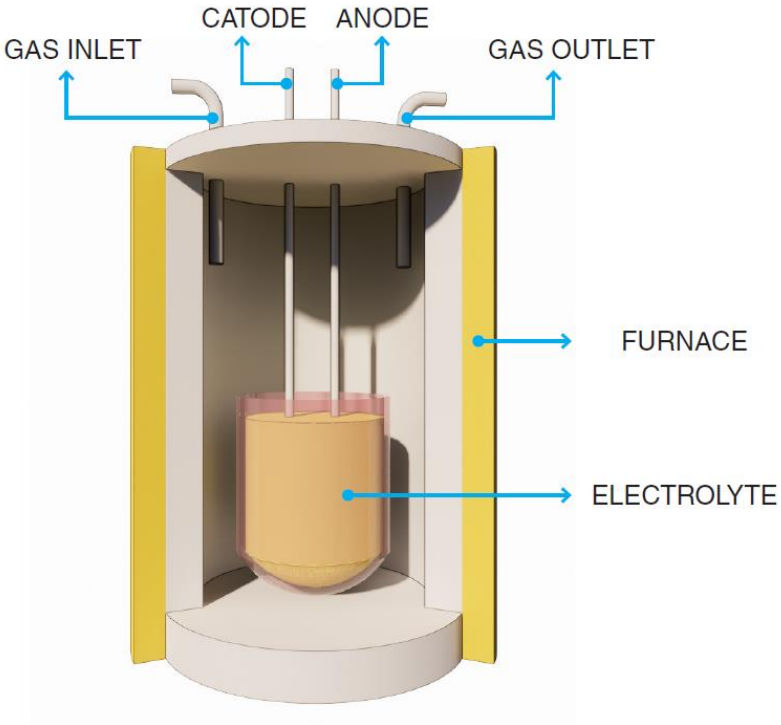

Figure 13 Electrodeposition setup

2.4 State-of-the-art Electrodeposition method to produce CNT

As mentioned in chapter 2.3.4, the Electrodeposition method was introduced as carbon capture technology in 1966[75]. The first attempt to apply this method to produce CNT was made by A.T. Dimitrov in 2009 [79]. In this experimental work, a carbon crucible was used as an anode, and a graphite rod (6.5 mm diameter) acted as a cathode. Molten LiCl + 5% Li_2CO_3 at a temperature of 700 ºC was used as an electrolyte. The result was that there was no CNT detected in the end product. Therefore, it was concluded that Electrodeposition is impossible to use as a CNT production method under their applied conditions. Another work of Electrodeposition was conducted by Happiness et al. in 2014 [80]. Utilising platinum wire electrodes was also concluded that no CNT was found. X. Qiao et al. in 2013 [81] and D. Tang et al. in 2013 [82] also studied the Electrodeposition method resulting in no evidence of CNT. However, all of these studies increase the production rate of the carbon capture process.

Electrodeposition has received a better response to produce CNT since the work of J.Ren et al. [56] was published and provides a roadmap to guide electrodes used in the research (Figure 14). This work successfully converted CO_2 to high-yield uniform Carbon nanofiber, and later in 2017, the work continued and confirmed that the end product was CNT[83]. The novelty research finds CNT in the end product is that they enable metal nuclei growth mechanism with supporting metal initiation from molten salt. Further tracking airborne CO_2 research also shows that CO_2 reactant in the Electrodeposition method provides an additional economic incentive to remove CO_2 from the air or stack emissions [76].

After J.Ren's work, more research confirmed and added more information regarding the growth of CNT in the Electrodeposition method. Douglas et al. in 2017 [55], [84] confirm the Ni nuclei growth with Zinc initiated path suggested by J.Ren in this research, MWCNT produced up to 30 nm in diameter. Further study in 2019 by S. Arcaro et al. [57] proves that not only Zinc can be used as a metal initiator but also Cr. Douglas et al. [55] also successfully produced SWCNT

alongside MWCNT with additional catalyst preparations, including the Ni coating process with 500 cycles (~50 nm) of Al_2O_3.

From all the previous work, some gaps need to be filled to improve the Electrodeposition method. The important one is using pre-CNT findings (before 2015) to improve the production rate of CNT. For example, D. Tang et al. 2013 [82] improved the productivity of carbon products compared to Happiness et al. in 2014 [80] which proves the upscale capability of the Electrodeposition method. Combining the metal nuclei growth mechanism with supporting metal initiation from molten salt knowledge [56] with the improvement of production rate is necessary to stimulate this method to gain more valuable products. The gap in material types as the electrode also needed further study since the metal initiator might be replaced with an unknown effect. All profound studies are also incomplete, with a wide range of parameters used. Therefore, a complete study is needed to wrap up all of the previous research. Furthermore, a study which improves CNT production while maintaining the uncomplex characteristic of Electrodeposition is necessary.

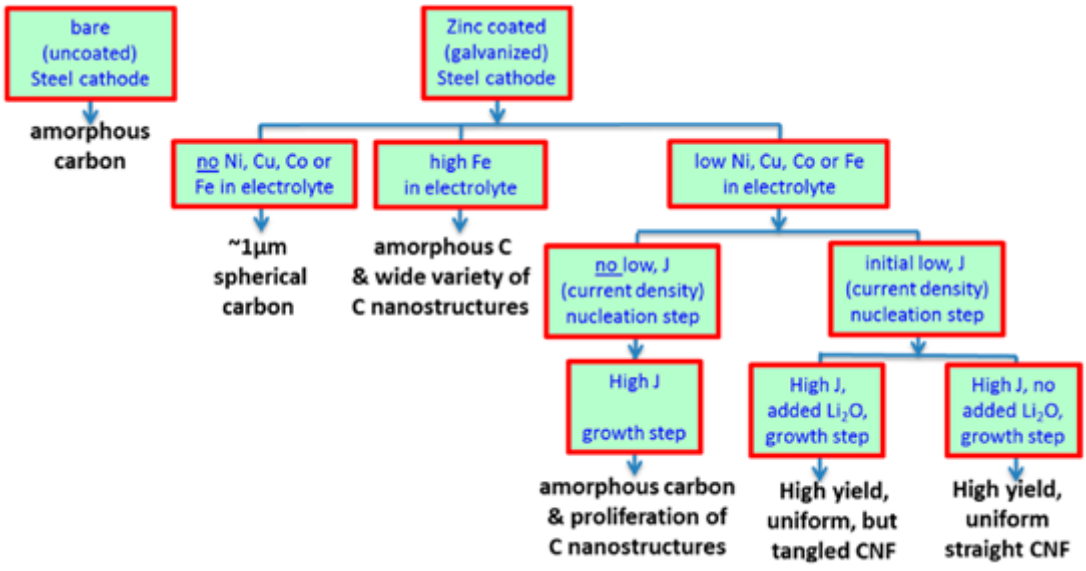

Figure 14 Roadmap research of electrode used in carbon Electrodeposition method to produce CNF [56]

2.5 Effect of variables in Electrodeposition method

Research on carbon nanotubes has been conducted for more than 20 years since their discovery. The CNT's growth and chiral control have been a scientist's ultimate goal. It is essential because these controls will open new opportunities for CNT application, reduce the purification process's effort, and reduce the production cost of CNT. In the initial study, the researchers attempt to control the synthesis by tweaking the Electrodeposition Variables. This chapter will discuss the current research on adjusting Electrodeposition process variables.

2.5.1 Temperature

The second factor is the synthesis temperature. Ijije et al. [80], [85], [86] used a temperature variation of 450-900 °C. The research results explained that carbon growth was influenced by the calculation of Gibbs free energy in the Electrodeposition process. In the potential free energy of alkali metal calculation, the standard value of pure metal potential (E_{M}°) and the potential required for carbon to occur or the standard value for carbon potential (E_{C}°) will determine the ease of carbon deposits. Among the options for the alkaline metal, Li has a value of E_{M}° which is relatively more negative than E_{C}°. Therefore, Li is a good choice in electrolyte selection. Alkali alternatives and other alkali metals, for example, K and Na. Tends to have E_{M}° a value that is equal to or more positive than E_{C}°. This study explains that the optimal carbon formation occurs at a temperature of 900 °C because the value of E_{C}° is closer to the value of 0 compared to the value of E_{C}° at a temperature of 700 °C. However, the formation of better carbon occurs at lower temperatures due to the value of (E_{M}°) minus the E_{C}° value is greater.

Tang et al. [82]explain that temperature variations affect the Electrodeposition method because the more significant the temperature used, the bigger the carbon. It can be seen from the results of these studies that at temperatures of 450 °C, the results obtained are 50-250 nm, while at temperatures of 550 °C of carbon obtained between 500 nm - 1 μm and at temperatures of 650 °C obtained size of more than 2 μm. In addition, Arcaro et al. [57] research used a temperature

of 770 ºC. The results obtained in this study are MWCNT (Multi-Wall Carbon nanotubes) carbon deposits with a purity of 90% for an outer diameter of 100-125 nm and an inner diameter of 25-40 nm.

The Electrodeposition temperature affects overall synthesis in several ways. One example is the changes in temperature resulting in changes in the electronegativity and conductivity of the salt. The changes in electronegativity and conductivity result in different sizes, purity, and quality of CNT products, which sometimes conflict. Therefore, further studies are needed regarding the effective temperature in producing large amounts of carbon while considering CNT quality, size and purity.

The temperature effect in the Electrodeposition process is that the higher temperature will produce a bigger particle carbon deposit. The study conducted by D. Tang et al. in 2013 fabricated 50-250 nm of carbon product at 450 °C while at 550 °C and 650 ˚°C produced bigger particles which are 500 nm-1 μm and > 2 μm, respectively. The carbon product morphology was amorphous, flake-like, and sheet carbon at each respective temperature [82].

Further investigation of molten salt working temperature is conducted using the potential energy of earth alkali reduction and comparing it to the need for potential energy to deposit carbons. This study investigates the reduction of Li, Na, and K in 450-900 °C range temperature. When analysing the data of metal alkali reduction energy (E_M^o) and energy needed to cause carbon deposit (E_C^o) (Table 2), carbon deposit will be favourable in approximation 700 °C either to produce CO or to produce C deposit using Li-based electrolyte [85]. However, Na and K-based electrolytes are not favourable in the carbon capture system because they have lower potential energy differences than Li.

Table 2 Standard potentials vs $CO_3^{2-}/CO_2^{-}O_2$ for converting metal carbonate to pure metal, carbon and carbon monoxide for Li, Na and K carbonates at different temperatures [85].

T (°C)	Metal	E_M^o (V)	E_C^o (V)	E_{CO}^o (V)
450	Li	-3.12	-1.78	-2.15
	Na	-2.71	-2.61	-2.61
	K	-2.77	-3.15	-3.98
540	Li	-3.01	-1.71	-2.01
	Na	-2.59	-2.53	-3.11
	K	-2.65	-3.06	-3.81
620	Li	-2.91	-1.65	-1.89
	Na	-2.49	-2.47	-2.98
	K	-2.54	-2.98	-3.66
700	Li	-2.82	-1.59	-1.79
	Na	-2.39	-2.4	-2.86
	K	-2.43	-2.9	-3.52
900	Li	-2.5	-1.48	-1.53
	Na	-2.14	-2.26	-2.59
	K	-2.19	-2.73	-3.2

Studies of temperatures greater than 900 °C show ineffective in capturing atmospheric carbon dioxide. First, by observing Table 2, the pattern of differences between E_M^o and E_C^o It will be decreased at a higher temperature. This decrease could mean that the system's energy will be less favourable for using carbon deposit energy. Secondly, Liwen Hu et al. show that at 950 °C, there is no carbon deposit [87]. This case proposed by the writer explains that at 950 °C, the reduction energy from CO_3^{2-} to CO is lower than CO_3^{2-} to C. This study also might indicate that temperature will affect the shape of the carbon product in the Electrodeposition. This study uses 650 °C, 750 °C, 850 °C, and 950 °C as temperature variables. At 650 °C, 750 °C, and 850 °C, the carbon deposit tends to be shaped flake-like, rolled ball-like, and flat-shaped, respectively. At 850 °C, fewer layers were formed if we compared them to lower temperatures.

Experiment research conducted by Aracaro et al. might indicate that the Electrodeposition process's optimal temperature is around the melting point (723 °C) of lithium carbonate[57]. This research was conducted using 770 °C temperature, 0.5-2 A current, 1-4 hours synthesis

time, and galvanized steel-nichrome electrode. As a result, this experiment produces carbon deposits in MWCNT form with 90% purity with 75-85 nm wall thickness.

2.5.2 External potential and current

External potential use in Electrodeposition needs to be investigated further due to two factors. The first factor is that the layer thickness deposited varies based on the size of the external potential. Based on previous research [88], the more significant the external potential, the thicker the resulting carbon deposit and vice versa; the smaller the external potential, the thinner the carbon deposit will be. The second factor is the current stability, which is different for each external potential value. Research in 2013 [82], the external potential used was 3V-6V and at specified temperatures of 450, 550, and 650 ℃ with a carbon source of CO_2. The result shows that the external potential at 3 V and 3.5 V tends to reach stable conditions quickly. The current reaction increases with increasing external potential and temperature. The particle size of carbon increases with increasing temperature, but the potential external effect on carbon particle size is more complicated than the temperature effect. Research in 2013 [82] obtained information on the relationship between external potential and current in the Electrodeposition process. The increase in current at constant external potential is an indication of the acceleration of the reaction between CO_2 and O^{2-} increasing CO_3^{2-}. With the rise in CO_3^{2-} concentration, the conversion of C and CO from CO_2 occurs faster. Based on its complex nature found in former research, external potential in Electrodeposition needs to be studied to optimize the CNT yield.

External potential acts as an electron composition changer in the Electrodeposition system. For example, in equation 1, the oxidation of CO_2 into CO_3^{-2} ions is possible because the excess of an electron in the system provides external potential. One way to achieve the attempt to control CNT growth in terms of external potential is by varying current or external potential. The value

of current and external potentials will vary depending on the electrolyte and electrode used. In general in Li_2CO_3 external potential values are 2-6 volt [82].

$$3CO_2 + 4e^- \rightarrow C + 2{CO_3}^{2-} \qquad \text{Equation 1}$$

The stability of external potential also needs to be considered in the Electrodeposition Study conducted by Diyong Tang et al. using 3-6 V external potential, Li_2CO_3-Na_2CO_3-K_2CO_3 mixture electrolyte, and Ni electrode. This study showed the time needed to stabilise the current in the constant external voltage [82]. Therefore initial low current (approx 0.05-0.4 A for 5-10 minutes) might be needed during Electrodeposition preparation to prevent rapid stabilization in the system [83].

Other research also suggests that during the Electrodeposition process, the increase of the current value is one of indication the reaction between CO_2 and O^{2-} in the system, which generates a higher concentration of CO_3^{2-}. A high concentration of CO_3^{2-} will promote the faster conversion of C and CO from CO_2 [87].

Some evidence also suggests that a high external potential effect increases carbon deposit amount. M. Gao et al. conducted experimental research using -2.1, -2.4 and -2.6 volt external potential at 723 °C for 5000 second synthesis time[89]. The result shows that the carbon deposit covered Ni cathode, and the carbon amount increases with the rising external potential value. XRD analysis also supports this result, which shows that Li_2O composition is lower in the -2.6 V than lower external potential.

2.5.3 Synthesis time

In Ijije et al. research, the Electrodeposition time was 30 minutes and 60 minutes. The highest growth rate produced was 0.1107 g cm^{-2} h^{-1} with 30 minutes of Electrodeposition time at a temperature of 540 ℃, and a decrease in the carbon growth rate of 0.0917 g cm^{-2} h^{-1} at a

temperature of 900 ℃ [80]. In their study, Tang et al., 2013 used a time variation of 150-900 minutes for the Electrodeposition process, with the highest results obtained at 250 minutes with 856.26 cm^2 g^{-1} [82]. In Douglas et al. research in 2018, the time used was 60 minutes in all experiments. The CNT obtained on the electrode with a thickness of 0.5 nm of Fe layer, namely the average diameter between 10-38 nm and an average diameter of 23 nm, while for the thickness of the Fe 5 layer nm CNTs obtained are 19-62 nm in diameter with an average diameter of 33 nm [55]. From these researches, there the optimum timing in Electrodeposition which still unknown. Finding the right deposition time is needed to optimize Carbon Nanotubes' growth rate.

The longer synthesis time likely produces more carbon deposits. However, the optimum carbon growth rate needs to be considered. In general, Electrodeposition process is taking 15 to 900 minutes which also depends on other parameters [55], [80], [82], [83]. It is hard to pinpoint the adequate time because of the wide range of Electrodeposition time. Furthermore, it is also affected by various variables, making the optimization of Electrodeposition time intricate.

Many factors influence the carbon deposition rate that occurs in the electrode. Some of them are physical and metallurgical factors, which as the thickness of deposited carbon. For example, the thickness of the deposited is closely related to the electrolyte's conductance. The electrolyte's conductance determines the number of ions and ions' speed movement in the electrolyte solution. The thicker the carbon deposited, the smaller the deposit rate [90].

More carbon will be deposited in the longer Electrodeposition time, but the carbon growth rate will be low. This phenomenon is due to the thickness of the layer getting thicker; the electrolyte's conductance becomes low and results in a lower number of ions. These thick layers of deposited carbon cause high resistance in the electrode[91]. Furthermore, the movement of ions in the electrolyte decreases. If the resistance is considerable, which results in smaller conductance, the rate of carbon deposits will decrease.

An experiment study by H.V. Ijije et al. employs 30-60 minutes of synthesis time. The highest carbon growth rate value is achieved in the 30 minutes of Electrodeposition time, 4 V external voltage, and 540 °C temperature settings, 0,1107 g cm^{-2} h^{-1} utilising platinum electrode and Li_2CO_3–K_2CO_3 electrolyte [80]. In the different settings, Douglas et al. Implemented 60 minutes of synthesis time in all their experiment. CNTs produced in this experiment ranged from 10-62 nm depending on Fe catalyst size [55]. These two research indicates that a longer deposition time will decrease the deposition rate.

Research by Tang et al. Using 150,170,250, and 400 minutes Electrodeposition time in 450 °C temperature setting[82]. Carbon deposit produce in these settings are 306,67 m^2g^{-1}, 558,10 m^2g^{-1}, 536,41 m^2g^{-1}, and 613,76 m^2g^{-1} respectively. From this research and specific setting, 170 minutes of Electrodeposition was suggested. Based on previous research, Electrodeposition time will affect the deposition rate differently. Therefore it is needed to optimize the Electrodeposition time to produce a better product.

2.5.4 Electrode and Catalyst

The electrode material used is an interesting variable because it has a significant role in the Electrodeposition method. There were at least two roles of the electrode in the Electrodeposition; the first was to deliver external potential into the system and the second one as a catalyst. An early research assessment was that a synthesis of CNT and CNF is not possible using electrolysis in molten lithium carbonate because of the reversible inclusion of carbon into the cathode[92]. However, later research shows that the carbon growth mechanism in the Ni and the zinc-initiated path will promote CNT growth[56].

In the major experiment research, the electrodes' role in the Electrodeposition method is the location of carbon growth or carbon collection, application of external potential, and catalyst. In the previous research, an electrode's effect on carbon growth is limited to producing graphite

in the nanoparticle form [79]. However, later research shows that a metal catalyst in the electrode results in an MWCNT product in the electrodeposition[56].

The utilization of catalysts in the Electrodeposition transforms these processes into advantages by affecting the types, sizes and shapes of the carbon growth. Therefore, it makes a catalyst to achieve the ultimate goal of CNT growth research, which is controlling the growth of CNT. Catalysts used are varied in the metal transition types of materials. The existence of metal transition, such as Ni, Cu, Fe, Co and Zn, is vital as nucleation points of CNT growth.

A study by M. Johnson uses Zn-coated steel and Monel cathode with Ir, Ni, and Ni-Cr anode. The Zn-coated steel cathode and Ir anode experiment resulted in no CNT growth. The Zn-coated steel with Ni anode produces CNT with a wavy profile. Monel cathode with Ni-Cr anode resulting in mixed straight and wavy CNT. The report suggests it is also an effect of pre-conditioning the Electrodeposition system, not only catalyst or electrode selection [20].

Research by Arcaro et al. using galvanized steel and Ni-Cr electrode, 1-4 hours of synthesis time, Li_2CO_3 electrolyte, 770 °C temperature and 0.5-2 A current. Ni-Cr cathode and galvanized steel anode resulted in an MWCNT outer diameter of 135 nm and 40 nm of inner diameter. However, the galvanized steel cathode and Ni-Cr anode result in the inner diameter of MWCNT 154 nm and 25 nm of inner diameter [57]. These different results indicate that changing the cathode and anode will produce different diameters of CNT.

The type of cathode used in Electrodeposition will affect the amount of carbon obtained on the cathode. Based on the research of Sigit et al. [93], it was revealed that the Pt-Pt electrode and the Pt-SS electrode had different amounts of sediment. More deposits were obtained at Pt-Pt electrodes with the same experimental method. Gunawan et Al. have also researched electrode material's effect on the quantity of sediment received [94]; they revealed that Cu-C, Zn-C, and CC electrodes could be used, but the efficiency and precipitation results are different. Hannula et al. [95] have researched CNT production by Electrodeposition. In this study, Ni and

Cu electrodes were used. However, no further research was carried out in this study regarding the effect of variations in electrode materials on the resulting carbon nanotube growth rate. The electrode material's impact on the formed CNT, Arcaro et al. [57] revealed that galvanic and Ni-Cr cathodes have almost the same outer and inner MWCNT diameter. However, the Ni-Cr cathode MWCNT has better wall quality and is smaller. The electrodes have significant roles in Electrodeposition, affecting the amount of end product of Electrodeposition. The effect of the electrode in the synthesis is complicated since it also acts as a catalyst. Therefore, it is necessary to understand further the relationship between the electrode used and the characteristics of carbon nanotubes (CNT) produced using the Electrodeposition method.

2.5.5 Carbon source

There are several choices of gases which previously been studied in Electrodeposition. However, the technology of greenhouse gas reduction is preferable; therefore, methane and carbon dioxide are the primary gasses of interest [96][97]. Two types of gas delivery systems are directly from absorbed atmospheric CO_2 or bubbled into molten salt. The bubbled method is superior, indicated by lowering potential in the system[98]. Concerning CO_2 flow rate, research in 2007 by Chen Mi et al. explained that the amount of CO_2 that enters affects the growth rate of carbon nanotubes in the carbon deposit process. The more CO_2 enters, the more carbon is formed, but CNT is rare.

Meanwhile, reducing the incoming CO_2 flow tends to develop more CNTs [99]. The reduction of CO_2 flow also means the carbon source in the system is also being reduced, limiting the Electrodeposition process. Therefore, further studies are needed to obtain optimal carbon source flow, which increases CNT growth.

Two primary greenhouse gasses are carbon dioxide and methane, which can be used in Electrodeposition. However, This research will be focused on CO_2. Several factors affect carbon nanotubes' growth rate in depositing carbon nanotubes. The main influence factors

were atmospheric CO_2 (carbon source), temperature, external potential, time, and electrode. An indication of the effect of CO_2 on the growth rate of carbon nanotubes is that using more CO_2 in the depositing process will produce more carbon deposits, but it does not guarantee that more CNT will be created. Chen mi et al. discussed this topic in a 2007 study, explaining that the amount of CO_2 that enters affects the carbon nanotube growth rate. The more CO_2 enters, the more carbon is formed (0-100 sccm CO_2 flowrate), but the CNT is rarely formed. Meanwhile, reducing the incoming CO_2 flow tends to develop more CNTs [99].

Previous research shows that Electrodeposition systems utilize CO_2 and convert it into carbon products. The carbon formed in the system can be produced by two processes which are direct and indirect. The direct process is a process without metal alkali, which is shown in Equations 2-4.

$CO_2 + 4e^- \rightarrow C + 2O^{2-}$ Equation 2

$CO_2 + O^{2-} \rightarrow {CO_3}^{2-}$ Equation 3

${CO_3}^{2-} + 4e^- \rightarrow C + 3O^{2-}$ Equation 4

The direct carbon capture process occurs with the presence of ${CO_3}^{2-}$ that changed into C and O ions. The indirect process involves metal alkali, which, in this case, is Li. This process is described in Equations 5-9.

$Li_2CO_3 \rightleftharpoons Li_2O + CO_2$ Equation 5

${CO_3}^{2-} + 2e^- \rightarrow {CO_2}^{2-} + O^{2-}$ Equation 6

${CO_2}^{2-} + 2e^- \rightarrow C + 2O^{2-}$ Equation 7

$Li^+ + e^- \rightarrow Li$ Equation 8

$2Li + Li_2CO_3 \rightarrow C + 3Li_2O$ Equation 9

Indirect carbon capture involves the presence of alkali metals. Li presence promotes carbon deposit from CO_2 by side product of Li_2O. This process is likely to occur because the value of E_M^o is more negative than E_C^o [80].

In general, CO_2 needed in the Electrodeposition is discussed in the study by J. Ren et al., which utilized ambient CO_2 directly from CO_2, which estimated CO_2 content is 0.04% or equal to 1.7 × 10^{-5} mol of tetravalent carbon per litre. The diffusion process of CO_2 in lithium carbonate depends on how much Li_2O is formed. Because the process is reversible, the faster the reaction process from lithium carbonate to $Li_2O + CO_2$ and CO_2, which is separated from lithium carbonate into carbon, the faster the diffusion process of CO_2 which is introduced from outside the system, meaning more carbon will be deposited in the process.

2.5.6 Electrolyte

In the Electrodeposition process, Gibbs's free energy can determine the ease of carbon deposit. E_m, and E_c values will determine the carbon deposit tendency in the calculation. The presence of alkali metal will promote indirect carbon capture, as discussed in the carbon source section. Several alkali metal options are Li, Na, and K. all of these alkali metals can promote this process.

Using Table 2 and comparing alkali metal, C and CO potential energy values, we can determine that the highest value of potential energy difference (E_m – E_c and E_m – E_{co}) is achieved by Li at 450-900 °C. This value means the Li-based electrolyte is more favourable to use in the carbon capture system than Na and K-based electrolytes [85].

Adding a substance to the primary electrolyte might affect the Electrodeposition product. For example, the addition of $LiBO_2$ with less than 10% of Li_2CO_3 could improve the quality of the CNT product. J.Ren et al. [56] used 50 gr Li_2CO_3 with 1.5, 3, and 5 gr $LiBO_2$. This addition resulted in a 200-500 nm CNT product alongside 10% of amorph carbon. The addition of $LiBO_2$ of more than 10% shows the inconsistency of carbon products.

2.6 Molecular dynamics simulation of the Electrodeposition process

Molecular dynamics (MD) is a method for analyzing the movement of atoms and molecules by solving the classical equation of motion. The law that presents how particles interact in the system is needed for this equation numerically. Although the perfect law generally does not exist, we can use the force field or constructed model approximations. These approximations will be varied in accuracy, and realism depends on the levels of theory and source used.

The molecular dynamics (MD) approach is a method to investigate an atom's location in space. In this approach, a single-point model is substituted with a dynamic model where the nucleus system is adjusted with a motion equation. Simulation of motion equations applied using Newtonian dynamics classic equation [100]. This simulation describes natural motion from a molecular structure driven by energy procedure, so atomic movement and interaction are possible. Molecular dynamics, in general, is used in the system with nanometer and femtosecond scales. However, MD can be used on a bigger scale using the MD acceleration method [101], [102]. The illustration of the MD position in the simulation selection can be analyzed in Figure 15.

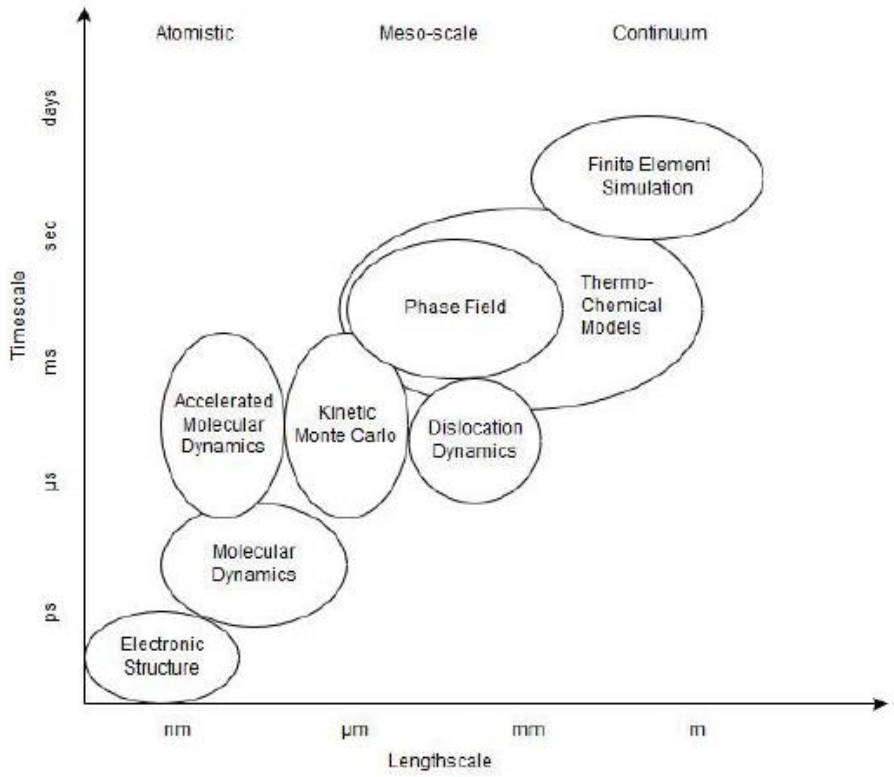

Figure 15 Simulation selection based on length scale and time scale[103]

Using the molecular dynamic method to simulate carbon Nano-tube growth is convenient because molecular dynamics can be considered adequate to simulate material on the nanoscale, as described in picture 12. The Finite element method will be suitable if the simulation is on the macro scale. While if the simulation is on the Pico scale, the quantum mechanics-based method will fit. In addition, the molecular dynamics time scale can stretch by accelerating it.

Many approaches were used to perform Molecular dynamics, but the essential requirement is that we provide initial values such as initial velocity and position for every atom in the system. In MD, the system's total energy is the sum of the kinetics and potential energy. While kinetics energy is affected by the system's temperature, the acceleration given to each atom is estimated from the forces it accepts, regulated by the force field[104].

The interest in MD was driven by its comprehensive utilities and convenience. one of them was its graphic representation of moving atoms and how they interact, which also gives benefit in detailing how distinct atoms act. Another benefit is the ease of controlling and configuring the environment, such as temperature and pressure, compared to the experiment counterpart.

In most cases, some assumptions need to be addressed during MD simulation. The first one is atom's behaviour is similar to a rigid body and obeys Newton's law. In general conditions, the quantum effect on atomic dynamics is negligible except for light atoms such as liquid helium. The second assumption is related to modelling how particles interact with each other and how specific or detailed the interaction would be. In this assumption, it is required to capture essential features without negatively impacting the simulation's productivity [105].

Fabrication of CNT is expensive, and optimisation using an experiments approach can be a disadvantage in terms of effectiveness, cost and general performance. Therefore simulation approach can be used as an alternative. Two simulation techniques that are commonly used are Ab Initio and Molecular Dynamics. However, the Ab Initio approaches are CPU intensive. Therefore, Molecular Dynamics is more favourable.

Molecular dynamics tools can vary depending on the simulation object, such as Abalone (Protein and DNA) and CHARMM (molecular mechanics). There were two types of force fields in general: reactive and non-reactive. The main difference between these force fields is in the Reaxff bond determined by bond order calculation which is the product from interatomic distance that updated each MD step. ReaxFF is force filed depending on bond order that provides accurate information on bonding and breaking the bond.

2.7 Molecular dynamics state-of-the-art and limitation

To perform MD, the embedded atom method (EAM) is a popular choice for the energy functional [106] because it has been shown to predict relevant dynamics for a system, including hydrogen adsorption and dissociation onto nickel [107][108]. This MD-EAM simulation is an up-and-coming method that could be adapted to the Electrodeposition simulation.

However, some authors report that MD-EAM has a downside in that it is an expensive simulation. This problem is because although parallel large-scale MD codes [48] and a large number of parallel processors run over several days, simulations can only resolve time scales on the order of nanoseconds. Even accelerated MD methods such as hyper dynamics [102] are limited to small systems. To solve this problem and increase the performance of simulation, T. Treeratanaphitak et al. [109] successfully performed the kinetic Monte Carlo methodology, which uses the embedded atom method potential and includes collective diffusion mechanisms (KMC-EAM), resulting in an accurate representation of the Electrodeposition process in relevant length (microns) and time (seconds) scales. This development of the KMC-EAM technique is also very suitable for simulating the process of carbon Electrodeposition, and it is an excellent method to run this simulation using both methods to set a solid baseline of simulation.

One research that successfully performs MD simulation in the process of single-wall carbon nanotube growth is Y. Shibuta et al. [110]. This simulation is robust research which performs nickel as a metal catalyst and randomly distributed carbon-source molecules as a carbon source. Figure 16 describes the initial condition of the simulation; three types of face-centred nickel crystals are used, which are Ni256, Ni108 and Ni32. Some of the results of the simulation using Ni108 are described in Figure 17. Between 2 ns and 130 ns, the structure of the hexagonal carbon network was growing. Some conclusions that can be achieved in this study are the effect of metal cluster size, vapour density, and the step of the growth of the single-wall nanotube. Based on other research, this simulation can be improved.

It is possible to use KMC-EAM to improve the time scale [109]. This improvement could be significant because if the timescale is improved, it might give more information about the amount of energy required for CNT growth. Another possible improvement was maximising the graphics processing unit (GPU) to speed up the simulation. The previous author reports that applying their algorithm design could increase simulation performance by making the calculation 700 times faster than conventional implementation [101]. This algorithm could help perform the simulation of carbon Electrodeposition. Unlike previous research, which performs two types of molecules (nickel and carbon), several molecules must be considered to perform this simulation. Ni, Li, CO_2 and CO3 will be calculated, and this molecule addition will add more computation requirements. The improved performance might promise a solution to the requirements problem.

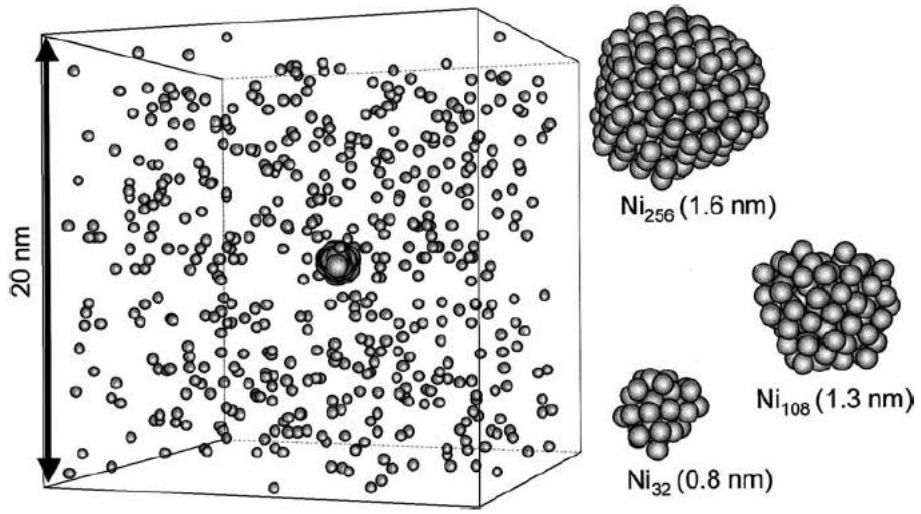

Figure 16 Initial condition of growth simulation [110]

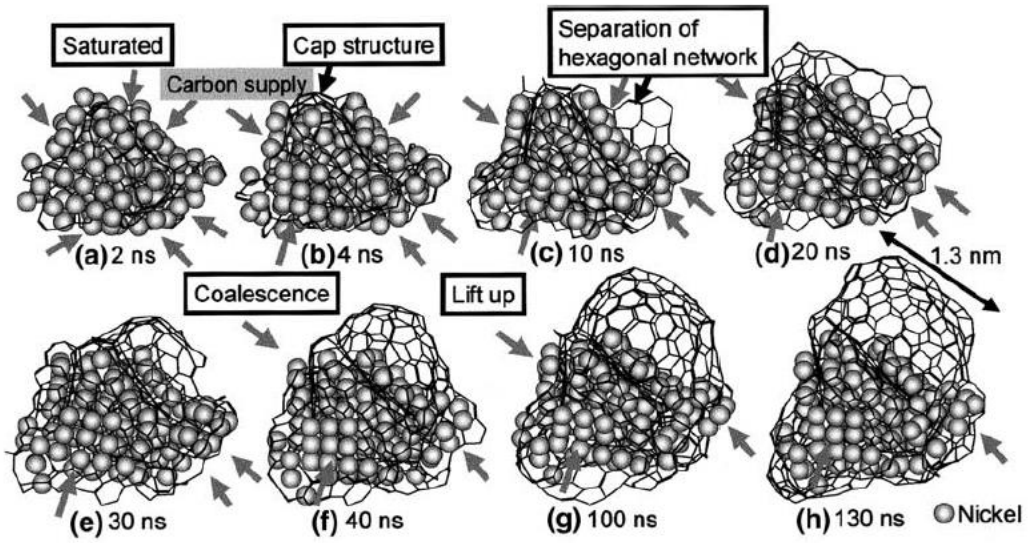

Figure 17 metal-catalysed growth process [110]

Despite the possibilities of simulation process improvement, some counterproductive points might occur. The first point is that the condition of the simulation may not be able to imitate the experiment's condition entirely. For example, the metal catalyst shape in the simulation is a perfect sphere [110]. In the experiment, the shape of this metal catalyst might be varied. This point needs to be investigated more to determine how it might affect the accuracy of the simulation. The second point is that the time scale resulting from MD simulation might not contain enough information needed to optimise the synthesis process. Although using KMC and GPU optimisation, the time scale from MD simulation is still a few seconds. In actual synthesis process will take at least 15 minutes.

The scale issue is the most obvious, with a few nanoseconds scales. Slow diffusion with many chemical and physical processes happened, resulting in many order magnitudes that may need another method to help solve. Energy and force calculation is the prime source of time scale limitation. Another method was in the work progress besides GPU acceleration and parallel calculation to solve this limitation. One of them is using custom design neural network prediction. Feeding a neural network with enough data obtained from simulation results extends the length of time scale accessible[111].

2.8 Conclusions

The need for a new approach to CNT production is justified in the literature review. Comparing the Electrodeposition method with well-established methods shows that Electrodeposition has its value to explore. Electrodeposition is an inexpensive method due to an uncomplicated setup. CO_2 as raw material has abundant availability. The Electrodeposition method can produce MWCNT using a relatively low-temperature set-up and large-scale possibility.

However, there are some disadvantages and challenges to the Electrodeposition method. One of the disadvantages is that SWCNT production will sacrifice the simple set-up with the addition of catalyst preparation. The challenge of this method is the consistency of CNT production. Some of the research found the CNT, while others reported the absence. Impartial variable studies are also the central knowledge gap of the Electrodeposition method. Comparing studies is difficult because researchers use different variable values resulting in different outcomes. Furthermore, despite the challenges, the opportunity is the possibility of optimising the method parameters to produce CNT with its advantages.

Chapter 3 – Molecular dynamics simulation study

3.1 Method

In the MD, there are four main components described in Figure 18. MD calculation starts at atom position determination. These atoms' positions are used in the interatomic energy calculation. There are many methods to calculate interatomic energy. This calculation is divided into two main categories: reactive and non-reactive interatomic energy. These energy calculations are EAM, MEAM, and ReaxFF [109], [112], [113]. After energy is calculated, acceleration and a new position of atoms can be determined. This process will be repeated each time until the desired step is reached.

The molecular dynamics simulation assessed five factors: temperature, external potential, carbon atom, step, and cathode materials. Temperature is applied as an argument for the Fix

NVT command (Appendix 1). Four temperatures are used in the simulation, ranging from 723 to 873 ºC. The 723ºC was used since its realistic value of Li_2CO_3 melting temperature, and a higher temperature was used to determine the behaviour of carbon bond in temperature change. The external potential is applied using a Fix Echemdid command. Echemdid is LAMMPS external package to apply external potential[114]. The carbon atom number is determined in the simulation cell creation. The goal is to understand the effect of lower or higher carbon atoms in the system on carbon bonds created during simulation. The carbon atom is used instead of CO_2 because the force field cannot yet describe CO_2 separation and creation. However, it is sufficient to understand the carbon atom's behaviour in the system[110]. The step represents the timescale of the simulation and is applied by the Run command. The cathode used in the simulation used is Ni and Cu. These two materials are used since they are the standard material used as an electrode in Electrodeposition[82]. Other electrode materials, such as Zn and Cr, cannot be simulated since the force field for these materials is non-existent yet. The electrode type used is created in the simulation cell creation.

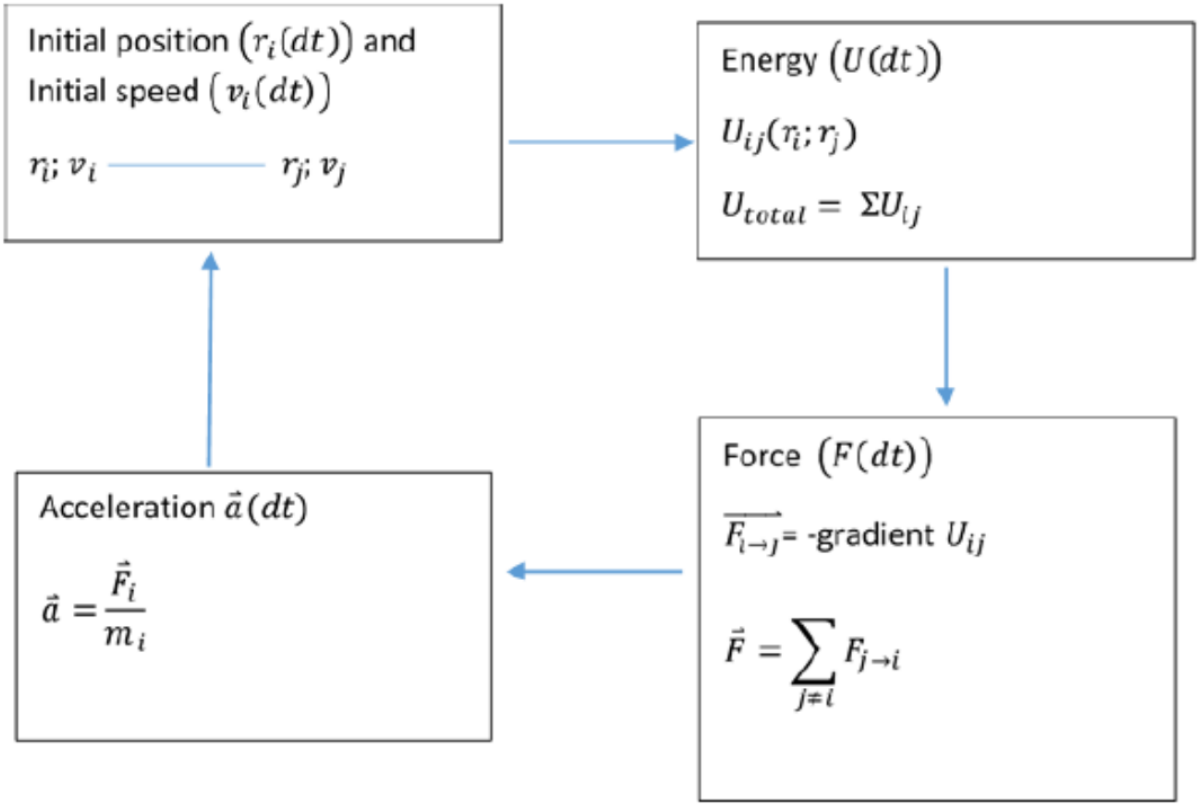

Figure 18 MD Calculation component

The Electrodeposition molecular dynamics simulation model utilises LAMMPS [106] as a major source code. However, as discussed in this section, several additional tools were used to support the simulation. Preparation of LAMMPS made with additional package such as Rigid, Reaxff [113], [115], Echemdid [116]. After Analyzing and testing all the packages compiling an executable file with all packages is necessary.

A simulation cell using LAMMPS consists of 3 regions: anode, cathode, and space between them where carbon atoms will generate. Figure 19 is an example of this simulation cell. Three atom materials in this simulation are Ni, Cu and C, with atom weights of 58.69 u, 63.55 u, and 12.011 u, respectively. Ni is used as an anode in all simulations with Face Centered Cubic (FCC) structure. The cathodes in the simulation are Ni and Cu, also in FCC structures. Carbon atoms were generated randomly in the space between the anode and cathode.

The energy minimization was conducted using the built-in LAMMPS command. These commands should be used under the correct iteration and evaluation number. After the minimization process, an annealing process was completed above the recrystallization temperature. The high temperature was used to ensure that the atoms did not collide. NVT calculation was held on various variables. The energy minimization, annealing and NVT were performed using the Reaxff force field [117]. Analyzing structure in this study using Ovito software [118]. Variables used in the simulation are temperature, external potential, amount of carbon atoms in the simulation and running step.

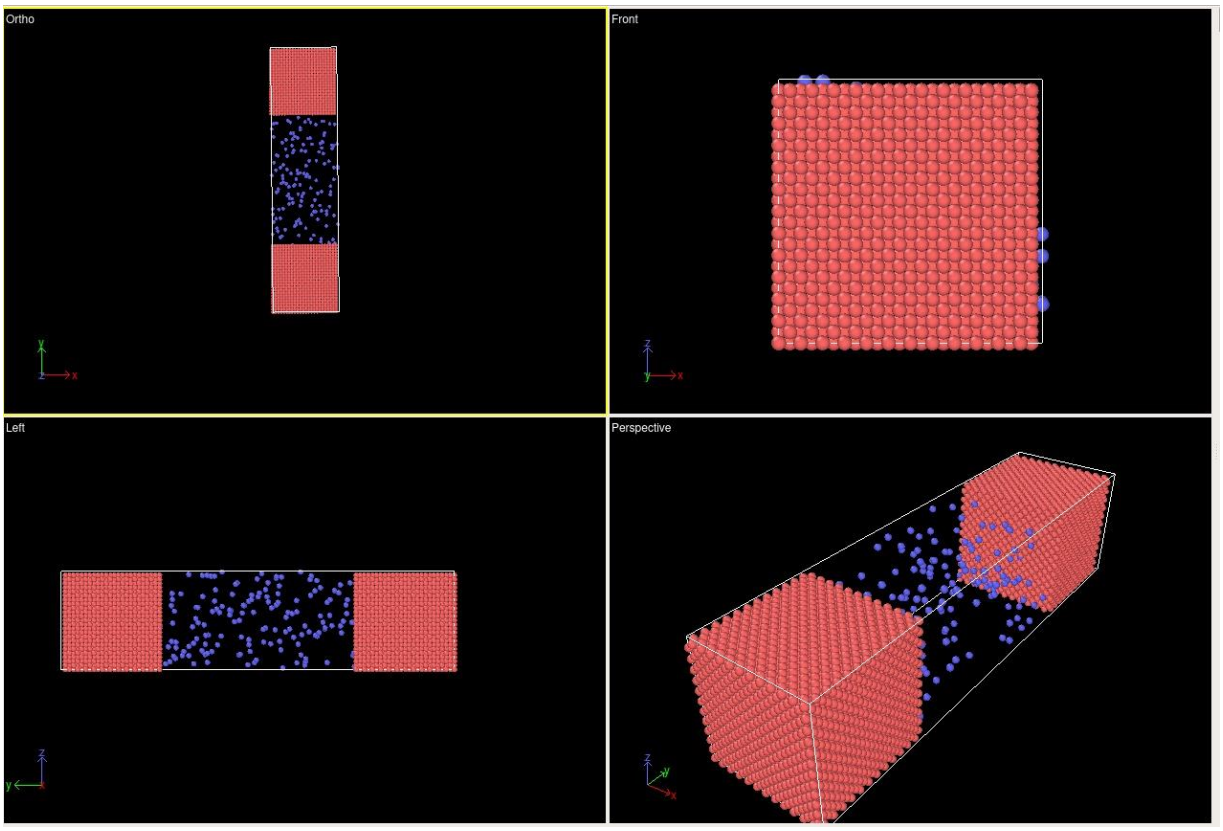

Figure 19 Simulation cell design

One of the Lammps input scripts developed for this simulation can be found in Appendix 1, while the LAMMPS simulation workflow is described in Figures 21-22. The input script file contains the units that are used, the atom style, the boundary of the cell, the instruction of the task to perform, the parameters, the force field or empirical potential. LAMMPS provide several

options for each variable and input file parameter, and many developers and users expand the option to each case that might be more suitable. The first input is the unit of the simulation unit that can be used in the simulation and could be varied, such as real, metal, and si. However, this simulation used a real unit, which means:

- energy = Kcal/mole
- velocity = Angstroms/femtosecond
- force = Kcal/mole-Angstrom
- pressure = atmospheres
- dynamic viscosity = Poise
- charge = multiple of electron charge (1.0 is a proton)
- dipole = charge*Angstroms
- electric field = volts/Angstrom
- density = gram/cm^{dim}
- mass = grams/mole
- distance = Angstroms
- time = femtoseconds
- torque = Kcal/mole
- temperature = Kelvin

The second input script is the atom style. The choice of atom style affects what properties are stored by each atom. This simulation considers both molecule's form and charge quantity; therefore, full atom style is used.

The third condition that needs to be specified is the boundary of the simulation system. in LAMMPS, four boundary options can typically be used: periodic, non-periodic-fixed, non-periodic-shrink-wrapped, and non-periodic-shrink-wrapped with minimum value. This simulation uses periodic in x and y directions and non-periodic shrink-wrapped in the z-direction. This condition means that an atom can always appear in the cell even though it passes through the x and y directions. However, if atoms pass through the boundary in the z-direction, the boundary will adjust as the atom moves and not move from one side to the other side of the box. The purpose of z boundary adjustment is to make the anode atom not interact with the cathode atom and vice versa.

Several of the following input scripts are straightforward. These input scripts are called data files, grouping atoms into a particular group for easier access and determining the time step. The smaller number of time steps will increase the accuracy of the simulation. The next step is to input the interatomic potential by calling pair style potential and the pair coefficient potential files.

The next step is to give an instruction script for calculating and displaying thermodynamics information on the time step. The thermodynamic components are potential, kinetic, temperature and Vander Waal pairwise energy. Instructing to display the result of every desired step is also essential in this step.

After setting the output calculation and display, the electrochemical potential is applied. Applying this external electrochemical potential requires some adjustment using Echemdid [116]. Echemdid is an external user package that can be implemented in LAMMPS based on the reax/c package.

The further action of this simulation is the energy minimisation process. This process also uses reax/c atomic interaction because it can apply a reactive force field, not only the attractive and repulsive force field. Minimisation is an essential process to prepare all the atoms as in an actual experiment because it is the nature of an atom to be in its lowest energy level. After the atom is prepared, the electronegativity in the electrode area is applied.

The last step before running the simulation is writing a fix command about the thermodynamic ensemble and what kind of Echemdid will be applied in this simulation. Figure 20 can be used as a general rule to make this command easier to understand.

N	μ
V	P
E	T

Figure 20 General rule fix command (N = Number of atom; μ = Chemical potential; V = Volume; P= Pressure; E= Energy; T= Temperature)

Six variables can be used to apply this command: the number of atoms; chemical potential, volume; pressure; energy; and temperature. However, one variable is not working with another variable. In Figure 20, the variable in the same horizontal line can not be used together. When the number of an atom is fixed, the chemical potential cannot be fixed simultaneously. A similar condition is applied for two other pairs: volume-pressure and energy-temperature. When volume is static, pressure cannot be fixed.

In this simulation fix, the NVT command is used. These commands will perform time integration on Nose-Hoover style non-Hamiltonian equations of motion [119] which are designed to generate positions and velocities sampled from the canonical (NVT)*.

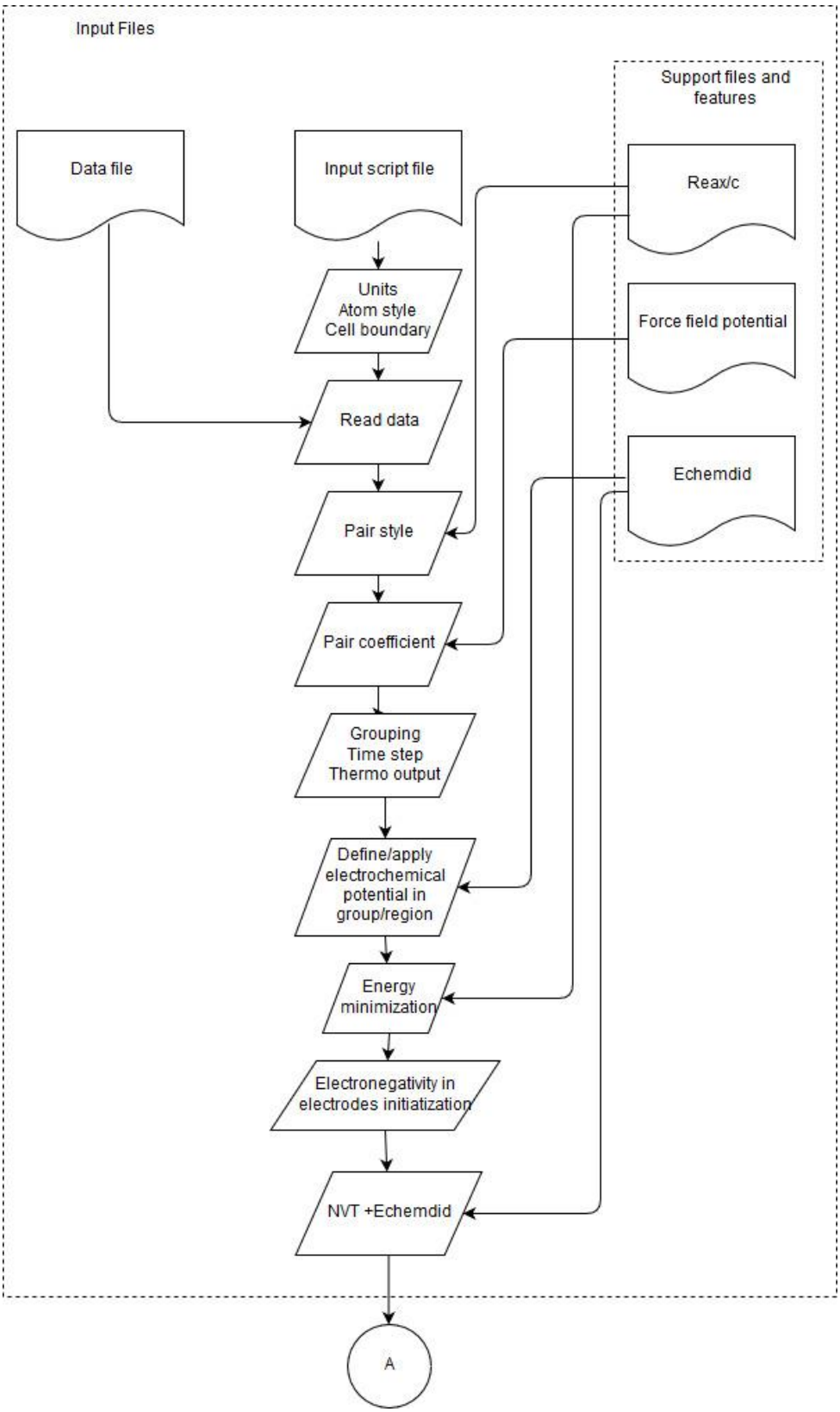

Figure 21 LAMMPS workflow

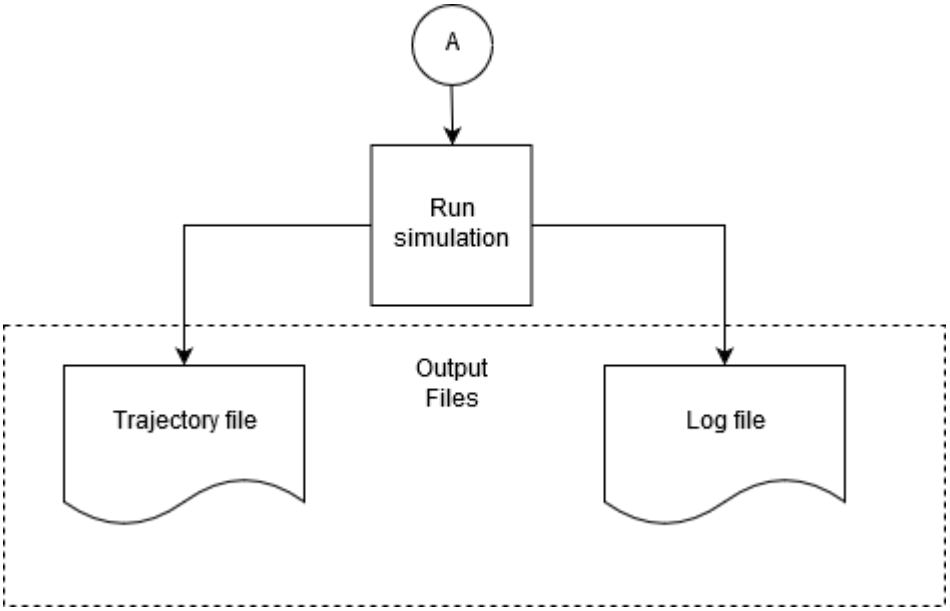

Figure 22 LAMMPS workflow continued

3.2 Support files and features

3.2.1 Pair style – reax/c

In molecular dynamics, the pair style is used to describe the relation of each atom to another atom. The reax/c pair style is used here. Reax/c was originally standalone C code but is now also integrated into LAMMPS. The primary purpose of reax/c is to compute the total energy generated by chemical bonding based on ReaxFF. ReaxFF uses empirical interatomic potential, which can be called distance-dependent bond order function. The total potential energy of the system is calculated in equation 10 and described in Figure 23.

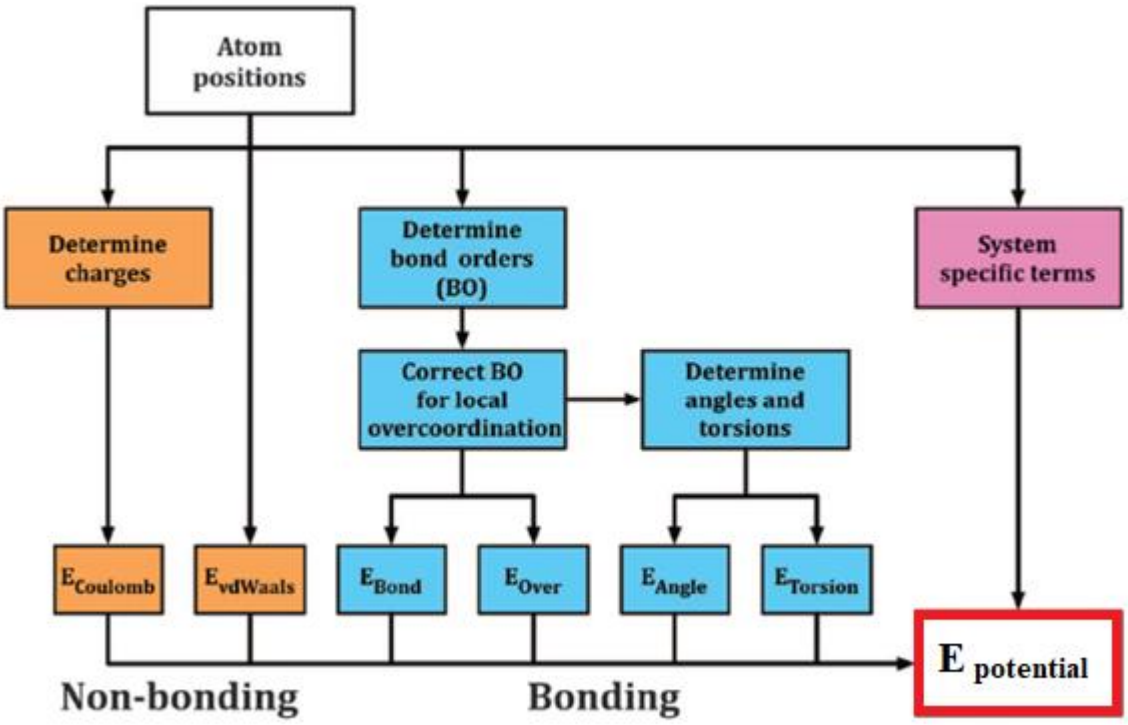

Figure 23 Total energy potential components of ReaxFF interatomic [120]

$$E_{potential} = E_{bond} + E_{over} + E_{tors} + E_{angle} + E_{vdWaals} + E_{Coulomb} + E_{specific} \quad \text{(Equation 10)}$$

$E_{potential}$ is a total energy potential related to the distance of an atom to other atoms. E_{bond} is bond energy based on bond order between a pair of the atom from an interatomic distance. E_{angle} and E_{tors} are the energies from valence angle strain and torsion angle strain. E_{over} is an energy penalty preventing the over-coordination of atoms. $E_{Coulomb}$ and $E_{vdWaals}$ are attractive and repulsive contributions calculated between all atoms, despite connectivity and bond order. $E_{specific}$ represents system-specific of interest, such as lone-pair, conjugation, and other corrections [120].

3.2.2 Force field potential

Force field potential is used to specify the pairwise force field by providing coefficients that are related to pair style. There are two ways to do this. The first is writing explicitly in the input

script, and the second is by calling the force field potential file. The second method is used in this research because of the same reason as using call data in the data file. It is much easier to manage the input script this way. The force field potential file contains all the C, Ni, and Cu atoms coefficients, such as the over and under coordinator coefficient, double and triple bond stabilisation, and valency angle coefficient.

3.2.3 Echemdid

Echemdid is external user package in LAMMPS that integrated to reax/c [116], [121]. The main purpose of the Echemdid is to solve how to apply external potential in the electrode by allowing switching constant electronegativity to dynamical electronegativity. The first thing Echemdid calculated is the electrostatic energy produced by electronegativity equalization in ReaxFF. Then by applying external electric external potential, the relative energy of the electron in the applied region will be changed. Then echemdid will calculate the atom's loss and gain during the electrochemical process based on the energy change.

3.2.4 Output files and post-processing

This simulation will generate two output files: trajectory file and log file. The trajectory file contains the movement of all atoms during the process, and the log file contains all of the thermodynamics calculation results. The trajectory files can be visualized using molecular dynamics visualisation software. A log file can be extracted into the desired graph to analyze the value pattern of the calculation result. Ovito software was also used in this research to extract the carbon-carbon bond created.

3.3 Molecular Dynamics simulation result

The molecular dynamics simulation assessed five factors: temperature, external potential, carbon atom, step, and cathode materials. The exact value of levels on each factor is given in Table 3.

Table 3 Description of factors and levels for C-C Bond.

Level	Temperature (°C)	External potential (V)	Carbon Atom	Step (k)	Cathode
1	723	3	200	50	Ni
2	773	4	300	75	Cu
3	823	5	400	100	
4	873	6	500	125	

The next step is designing the experiment using the Taguchi method. For five factors at four levels, the L16 orthogonal array was selected and is given in Table 4. After the simulation based on the orthogonal arrays are complete, two statistical tools are used: signal-to-noise ratios (SNR) and analysis of variance (ANOVA). There are three options for the SNR based on the user's need: nominal is the best, smaller the better, and larger the better. In this case, the larger, the better the suitable one. The equation to calculate the SNR is given in equation 11.

$$\frac{S}{N} = 10 \times Log10 \left(\sum \left(\frac{\frac{1}{Y^2}}{n} \right) \right) \qquad \text{Equation 11}$$

Where Y are responses for the given factor level combination and n si the number of responses in the factor level combination.

The signal-to-noise ratios (SNR) were used to distinguish the output signal from unwanted data (noise) to maximise the response. A Taguchi-designed manipulation of noise factors to force variability to occur and, from the results, identify optimal control factor settings that make the process or product robust or resistant to variation from the noise factors[122]. ANOVA was used to distinguish the significance of the different result groups[123].

Information on each factor's relative importance can be plotted from the SNR values to identify each factor's optimum levels. The ANOVA is conducted using SNR results to provide information on each factor's contribution to maximising the carbon-carbon bond.

Table 4 Orthogonal array illustrating the configuration of the simulation.

Run	Temperature (°C)	External potential (V)	Carbon Atom	Step (k)	Cathode
1	723	3	200	50	Ni
2	723	4	300	75	Ni
3	723	5	400	100	Cu
4	723	6	500	125	Cu
5	773	3	300	100	Cu
6	773	4	200	125	Cu
7	773	5	500	50	Ni
8	773	6	400	75	Ni
9	823	3	400	125	Ni
10	823	4	500	100	Ni
11	823	5	200	75	Cu
12	823	6	300	50	Cu
13	873	3	500	75	Cu
14	873	4	400	50	Cu
15	873	5	300	125	Ni
16	873	6	200	100	Ni

Table 5 C-C Bond for each experiment.

Run	∑ C-C Bond
1	55.91
2	98.40
3	112.43
4	183.14
5	72.87
6	68.02
7	289.55
8	242.49
9	175.91
10	283.17
11	89.01
12	121.37
13	182.67
14	140.33
15	208.36
16	187.96

The C-C bond result for each run is presented in Table 5. The SNR values were used to identify which factor levels maximise the CNT C-C bond. Table 6 shows the response of SNR. With the

higher is better SNR higher value in Table 6 will maximise the C-C bond. The optimum value is: carbon atom = 500; Temperature = 873°C; external potential = 7V; Cathode = Ni and; Step =1 25 k.

Table 6 Response table for the signal to noise ratio (SNR) larger is better.

Level	Temperature	External Potential	Carbon Atom	Step	Cathode
1	40.27	40.58	39.02	42.20	41.13
2	42.71	42.12	41.29	42.94	44.69
3	43.65	43.9	44.14	43.20	
4	45.01	45.03	47.19	43.30	
Delta	4.74	4.44	8.17	1.10	3.56
Rank	2	3	1	5	4

Delta value from Table 6 presents a ranking of the factors based on the C-C bond's importance when ranged on five levels. The sequence follows carbon atom > temperature > external potential > cathode > step. The optimum levels value on each factor is presented graphicly in Figure 24.

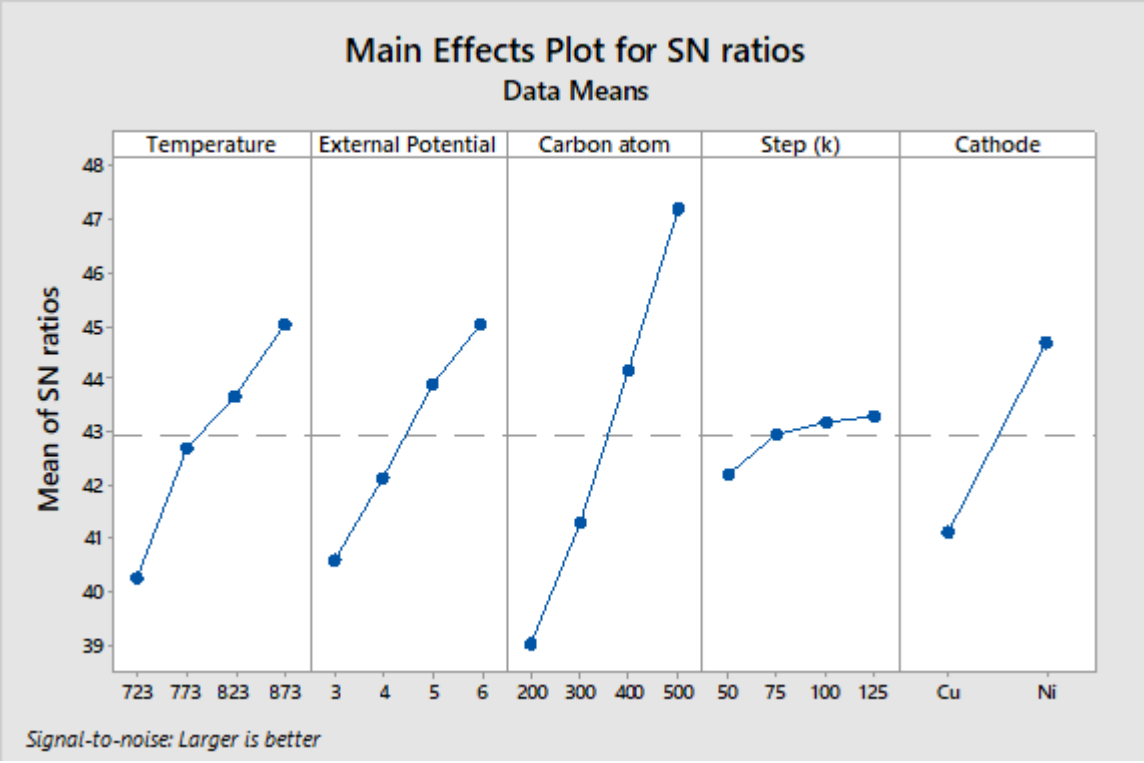

Figure 24 Main Effects Plot for SN Ratio

A confidence level of 95% or the significance level of 5% was used in ANOVA using the SNR value from Table 6. The ANOVA p-value results in Table 7 present the statistical significance of the factors in the Electrodeposition method. A p-value of less than 0.05 considered rejecting H_0, which means that the factors significantly affect the response value. All of the factors have a p-value less than 0.05, which means that all the factors statistically significantly impact the C-C bond except step factors. the sequence of these value carbon atom > temperature > external potential > cathode > step.

Figure 25 describes the contributor percentage of each factor in maximising the Electrodeposition growth rate Graphically. This result is in line with the sequence of the p-value, in which the more significant contributors are a carbon atom and cathode with 50,06% and 24,66%, respectively, followed by temperature, external potential and step.

Table 7 ANOVA table for the mean SNR.

Factor	Degree of Freedom (DF)	Sum of Square (SS)	Contribution (%)	Mean of squares (MS)	F-Value	*p*-Value
Temperature	3	10950.6	13.21%	10950.6	3650.2	0.024
External Potential	3	9440.2	11.39%	9440.2	34.64	0.028
Carbon Atom	3	41498.6	50.06%	41498.6	152.27	0.007
Step	3	384.1	0.46%	384.1	1.41	0.441
Cathode	1	20442.2	24.66%	20442.2	20442.2	0.004
Error	2	181.7	0.22%	181.7	90.8	
Total	15	82897.4	100.00%			

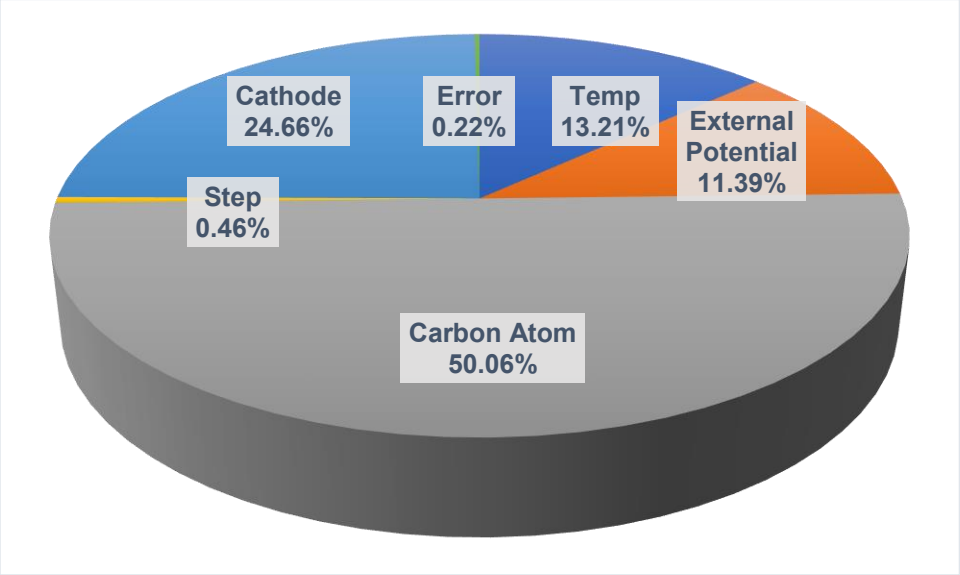

Figure 25 Contribution of variables on ANOVA

The main effects plot for the means of each factor on the C-C bond is presented in Figure 26. The carbon atom was seen to increase the C-C bond. Contradictory to the carbon atom and cathode, the step seems to have the lowest effect on the C-C bond.

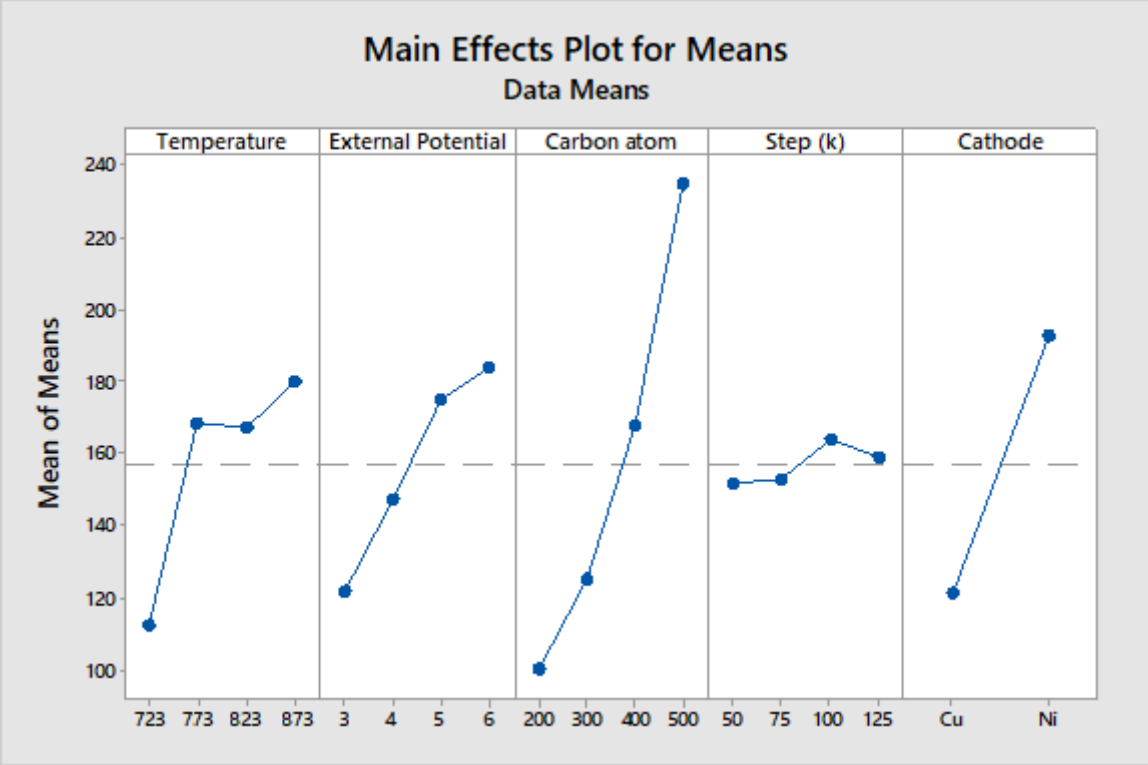

Figure 26 Main Effects Plot for Means

The interaction plot in Figure 27 aims to assess the interaction between factors to interpret the main effects—the interaction plot for five factors connected with the line. When the line is parallel indicates the interaction is small, and the more non-parallel the line, the greater the interaction.

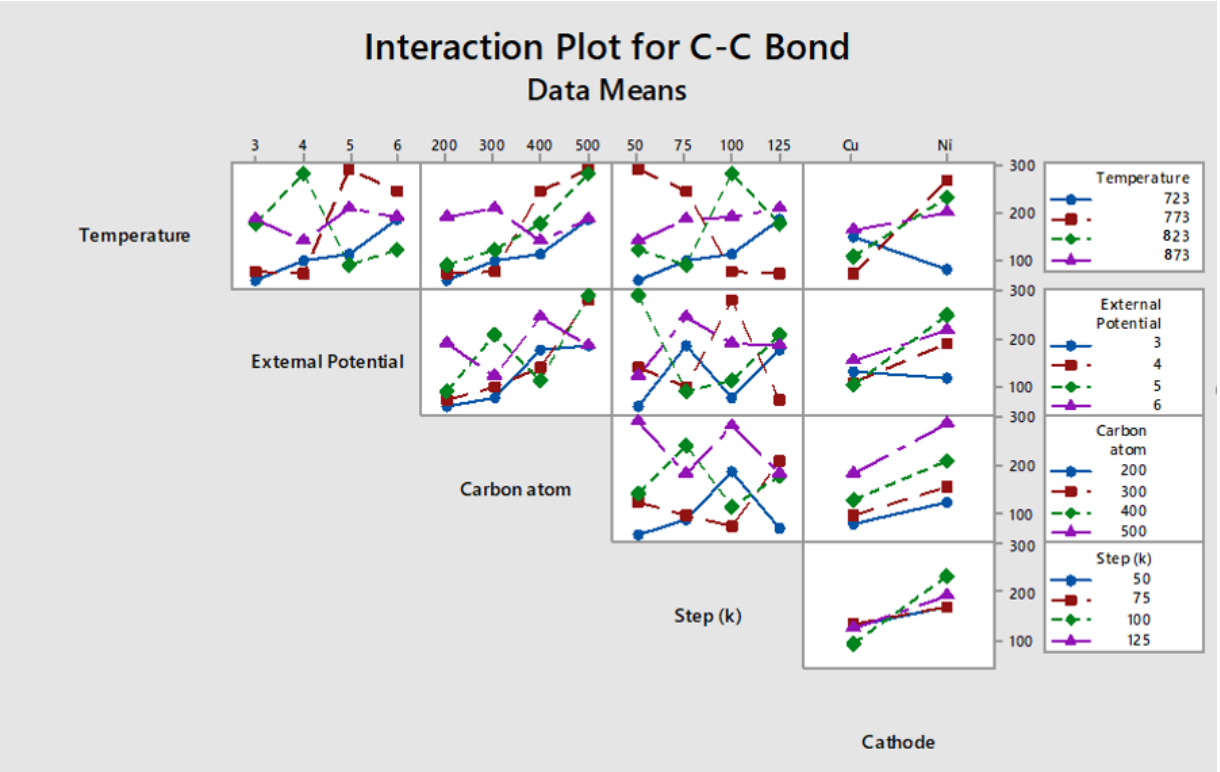

Figure 27 Interaction Plot for C-C Bond

3.4 Discussion and validation study

The molecular dynamics simulation show carbon-to-carbon (C-C) bonds created in the simulation. The main objectives are to understand the basics of parameters behaviour. The result is higher value parameter will promote more carbon-carbon bonds.

Figure 25 shows the contribution of variables. The highest contribution is by carbon atom number. This was expected since the calculation of density of molecules (800 ºC, 10 Torr) in previous research in normal conditions is roughly 0.7 molecules in 20 nm cubes. In this

simulation, the highest carbon atom is 500 carbon, roughly 200 times higher than the usual condition[110].

The interaction plot's notable aspect is the carbon atom variable and cathode relation. In these interactions, introducing more carbon atoms will consistently increase the number of C-C bonds. Using Ni cathode also follows these patterns with minimum interaction with carbon atom quantity variable. This evidence suggests that using Ni as a cathode and a higher quantity of atom carbon will increase the carbon-to-carbon bond without affecting each other. The next notable feature in the interaction plot is that increasing carbon quantity in the system reduces the C-C bond number when using the highest temperature (873 °C), which is the opposite when using a lower temperature. Although changing into the higher value of the other variables (external potentials and simulation step) does not decrease the C-C bond, the changes are not as significant at lower temperatures.

The simulation pattern shows that increasing temperature, external potential, carbon atom amount, step (time in femtosecond) and cathode material also increase the number of C-C bonds. The increase of the C-C bond can be related to the total energy in the system. The total energy of the MD is calculated by $kinetic\ energy + potential\ energy$. $\frac{1}{2}mv^2$ is used to compute kinetic energy, where v and m are the velocity and mass of the particle. In thermodynamics terms, kinetic energy is also calculated as $\frac{1}{2}k_BT$, where k_B and T are The Boltzmann constant and temperature. From the relation of $\frac{1}{2}mv^2 = \frac{1}{2}k_BT$, when the particle mass is the same increasing temperature will also increase kinetic energy, followed by total energy in the MD system and velocity of the particle. Especially in the temperature increase case, the velocity of carbon particles will be higher, and it easier to collide with each other and create a bond.

Higher external voltage also increases the potential energy resulting in higher total energy in the simulation system. Higher potential energy allows the particles to create more C-C bonds[124][125]. More carbon atom appearance also indicates more C-C creation; this was to

be expected since it is reasonable to create more C-C bonds if more carbon atoms are available—furthermore, more atoms in the system cause higher total energy, promoting C-C bond creation.

Although the cathode material does not directly affect the total energy, it also contributes to the C-C bond created; this can be the effect of the electronegativity of the cathode atoms. The last parameters are the step that represents of time of the simulation in a femtosecond. Time parameters seem to have little effect on the C-C bond; this justifies that more extended time simulation might not be needed.

3.5 Conclusion

In summary, the base expectation of Electrodeposition variables was created in this finding. Molecular dynamics simulation can predict the carbon-to-carbon bond created during Electrodeposition. The parameter effect is also related to the total energy generated in the system. Higher potential energy results in more carbon-to-carbon bonds created. Higher temperature results in higher kinetic energy followed by the system's total energy; therefore, more carbon-to-carbon bonds are created—higher external voltage affecting the rise of potential energy in the system.

More carbon atom appearance is expected to create more C-C bonds. The atom's electronegativity affects the system's potential energy; therefore, using Ni as a cathode will be expected to create more carbon-to-carbon bonds than Cu. Time parameters seem to have little effect on the C-C bond; this justifies that more extended time simulation might not be needed.

Chapter 4 – Experiment study of Electrodeposition

4.1 Method, setup and materials

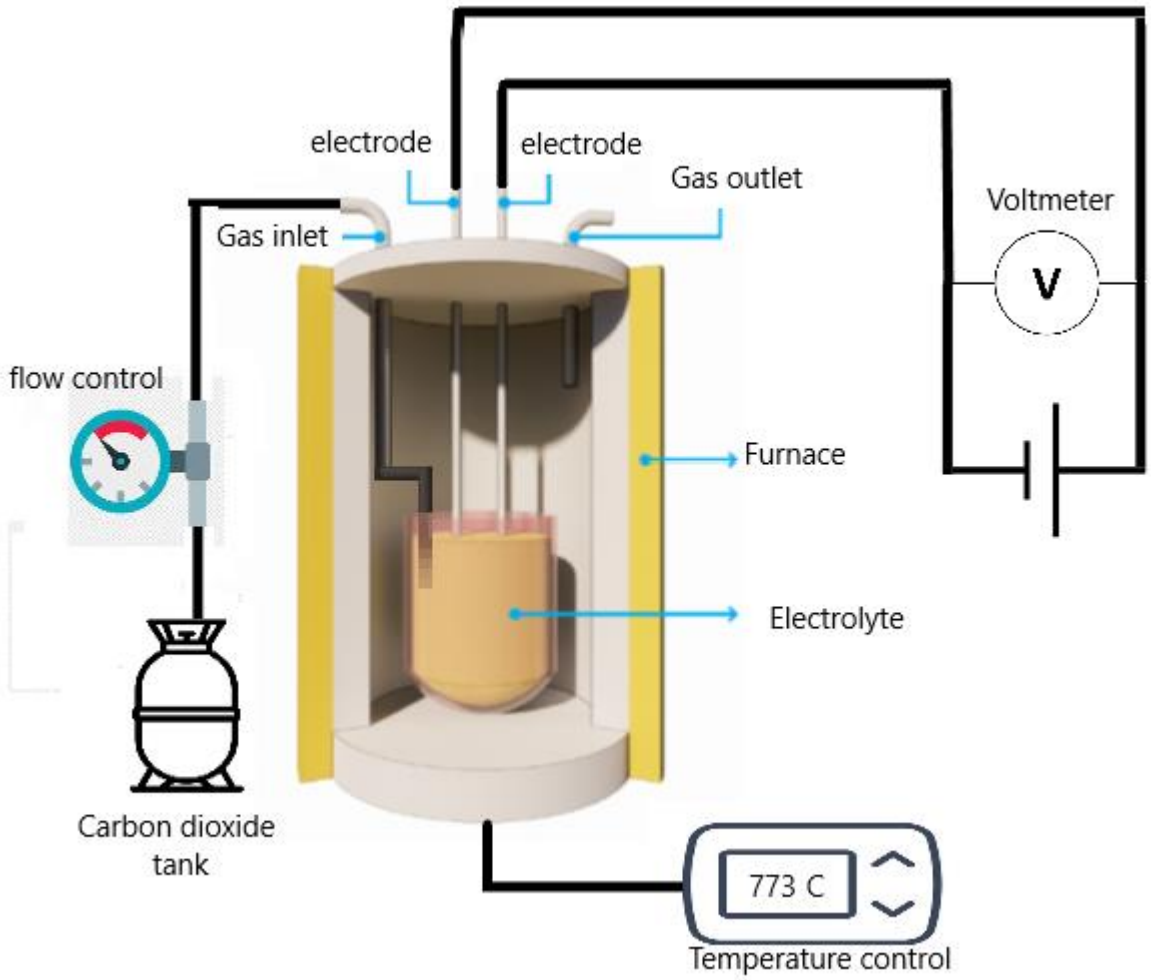

Figure 28 Electrodeposition diagram

The Electrodeposition setup diagram can be seen in Figure 28. The first step to conducting Electrodeposition is heating 50 gr lithium Li_2CO_3 (99% purity, Merck 105680) in the alumina crucible placed in the furnace. Lithium was slowly heated until it reached 823 °C and held this temperature for 4 hours; then, the temperature was gradually reduced or raised to the targeted temperature. The holding process is carried out at a higher temperature than the melting point

of Li_2CO_3, which is 723°C, to ensure that the lithium carbonate is wholly melted and homogeneous. The electrolyte was replaced with a new one, each Electrodeposition complete. On some occasions, carbon debris was found in the electrolyte, especially in longer synthesis time, high temperature, and high external potential; therefore, electrolyte replacement is needed.

The electrode used in this Electrodeposition method is metal wires of five varieties. Nickel as the anode uses 0.4 mm diameter (Merck 99.99% purity). Nickel cathode also uses the same material as the anode, while other cathode uses stainless steel (Fe 69.5%, Cr 22% Ni 5.5% Mo 3%), Nichrome (Ni 80%, Cr 20%), Copper (Cu 99.995%), Galvanised steel (Zn thickness 80 μm), in 0.5 mm diameter. The wire was shaped into a circle with a diameter of 2 cm and placed 1 cm apart in the furnace. The electrodes that have been prepared earlier are inserted into the furnace. The carbon source in the form of CO_2 gas is inserted into the furnace through a stainless steel hose. The following process connects the electrodes to the power supply, which provides external potential. The system's initial external potential of 0.2 V was applied for 60 minutes to achieve the current and external potential stability. Also, this process will stimulate further CNT nucleation.

The Electrodeposition process was carried out at a predetermined time. After the Electrodeposition process is complete, the electrodes are removed from the furnace. After removing the electrodes from the furnace, the cathodic product was separated from the electrode in a sonic bath and washed using a 2M HCl solution. After washing, the product was dried for 3 hours at a temperature of 100 °C. The material characteristic was evaluated with Raman for its graphitization degree analysis performed using a Horiba Raman iHR320 with an excitation wavelength of 532 nm. XRD for the crystallinity analysis performs using PanAnalytical and FTIR for Functionalities analysis utilizing Shimadzu IRPrestige 21. Lastly, SEM-EDX for morphology analysis employs FEI Inspect-S50.

4.2 Taguchi and OFAT design on Electrodeposition method

Two types of models are used in this experiment. The first is utilising Taguchi methods consisting of five levels and five parameters. Therefore using Taguchi design L25 is appropriate (Table 10). The second is One Factor at a time (OFAT), varying parameters as independent variables (Table 8).

The Taguchi method was used due to its practicality in providing a high-quality experiment design. Furthermore, this method reduces variance for experiments with an optimum parameters setting[122]. The alternative to the Taguchi method is a factorial design which demands a significant number of factors and a full factorial design performing a large number of experiments. In the One Factor at a time (OFAT), only one factor is changed at one time while the other factors are kept fixed. Therefore, it is suitable for examining parameters individually.

The temperature used in the experiment was 723, 773, 823, 873, and 923 °C. 723 °C was chosen because it is the minimum temperature that can be used to melt Li_2CO_3; as 723 °C is the Li_2CO_3 melting point, the temperature is increased to examine the effect of temperature on the end product of electrodeposition. The 923 °C was chosen as the highest temperature since numerous reports that temperatures higher than 923 lead to a performance drop[57], [80], [85]. The external voltage ranged from 2V to 6V; the minimum external potential used in the Electrodeposition is ~2V from the calculation (equation 14) [98]. The highest external potential is 6V since the previous report suggests that an external voltage higher than 5.5V resulting current instability[82]. The CO_2 flow rate ranges from 5 ml/min to 185 ml/min. The minimum value of 5ml/min was adapted from the previous research [56], [126], and the highest value of 185 ml/min was chosen because the report suggests that excessive CO_2 flow rate resulted in

excessive carbon debris in the molten salt[82], [98], [127][85]. The cathode selection in this experiment was Cu, Galvanized steel Ni, NiCr and Stainless steel. Ni cathode is used because it is an excellent catalyst choice from numerous studies. Other than the Electrodeposition method, Ni is also used in other methods such as Laser Ablation and CVD. Ni is favourable because it provides a nucleation mechanism for CNT[72][128][76]. Cu was used because its ions are sensitive to anions formed in the Electrodeposition process combined with Ni anode, which provides a metal nucleation mechanism it provides the excellent potential to produce CNT[129]. Galvanized steel, NiCr, and stainless steel were excellent cathodes for the Electrodeposition method since previous research reports on metal alloys and mixtures increased the growth and yield of CNT production[98][92]. Galvanized steel containing Zn which a prime candidate for metal initiation of CNT growth in the Electrodeposition. NiCr and stainless steel containing Cr also perform well compared to Galvanized steel in the previous research [57].

Temperature is set as an independent variable in the first cluster in the OFAT design. 723, 773, 823, 873, and 923 °C synthesis temperature were used, while Other variables such as external voltage, CO_2 flow, synthesis time, and electrode were controlled variables. This pattern was used in the experiment switching parameters as an independent variable in the second to fifth cluster sets.

Table 8 OFAT experiment design

Run	Temperature (°C)	External potential (V)	CO_2 Flow (ml/min)	Time (m)	Cathode
First OFAT experiment cluster - Temperature					
1	723				
2	773				
3	823	5	185	60	NiCr
4	873				
5	923				
Second OFAT experiment cluster – External Potential					
1		2			
2		3			
3	773	4	185	60	NiCr
4		5			
5		6			
Third OFAT experiment cluster – CO_2 Flow rate					
1			5		
2			50		
3	773	5	95	60	NiCr
4			140		
5			185		
Second OFAT experiment cluster - Cathode					
1					Cu
2					Galvanis
3	773	5	185	60	Ni
4					NiCr
5					SS
Third OFAT experiment cluster – Electrodeposition time					
1				60	
2				90	
3	773	5	185	120	NiCr
4				150	
5				180	

Optimisation and sensitivity analysis was carried out using the Taguchi method, a statistical technique in the experiment's design. This method outperforms the complete factorial design by using orthogonal arrays. These sections will show the result of implementing the Taguchi

method to obtain the optimum Electrodeposition parameters. A further study of temperature, external voltage, carbon source rate, synthesis time, and electrode as individual controllable factors.

Based on the literature review, five factors were assessed in this work: temperature, external voltage, CO_2 flow rate, Electrodeposition time, and cathode materials—the exact value of levels on each aspect is given in Table 9.

Table 9 Description of factors and levels for the growth rate.

Level	Temperature (°C)	External potential (V)	CO_2 Flow (ml/min)	Time (m)	Cathode
1	723	2	5	60	Cu
2	773	3	50	90	Ni
3	823	4	95	120	Galv
4	873	5	140	150	SS
5	923	6	185	180	NiCr

The next step is designing the experiment using the Taguchi method. For five factors at five levels, the L25 orthogonal array was selected and is given in Table 10. After the experiment based on the orthogonal arrays are complete, two statistical tools are used: signal-to-noise ratios (SNR) and analysis of variance (ANOVA). There are three options for the SNR based on the user's need: nominal is the best, smaller the better, and larger the better. In this case, the larger, the better the suitable one. The equation to calculate the SNR is given in equation 11.

Information on each factor's relative importance can be plotted from the SNR values to identify each factor's optimum levels. The ANOVA uses SNR results to explain each factor's contribution to maximising the growth rate.

Table 10 Taguchi Orthogonal array illustrating the configuration of the experiment

Run	Temperature (°C)	External potential (V)	CO_2 Flow (ml/min)	Time (m)	Cathode
1	723	2	5	60	Cu
2	723	3	50	90	Ni
3	723	4	95	120	Galv
4	723	5	140	150	SS
5	723	6	185	180	NiCr
6	773	2	50	120	SS
7	773	3	95	150	NiCr
8	773	4	140	180	Cu
9	773	5	185	60	Ni
10	773	6	5	90	Galv
11	823	2	95	180	Ni
12	823	3	140	60	Galv
13	823	4	185	90	SS
14	823	5	5	120	NiCr
15	823	6	50	150	Cu
16	873	2	140	90	NiCr
17	873	3	185	120	Cu
18	873	4	5	150	Ni
19	873	5	50	180	Galv
20	873	6	95	60	SS
21	923	2	185	150	Galv
22	923	3	5	180	SS
23	923	4	50	60	NiCr
24	923	5	95	90	Cu
25	923	6	140	120	Ni

4.3 Result - Experimental Taguchi method

SEM-EDX, Raman and XRD spectroscopy was used to confirm CNT's presence. Raman spectroscopy is often used as a characterisation tool of carbon nanotubes. This method is relatively fast and non-destructive and can be conducted without sample preparation. In Figure 29, two main features can be observed: the D band and the G band. D band shows the disordered graphene, and the G band structure represents C-C bond stretching. Figure 29 shows these features in 1353 cm^{-1} as the D band and 1602 cm^{-1} as the G band. Figure 30 shows the XRD result, representing (002) and (100) carbon peaks. XRD characterisation is an indestructive test and aims to obtain impurities information. Comparing the Raman and XRD

results to typical CNT data (Figures 8 and 9), both Raman features and XRD miller indices were present. Therefore, it is a strong indication that MWCNT present

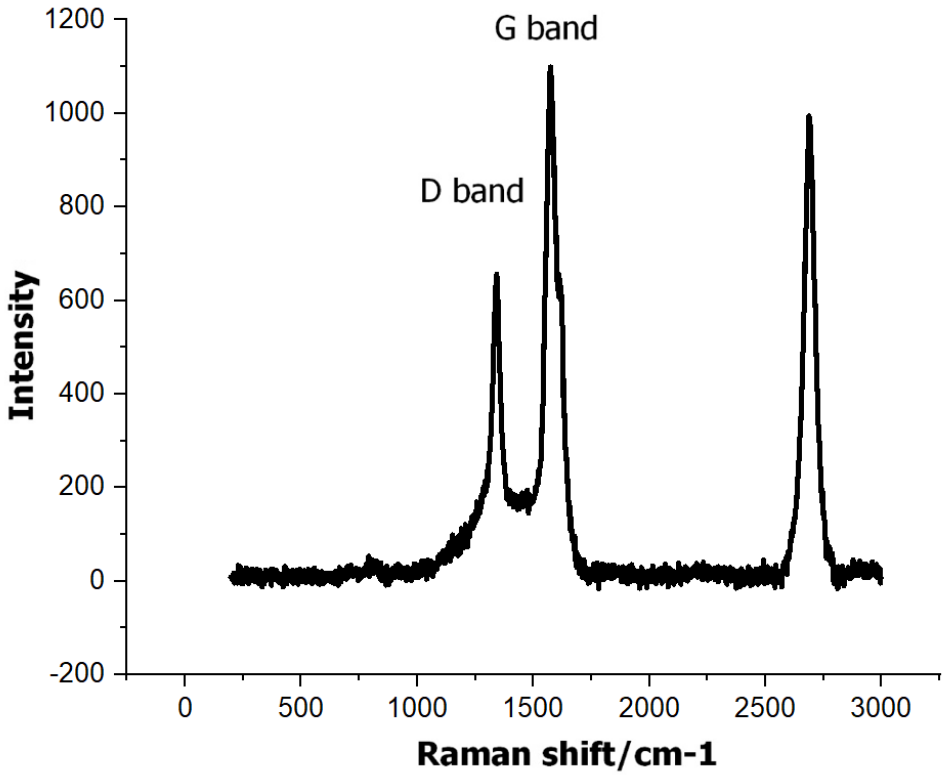

Figure 29 Raman Spectroscopy of cathodic carbon product on Electrodeposition Taguchi run 4 with an excitation wavelength of 532 nm

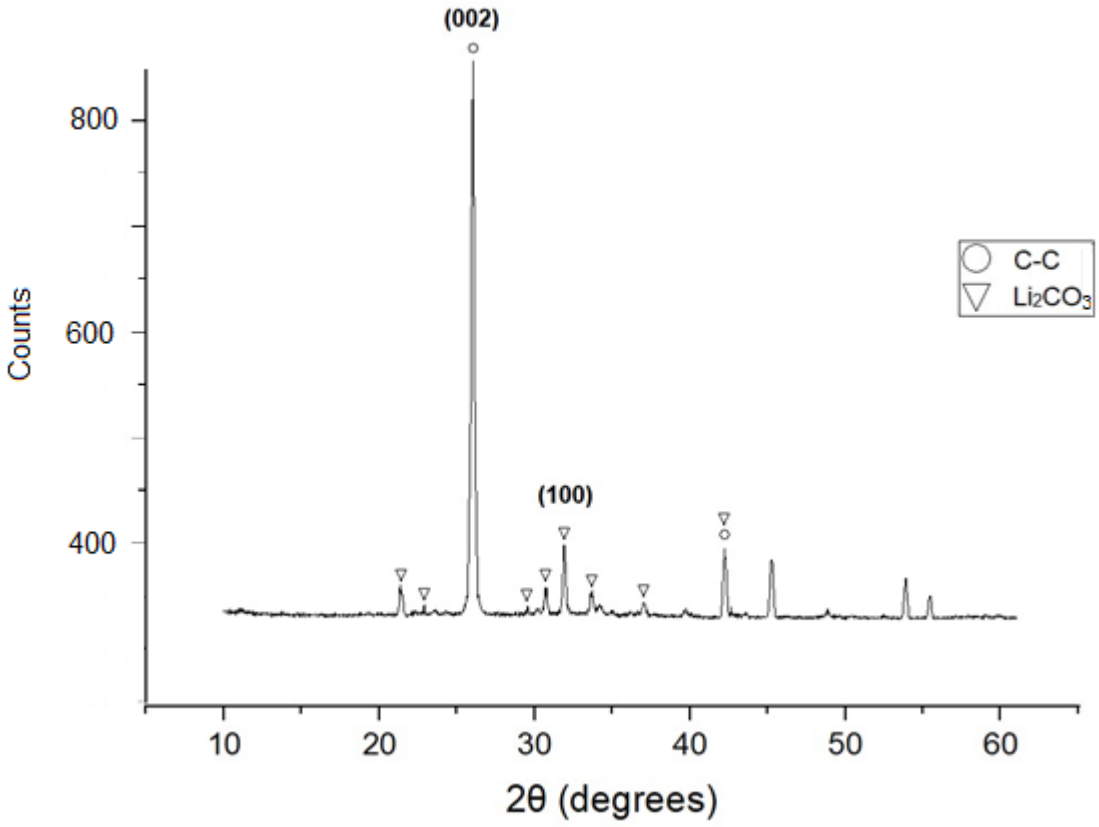

Figure 30 XRD of cathodic product on Electrodeposition Taguchi run 4

The optimisation's objective is to achieve the maximum growth rate of carbon nanotubes in the Electrodeposition system. The growth rate is calculated using equation 12. Total mass is the amount of sediment obtained from the Electrodeposition process; Wt% carbon is the weight percentage of carbon in the deposit obtained in the EDX analysis. The deposition area is an area of a cathode used for carbon capture, and time is the length of the Electrodeposition process.

Deposited carbon and wt% from EDX of each experiment run are taken as output, and from these values, the growth rate is calculated based on equation 12. The Growth rate result for each run is presented in Table 11.

Table 11 Growth Rate for the experiment using the Taguchi method.

Run	∑ Growth Rate
1	0.230
2	0.408
3	0.393
4	0.935
5	0.760
6	1.056
7	1.195
8	0.695
9	1.282
10	0.696
11	0.485
12	0.665
13	1.106
14	1.079
15	0.441
16	0.751
17	0.509
18	0.401
19	0.498
20	1.007
21	0.521
22	0.347
23	0.904
24	0.683
25	0.640

The SNR values were used to identify which factor levels maximise the CNT growth rate. Table 12 shows the response of SNR. With the higher is better SNR higher value in the Table 12 will maximise the carbon growth rate. The optimum value is: temperature=773 ^{o}C; external potential=5V; CO_2; Flowrate=185 ml/min; Electrodeposition time=60 min and; cathode=NiCr.

Table 12 Response table for the signal-to-noise ratio (SNR) larger is better.

Level	Temperature	External potential	CO_2 Flow	Time	Cathode
1	-9.87	-9.86	-9.08	-3.37	-9.96
2	-1.50	-7.30	-6.52	-4.02	-7.22
3	-4.43	-5.33	-5.36	-5.70	-8.07
4	-6.06	-2.60	-4.10	-6.95	-2.42
5	-7.12	-3.88	-3.91	-8.94	-1.32
Delta	8.38	7.27	5.16	5.57	8.64
Rank	2	3	5	4	1

Delta value from Table 12 presents a ranking of the factors based on the importance of the growth rate when ranging on five levels. The sequence follows cathode > temperature > External potential > CO_2 Flow > time. The optimum levels value on each factor is presented graphicly in Figure 31.

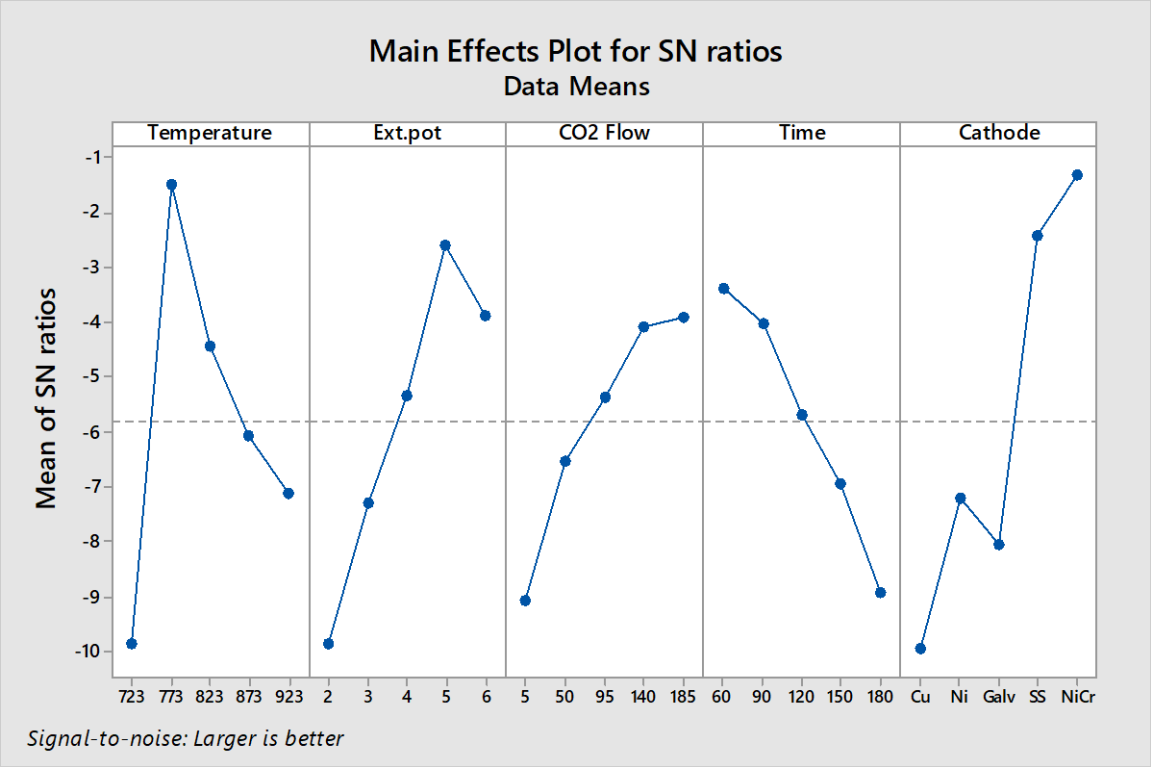

Figure 31 Main Effects Plot for SN Ratios

A confidence level of 95% or the significance level of 5% was used in ANOVA using the SNR value from Table 12. The ANOVA p-value results in Table 13 present the statistical significance of the factors in the Electrodeposition method. A p-value of less than 0.05 considered rejecting

H0, which means that the factors significantly affect the response value. All of the factors have a p-value less than 0.05, which means that all the factors statistically significantly impact the growth rate.

Figure 32 describes each factor's contributor percentage in maximising the Electrodeposition growth rate. This result is in line with the sequence of the p-value, in which the more significant contributors are electrode and temperature with 33.93% and 20.10%, respectively, followed by external potential, CO_2 flow and Electrodeposition time. Graphically contributor factors data are presented in Figure 32.

Table 13 ANOVA table for the mean SNR.

Factor	Degree of Freedom (DF)	Sum of Square (SS)	Contribution (%)	Mean of squares (MS)	F-Value	*p*-Value
Temperature	4	0.7506	20.10%	0.1877	9.06	0.028
External Potential	4	0.5487	14.69%	0.1372	6.62	0.047
CO_2 Flow	4	0.3317	8.88%	0.0829	4	0.104
Time	4	0.7534	20.18%	0.1884	9.09	0.028
Cathode	4	1.2670	33.93%	0.3167	15.29	0.011
Error	4	0.0829	2.22%	0.0207		
Total	24	0.7506	100.00%			

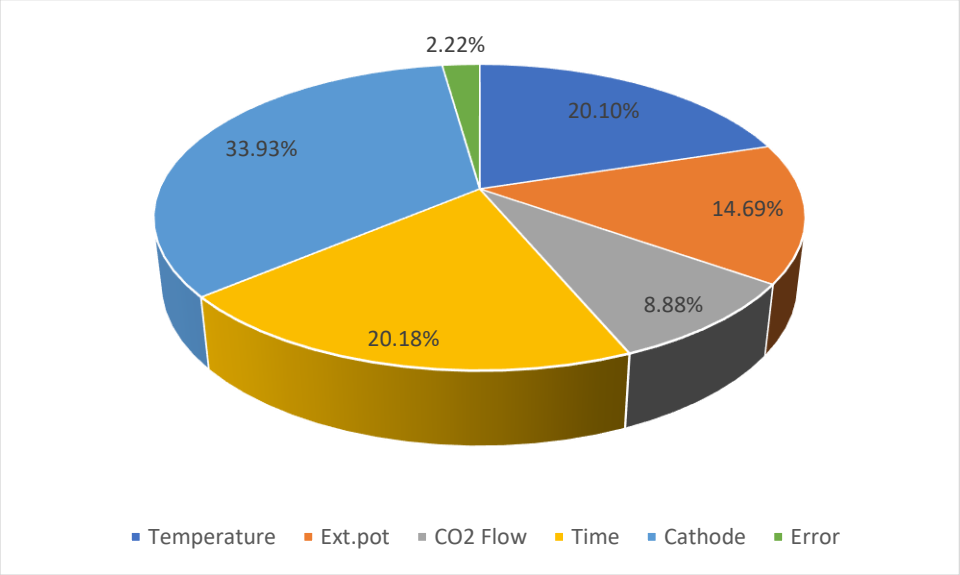

Figure 32 Contribution of variables on ANOVA

The influence levels of each factor on the CNT growth rate are presented in Figure 33. Temperature and cathode changes were seen to increase the growth rate of CNT. Contradictory to temperature and cathode, CO_2 flow seems to have a minor effect on growth rate. The lowest temperature (723ºC) produces the lowest carbon and carbon growth value since the electrolyte might not completely melt since the Electrodeposition operates in the precise lithium carbonate melting point. The complex nature of the technical operation of Electrodeposition at this temperature might reduce the result significantly. Therefore temperature response contribution is reasonable to be the highest.

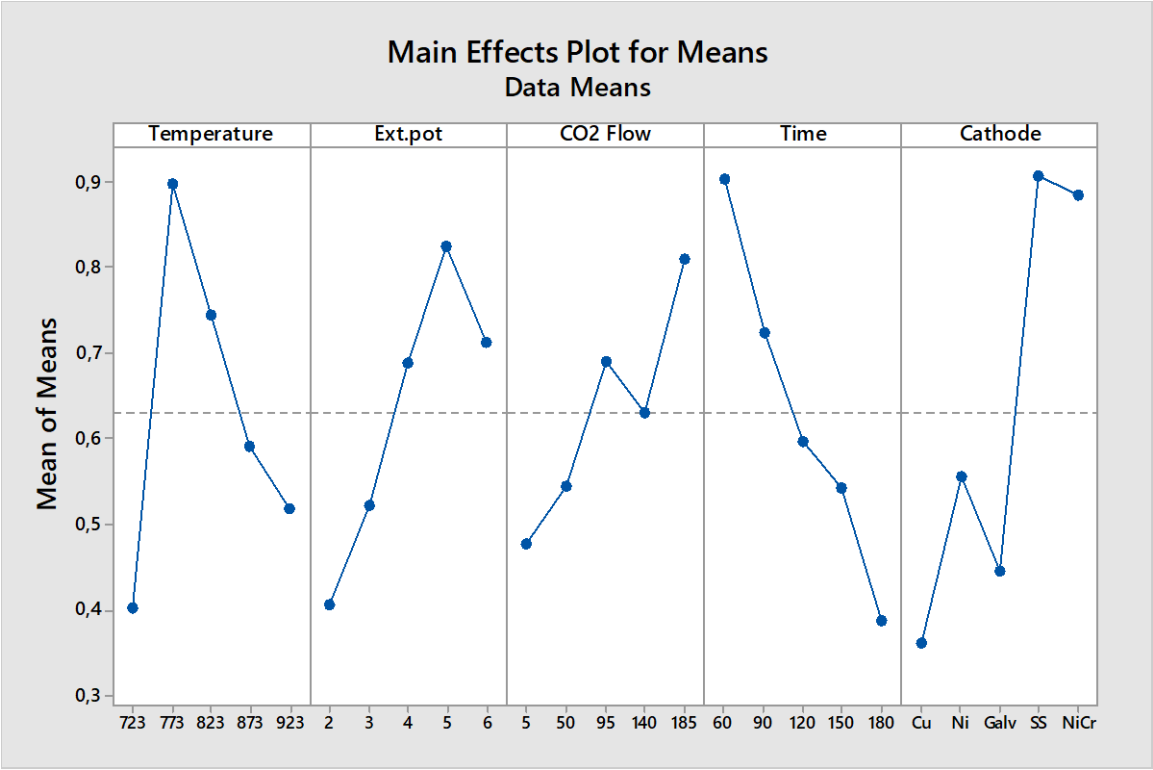

Figure 33 Main Effects Plot for Means

The interaction plot in Figure 34 aims to assess the interaction between factors to interpret the main effects—the interaction plot for five factors connected with the line. When the line is parallel indicates the interaction is small, and the more non-parallel the line, the greater the interaction. Although the interaction of the variables is relatively complex, there were some notable patterns in the interaction plot. The higher temperature (923 and 873 °C) tend to have

less response/negative response toward other variables. For example, the interaction of temperature and Electrodeposition time results in a sloping pattern. Longer Electrodeposition results in less carbon overall, but the higher temperature is the most noticeable. This temperature pattern can also be found in previous reports[22][77], agreeing that higher temperature is less favourable in Electrodeposition. In addition, the higher temperature also produces a more prominent crystallite morphology. Another notable feature is cathode interaction with other variables. Two dominant cathodes in carbon growth are stainless steel and nichrome, with nichrome's slightly higher signal-to-noise ratio. In the interaction plot, nichrome is a more stable response to other variable changes than stainless steel. However, stainless steel produces higher responses in some cases.

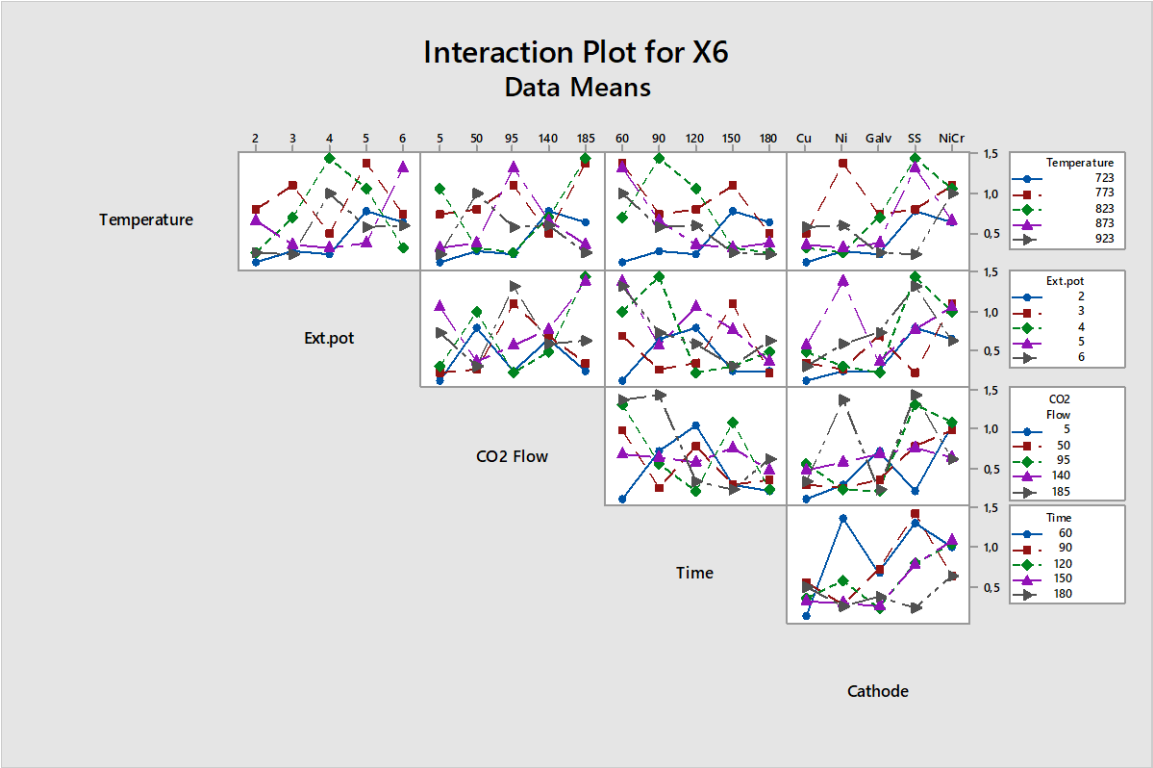

Figure 34 Interaction Plot for Growth Rate

4.4 Result - Experimental OFAT method

4.4.1 Temperature variable effect on Electrodeposition

The previous reports suggested that Electrodeposition in the molten salt is not possible below a temperature of 500 °C and suggested using 723 °C and higher on Lithium carbonate[79]. Other than general ranges of working temperature, there is only little known about the effect of temperature and electrode potential on the end product of Electrodeposition. An inevitable effect is the oxidation of CO_3^{2-} which become dominant at high current density and temperature. This oxidation also means that temperature and voltage affect anodic products, mostly O^{2-}[85]. Therefore, a deeper understanding of cathodic product behaviour on different Electrodeposition temperatures will help to improve this method.

Table 14 One Factor at a Time Experiment Design Varying Temperature

Run	Temperature (°C)	External potential (V)	CO_2 Flow (ml/min)	Time (m)	Cathode
1	723				
2	773				
3	823	5	185	60	NiCr
4	873				
5	923				

The cathodic product of Electrodeposition in different temperatures, which are 723 °C, 773 °C, 823 °C, 873 °C, and 923 °C, is present in Figure 35. The OFAT varying temperatures were employed (Table 14). The syntheses used an external voltage of 5 V, an Electrodeposition time of 60 minutes, a CO_2 flow rate of 180ml/min and NiCr cathode—all of the temperatures resulting in carbon deposits with some electrolyte residue. However, at 873 and 923 °C, the result tends to be porous compared to lower temperatures. The porous structures of the deposited carbon promote electrolyte residue to fill the space, resulting in intricate carbon separation from the cathode. These phenomena were reported in a previous study [75][91] and predicted it was caused by O^{2-} ion from OH^- made contact with molten carbonate.

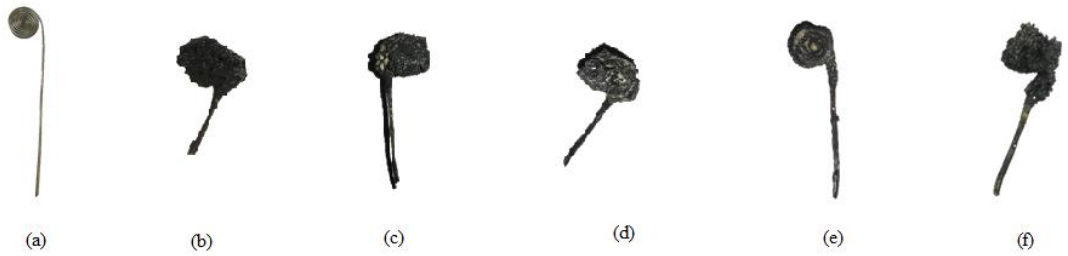

Figure 35 Example of the electrode before and after the Electrodeposition process with temperature variance. a) Before Electrodeposition, b) after Electrodeposition at 723 °C, c) after Electrodeposition at 773 °C, d) after Electrodeposition at 823 °C, e) after Electrodeposition at 873 °C, f) after Electrodeposition at 923 °C.

After separating the soot using an ultrasonic bath and washing it using an acid solution, phase identification of the Electrodeposition result was made using XRD analysis. This analysis aims to identify the composition of the Electrodeposition product and measure the crystal size. (illustrated in Figure 36). Based on the XRD result, two types of peaks can be analysed. The first one is in the $2\theta = \sim 26^{o}$, which can be the C (002) miller indices graphite reflection, representing the C-C bond present that can be concluded as CNT or graphite [33]. The second peak is at $2\theta = \sim 33^{o}$This peak contributes to the presence of Li_2CO_3 residue [130]. At 723 °C, this peak is lower compared to other temperatures. This lower peak might indicate that the crystal is not well organised, and it can be assumed that during 723 °C, the crystal is not unravelled well during the Electrodeposition process.

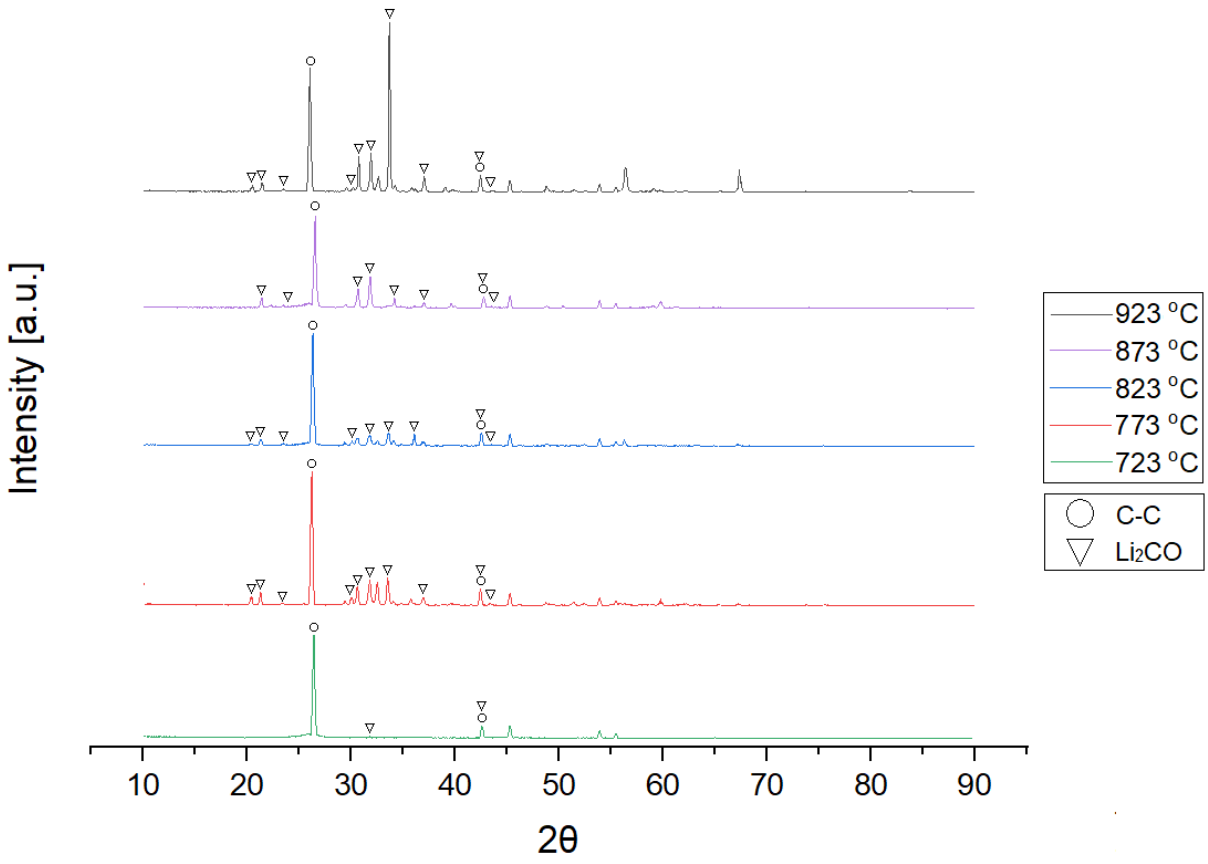

Figure 36 Diffractogram XRD deposited carbon in different synthesis temperature

Table 15 Phase of XRD test result on carbon

No	Temperature	FWMH	Crystalline size D (nm)
1	723	0.472	17.285
2	773	0.468	17.43
3	823	0.364	22.424
4	873	0.286	28.547
5	923	0.212	38.523

The FTIR analysis (Figure 37) characterises carbon nanotube functional elements shaped in the Electrodeposition. The dominant peaks representing primary mode (A_{2u} and E_{1u}) are present in 868 and 1575 cm^{-1}, indicating the MWCNT. Both A_{2u} and E_{1u} peaks appear at all temperatures except for 723 °C showing that CNT is not formed at the lowest temperature. The most noticeable peaks are in the region 1400-1600 cm^{-1} which are active because of the response of aromatic C=C. Since nanotubes are carbon atoms arranged in a hexagonal pattern

from benzenoid derivatives of sp^2, it is classified as aromatic. Therefore this region is expected to be active[131].

The functionalities related to oxygen in the CNT surface can be confirmed by a broad peak around 3430 cm^{-1}, corresponding to the O-H stretching mode[132]. This functionality also does not arise at 723 °C. The absence of oxygen functionalities in the product suggests a limited oxygen-related reaction. Therefore the Electrodeposition in the lowest temperature can be assumed not to work well since the anode product is mainly O_2. Another functionality is CH_2 related, which appears in two forms: asymmetric CH_2 (aCH_2) at 2950 cm^{-1} and symmetric CH_2 (sCH_2) at 2830 cm^{-1}.

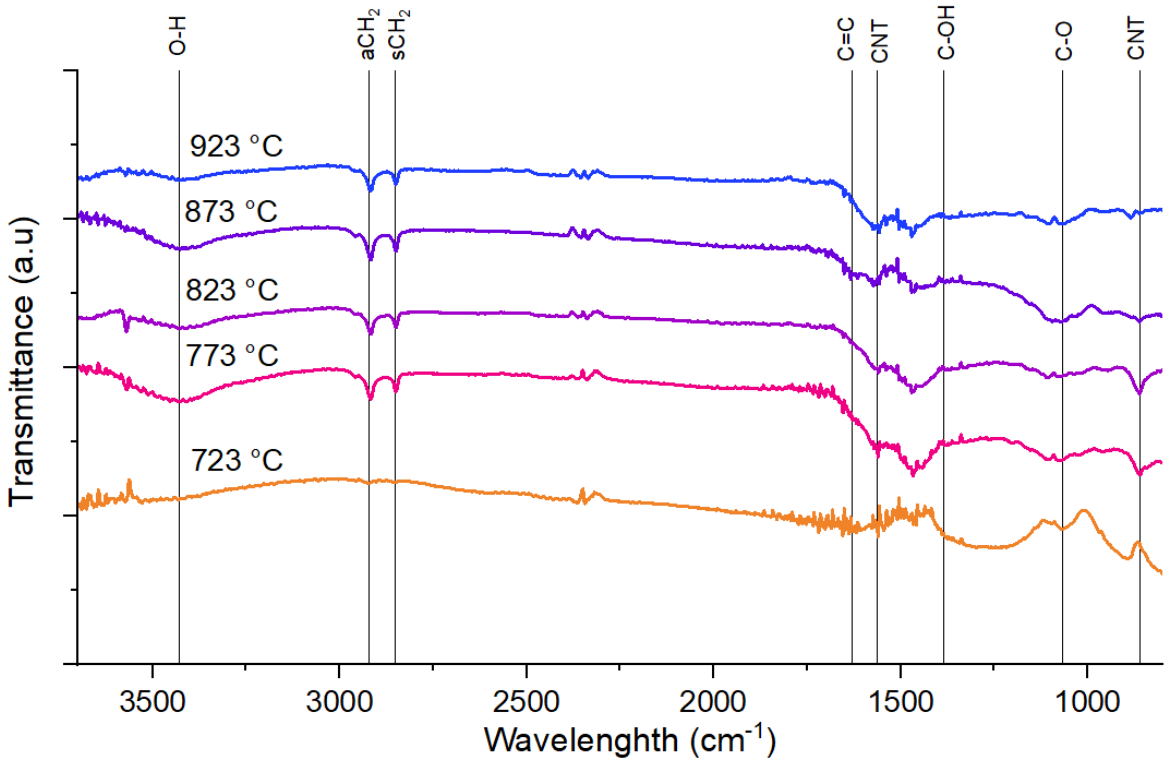

Figure 37 FTIR spectra of cathodic product produced in different temperatures

The rewash process is done to minimize the remaining residue before further analysis. The Raman analysis contains some notable features: D, G, and G' bands. In all temperatures, the D band peaks are 1340-1351 cm^{-1}, while the G and G' bands are 1455-1580 $cm^{-1}$and 2683-

2700 cm^{-1}, respectively. There are at least two possible causes of the shifting frequency: the difference in the sp^2 carbon structure and the nanotube's diameter[34]. The G split and features are seen at all temperatures except 723 °C. G band splits indicate the bending of the graphene system, such as CNT[133]. Therefore, because of the lack of RBM feature in the Raman analysis and combining the presence of D, G, and G' features, it can be concluded that the soot composition from 773-923 °C is mainly MWCNT. However, using 723 °C synthesis temperature, the presence of CNT in the cathodic product is inconclusive. Based on Raman analysis, the broader linewidth (>100 cm^{-1}) was typically for amorphous carbon while the linewidth of SWCNT is 10-30 $cm^{-1}$and MWCNT is 30-60 cm^{-1}. Also, when comparing the pattern from the previous study, the pattern of the Raman analysis graph is toward amorphous carbon[33], [35], [82].

MWCNT Purity calculation is based on the previous work using I_G'/I_G[36][35], resulting in the best purity achieved at 773 °C in 88.27%. The MWCNT is not found in the lowest temperature, 723 °C. Increasing the temperature from 723 °C to 773 °C improves the purity drastically, and a further temperature increase will decrease the purity value of MWCNT. The normalised intensity I_D/I_G ratio from Raman analysis can be used to measure disorder [34]. This ratio value in carbon products has been recorded from approaching 0 to 3.3, with ~0 being perfectly oriented graphite, and 3.3 is amorphous carbon[133][134]. Therefore analyzing Figure 38 and Table 16 indicates that changing the Electrodeposition temperature resulting different I_D/I_G ratios. The lowest temperature achieves the highest ratio. Increasing the temperature to 773 °C lowers the I_D/I_G ratio; however, increasing the further temperature increases, the ratio also increases, indicating that increasing temperature will extend defects.

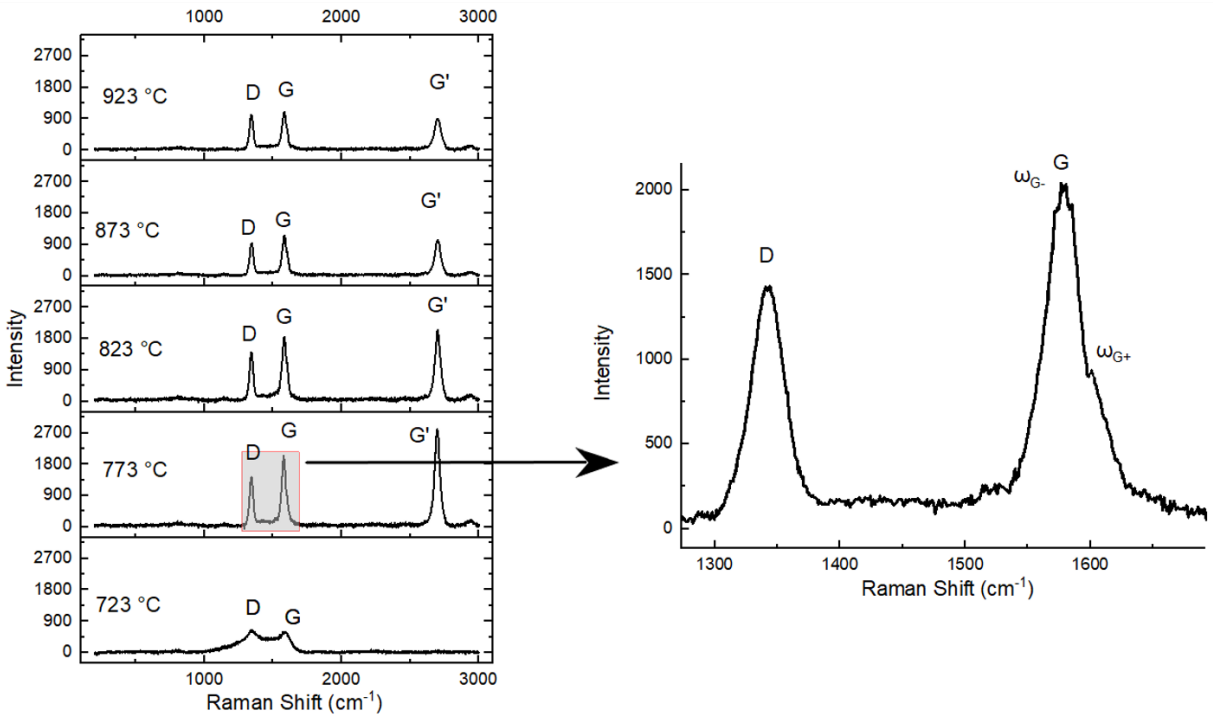

Figure 38 Raman analysis of cathodic product produced in different temperatures

Table 16 Raman analysis result of cathodic product produced in different temperatures

Temperature	ID/IG	IG'/ID	Purity (%)
723	1.22	-	0%
773	0.73	2.01	88.27%
823	0.76	1.39	70.98%
873	0.85	1.01	56.09%
923	0.96	0.93	52.05%

The composition of soot products in various temperature syntheses is evaluated using EDX. The cathodic product mainly contains carbon and oxygen, representing oxygen-containing functional groups[82][135]. Analyzing the EDX spectrum, the lowest carbon weight percentage (39.88 wt%) is at 723 °C and significantly improves when increasing the temperature to 773 °C. Further temperature increases will also reduce the wt% suggesting that 773 °C is ideal for optimizing the Electrodeposition process to increase carbon production.

The morphology of deposited carbon is investigated further using SEM. Based on the SEM result (shown in Figure 39), from 773 °C to 923 °C, the CNT outer diameter ranges from 50-100 nm. The size of CNT gradually increased with higher synthesis temperature. There are no

visible carbon nanotubes at the lowest temperature, which is also in line with the FTIR and Raman analysis. The lowest normalized diameter is 773 °C, followed by 823 °C, 873 °C 923°C, with values of 65, 77.5, 87.5, and 100 nm, respectively.

This evidence suggests that the higher synthesis temperature leads to a more extensive particle form of deposited CNT. This phenomenon can also be seen in the crystallite calculation result [53], presented in Table 15. The average crystal size value increases due to the temperature increase.

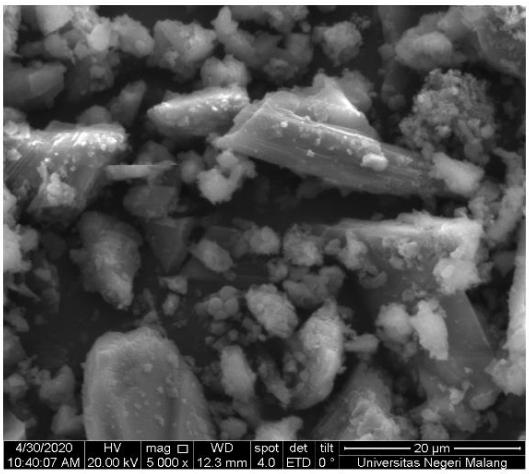

1(a)

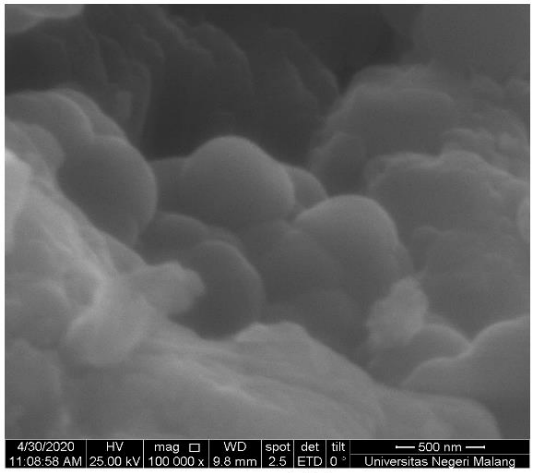

1(b)

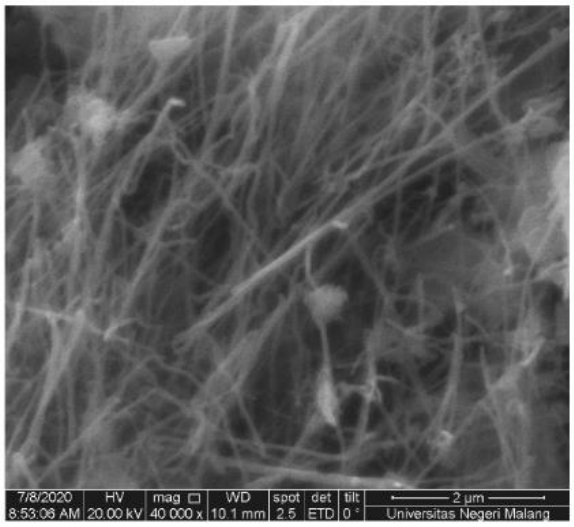
7/8/2020 8:53:08 AM
HV 20.00 kV
mag 40 000 x
WD 10.1 mm
spot 2.5
det ETD
tilt 0 °
2 µm
Universitas Negeri Malang

2(a)

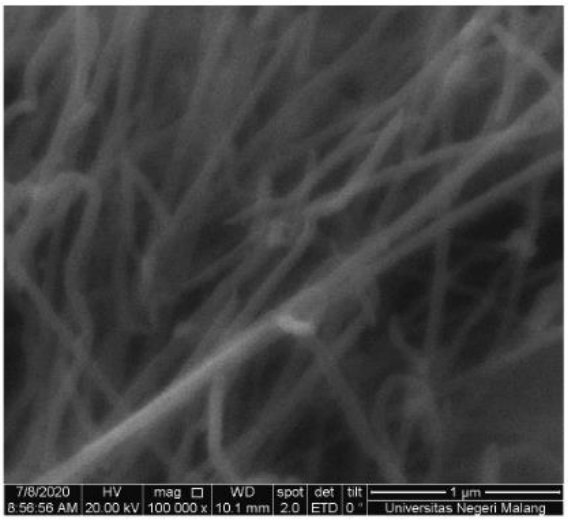
7/8/2020 8:56:56 AM
HV 20.00 kV
mag 100 000 x
WD 10.1 mm
spot 2.0
det ETD
tilt 0 °
1 µm
Universitas Negeri Malang

2(b)

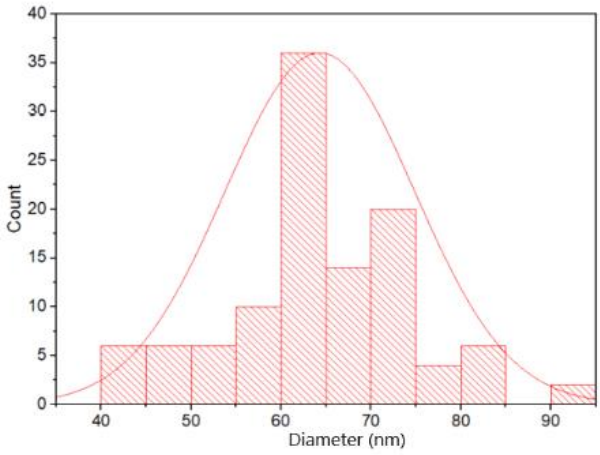
Count
Diameter (nm)
0
5
10
15
20
25
30
35
40
40
50
60
70
80
90

2(c)

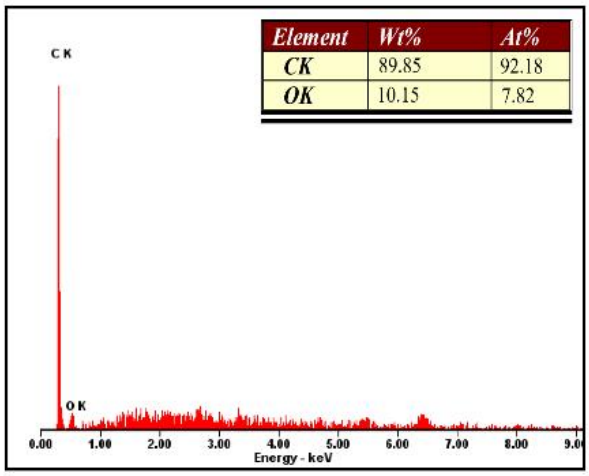
Element | Wt% | At%
CK | 89.85 | 92.18
OK | 10.15 | 7.82
C K
O K
0.00
1.00
2.00
3.00
4.00
5.00
6.00
7.00
8.00
Energy - keV

2(d)

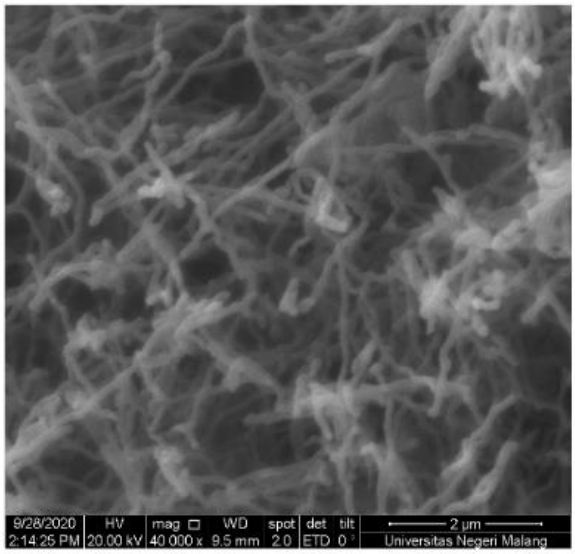
9/28/2020 2:14:25 PM
HV 20.00 kV
mag 40 000 x
WD 9.5 mm
spot 2.0
det ETD
tilt 0 °
2 µm
Universitas Negeri Malang

3(a)

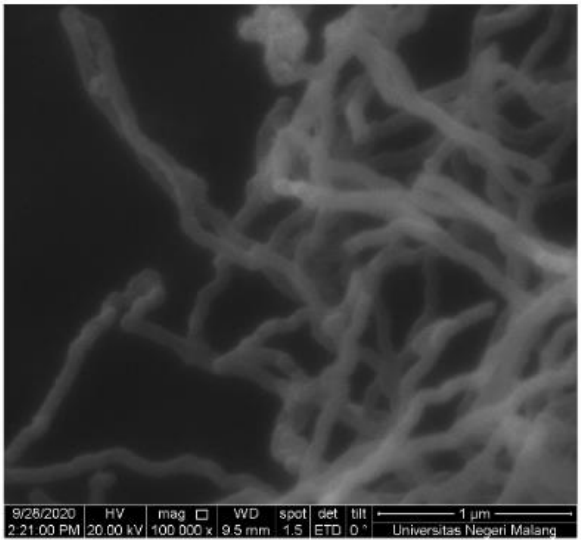
9/28/2020 2:21:00 PM
HV 20.00 kV
mag 100 000 x
WD 9.5 mm
spot 1.5
det ETD
tilt 0 °
1 µm
Universitas Negeri Malang

3(b)

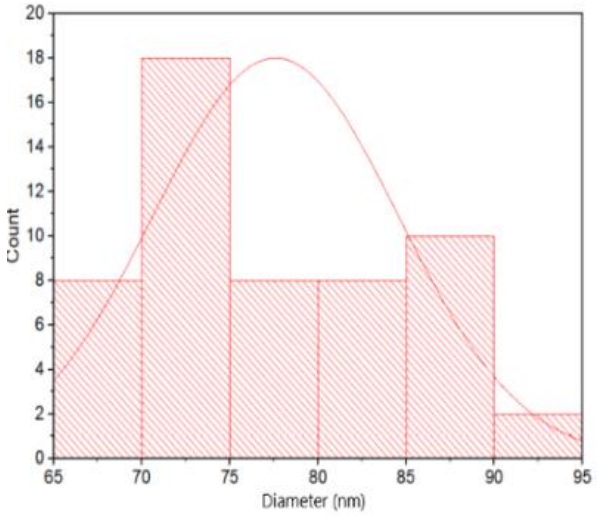
Count
Diameter (nm)
0
2
4
6
8
10
12
14
16
18
20
65
70
75
80
85
90
95

3(c)

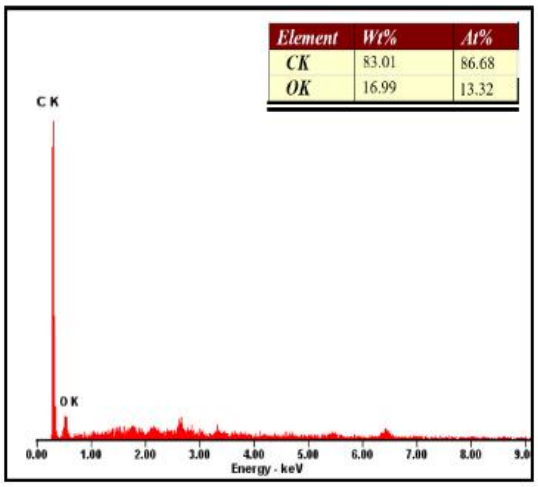
Element Wt% At%
CK 83.01 86.68
OK 16.99 13.32
C K
O K
0.00 1.00 2.00 3.00 4.00 5.00 6.00 7.00 8.00 9.0
Energy - keV

3(d)

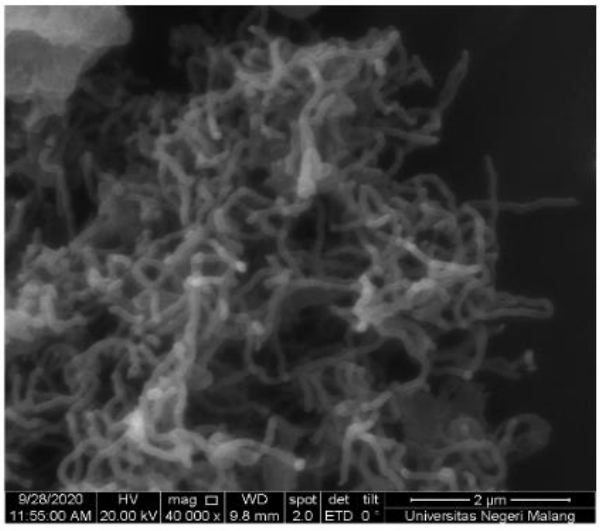
9/28/2020 HV mag WD spot det tilt 2 µm
11:55:00 AM 20.00 kV 40 000 x 9.8 mm 2.0 ETD 0 °
Universitas Negeri Malang

4(a)

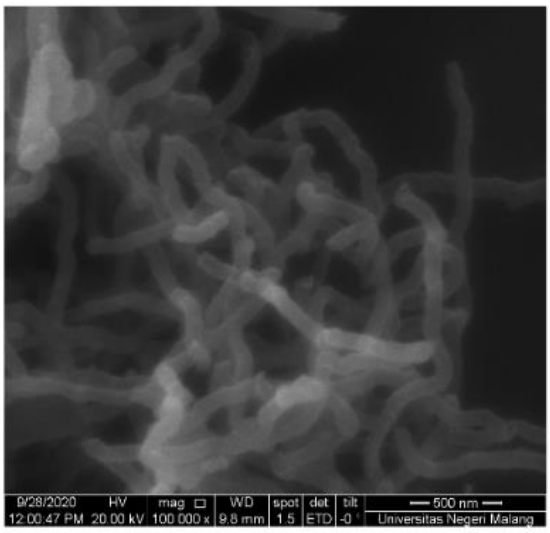
9/28/2020 HV mag WD spot det tilt 500 nm
12:00:47 PM 20.00 kV 100 000 x 9.8 mm 1.5 ETD -0 °
Universitas Negeri Malang

4(b)

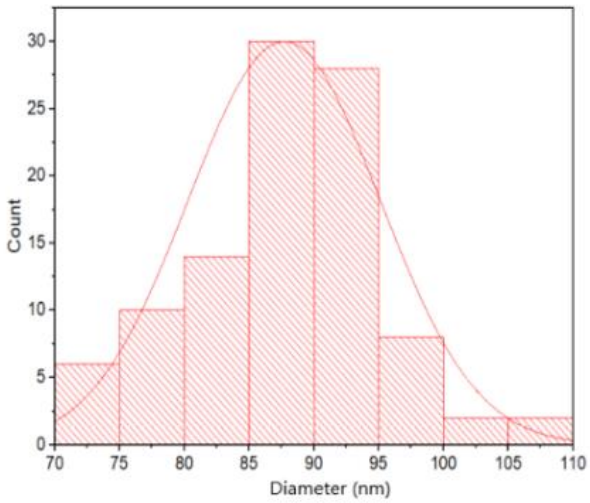
Count
Diameter (nm)
0
5
10
15
20
25
30
70
75
80
85
90
95
100
105
110

4(c)

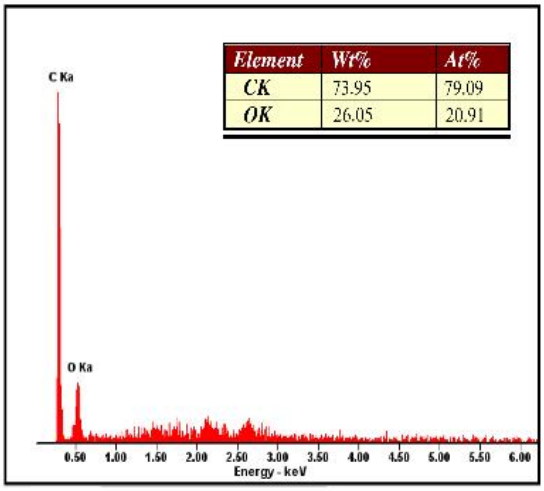
C Ka
O Ka
Element Wt% At%
CK 73.95 79.09
OK 26.05 20.91
0.50 1.00 1.50 2.00 2.50 3.00 3.50 4.00 4.50 5.00 5.50 6.00
Energy - keV

4(d)

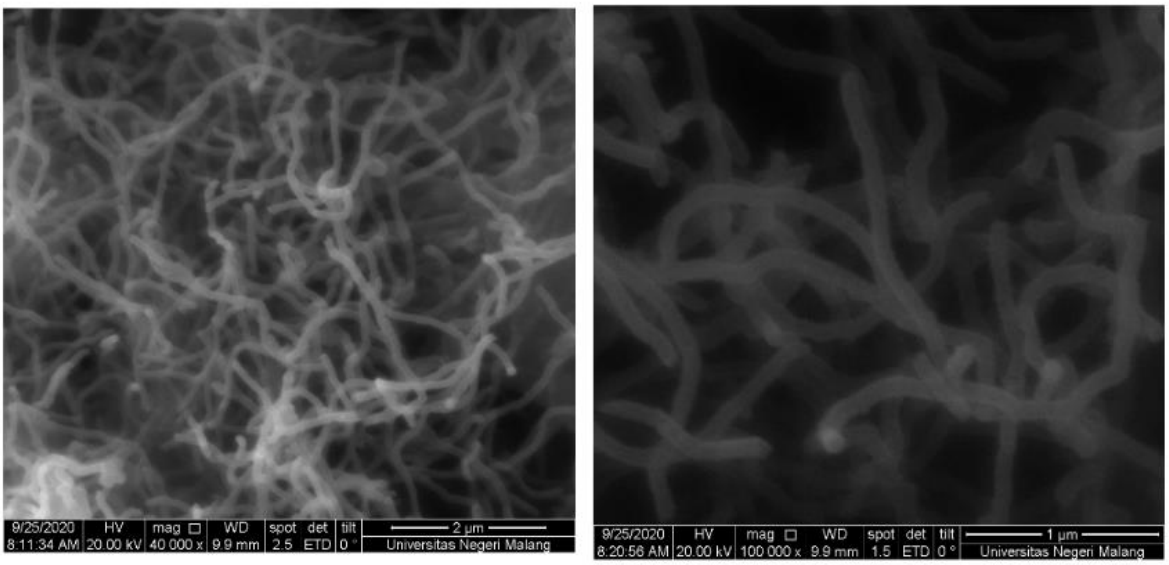

5(a) 5(b)

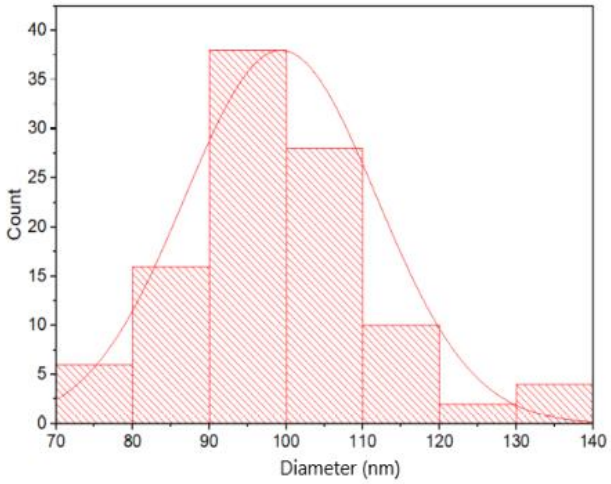

5(c)

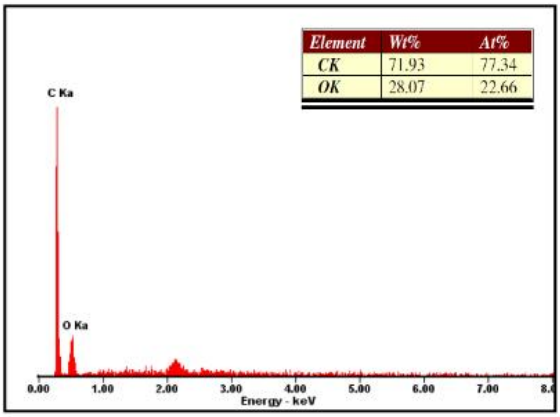

5(d)

Figure 39 SEM and EDX analysis of deposited carbon in different synthesis temperatures. a,b) SEM image c) Diameter distribution d) EDX (1) 723 (2) 773 (3) 823 (4) 873 (5) 923 All measurement (c) is based on image (a)

$$Carbon\ growth\ rate = \frac{Total\ mass\ of\ deposit \times wt\ \%\ Carbon}{Deposition\ area \times time}$$ Equation 12

$$MWCNT\ yield = \frac{Total\ mass\ of\ deposit \times \%purity}{Deposition\ area \times time}$$ Equation 13

The carbon growth rate and CNT yield (Figure 40) are calculated using Equations 12 and 13. Electrodeposition with temperature 723 °C, 773 °C, 823 °C, 873 °C, 923 °C resulting carbon growth rate of 0.852, 1.787, 1.648, 1.687 and 1.557 g cm^{-2} $Hour^{-1}$ respectively. 773 °C is the best temperature in carbon deposition rate, followed by 823 °C, 873 °C, 923 °C and 723°C. 723 °C is the lowest deposition rate due to the melting temperature of Li_2CO_3, and keeping lithium carbonate's stability in the molten form will be a challenge at this temperature. A temperature higher than 773 °C produces a lower deposition rate. Although higher temperature increases electrolyte conductivity, it does not mean a better deposition rate, as shown in Table 17.

Table 17 temperature variable effect on Electrodeposition growth rate and MWCNT yield

Run	Temperature (°C)	Total deposit mass (gr)	Wt% Carbon	Carbon Growth Rate (g cm-2 h-1)	Purity (%)	MWCNT yield (g cm-2 h-1)
1	723	3.35	39.88	0.852	0	0
2	773	3.12	89.85	1.787	88.27%	1.76
3	823	3.12	83.01	1.648	70.98%	1.41
4	873	3.58	73.95	1.687	56.09%	1.28
5	923	3.40	71.93	1.557	52.05%	1.13

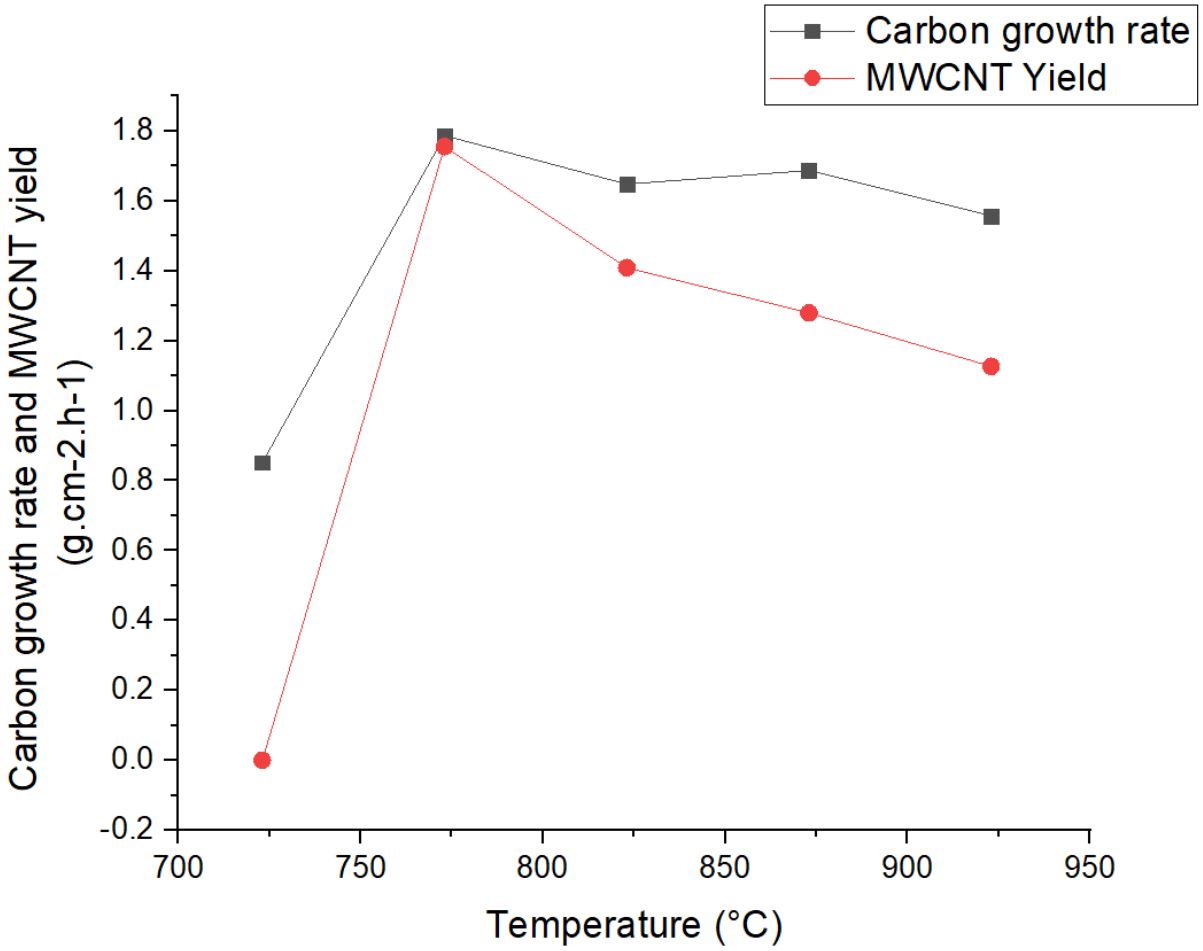

Figure 40 Carbon growth rate and MWCNT yield In different temperatures

After analysing all the analysis results of the cathodic product synthesized in different temperatures, the Electrodeposition temperature significantly affects the carbon product. The most significant improvement is achieved in changing the temperature from 723 to 773 °C. Not only producing more carbon deposits and a higher carbon growth rate, but 773 °C also produces MWCNT in the process. However, increasing temperature further does not improve carbon growth rate and MWCNT yield.

4.4.2 External potential effect on Electrodeposition

The particular effect of external potential in the Electrodeposition is the domination of CO_3^{2-} in higher voltage, which results in the oxidation of CO_2. Lower voltage will interrupt these oxidation processes. The thermodynamic calculation determines the least energy to remove CO_2 by

electrolysis. This calculation uses the standard thermodynamic potential of reaction and resulting 1.7 volts at 600 °C [98].

$$3Li_2CO_3 \rightarrow 3Li_2O + 2CO_2 + C + O_2 \quad E°(600) = 1.719\,V \qquad \text{Equation 14}$$

However, a current instability event might affect the cathodic product in the stable external potential condition. Previous research suggests that the current instability is an issue in the 5.5 V and higher external potential conditions [82]. Hence, the ideal electrochemical window of the Electrodeposition using pure Li_2CO_3 is in the 2-6 V. One Factor at a time (OFAT) model clusters are used in this experiment, varying external potential. Table 18 present the experiment settings.

Table 18 One Factor at a time (OFAT) model clusters varying external potential

Run	Temperature (°C)	External potential (V)	CO_2 Flow (ml/min)	Time (m)	Cathode
1		2			
2		3			
3	773	4	185	60	NiCr
4		5			
5		6			

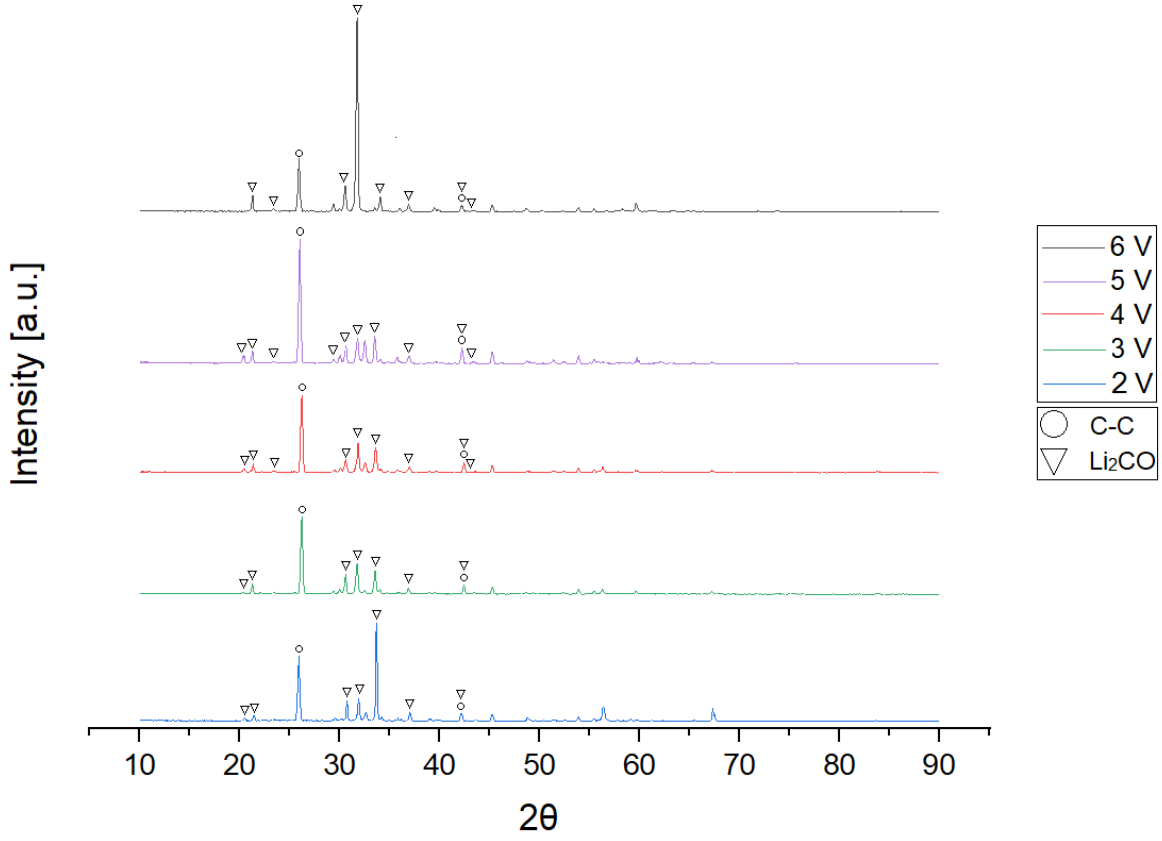

Figure 41 XRD deposited carbon in different external potentials

Table 19 Phase of XRD test result on carbon

No	External Potential	FWHM	Crystalline size D (nm)
1	2 V	0.348	23.46
2	3 V	0.386	21.15
3	4 V	0.429	19.04
4	5 V	0.468	17.43
5	6 V	0.454	17.98

Table 19 and Figure 41 show the carbon powder's XRD test phase results. The XRD analysis has shown that the Li_2CO_3 and Li_2O are present after the purification process, which means the impurities remain after acid treatment. Therefore the rewash process is needed to minimize impurities. Calculation of the crystalline using the equation from previous research[136]. The result is that the crystallite size is slightly decreasing using higher voltage Electrodeposition. However, this result is not as significant as the temperature changes used

in the Electrodeposition synthesis. This phase pattern showed that the crystal structures are formed and affected by the changes in voltage used.

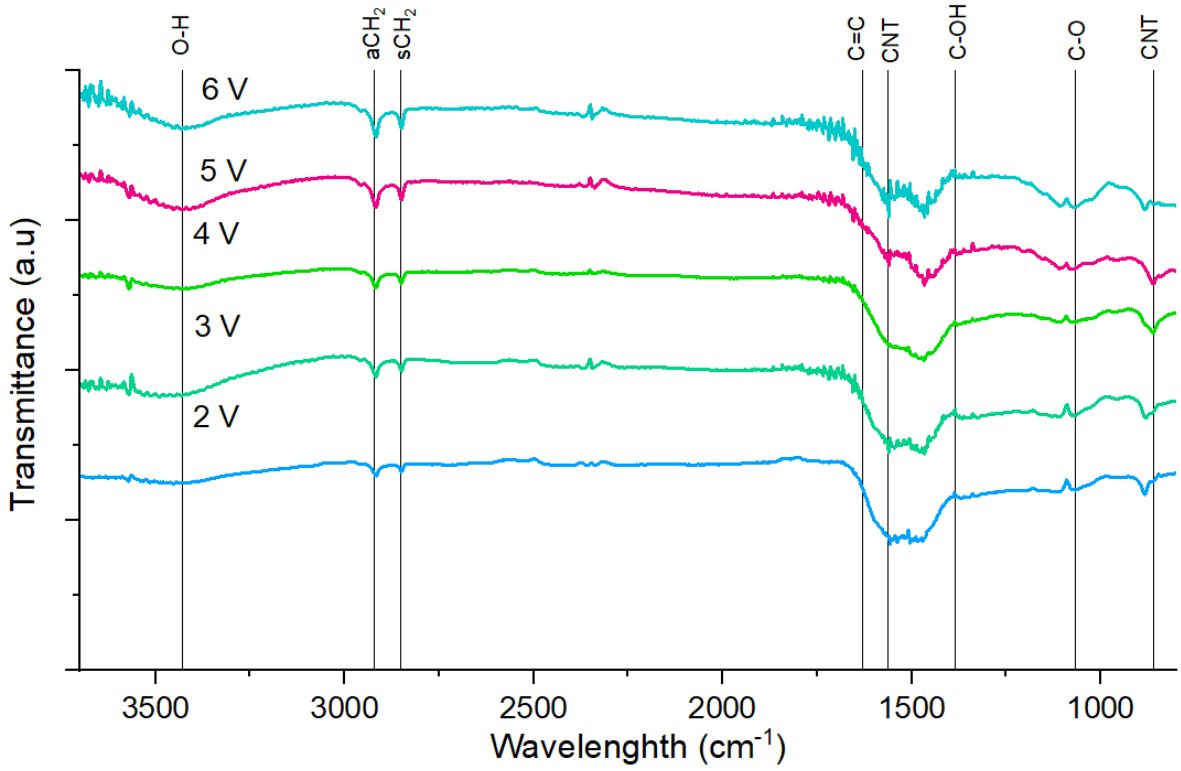

Figure 42 FTIR spectra of cathodic product produced in different external potentials

The FTIR analysis (Figure 42) analyses CNT functional elements in different cathodic products produced in different voltages, especially carboxylic and hydroxylic groups. The A_{2u} and E_{1u} peaks (868 and 1575 cm^{-1}) appear in all voltage. However, the A_{2u} are sifting to a higher wavelength at 2, 3 and 6 volts. The shifting wavelength is correlated to the level of molecular interaction or changes in the population of different chemical species. There are conflicting hypnotises regarding the upshift and downshift of IR-active frequency. The experimental hypothesis suggests that downshift arise when the diameter increase[137]. Another theory is based on ab initio calculation which indicates the opposite[138]. However, it also must be considered that CNT's functionalization commonly occurs under purification treatment. The shifting could be part of the functionalization of the vibrational modes, which do not reflect the

phonon dynamic of CNT[139]. The other IR-active are 1400-1600 cm^{-1}, 3430 cm^{-1},2830 cm^{-1}, and 2950 cm^{-1} attribute of C=C, O-H, sCH_2 , and aCH_2 respectively.

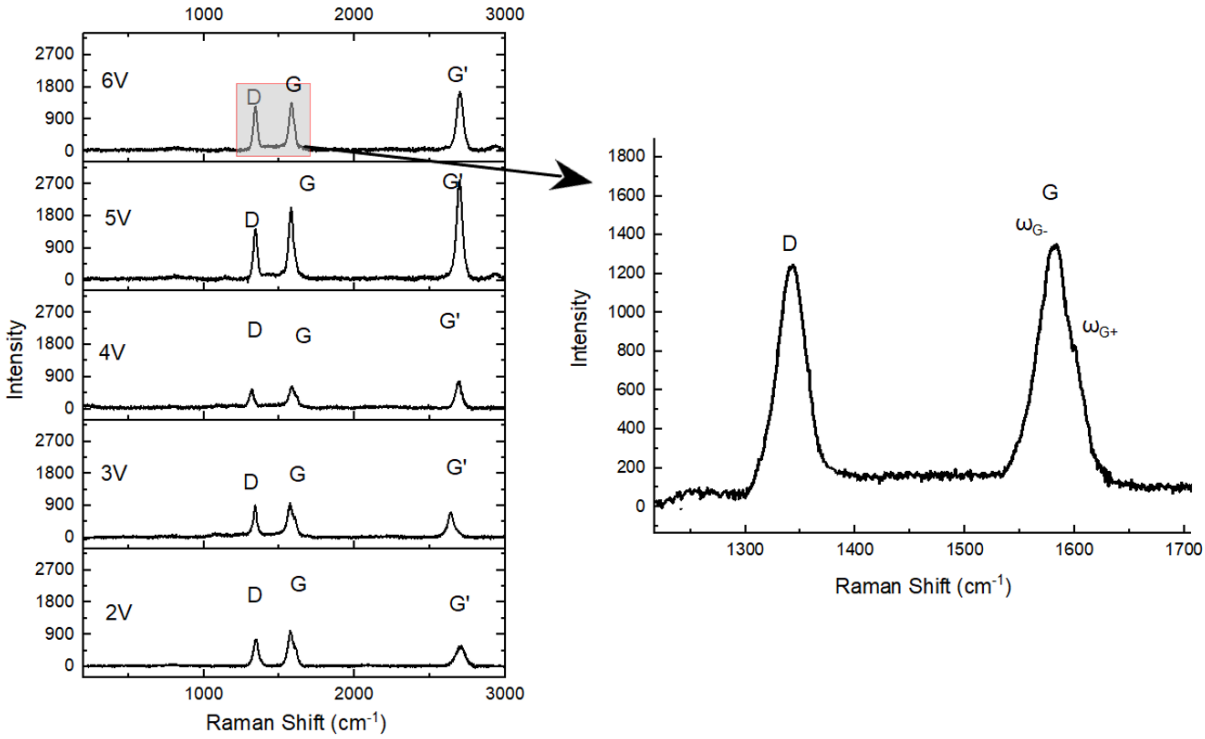

Figure 43 Raman analysis of cathodic product produced in different external potentials

Table 20 Raman analysis result of cathodic product produced in different external potentials

External potential (V)	ID/IG	IG'/ID	Purity (%)
2	0.75	0.76	42.81
3	0.90	0.79	44.66
4	0.86	1.21	64.56
5	0.73	2.01	88.27
6	0.96	1.40	71.47

The Raman analysis (Figure 43 and Table 20) aims to determine the graphitization degree of the Electrodeposition product. The Raman analysis results of all external potential show D, G, and G' bands' features, showing that 2-6 V Electrodeposition can fabricate CNT. The active D band is related to the sp^2 carbon defect, and the G band presents the signature of C-C bond stretching. The normalised intensity (I_D/I_G ratio) is used to measure the disorder because of the

complex nature of the measurement of absolute intensity disorder. The I_D/I_G ratio ranges from 0.73 to 0.96 with an inconclusive pattern.

G band, which signature of all sp^2 carbons is split into into ω_{G^-} and ω_{G^+} Indication of (LO modes) and perpendicular (TO modes) rolled graphene such as CNT. All Raman analysis results in 2-6 volts show this split feature. The second order of Raman signature in sp^2 (G' band) arises in the Raman spectrum. The purity calculation could be done using $I_{G'}/I_D$[36]. The highest purity is achieved in 5V, followed by 6V, 4V, 3V, and 2V, with 88.27%. 71.47%, 64.56%, 44.66%, and 42.81% respectively.

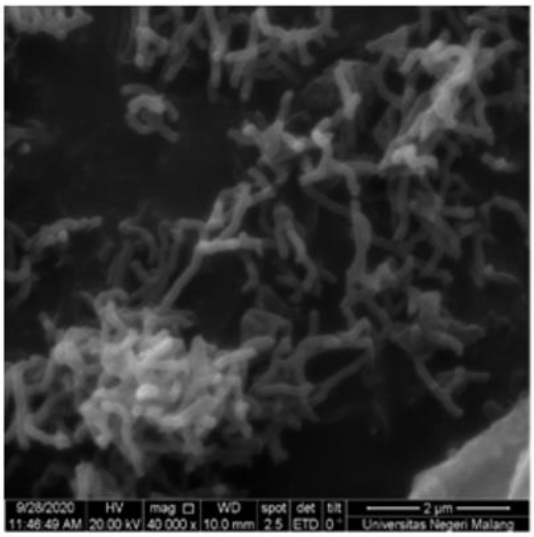
9/28/2020 HV mag WD spot det tilt 2 µm
11:46:49 AM 20.00 kV 40,000 x 10.0 mm 2.5 ETD 0 ° Universitas Negeri Malang

1 (a)

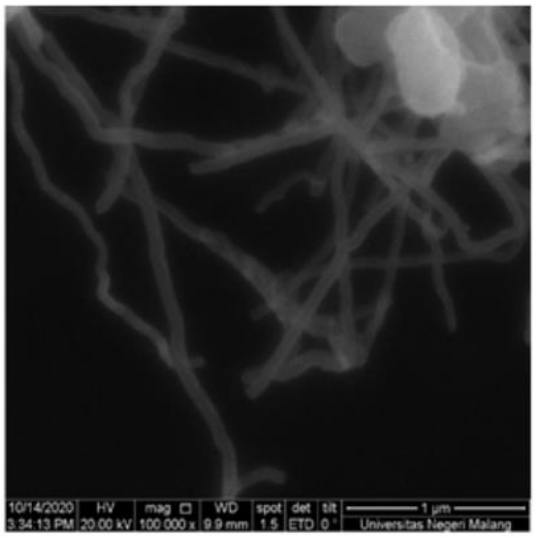
10/14/2020 HV mag WD spot det tilt 1 µm
3:34:13 PM 20.00 kV 100,000 x 9.9 mm 1.5 ETD 0 ° Universitas Negeri Malang

1 (b)

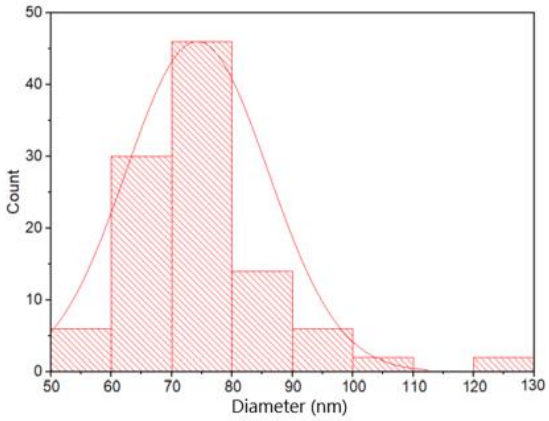
Count
Diameter (nm)
0
10
20
30
40
50
50
60
70
80
90
100
110
120
130

1(c)

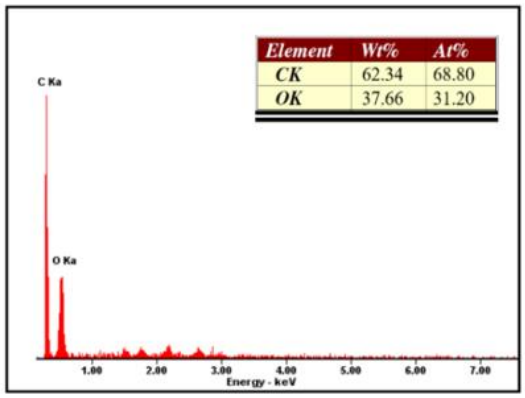
Element Wt% At%
CK 62.34 68.80
OK 37.66 31.20
C Ka
O Ka
1.00
2.00
3.00
4.00
5.00
6.00
7.00
Energy - keV

1(d)

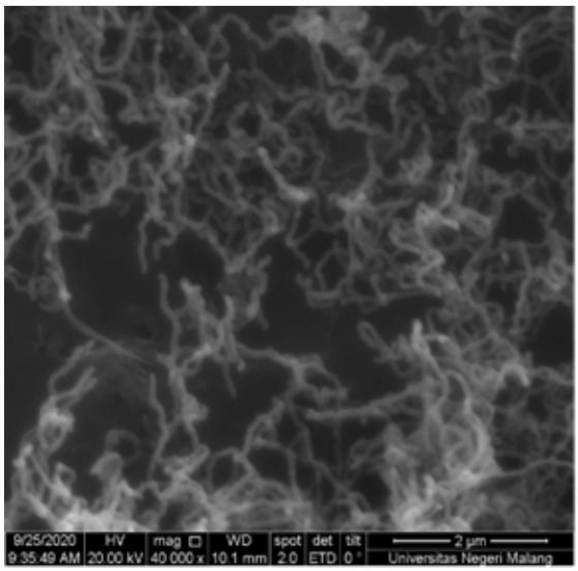
9/25/2020 9:35:49 AM
HV 20.00 kV
mag 40 000 x
WD 10.1 mm
spot 2.0
det ETD
tilt 0 °
2 µm
Universitas Negeri Malang

2 (a)

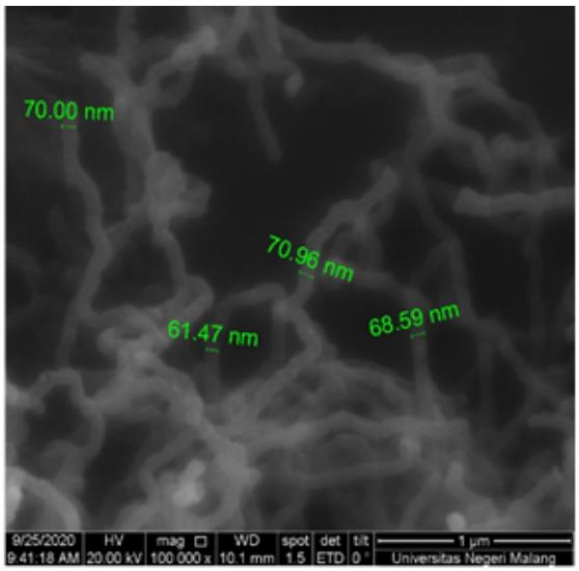
70.00 nm
70.96 nm
61.47 nm
68.59 nm
9/25/2020 9:41:18 AM
HV 20.00 kV
mag 100 000 x
WD 10.1 mm
spot 1.5
det ETD
tilt 0 °
1 µm
Universitas Negeri Malang

2 (b)

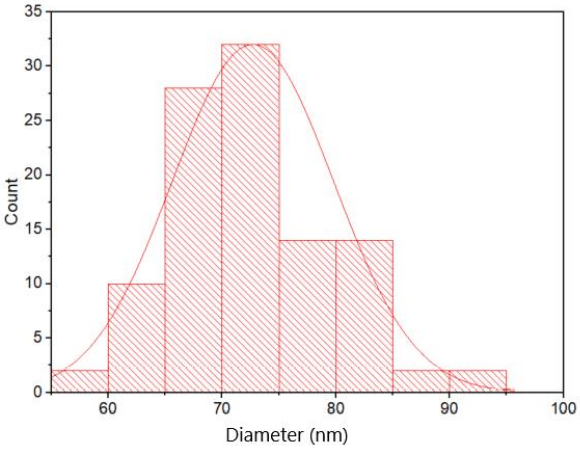
Count
Diameter (nm)
0
5
10
15
20
25
30
35
60
70
80
90
100

2 (c)

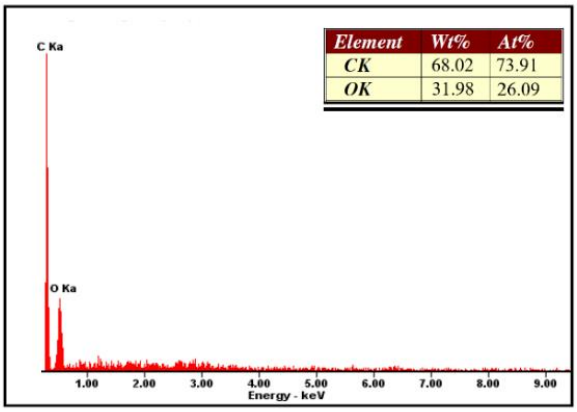
C Ka
O Ka
Element Wt% At%
CK 68.02 73.91
OK 31.98 26.09
1.00
2.00
3.00
4.00
5.00
6.00
7.00
8.00
9.00
Energy - keV

2 (d)

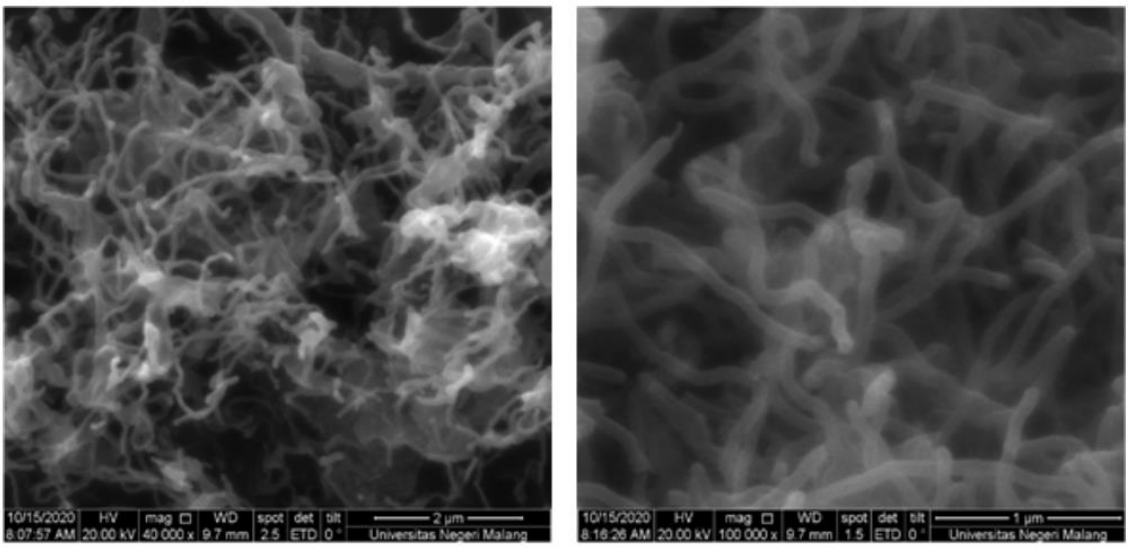

3 (a)

3 (b)

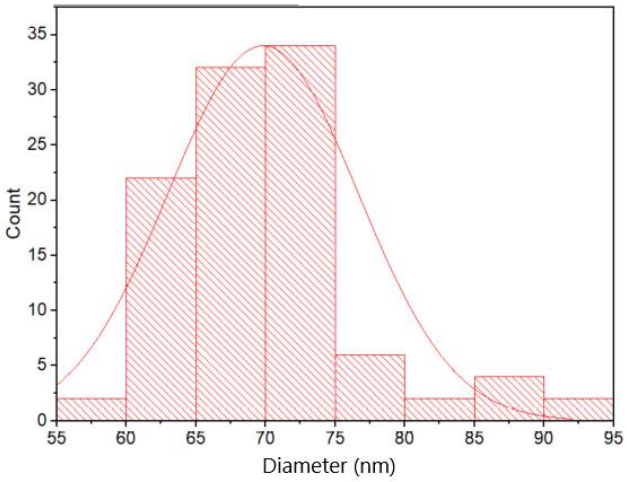

3 (c)

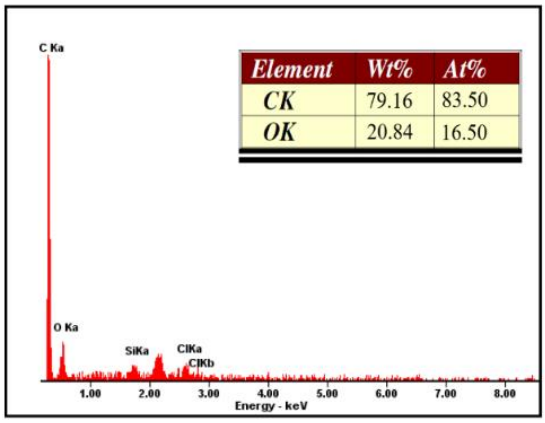

Element	Wt%	At%
CK	79.16	83.50
OK	20.84	16.50

3 (d)

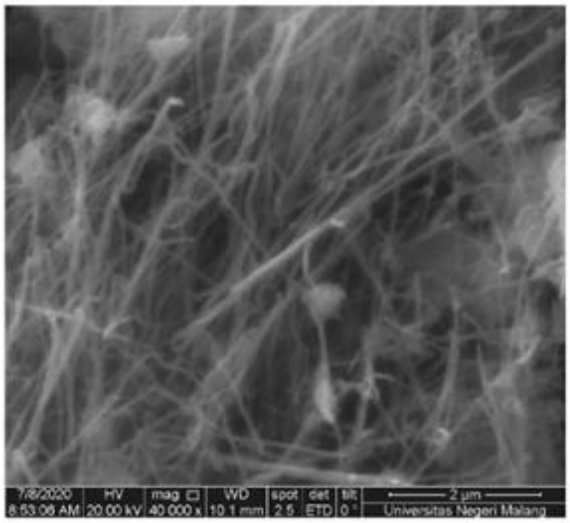
7/8/2020
8:53:06 AM
HV
20.00 kV
mag
40 000 x
WD
10.1 mm
spot
2.5
det
ETD
tilt
0 °
2 µm
Universitas Negeri Malang

4(a)

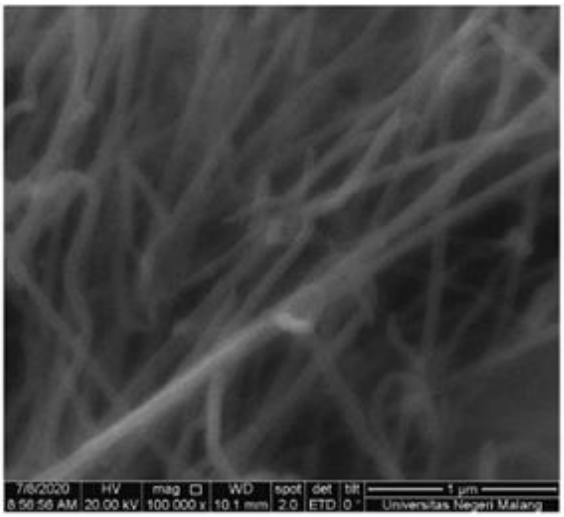
7/8/2020
8:56:56 AM
HV
20.00 kV
mag
100 000 x
WD
10.1 mm
spot
2.0
det
ETD
tilt
0 °
1 µm
Universitas Negeri Malang

4(b)

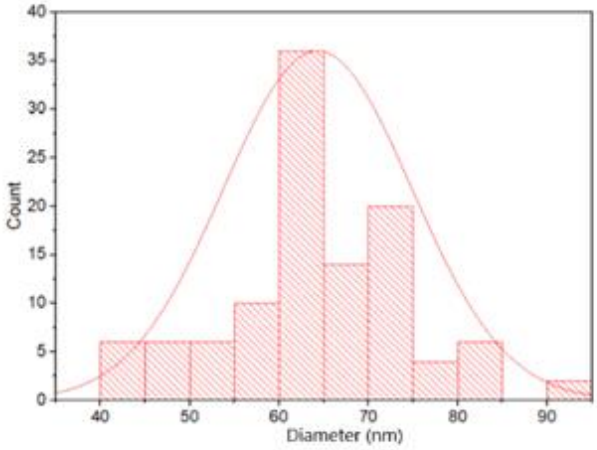
Count
Diameter (nm)
0
5
10
15
20
25
30
35
40
40
50
60
70
80
90

4(c)

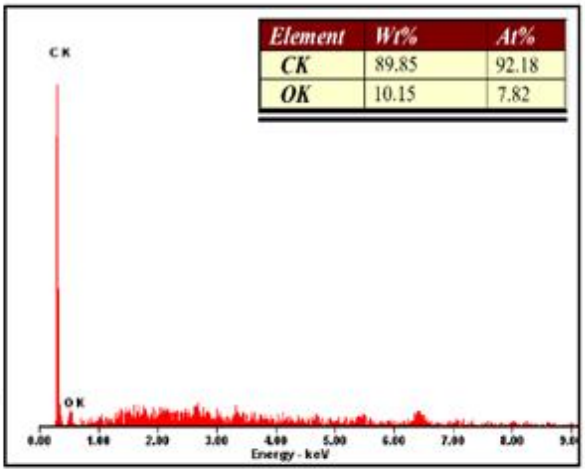
Element
Wt%
At%
CK
89.85
92.18
OK
10.15
7.82
C K
O K
Energy - keV

4(d)

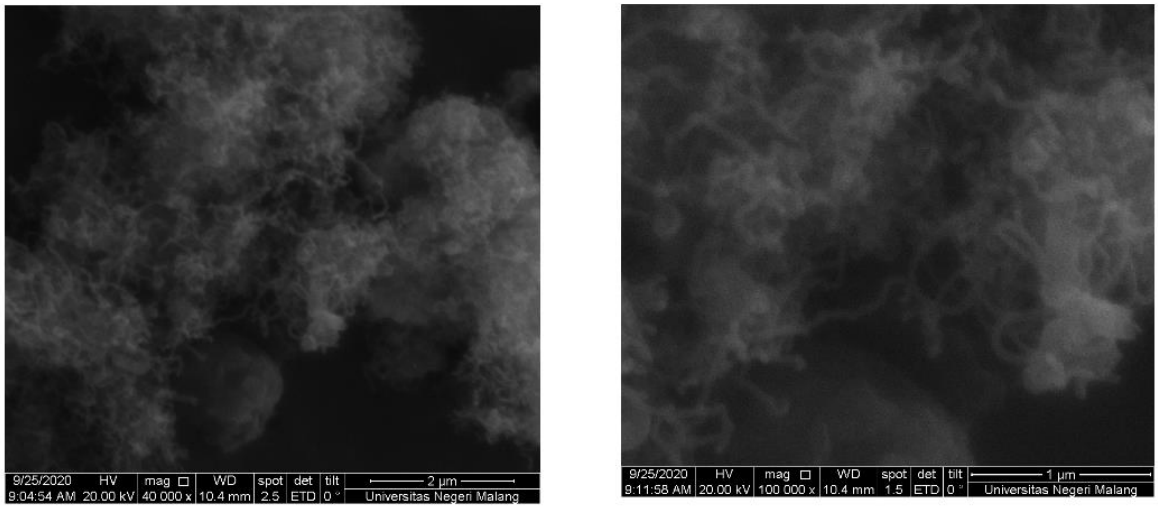

5 (a) 5 (b)

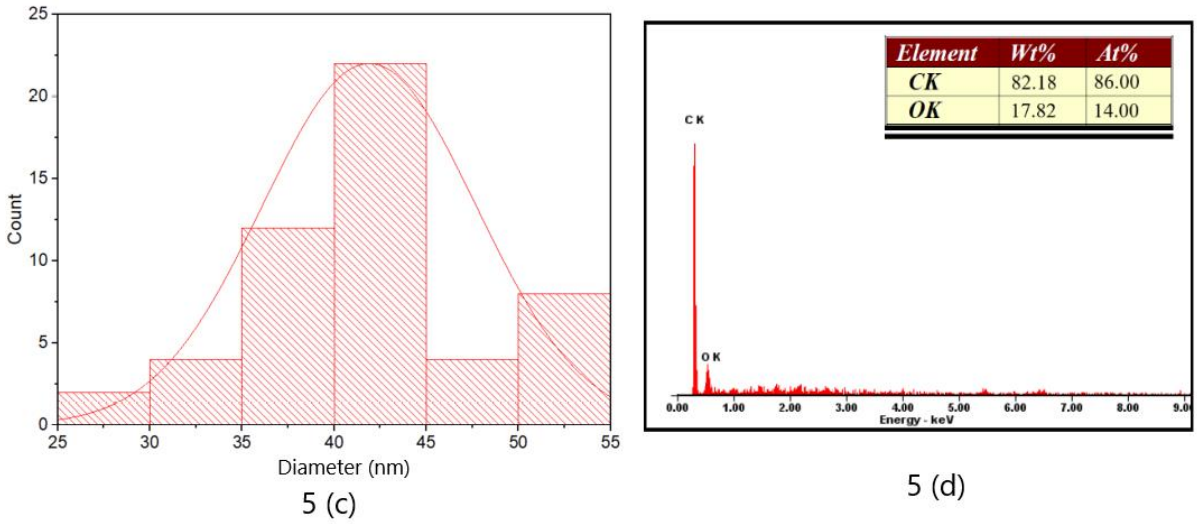

5 (c) 5 (d)

Figure 44 SEM and EDX of analysis of deposited carbon in different synthesis potentials
a,b) SEM image c) Diameter distribution d) EDX
(1) 2V (2) 3V (3) 4V (4) 5V (5) 6V
All measurement (c) is based on image (a)

Morphology of the carbon deposit samples was observed using SEM. SEM analysis on carbon powder with external potentials is shown in Figure 44. Before being tested, the Electrodeposition results were rewashed using HCl to minimize the impurities that might still be attached. SEM analysis shows that the MWCNT tend to be denser with a higher voltage value. This phenomenon might result in excessive energy to convert carbon dioxide to carbon. The

size of MWCNT tends to get smaller with higher voltage. The minor normalized diameter is achieved in 6V followed by 5V, 4V, 3V and 2V with normalised diameter values of 42.5, 65, 70, 72.5, and 75 nm. However, the crystalline size in this experiment might be little affected by voltage, as seen in Table 19. The crystalline size was typical in the ~17-23 nm range.

The identification of carbon growth rates uses the EDX test results, while the MWCNT yield calculation utilised purity value from Raman analysis. Calculate the carbon growth rate and MWCNT yield using equations 12 and 13. The deposition area or the large cross-sectional area of the NiCr cathode used in the Electrodeposition process is 1.57 $cm^{-2,}$ and the synthesis time is 1 hour. The results of calculating the carbon growth rate are shown in Table 21.

Table 21 External potential variable effect on Growth rate and MWCNT yield (1.57 cm^2 NiCr cathode area, 1 hour of Electrodeposition)

Run	External potential (V)	Total deposit mass (gr)	Wt% Carbon	Growth Rate (g cm-2 h-1)	Purity (%)	MWCNT yield (g cm-2 h-1)
1	2	0.72	62.34%	0.894	42.81	0.61
2	3	2.29	68.02%	1.264	44.66	0.83
3	4	3.31	79.16%	1.542	64.56	1.26
4	5	3.88	89.85%	1.787	88.27	1.76
5	6	3.36	82.18%	1.599	71.47	1.39

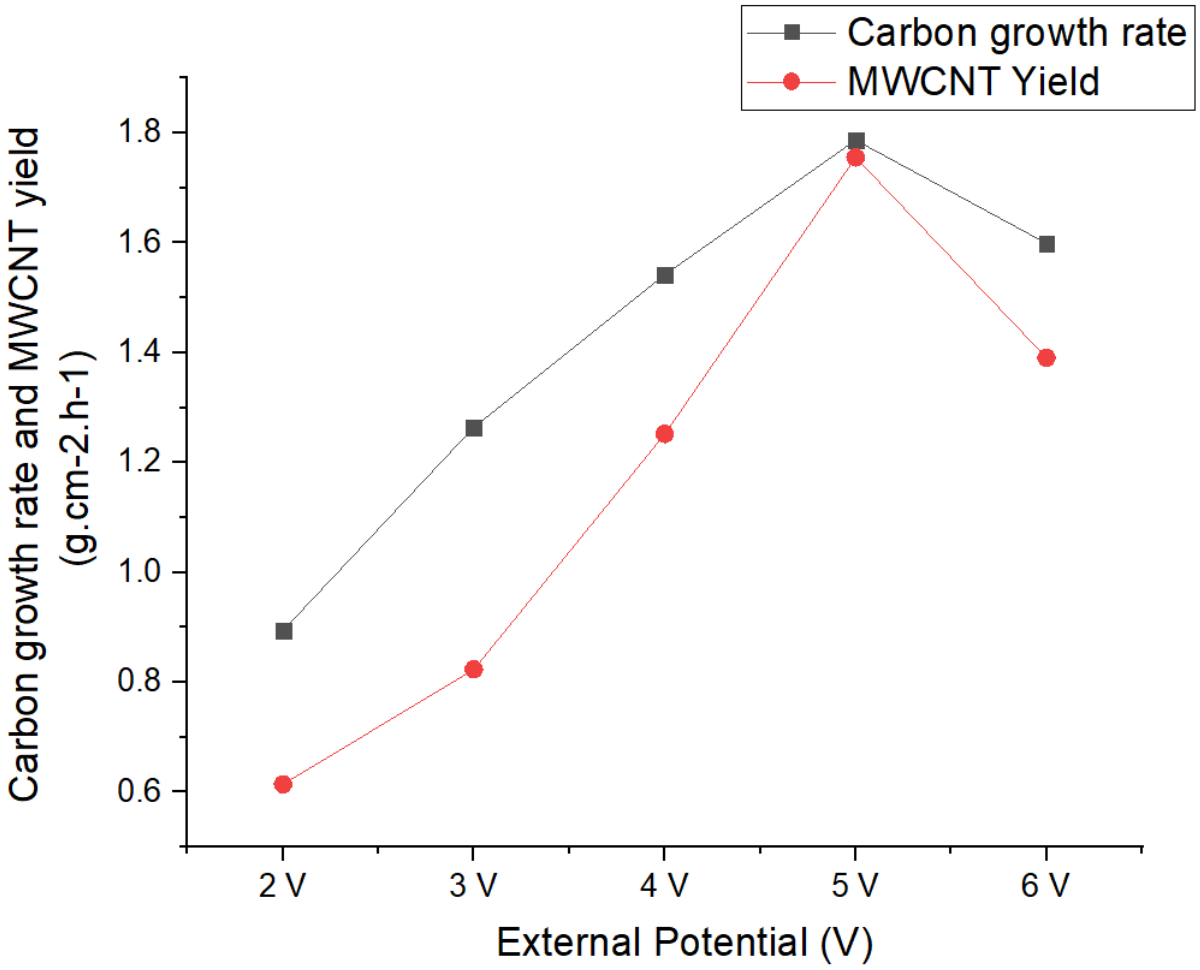

Figure 45 Growth rate of carbon and MWCNT yield in different external potential

Table 21 and Figure 45 show that the carbon growth rate increases in line with the value of the external potential until the 5V value, and the value decreases at 6V. The highest carbon growth rate was obtained at 5 V external potential with 1.787 gr.cm^{-2}.hour^{-1} at the temperature of 773°C for 60 minutes. It is also worth mentioning that the result is in line with this in a previous study; in addition, with higher voltage (> 5V), the current efficiency decrease and energy consumption increases [82].

4.4.3 Carbon source flowrate effect on Electrodeposition

The use of atmospheric CO_2 in the Electrodeposition is possible but bubbled (injection of CO_2 into molten carbonate) method is superior. The bubbled way lowers the voltage and increases the current, associated with the faster CO_2 reduction process[98]. The further rapid reduction also seems to happen with the increase of CO_2 injected into the system. The rapid reduction due to the reaction of Li_2O back to the original lithium carbonate may be strongly favourable (eq 25)[78]. However, it is hard to pinpoint the CO_2 needed in the Electrodeposition since it needs to match the reaction speeds. The reaction speed depends on many variables, and the instability of the variables also plays a role. The higher CO_2 introduced in the system potentially increases impurities, while a lower number might hold up carbon production. In this experiment, one factor at a time (OFAT) model clusters vary CO_2 flow rates. Table 22 present the experiment settings.

Table 22 One Factor at a time (OFAT) model clusters varying CO_2 flowrates

Run	Temperature (°C)	External potential (V)	CO_2 Flow (ml/min)	Time (m)	Cathode
First OFAT experiment cluster					
1	773	5	5	60	NiCr
2			50		
3			95		
4			140		
5			185		

$$Li_2CO_3 \rightarrow C + Li_2O + O_2 \qquad \text{Equation 15}$$

$$Li_2O + 2CO_2 \rightarrow Li_2CO_3 + C + O_2 \qquad \text{Equation 16}$$

$$CO_2 \rightarrow C + O_2 \qquad \text{Equation 17}$$

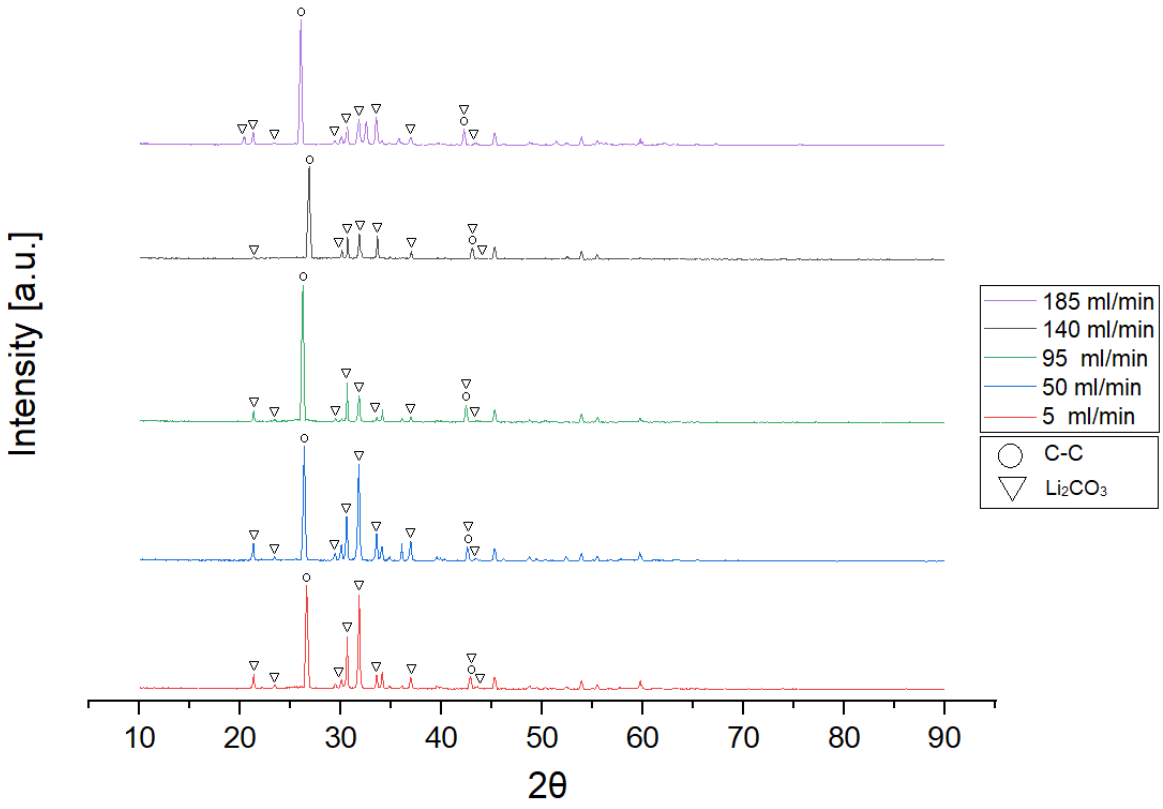

Figure 46 XRD carbon at 5 ml/min, 50 ml/min, 95 ml/min, 140 ml/min dan 185 ml/min

Table 23 Phase of XRD test result on various CO_2 flowrate

No	CO_2 Flowrate	FWHM	Crystalline size D (nm)
1	5 ml/min	0.422	19.38
2	50 ml/min	0.404	20.18
3	95 ml/min	0.442	18.46
4	140 ml/min	0.457	17.86
5	185 ml/min	0.468	17.43

The phase identification process of carbon powder was carried out by inspecting XRD characterisation results to compare the carbon powder's crystal phases. Based on Figure 46, it can be seen that the peak from the XRD graph shows the carbon phase, and the average location of the highest peak is 2θ 26°, with different peak heights. At the same time, the lithium carbonate is at ~2θ 33°. There is no clear pattern of the CO_2 flow rate effect on the crystalline soot size shown in Table 23, ranging from ~17-21 nm.

The outcome of Li_2CO_3 electrolysis is Li_2O, C and O_2 (equation 15). The appearance of the Li_2O and CO_2 in the system results in an extension reaction (equation 16). Equation 16 provides the reduction reaction of CO_2 into C and restores Li_2O to its original form, Li_2CO_3. It is also worth mentioning that direct reduction of CO_2 (equation 17) is possible. However, the indirect reduction (equation 15) is thermodynamically favourable and consistent[98].

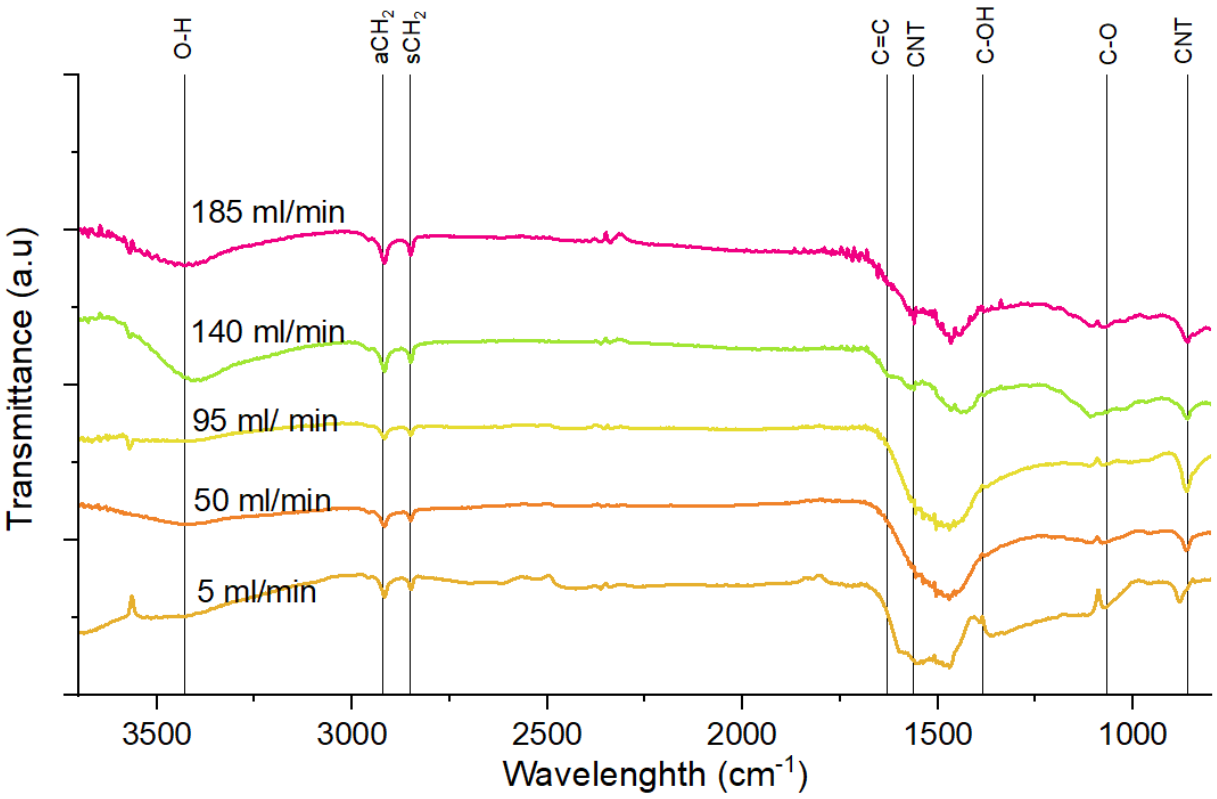

Figure 47 FTIR spectra of cathodic product produced in different CO_2 flow rate

Functional element identification in the cathodic product is analyzed using FTIR (Figure 47). The A_{2u} and E_{1u} arise in all flowrate. However, in the 5 and 50 ml/min, wavelength shifts occur. The shifting could occur due to changes in the level of molecular interaction, the population of chemical species, the functionalization of the vibrational modes or combinations of those three. The evidence of C=C, O-H, sCH_2, and aCH_2 functionalization is arise at 1400-1600 cm^{-1}, 3430 cm^{-1},2830 cm^{-1}, and 2950 cm^{-1} respectively.

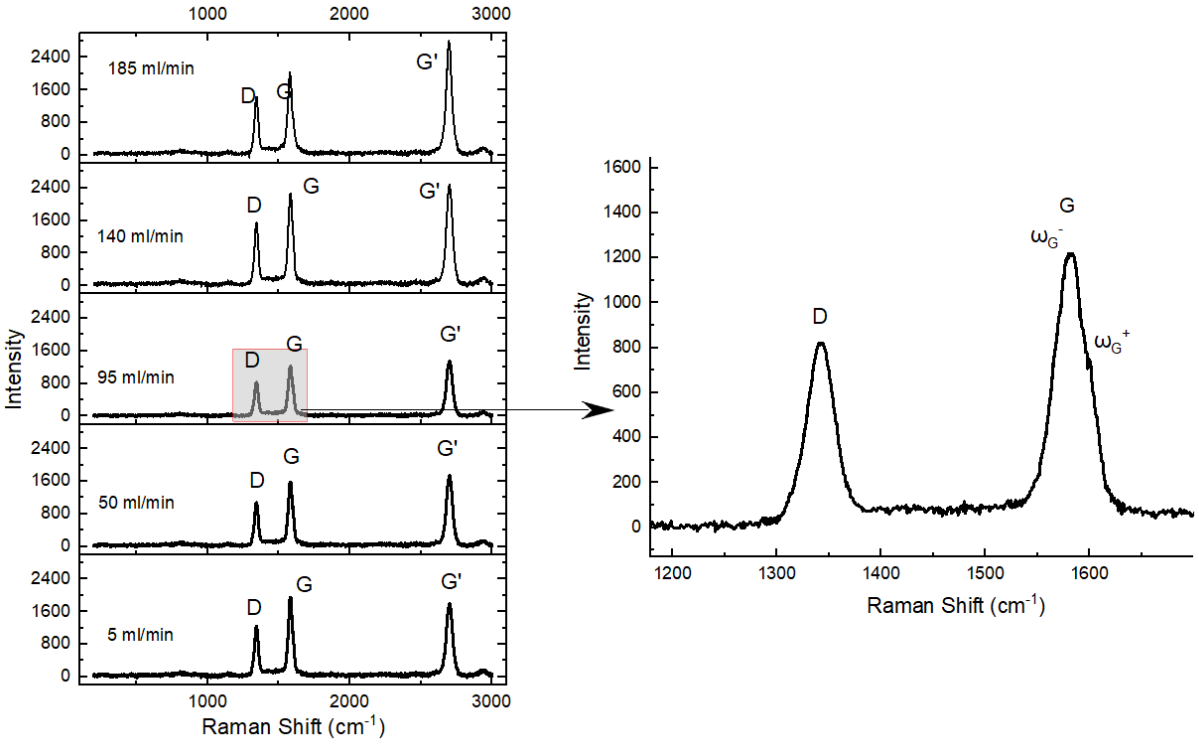

Figure 48 Raman analysis of cathodic product produced in different CO_2 flow rate

Table 24 Raman analysis result of cathodic product produced in different CO_2 flow rate

CO_2 flowrates (ml/min)	ID/IG	IG'/ID	Purity
5.00	0.65	1.55	76.20%
50.00	0.69	1.53	75.42%
95.00	0.71	1.71	80.86%
140.00	0.71	1.79	83.03%
185.00	0.73	2.01	88.27%

The Raman analysis of the cathodic product produced at different CO_2 flow rates (Figure 48 and Table 24) is used to determine the graphitization degree of the soot. The D, G, and G' bands' features consistently arise in all CO_2 flow rates. The normalized intensity I_D/I_G ratio is getting smaller in lower CO_2 flow rates. Since normalized intensity is related to the quality of MWCNT, the lower flow rate tends to produce better quality MWCNT. However, based on the purity value, the opposite pattern occurs: A lower flow rate tends to have low purity.

Morphology analysis utilised SEM to extract outer diameter information of MWCNT in all CO_2 flowrate. The MWCNT outer diameter does not affect the CO_2 flow rate changes with a normalized value of 75-80 nm. The EDX analysis reveals the composition of the soot resulting weight percentage, which changes slightly with the changes in the CO_2 flow rate. However, these changes result in an undefined pattern.

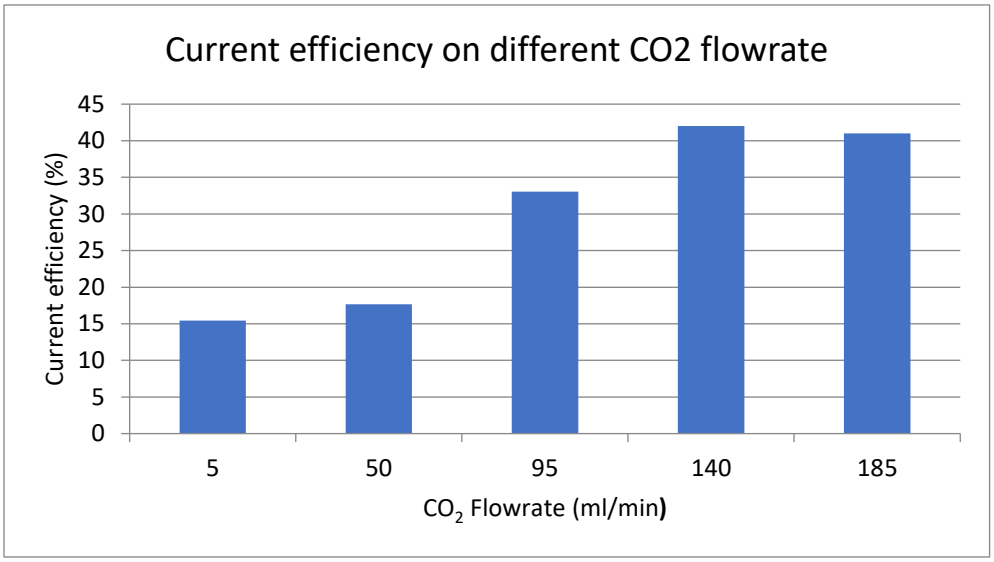

Figure 49 Current Efficiency on Different CO_2 Flowrate

Current efficiency is calculated using equation 18, and the result is described graphicly in Figure 49. The current efficiency seems to increase with the higher value of the CO_2 flow rate from this result. However, a slight reduction of the current efficiency value appears at 185 ml/min. This reduction can be used to predict that the flow rate higher than 185 will have a lower current efficiency value. The morphology of the carbon samples was observed using SEM. The differences in morphological variations of carbon source variations of 5 ml/min, 50 ml/min, 95ml / min, 140 ml/min, and 185 ml/min are shown in Figure 50. Following the potential external pattern, the MWCNT get denser with a higher value of CO_2 flow rate.

$$\text{Current efficiency} = \frac{\text{Deposited carbon}}{\text{Calculated deposited carbon}} \text{X}100\% \qquad \text{Equation 18}$$

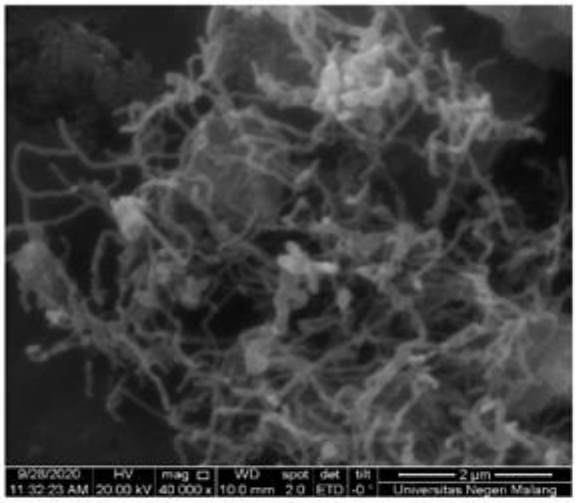
9/28/2020 11:32:23 AM
HV 20.00 kV
mag 40 000 x
WD 10.0 mm
spot 2.0
det ETD
tilt -0 °
2 µm
Universitas Negeri Malang

1(a)

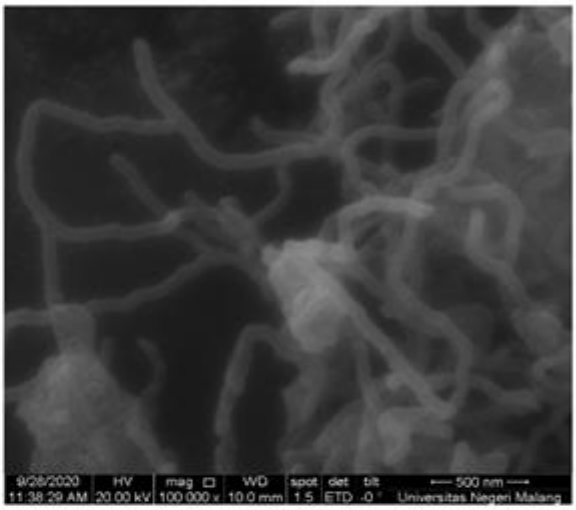
9/28/2020 11:38:29 AM
HV 20.00 kV
mag 100 000 x
WD 10.0 mm
spot 1.5
det ETD
tilt -0 °
500 nm
Universitas Negeri Malang

1(b)

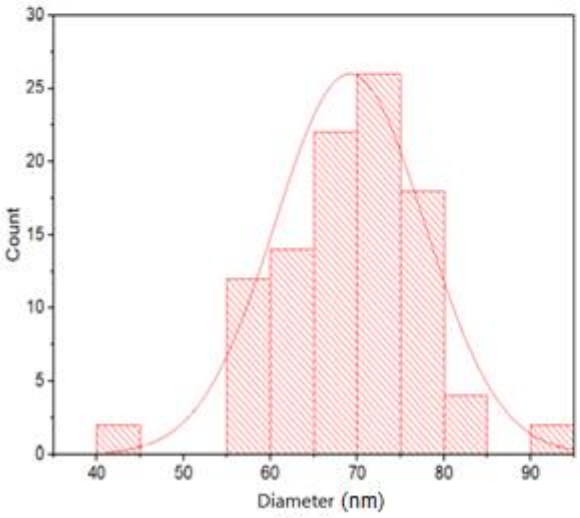
Count
Diameter (nm)
0
5
10
15
20
25
30
40
50
60
70
80
90

1(c)

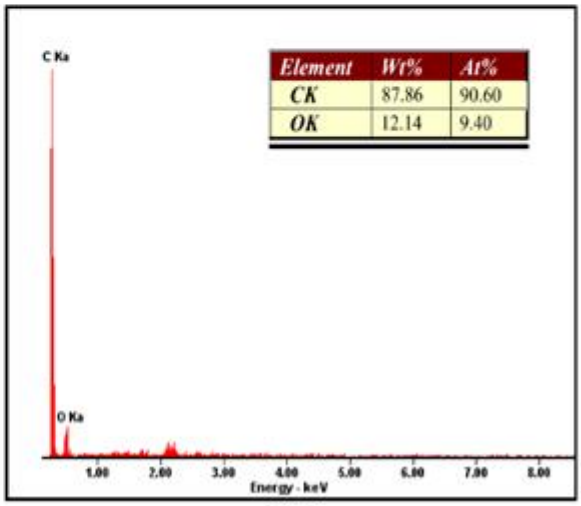
C Ka
O Ka
Element Wt% At%
CK 87.86 90.60
OK 12.14 9.40
1.00
2.00
3.00
4.00
5.00
6.00
7.00
8.00
Energy - keV

1(d)

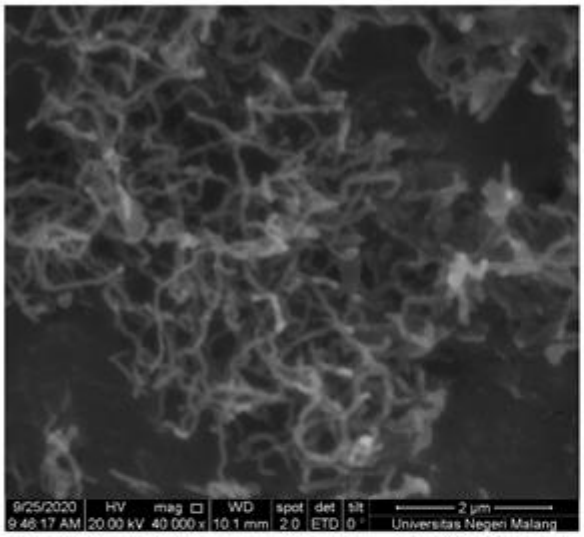
9/25/2020
9:46:17 AM
HV
20.00 kV
mag
40 000 x
WD
10.1 mm
spot
2.0
det
ETD
tilt
0 °
2 µm
Universitas Negeri Malang

2(a)

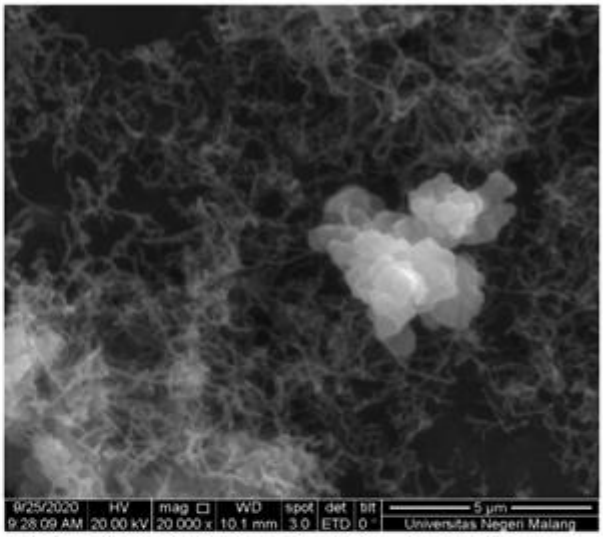
9/25/2020
9:28:09 AM
HV
20.00 kV
mag
20 000 x
WD
10.1 mm
spot
3.0
det
ETD
tilt
0 °
5 µm
Universitas Negeri Malang

2(b)

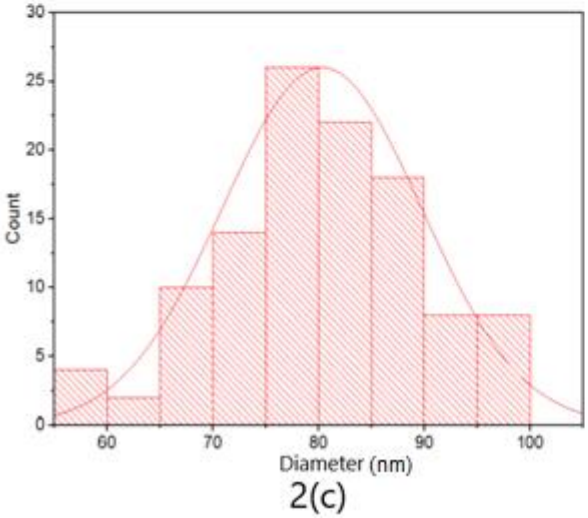
Count
Diameter (nm)
0
5
10
15
20
25
30
60
70
80
90
100

2(c)

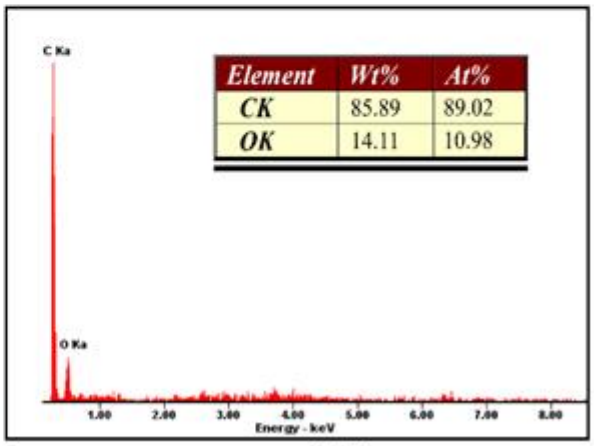
C Ka
O Ka
Element
Wt%
At%
CK
85.89
89.02
OK
14.11
10.98
1.00
2.00
3.00
4.00
5.00
6.00
7.00
8.00
Energy - keV

2(d)

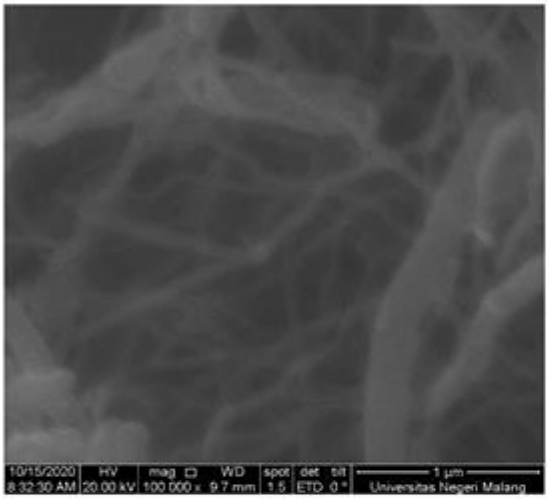

3(a)

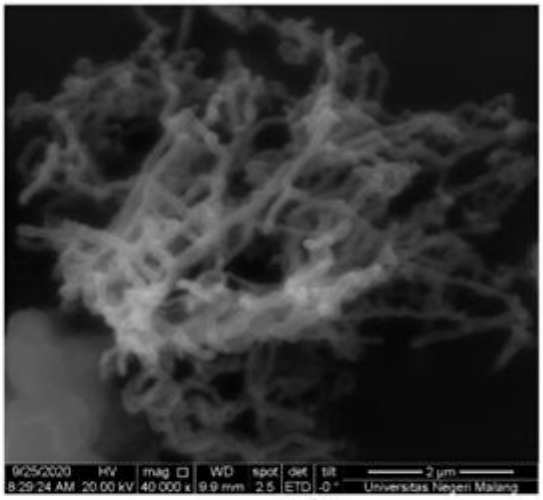

3(b)

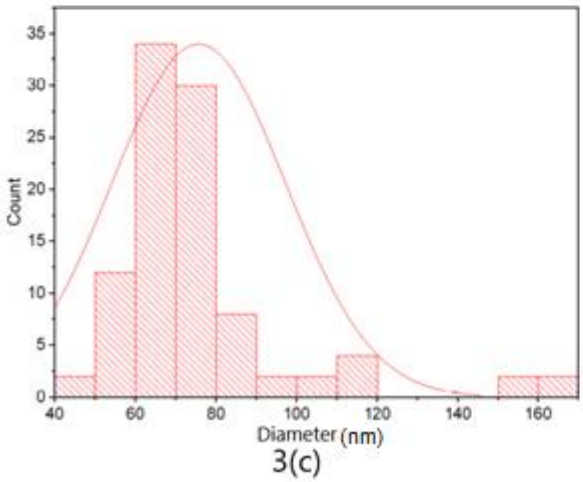

3(c)

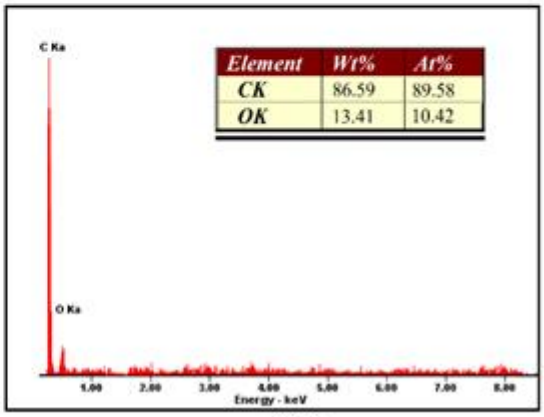

Element	Wt%	At%
CK	86.59	89.58
OK	13.41	10.42

3(d)

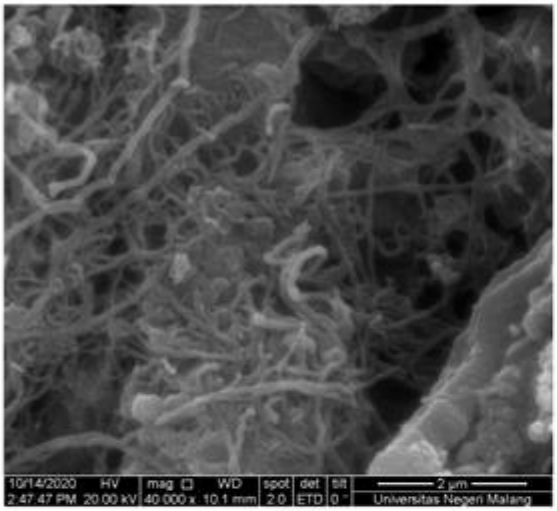
10/14/2020 HV mag WD spot det tilt
2:47:47 PM 20.00 kV 40,000 x 10.1 mm 2.0 ETD 0°
2 µm
Universitas Negeri Malang

4(a)

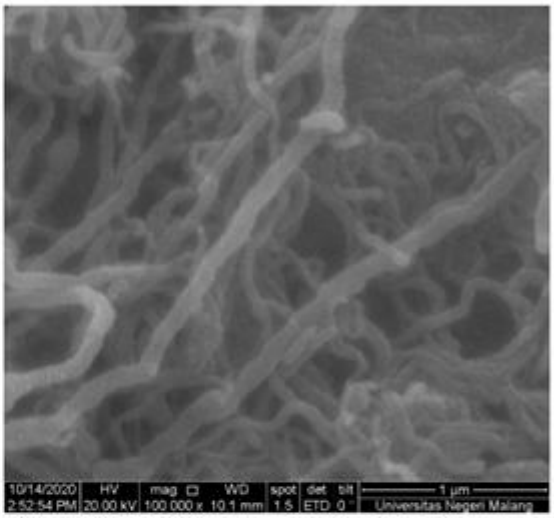
10/14/2020 HV mag WD spot det tilt
2:52:54 PM 20.00 kV 100,000 x 10.1 mm 1.5 ETD 0°
1 µm
Universitas Negeri Malang

4(b)

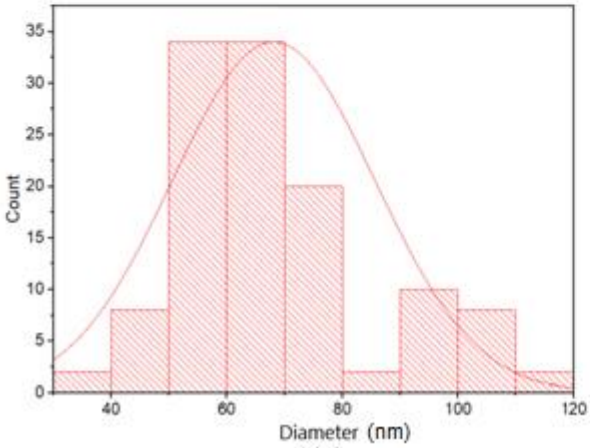
Count
Diameter (nm)
0
5
10
15
20
25
30
35
40
60
80
100
120

4(c)

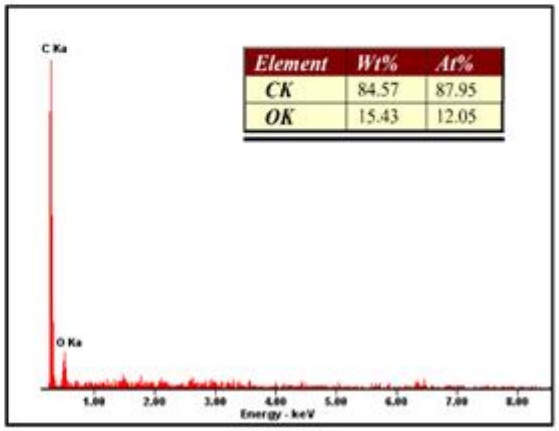
C Ka
O Ka
Element Wt% At%
CK 84.57 87.95
OK 15.43 12.05
Energy - keV

4(d)

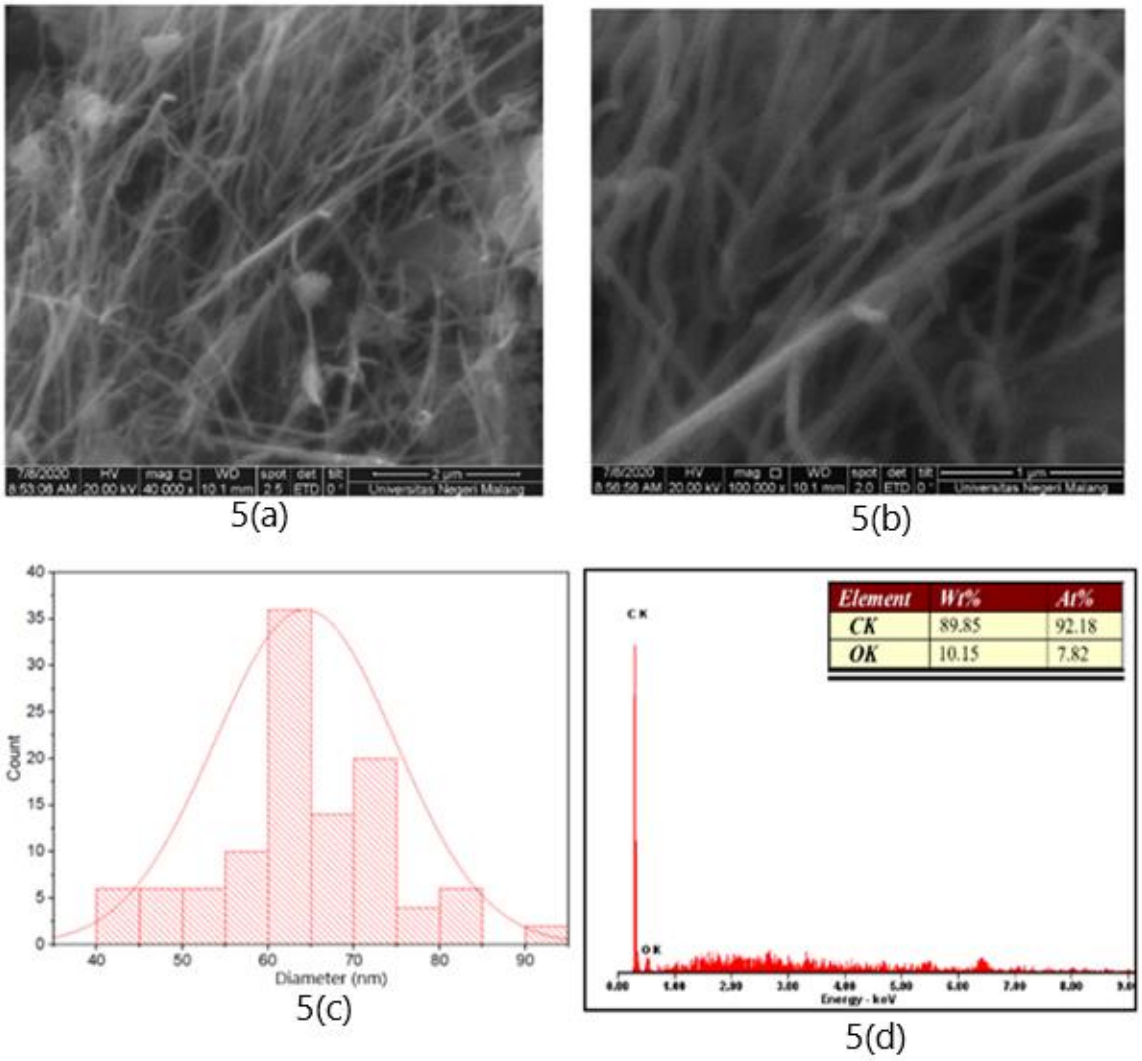

Figure 50 SEM and EDX of analysis of deposited carbon in different CO_2 Flowrate
a,b) SEM image c) Diameter distribution d) EDX
(2) 5 ml/min (2) 50 ml/min (3) 95 ml/min (4) 140 ml/min (5) 185 ml/min
All measurement (c) is based on image (a)

Table 25 Growth rate of carbon and MWCNT yield in different CO_2 flowrate

Run	CO_2 Flowrate (ml/min)	Total deposit mass (gr)	wt% carbon	Carbon Growth Rate (g cm-2 h-1)	Purity (%)	MWCNT yield (g cm-2 h-1)
1	5	2.63	87.86%	1.472	76.20%	1.277
2	50	2.79	85.89%	1.528	75.42%	1.351
3	95	2.67	86.59%	1.672	80.86%	1.375
4	140	3.26	84.57%	1.756	83.03%	1.724
5	185	3.12	89.85%	1.787	88.27%	1.756

The identification of the growth rate is used in EDX analysis results, and the MWCNT yield calculation utilized purity value from Raman analysis. Calculating the carbon growth rate and MWCNT yield can be done using equations 12 and 13, respectively. The total mass of deposit is the total mass-produced after acid treatment, wt% is the carbon weight percentage in the EDX results and %purity is the purity value from Raman analysis. In this experiment deposition area is 1.57 cm^2, and the Electrodeposition time is 1 hour. The results of calculating the carbon growth rate and MWCNT yield are shown in Table 25.

Table 25 shows that the carbon growth rate increases with the carbon source flow rate (CO_2). The highest deposition rate is in the variation of carbon source 185 ml/min of 1.787 g cm^{-2} h^{-1} with a temperature of 773°C for 60 minutes. Figure 51 describes the rate of carbon growth increasing. Nevertheless, in Figure 51, the increasing carbon sources, the impurities, and residues in the carbon also increase, indicating lower wt% in higher CO_2 flow value. Increased contaminant and residue make impurity processes more challenging to carry out, increasing the costs or effort for impurity processes.

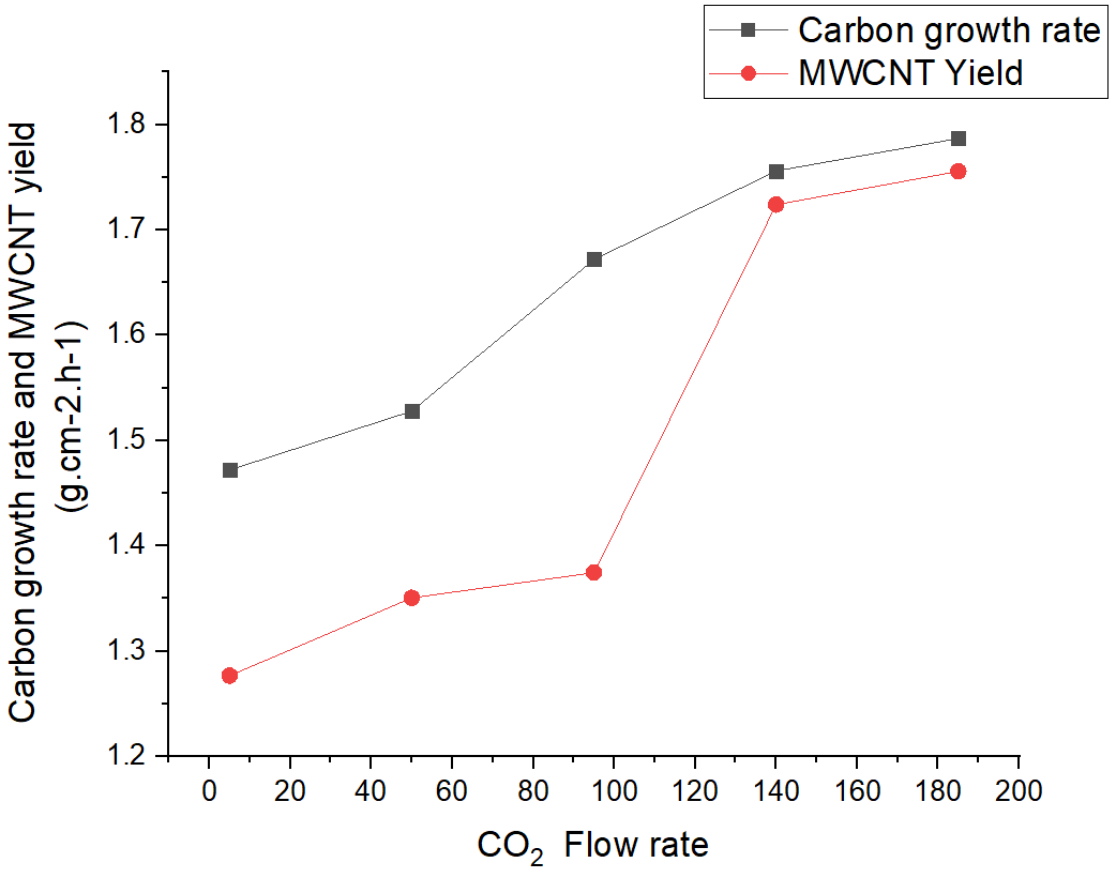

Figure 51 Growth rate of carbon and MWCNT yield in various CO_2 flowrate

4.4.4 Electrode effect on Electrodeposition

The Electrodeposition of CNT in this study used several electrodes (Nikel-Nikel, Cu-Nikel, Galvanis-Nikel, SS-Nikel, NiCr-Nikel) to study each behaviour on the final carbon product. The CNT formation process is directly influenced by the composition and properties of the electrode material. The choice of the electrode material to be used is crucial because it must withstand high temperatures, have good conductivity and stability, be inert, and, most importantly, act as a surface metal catalyst.

The introductions of surface metal catalysts open new possibilities for nanostructure formations in electrochemical techniques[140][141]. Many metal catalysts with their alloys can be used in the Electrodeposition, namely Ni, Fe, Co, Mo, Cu, and Zn. In a recent study, the most prominent metals are Ni, Cu, Fe, and Ni-Cr, galvanized steel and stainless steel[56][57].

In those studies, J. Ren et al. conclude that Ni, Cu, and Fe are vital to avoid spherical carbon shapes, and excessive Fe in the system will favour amorphous C growth. Therefore metal catalysts used in this study were Ni, Cu, Galvanized steel, Stainless steel, and Ni-Cr. Other factors that might also need to be considered in the electrode selection are the standard electrode potential value on each electrode used, which will affect the redox rate during Electrodeposition. However, this might only affect the carbon deposit and is unlikely to affect the growth of CNT since the more prominent factor is the metal catalyst. One factor at a time (OFAT) model clusters varying external potential in this experiment. Table 26 present the experiment settings.

Table 26 One Factor at a time (OFAT) model clusters varying electrodes

Run	Temperature (°C)	External potential (V)	CO_2 Flow (ml/min)	Time (m)	Cathode
1					Cu
2					Galvanis
3	773	5	185	60	Ni
4					NiCr
5					SS

The Electrodeposition process produces carbon deposits on the cathode with each electrode pair, resulting in a different sediment mass and CNT purities. The physical changes of the electrodes before and after the Electrodeposition process can be seen in Figure 52. After the Electrodeposition is complete, the electrodes are removed from the furnace and followed through purification by a sonic bath and acid treatment using the HCL solution to remove adhered electrolytes and other possible impurities.

Figure 52 Electrode profile before and after the Electrodeposition process

XRD analysis (Figure 53 and Table 27) examined the Electrodeposition samples' phase and crystallinity. This analysis was performed on the 2θ angle range of 10°-90°. Based on Figure 53, it can be seen that the peak of the C-C (002 miller indices) is in the range of 2θ 26°, with different peak heights on each cathode. It is also seen that each variation of the electrode material produces a distinct diffraction pattern. The highest C- C peak was found in cathodic product samples using Ni-NiCr electrodes with the peak position at 26,21° 2θ and with a height of 3843 counts. The XRD analysis showed that the Li_2CO_3 and Li_2O are present after the purification process, which means the impurities remain after the purity process, including ultrasonic bath and acid treatment. Therefore the second process is needed to minimize impurities. The crystalline calculation can be performed using the previous research method[136]. From the crystalline analysis, single metal electrodes seem to have more extensive crystalline compared to multi-metal electrodes.

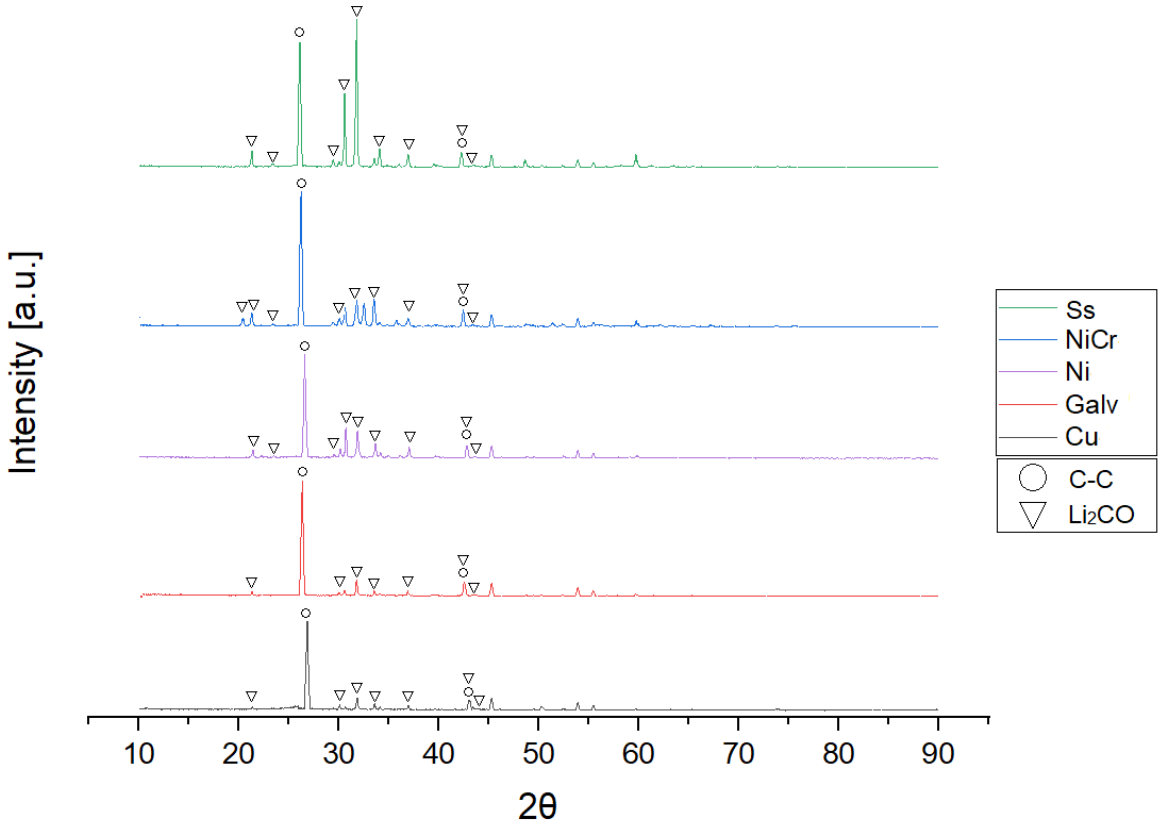

Figure 53 Diffractogram XRD deposited carbon in different cathodes.

Table 27 XRD Phase result in different electrode

No	Electrode	FWHM	Crystalline size D (nm)
1	Cu	0.352	23.188
2	Galvanis	0.386	21.142
3	Ni	0.472	17.285
4	NiCr	0.468	17.43
5	SS	0.472	17.288

The characterisation of functional elements absorbed by CNT is using FTIR (Figure 54). The IR-active attribute of C=C, O-H, sCH_2, and aCH_2 is 1400-1600 cm^{-1}, 3430 cm^{-1},2830 cm^{-1}, and 2950 $cm^{-1,}$ respectively, indicating carboxylic and hydroxylic functional groups in all cathodic products. Primary CNT modes A_{2u} and E_{1u} were also active at 868 and 1575 cm^{-1}. However, in galvanized steel (Galv), Nickel (Ni) and Copper (Cu), the wavelength upshift occurs. The shifting frequency is possible due to the changes in molecular interaction level or changes in

the population of different chemical species in the purification process. Therefore this shifting is related to the functionalization of the vibrational modes, which do not reflect the phonon dynamic of CNT.

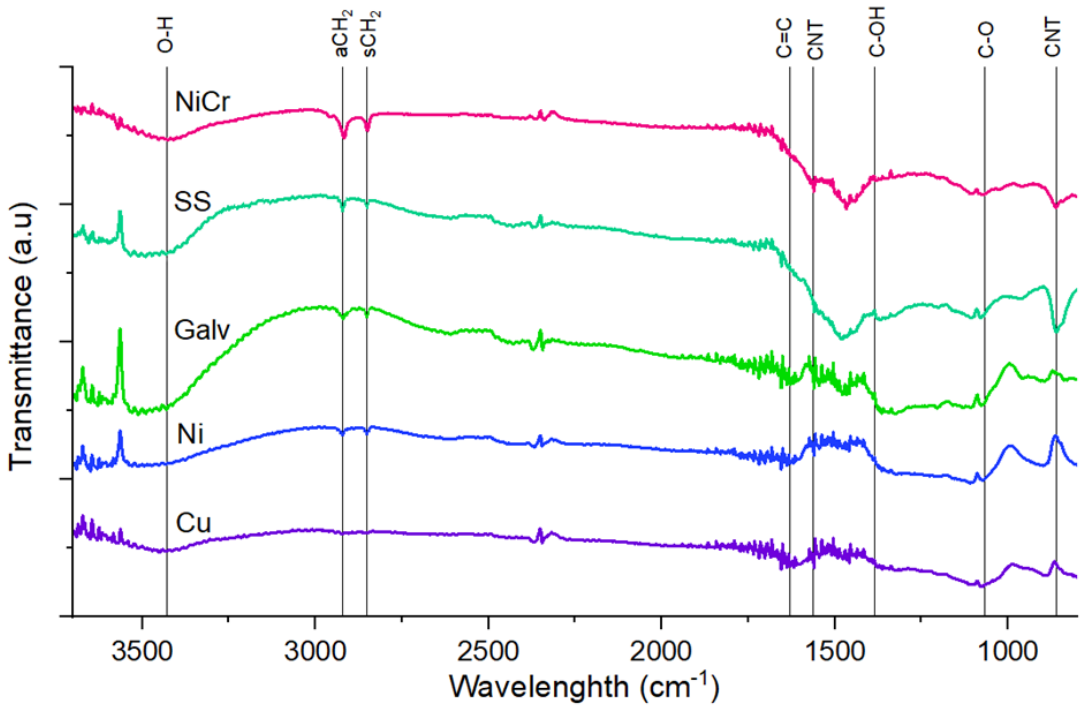

Figure 54 spectra of cathodic product produced in different cathodes

The interpretation of Raman analysis of carbon nanotubes has been studied extensively in previous research[142][143][144][27]. Raman spectra of carbon soot from Electrodeposition synthesis with various cathodes are shown in Figure 55 and Table 28. Five different cathodic products were examined. Three dominant Raman spectra features were seen: D band, G band, and second-order harmonic G' band. The first indication of nonappearance of the SWCNT is no indication of RBM. RBM are Raman spectra features exclusively to SWCNT with a diameter under ~2 nm. Apart from RBM, the absence position and intensity of Raman peaks are in good agreement with theoretical calculations and previous experimental studies. Another subtle feature is the split of the G band into ω_{G^-} and ω_{G^+} also distinguishable.

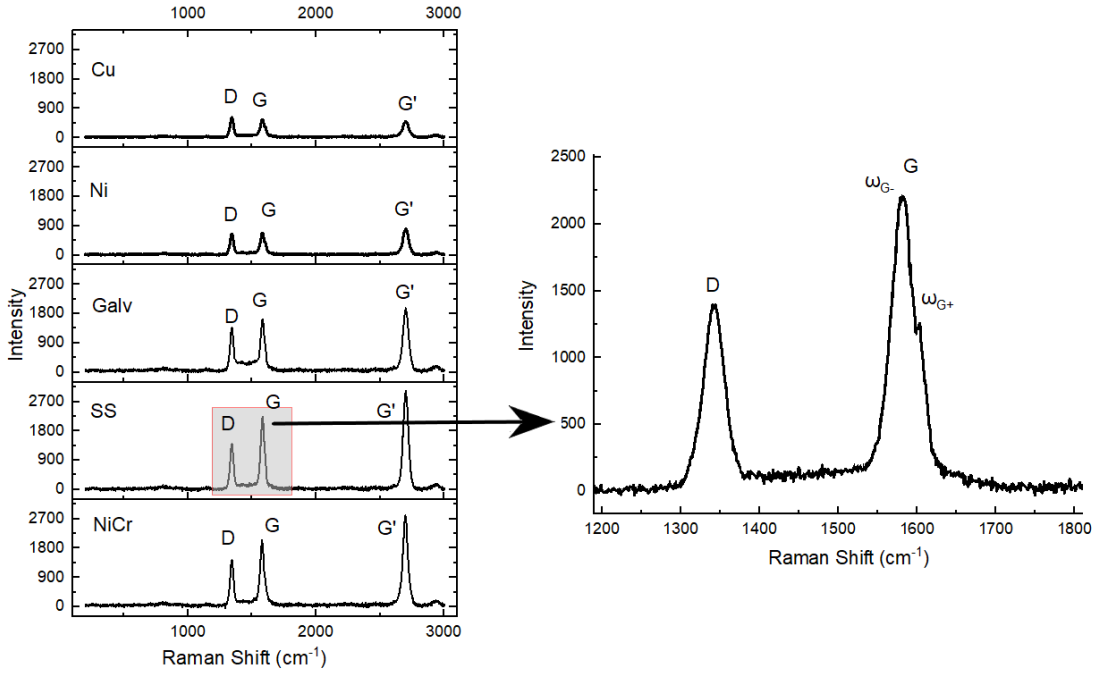

Figure 55 Raman spectroscopy from the cathodic product by Electrodeposition method using Nichrome (NiCr), Nickel (Ni), Galvanized steel (Galv), Copper (Cu) and Stainless steel (SS) cathode.

Table 28 Raman analysis result of cathodic product produced in different cathodes

Electrode	ID/IG	IG'/ID	Purity (%)
Cu	1.13	0.74	41.54%
Galvanise	0.87	1.16	62.47%
NiCr	0.73	2.01	88.27%
Ni	0.98	1.29	67.35%
SS	0.64	2.19	92.32%

The first sharp and third peaks from the left are the D and G bands, which indicate disorders of sp^2 and its second-order harmonic, seen at 1350 cm-1 and 2700 cm^{-1}, respectively. The RBM feature is not detected, indicating the cathodic product unlikely contain SWCNT. Being disorder related to graphene-based material, the D band can swift up to a hundred cm^{-1} of wavelength. It is also considered a unique feature distinguishing one carbon product from another. The weaker D band is regarded as higher purity or less defective product.

G band is related to the C-C bond stretching, the signature in all sp^2 carbon. The G band will split into ω_{G^-} The G band is related to the C-C bond. Because of the characteristics of rolling up graphene sheets such as carbon nanotubes, the G band will split into ω_{G^-} and ω_{G^+}. These G bands split arise from all variety cathode Raman results. Normalised intensity (I_D/I_G ratio) will provide information on CNT quality since the absolute measurement of I_D is problematic. The lowest I_D/I_G ratio is achieved by stainless steel cathode, followed by Nichrome and galvanized steel, and the highest ratio is achieved by copper, followed by nickel cathode.

G' band is related to the number of CNT layers and geometry, which appear at ~2700 cm-1 for Elaser = 2.41 eV. With a smaller diameter of SWCNT, these feature intensities will be higher than the G band. However, the G' band in Raman spectra will result in a Lorentzian shape with significantly reduced intensity with a multilayer CNT. Usually, the Lorentzian peak is inhabited by up to 13 peaks, which occur close in frequency, resulting in hard to distinguish from each other.

The purity assessment has been studied extensively either for SWCNT and MWCNT. The characteristic of the Raman peak ratio could be used as guidance for this assessment. However, using different E_{laser} will result in different ratios, affecting the Raman peak ratios. Previous research found that the $I_{G'}/I_D$ ratios profile remains identical with E_{laser} changes[47] because I_D is E_{laser} independent when measured in the 1.9-2.7 eV range[34]. Stainless steel produces the highest purity, followed by nichrome, nickel, galvanized steel, and copper from a purity value perspective.

SEM analysis examines the CNT's morphology for each variation of the electrode material. CNT is shown with an elongated tube shape that is visible, and a little lump is thought to be the residue of Electrodeposition. Figures 56 3(a),3(b),4(a), and 4(b) show that less residue appeared in NiCr and stainless steel cathode than in the other electrodes. The CNTs are relatively straight from the NiCr and stainless steel cathode from all the electrode materials,

which is also agreed by the normalised intensity (I_D/I_G ratio) result. The outer diameter of MWCNT analysis shows nickel produces the minor diameter at a normalised value of 55 nm, followed by stainless steel, nichrome, galvanized steel and copper at 60, 65, 70 and 300 nm, respectively. From EDX wt% value standpoint, the highest carbon wt% is achieved by stainless steel, followed by nichrome nickel, galvanized steel, and copper.

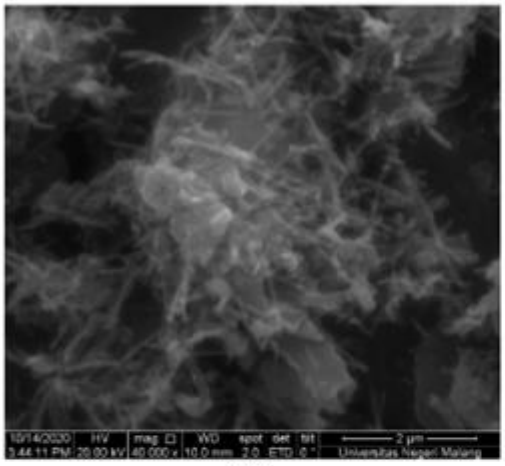

1(a)

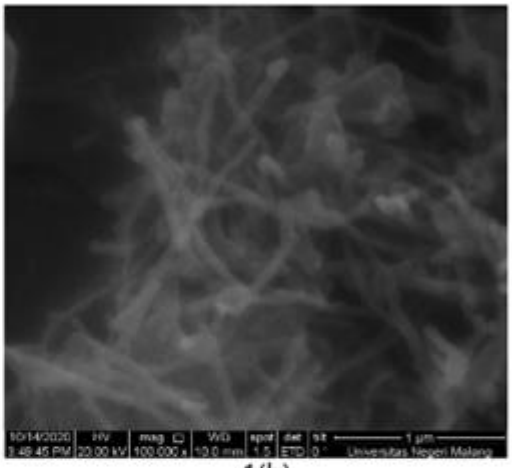

1(b)

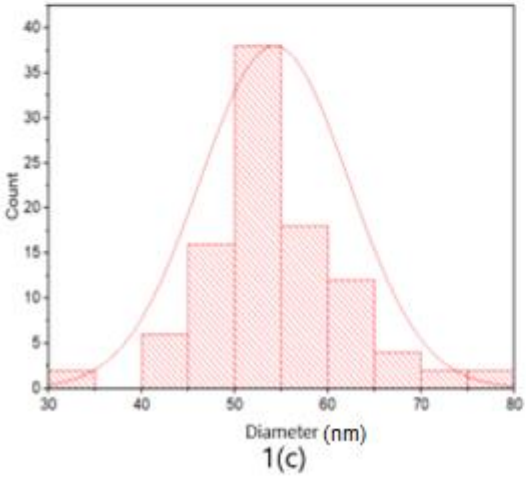

1(c)

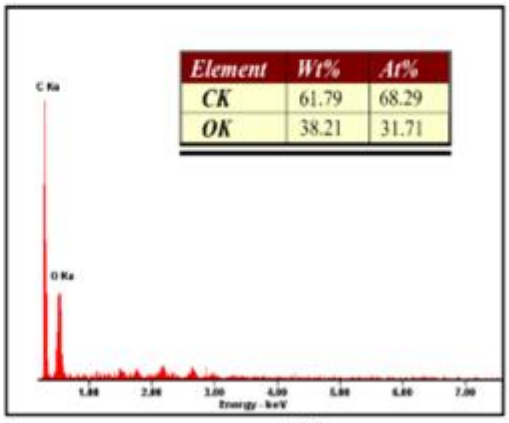

1(d)

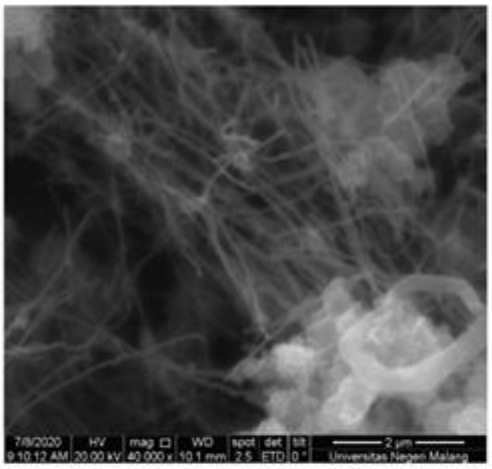

2(a)

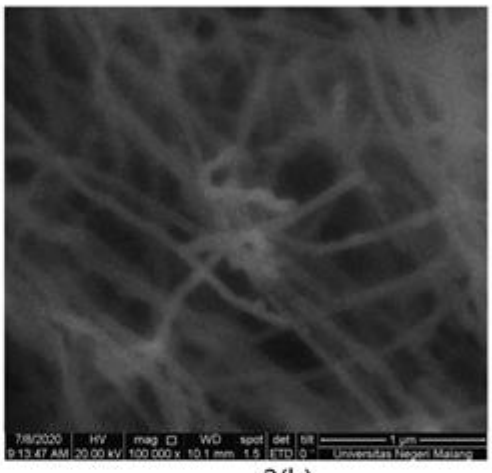

2(b)

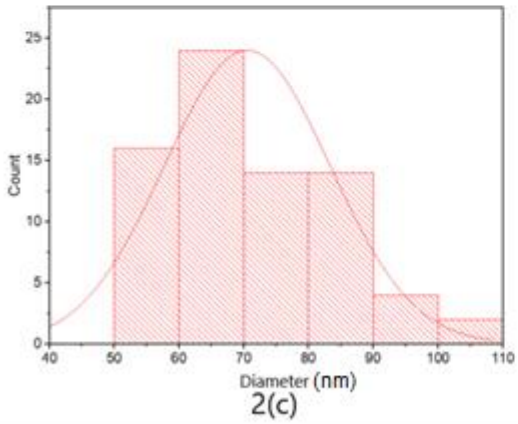

2(c)

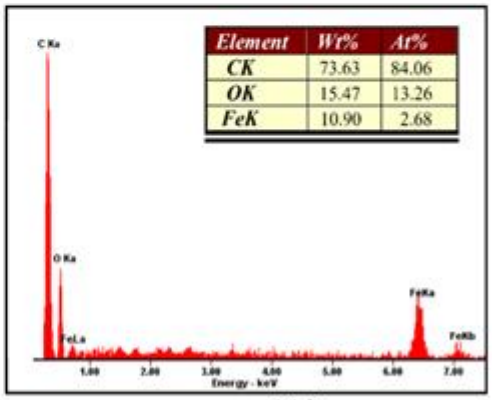

Element	Wt%	At%
CK	73.63	84.06
OK	15.47	13.26
FeK	10.90	2.68

2(d)

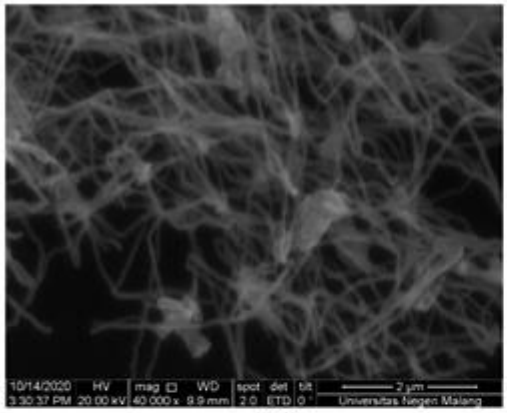

3(a)

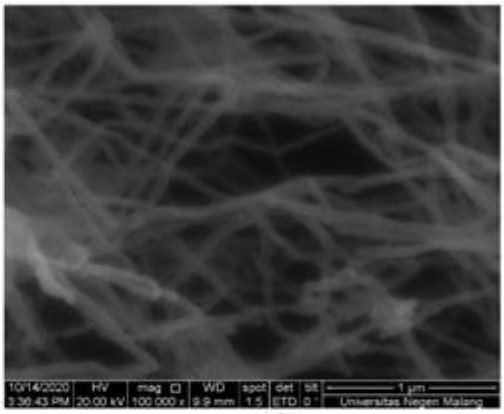

3(b)

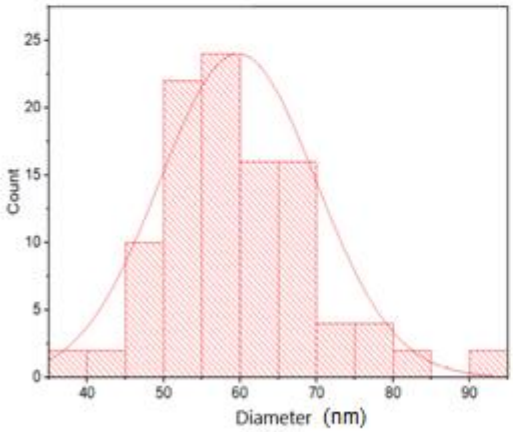

3(c)

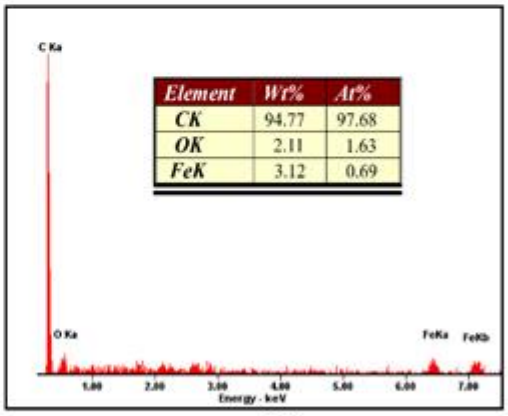

Element	Wt%	At%
CK	94.77	97.68
OK	2.11	1.63
FeK	3.12	0.69

3(d)

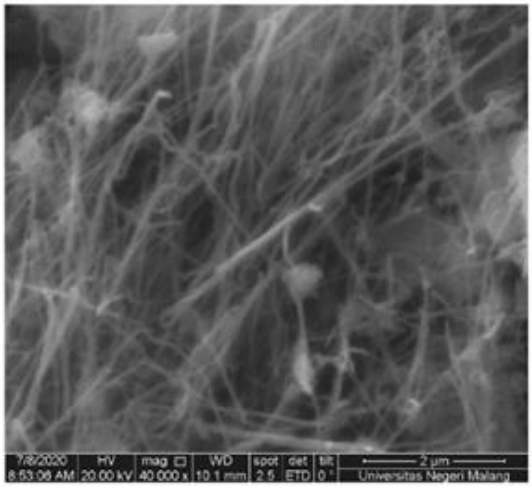
7/8/2020 8:53:08 AM
HV 20.00 kV
mag 40 000 x
WD 10.1 mm
spot 2.5
det ETD
tilt 0°
2 µm
Universitas Negeri Malang

4(a)

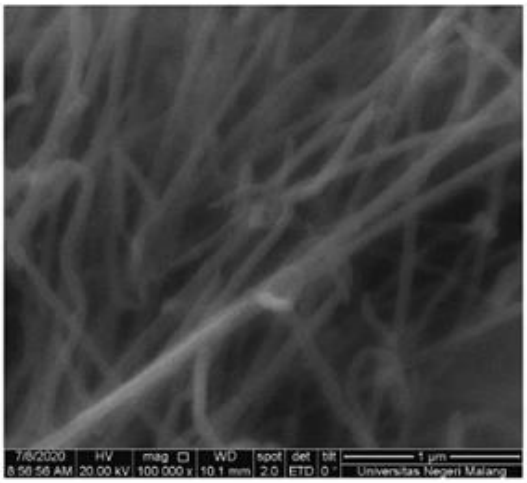
7/8/2020 8:50:56 AM
HV 20.00 kV
mag 100 000 x
WD 10.1 mm
spot 2.0
det ETD
tilt 0°
1 µm
Universitas Negeri Malang

4(b)

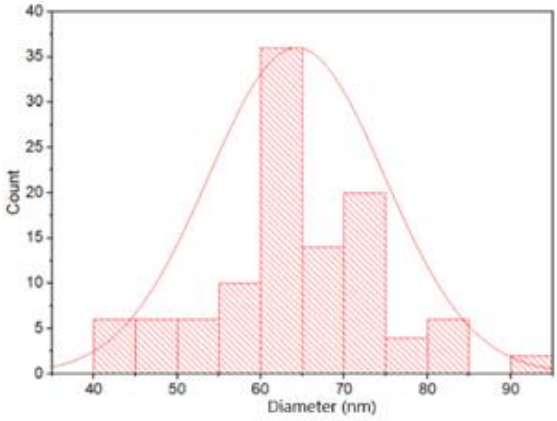
Count
Diameter (nm)
0
5
10
15
20
25
30
35
40
40
50
60
70
80
90

4(c)

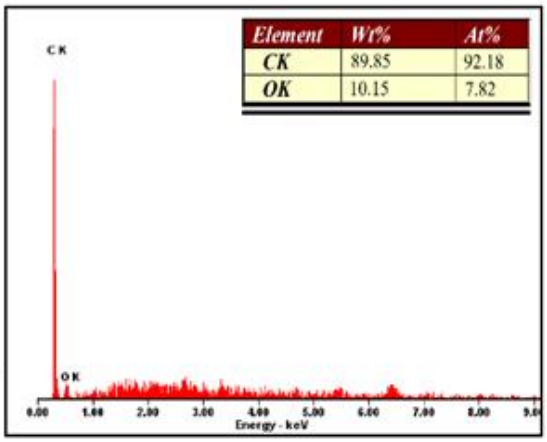
Element | Wt% | At%
CK | 89.85 | 92.18
OK | 10.15 | 7.82
C K
O K
Energy - keV

4(d)

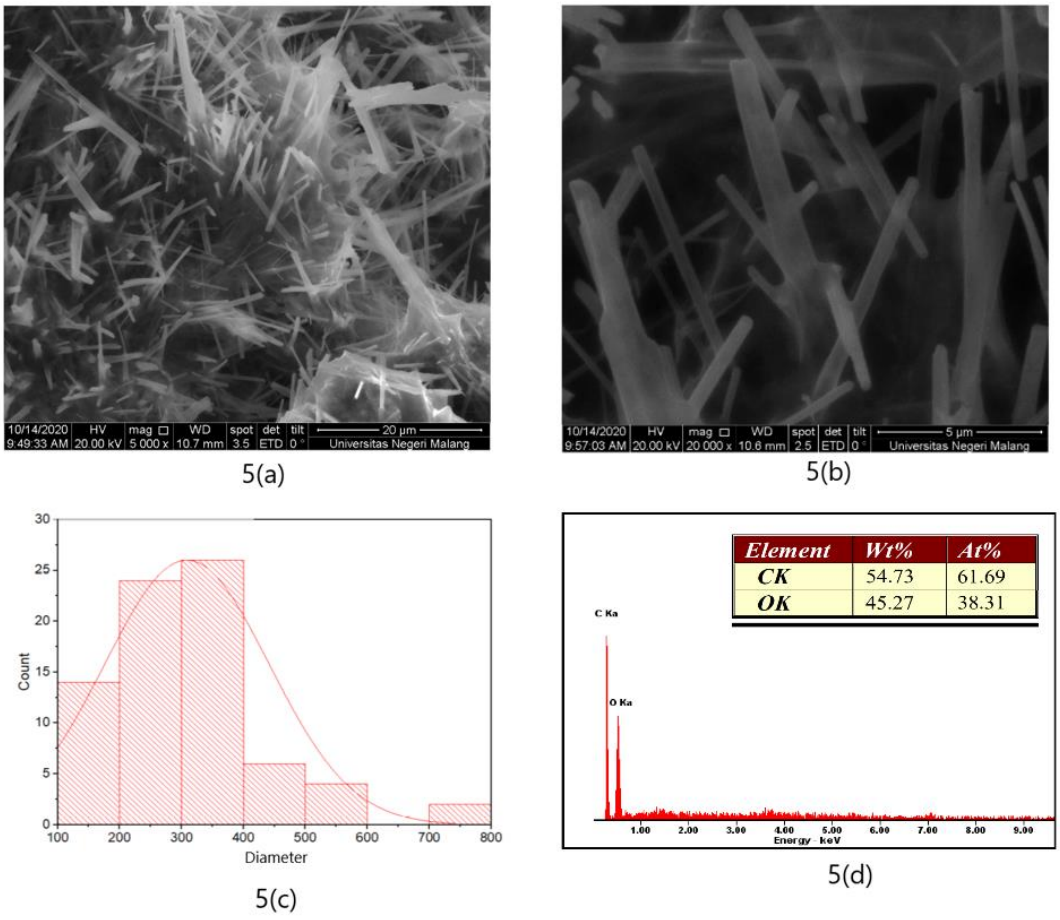

Figure 56 SEM and EDX of analysis of deposited carbon in different cathode
a,b) SEM image c) Diameter distribution d) EDX
(3) Ni (2) Galv (3) SS (4) NiCr (5) Cu
All measurement (c) is based on image (a)

Table 29 Growth rate of carbon and MWCNT yield in different cathode

Run	Electrode	Total deposit mass (gr)	wt% carbon	Growth Rate (g cm^{-2} h^{-1})	Purity (%)	MWCNT yield (g cm-2 h-1)
1	Cu	1.90	54.73%	0.664	41.54%	0.50
2	Galvanise	2.80	73.63%	1.312	62.47%	1.11
3	NiCr	3.12	89.85%	1.787	88.27%	1.76
4	Ni	2.50	61.79%	0.9854	67.35%	1.07
5	SS	2.82	94.77%	1.702	92.32%	1.66

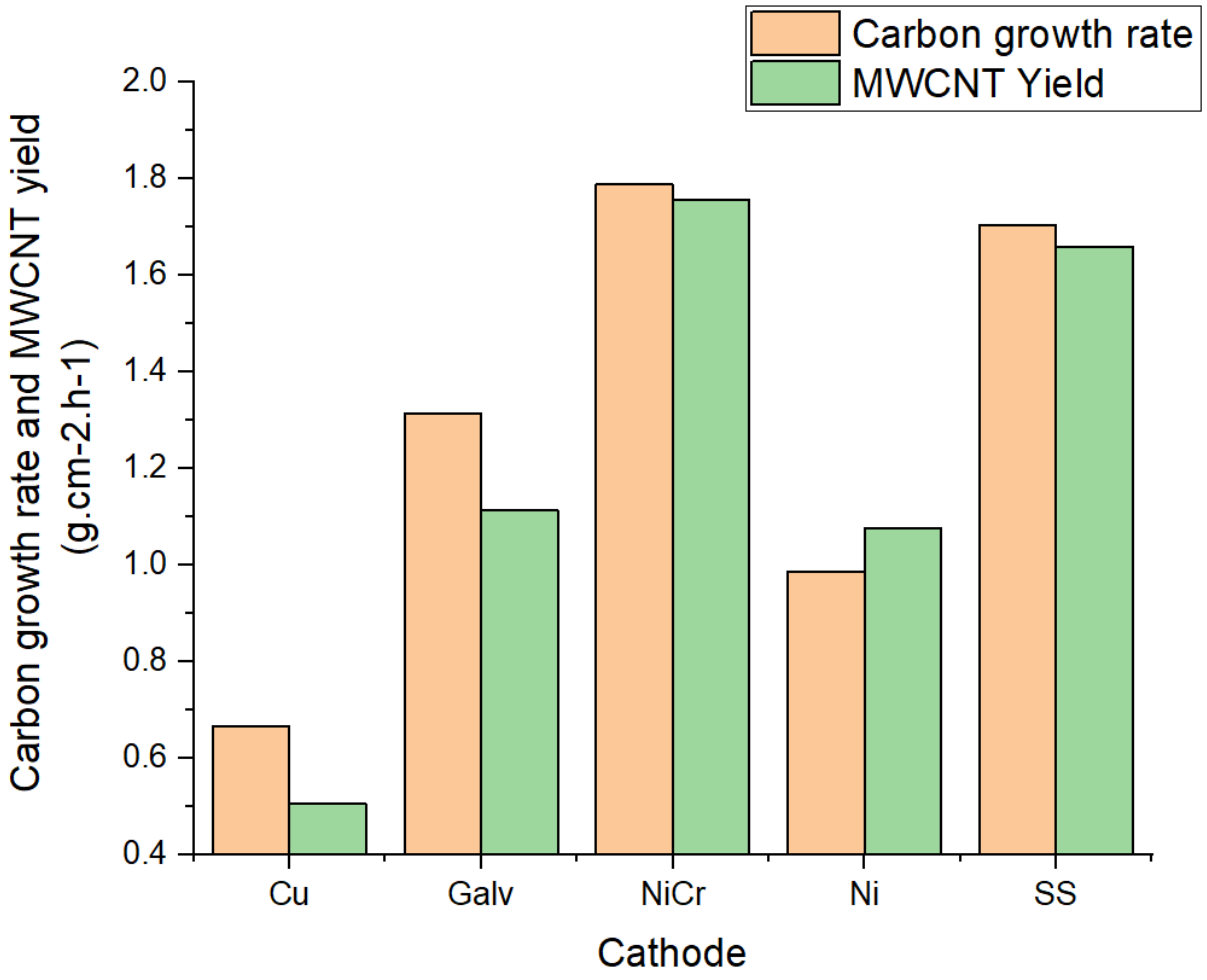

Figure 57 Carbon Growth rate and MWCNT yield in different cathode materials

Table 29 shows that various cathode produces a different mass of Electrodeposition results. This study's mass sequence of carbon was obtained from the Electrodeposition process: NiCr > Stainless Steel > Ni > Galvanised steel > Cu. These results describe graphicly in Figure 57. The highest deposited mass of carbon obtains using a Ni-NiCr electrode pair. This result is in accordance NiCr having good catalytic activity[57]. In the Electrodeposition results (Table 29), it can be seen that most carbon deposits are in the Ni-NiCr electrode pair. This phenomenon is because the Ni oxidation at the anode to the electrolyte causes the coating on the cathode. During The oxidation process, Ni also facilitates carbon Nanotubes structure nucleation on the cathode surface[145]. Also, the electrode potential value of the nickel anode is negative, which

means the nickel anode is easily oxidised and easy to release electrons. In addition, Cr alloy promotes this phenomenonone[56]. The characteristics possessed by the Ni-NiCr electrode will trigger a high Electrodeposition rate.

Carbon has grown quite well on stainless steel electrodes. Stainless Steel anode material contains iron (Fe) which is very dominant, so the amount of deposited Carbon yield and growth rate is higher than Ni, Cu, and galvanised anodes. Based on the Mukul Kumar et al. study, Ferrous metals (Fe), Cobalt, and Nickel have higher adhesion features in growing carbon than other transition metals. Iron (Fe), cobalt, and nickel also have a high diffusion rate and have an excellent ability to break down carbon at high temperatures when these metals act as catalysts. That is what causes Stainless Steel anodes to grow carbon better than Ni, Cu, and galvanised anodes[146]. The obtained deposits in the Ni-Ni electrode pair have a lower mass than the NiCr-Ni and SS-Ni electrodes. This fact follows J. Ren et al. (2015) research suggests that a mixture of metals is essential to promote carbon nanofibre and carbon nano-tubes deposit[56]. In addition, an anomaly result of the Ni-Ni electrode pair of Carbon growth rate and MWCNT yield is explained in appendix 11.

Galvanised electrodes (Fe coated with Zn elements) produced the lowest mass of CNT deposits after the NiCr electrodes. Based on the electrode potential value, the Galvanized electrode has the most considerable negative electrode potential value compared to other electrodes. This value should cause more CNT deposits on the Galvanised-Nickel electrode pair than on the other electrode pairs. However, Arcaro et al.; revealed that Zn metal has a low degradation rate. The Zn layer can slow the oxidation rate because Zn has a feature that can replace oxidation loss, and when Fe metal is exposed to outside air, it will be covered again by Zn. This slowed process happens because the Zn around it will be absorbed and deposited in the Fe, replacing metals previously lost due to oxidation. Therefore, the Zn layer blocks the Fe, which can catalyse the solution. In addition, the feature of the Zn metal causes low impurities in the carbon deposits[57].

The copper (Cu) electrodes showed the lowest cathodic product mass than the Electrodeposition mass using other electrodes. The different Electrodeposition results' mass is very significant than nickel and stainless steel electrodes. This result has been explained in Radhamani et al. (2018) research that carbon nanotubes using Cu electrodes produce a low amount of CNT[147]. In contrast, stainless steel shows a higher MWCNT[147]. In addition, Cu metal has a positive electrode potential value, which means that the Cu element will be challenging to oxidise. Therefore, it causes the oxidation particles of Cu metal to be minor, and the impurities in the carbon deposit are relatively small. This fact proves that the carbon growth process is directly controlled by the composition and properties of the anode material[57].

The carbon growth rate does not directly represent the CNT growth rate, but it can be ascertained that there is CNT on this carbon. This value can be proven by detecting the CNT phase in the XRD and SEM morphology analysis. The Wt% value is obtained from the EDX results, representing the sample's carbon composition. The carbon growth rate is obtained by using equation 12.

4.4.5 Deposition time effect on Electrodeposition

Further investigation of the time effect on Electrodeposition results is carried out using the One Factor at a time (OFAT) model in this experiment. Table 30 present the experiment settings. The phase identification is carried out by XRD characterisation to compare the crystal phases in carbon powder and analyse the crystalline size and phase structure. In Figure 58, the XRD graphs were shown, compared, and used to calculate crystalline size. The calculation result is presented in Table 31. XRD diffractogram shows the presence of 002 miller indices in the 2θ ~, 26°indicating C-C. Some impurities also occur, which indicate the presence of Li_2CO_3 and Li_2O. The crystalline calculation results in an inconclusive pattern of the Electrodeposition time effect on the crystalline soot size.

Table 30 One Factor at a time (OFAT) model clusters varying Electrodeposition times

Run	Temperature (°C)	External potential (V)	CO_2 Flow (ml/min)	Time (m)	Cathode
11				60	
12				90	
13	773	5	185	120	NiCr
14				150	
15				180	

Table 31 Phase result XRD in different deposition times

No	Time	FWHM	Crystalline size D (nm)
1	60 min	0.468	17.43
2	90 min	0.424	19.26
3	120 min	0.429	19.05
4	150 min	0.410	19.91
5	180 min	0.406	20.14

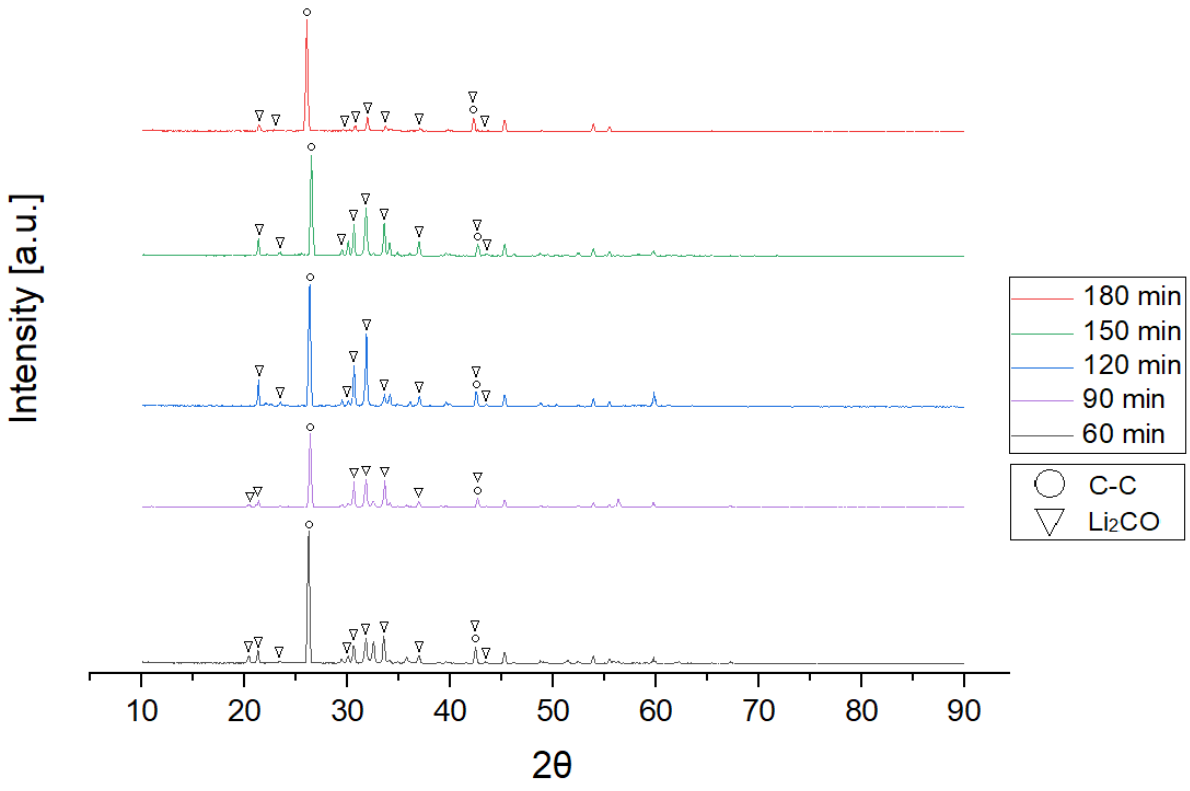

Figure 58 Diffractogram XRD deposited carbon in different deposition time

FTIR characterisation of functional elements absorbed by CNT on cathodic products is shown in Figure 59. Indication of carboxylic and hydroxylic functional groups are arises at 1400-1600 cm^{-1}, 3430 cm^{-1},2830 cm^{-1}, and 2950 cm^{-1} attribute of C=C, O-H, sCH_2, and aCH_2 respectively. Primary CNT modes A_{2u} and E_{1u} were active at 868 and 1575 cm^{-1}. However, in 180-minute Electrodeposition, the A_{2u} wavelength upshift occurs.

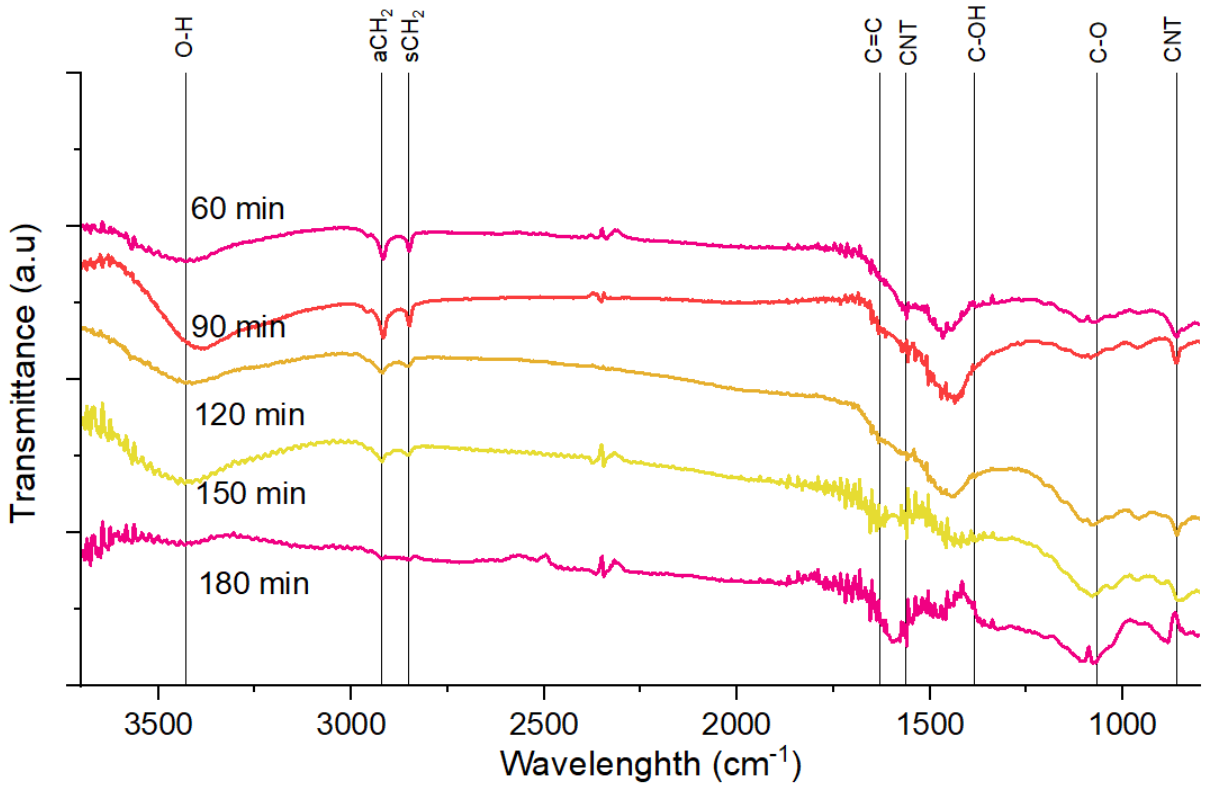

Figure 59 FTIR spectra of cathodic product produced in different Electrodeposition time

Cathodic products produced in different electrolysis times are analyzed using Raman analysis (Figure 60 and Table 32) to determine the graphitization degree. The D, G, and G' bands' features consistently arise in all Electrodeposition times, indicating that the soot contains MWCNT. Furthermore, a subtle feature of the G band into ω_{G-} and ω_{G+} also occurs. The normalized intensity I_D/I_G ratio gets higher in longer Electrodeposition time, which means that longer electrolysis reduces the quality of MWCNT. MWCNT purity value also follows this pattern; longer Electrodeposition promotes impurities.

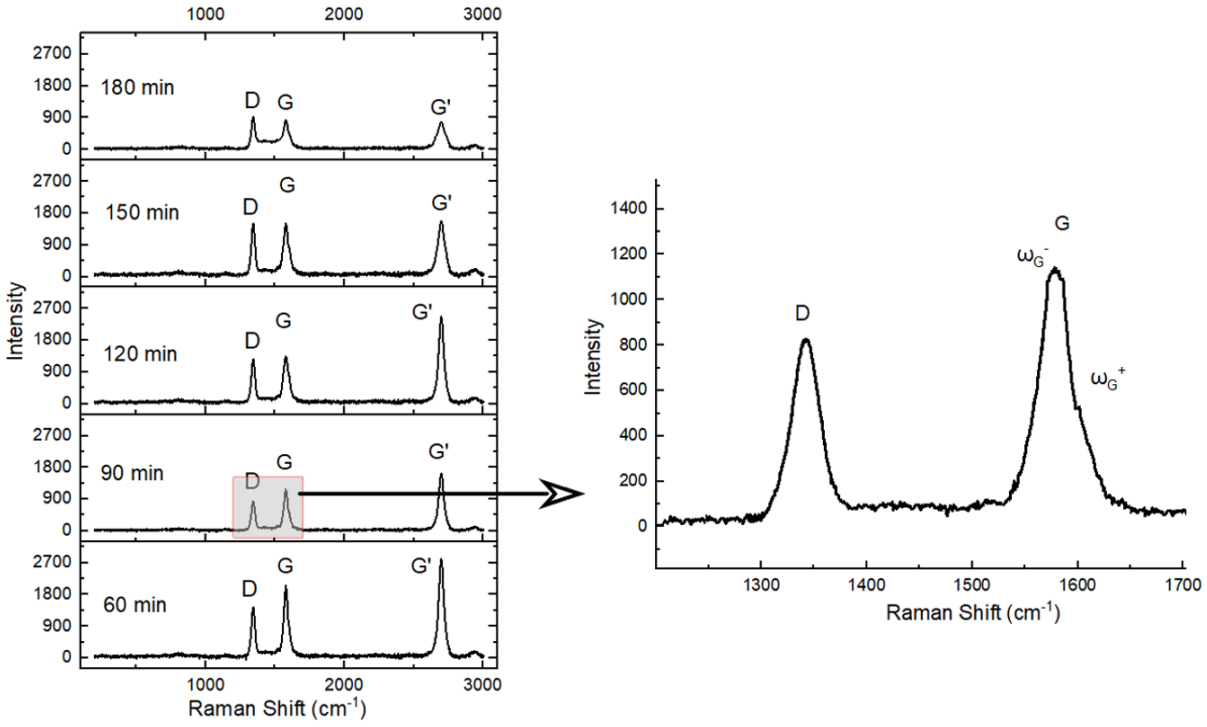

Figure 60 Raman analysis of cathodic product produced in different Electrodeposition times

Table 32 Raman analysis result of cathodic product produced in different Electrodeposition times

Time	ID/IG	IG'/ID	purity
60	0.73	2.01	88.27%
90	0.72	1.89	85.56%
120	0.98	1.48	73.85%
150	0.96	0.99	55.03%
180	1.24	0.86	48.44%

The morphology of the carbon powder samples was observed using SEM. SEM tests on carbon powder samples are shown in Figure 61, and comparing them to the previous experiment, all the CNT result is somewhat straight. Figures 61 1a and 1b show that the shape of the CNT looks straight and better structured. Figure 61 2a, 2b, 3a, and 3b also deliver the form that looks linear and structured with slight wavy. Figures 4 and 5 have more wavy structures, with noticeable impurities in the end product. This SEM result confirms the Raman analysis result, in which longer Electrodeposition promotes impurities and extend defect on the CNT. Table 33 indicates that Electrodeposition time affects carbon content produced. The EDX result shows

carbon content in 60 minutes is the highest at 89.85% and reduced with longer Electrodeposition.

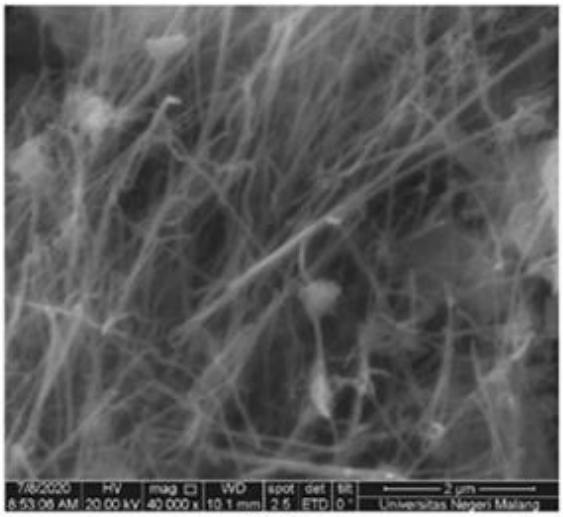

1(a)

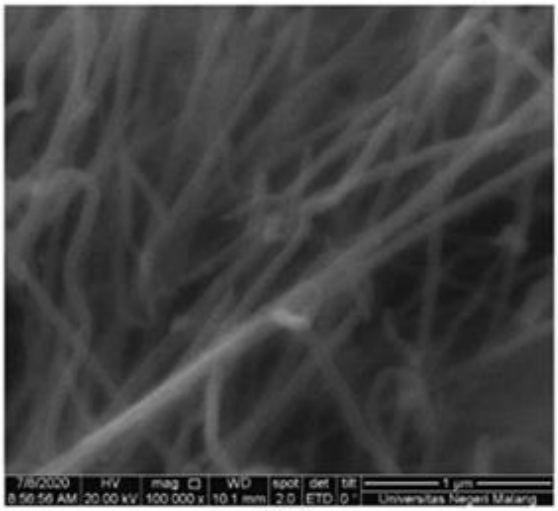

1(b)

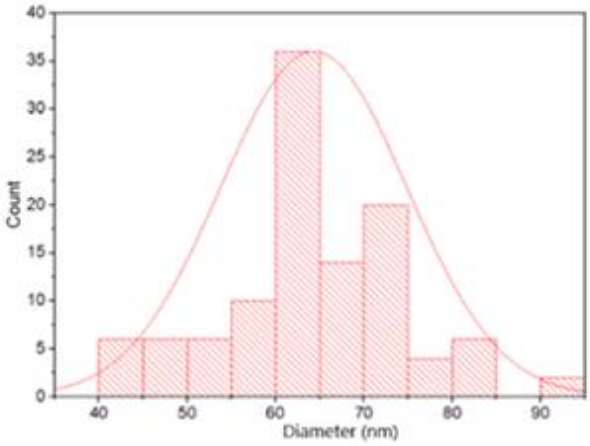
Count
Diameter (nm)

1(c)

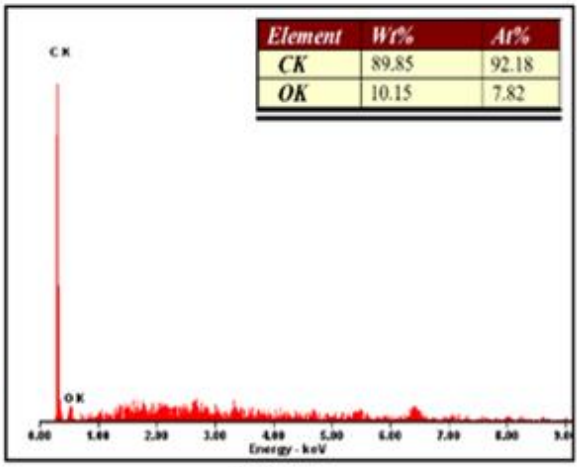
Element | Wt% | At%
CK | 89.85 | 92.18
OK | 10.15 | 7.82
CK
OK
Energy - keV

1(d)

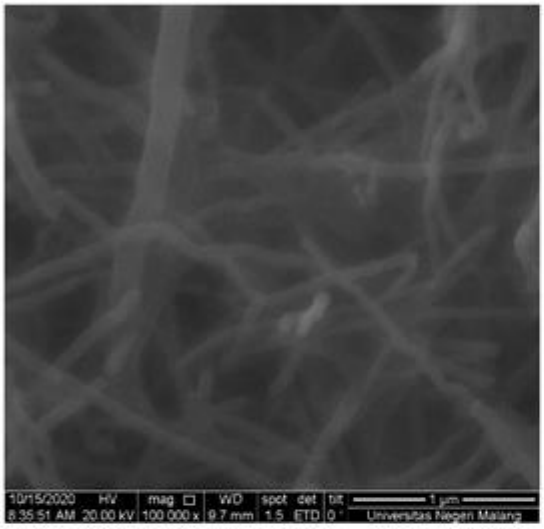
10/15/2020 HV mag WD spot det tilt 1 µm
8:35:51 AM 20.00 kV 100 000 x 9.7 mm 1.5 ETD 0 Universitas Negeri Malang

2(a)

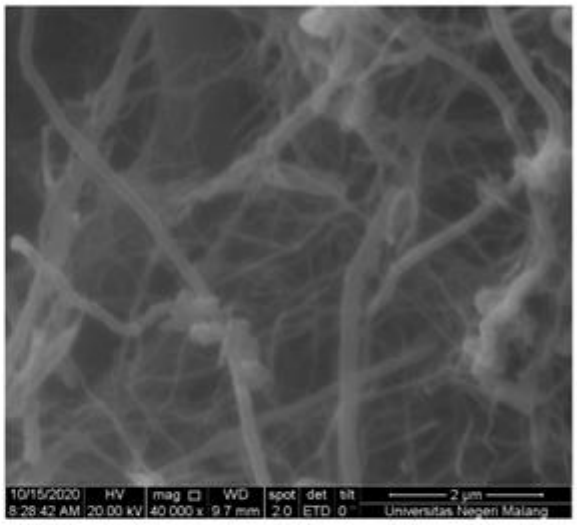
10/15/2020 HV mag WD spot det tilt 2 µm
8:28:42 AM 20.00 kV 40 000 x 9.7 mm 2.0 ETD 0 Universitas Negeri Malang

2(b)

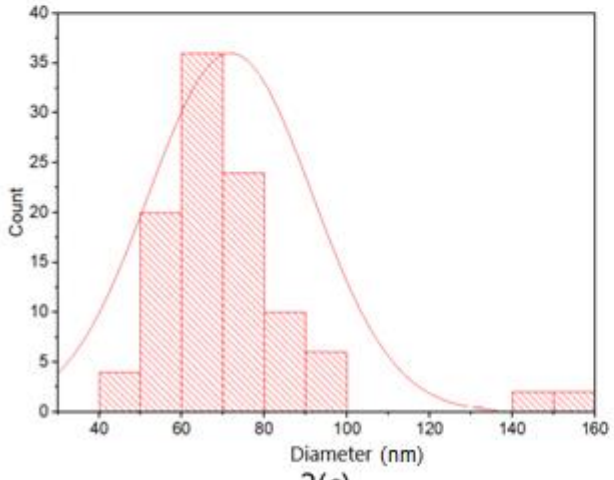
Count
Diameter (nm)
0
5
10
15
20
25
30
35
40
40
60
80
100
120
140
160

2(c)

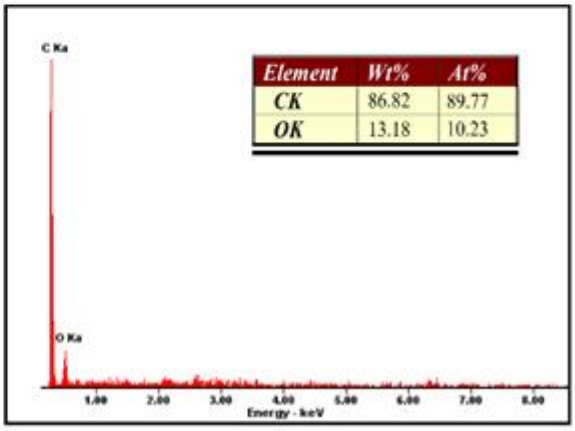
C Ka
O Ka
Element Wt% At%
CK 86.82 89.77
OK 13.18 10.23
1.00 2.00 3.00 4.00 5.00 6.00 7.00 8.00
Energy - keV

2(d)

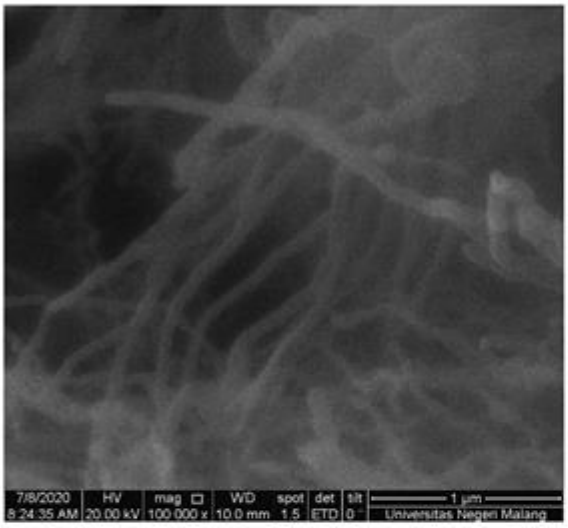
7/8/2020 8:24:35 AM
HV 20.00 kV
mag 100,000 x
WD 10.0 mm
spot 1.5
det ETD
tilt 0°
1 µm
Universitas Negeri Malang

3(a)

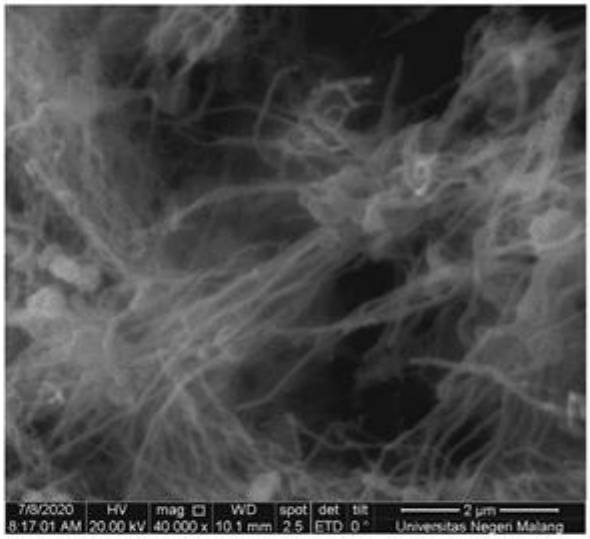
7/8/2020 8:17:01 AM
HV 20.00 kV
mag 40,000 x
WD 10.1 mm
spot 2.5
det ETD
tilt 0°
2 µm
Universitas Negeri Malang

3(b)

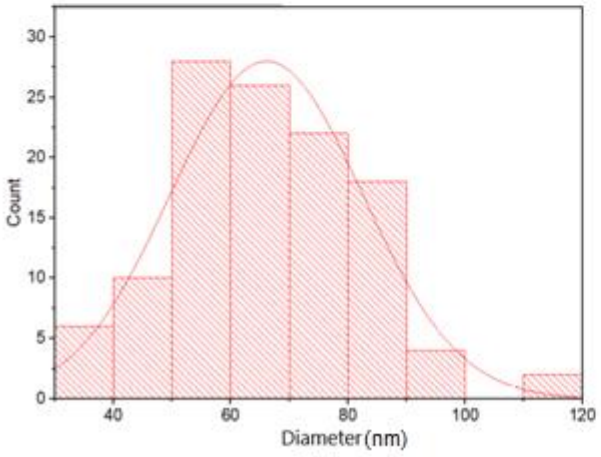
Count
Diameter (nm)
0
5
10
15
20
25
30
40
60
80
100
120

3(c)

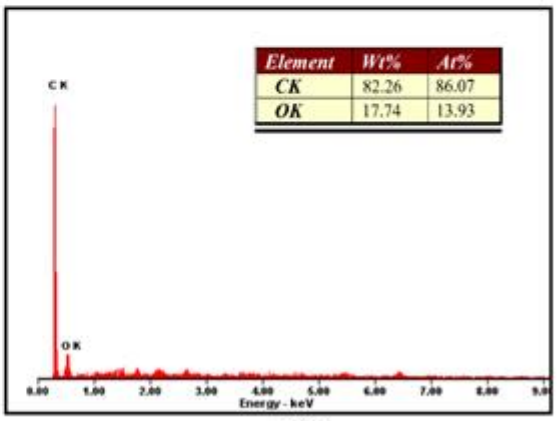
Element Wt% At%
CK 82.26 86.07
OK 17.74 13.93
C K
O K
Energy - keV

3(d)

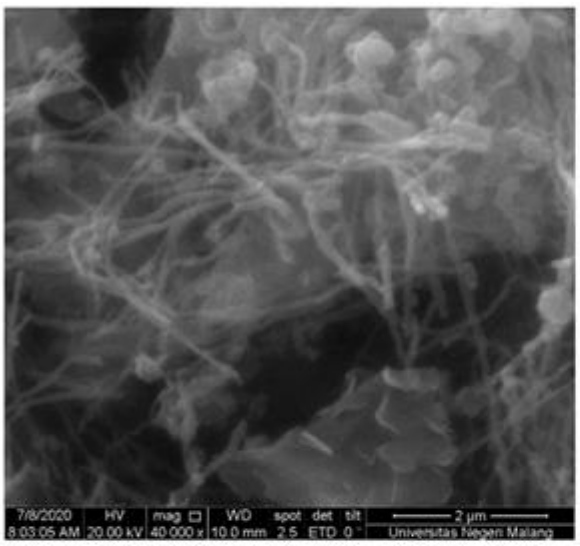
7/8/2020 8:03:05 AM
HV 20.00 kV
mag 40,000 x
WD 10.0 mm
spot 2.5
det ETD
tilt 0°
2 µm
Universitas Negeri Malang

4(a)

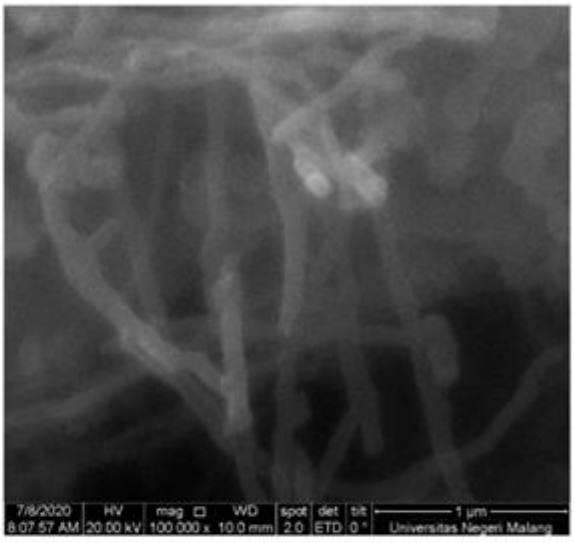
7/8/2020 8:07:57 AM
HV 20.00 kV
mag 100,000 x
WD 10.0 mm
spot 2.0
det ETD
tilt 0°
1 µm
Universitas Negeri Malang

4(b)

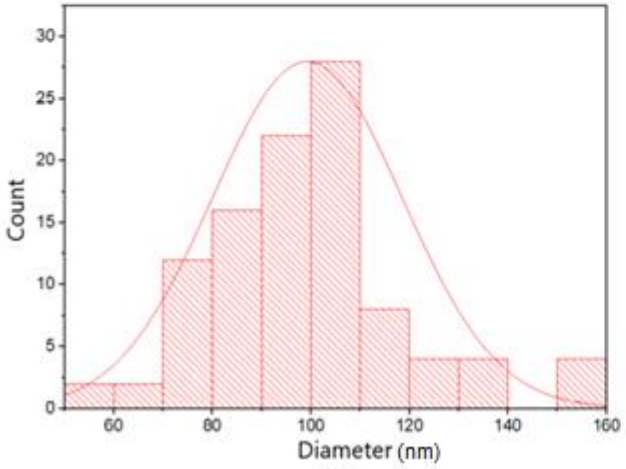
Count
Diameter (nm)
0
5
10
15
20
25
30
60
80
100
120
140
160

4(c)

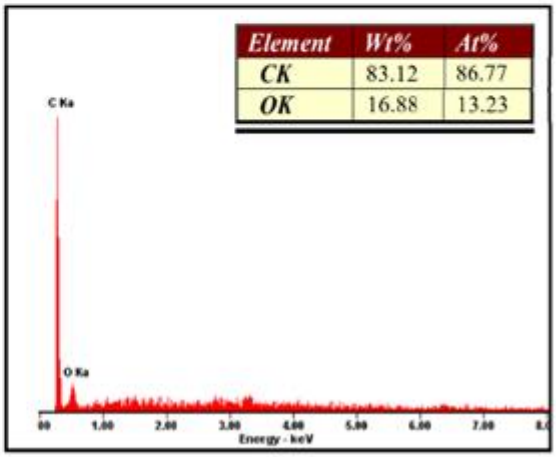
Element Wt% At%
CK 83.12 86.77
OK 16.88 13.23
C Ka
O Ka
Energy - keV

4(d)

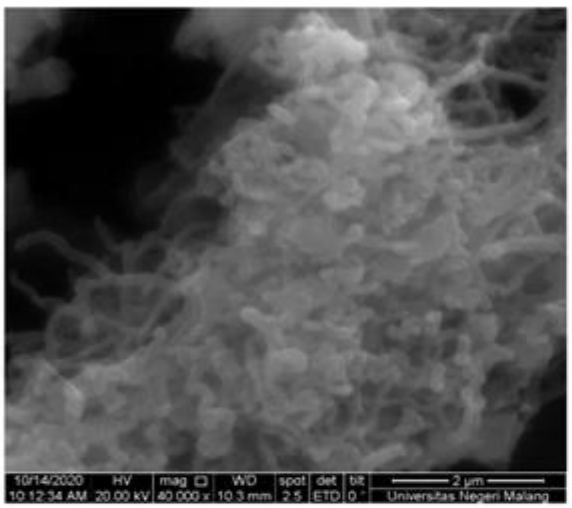

5(a)

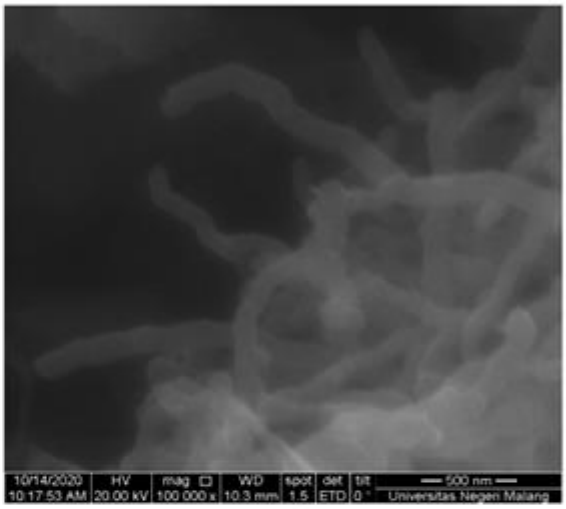

5(b)

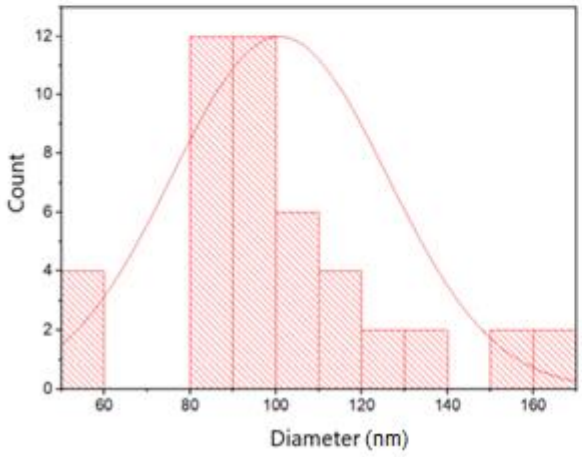

5(c)

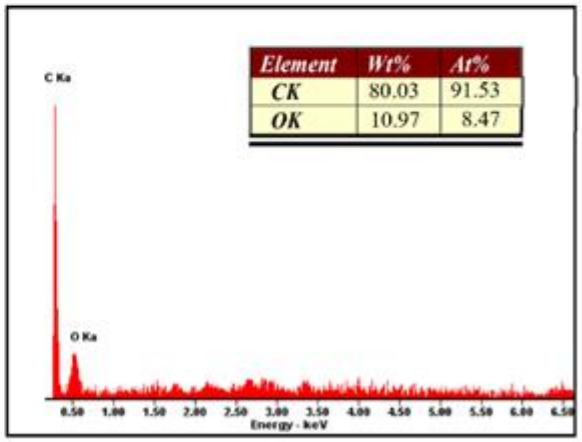

Element	Wt%	At%
CK	80.03	91.53
OK	10.97	8.47

5(d)

Figure 61 SEM and EDX analysis of deposited carbon in different synthesis times.
a,b) SEM image c) Diameter distribution d) EDX
(1) 60 min (2) 90 min (3) 120 min (4) 150 min (5) 180 min
All measurement (c) is based on image (a)

Table 33 Growth rate of carbon and MWCNT yield in different deposition times

Run	Time (min)	Total deposit mass (gr)	Wt% Carbon	Growth Rate (g cm-2 h-1)	Purity (%)	MWCNT yield (g cm-2 h-1)
1	60	3.12	89.85%	1.787	0.88	1.76
2	90	4.59	86.82%	1.692	0.86	1.67
3	120	6.01	82.26%	1.575	0.74	1.41
4	150	7.28	83.12%	1.542	0.55	1.02
5	180	8.63	80.03%	1.467	0.48	0.89

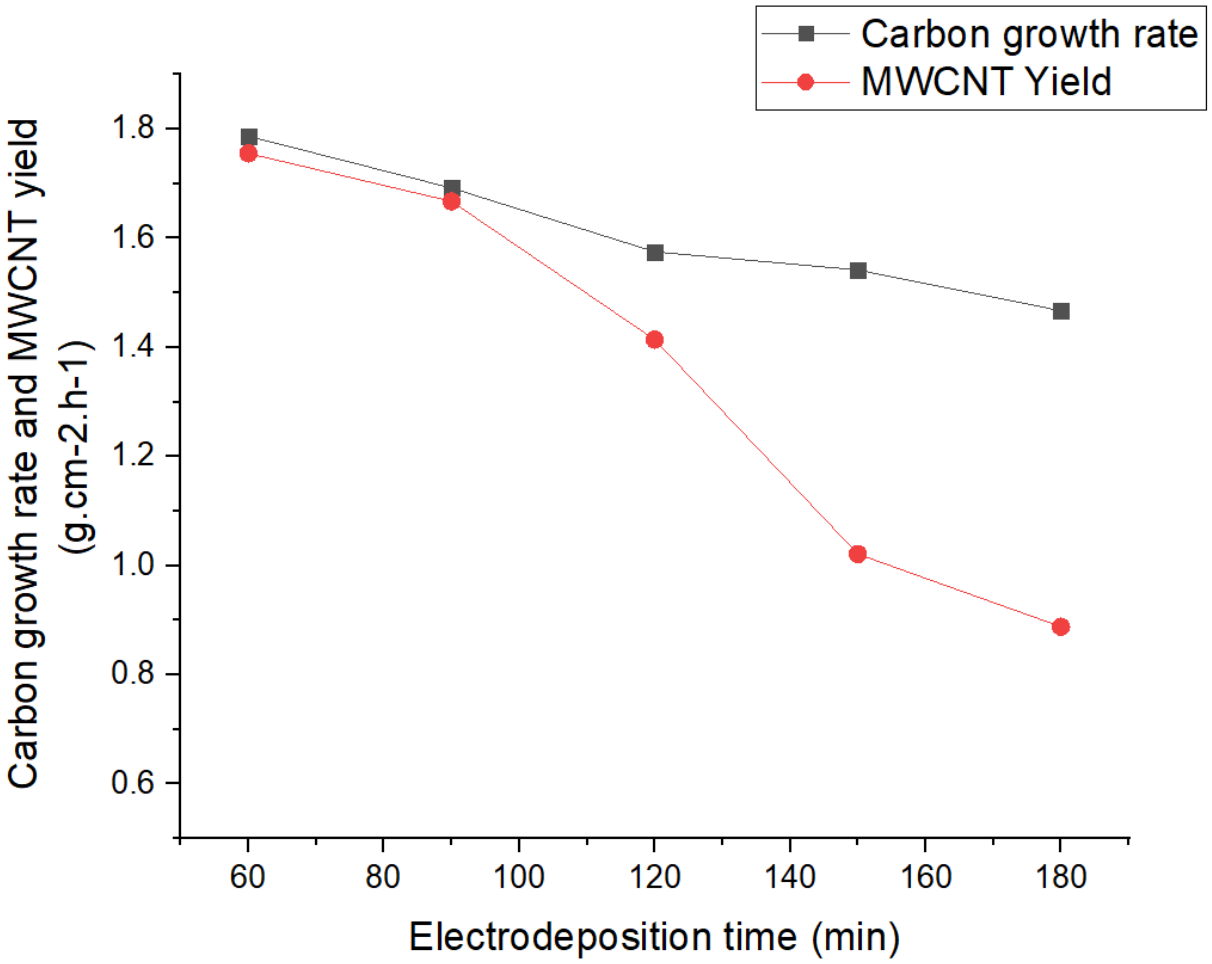

Figure 62 Carbon growth rate and MWCNT yield in different deposition time

Figure 62 shows the carbon growth rate value at different synthesis times and shows that an extended Electrodeposition time pattern will result in a lower carbon growth number. A similar way is also shown in Figure 63, which describes the current efficiency value on synthesis time variation. Longer Electrodeposition time results in lower current efficiency. It is also necessary to note that more prolonged deposition causes carbon debris to appear on

electrolytes. Table 33 shows that 60 minutes is the highest growth rate value among the other synthesis time, followed by 90, 120, 150 and 180 minutes, respectively.

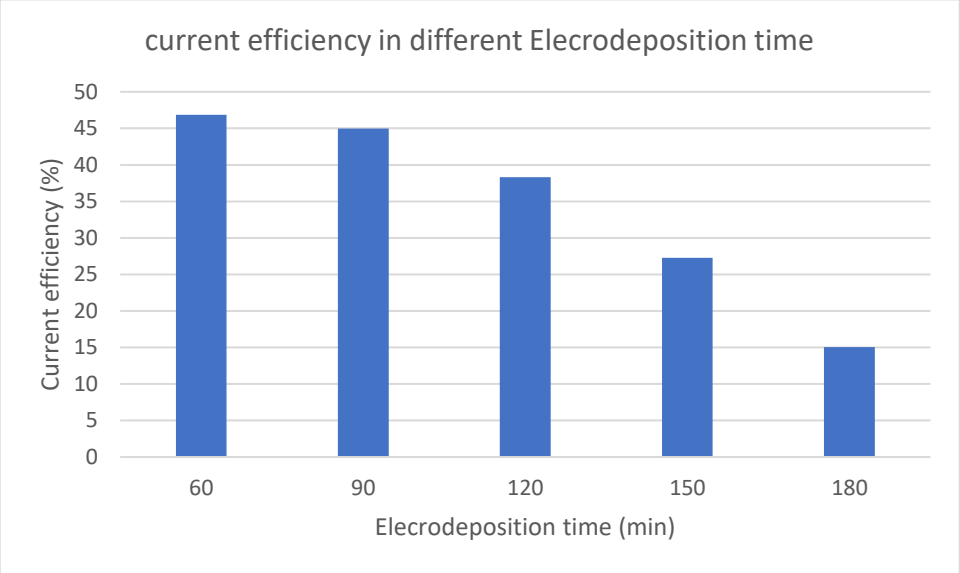

Figure 63 current efficiency in different deposition time

4.5 Discussion

Taguchi method results indicate that the highest growth rate was achieved at Temperature 773 ºC, external voltage 5 V, CO_2 flow rate 185 ml/min, synthesis time 60 min, utilising NiCr cathode. After confirming it with the OFAT experiment, the growth rate value is 1.787 g cm^{-2} $h^{-1,}$ and MWCNT yields 1.76 g cm^{-2} h^{-1}.

Sample from the Taguchi method was analyzed using XRD (Figure 30) and Raman spectroscopy (figure 29). The XRD result detected the (002) and (100) indices, indicating the carbon compound in the sample and typically the peak of the CNT (Figure 8) [33]. Alongside the carbon compound, Li_2CO_3 was also present. The XRD peak cannot be strong evidence of CNT; therefore, Raman spectroscopy was used to determine the graphitization degree of the sample. As discussed in chapter 2.1, four features indicate CNT. Out of four features, three of

the features were detected, which are D, G and G' bands. The undetected feature is RBM indicating the sample was not SWCNT but MWCNT.

The Taguchi method also shows each parameter's contributor factor (Figure 32), with the highest contribution received by Temperature at 33.93%. This high contribution is due to a significant difference in the growth result of 723 ºC to 773 ºC. Therefore the signal indicates a significant response resulting in high contribution.

The interaction plot (Figure 34) shows the complex interaction between each parameter. One notable feature is cathode interaction with other parameters, which indicates that the Stainless Steel cathode results in a slightly higher response in some cases and NiCr resulting a stable response; therefore, on average, NiCr resulting a better response. Both were excellent cathode materials because they are metal alloys containing Ni and Cr. Previous research suggests that metal alloys were essential to promoting the growth rate of CNT[76][98][92]. Ni provides growth mechanisms and Cr function as metal initiation from molten salt[56]. The Stainless steel also contains Fe, which received mixed reviews from the previous reports. From Figure 14, we can determine that pure Fe is not suitable for the Electrodeposition process to produce carbon nanotubes. However, adding other materials, such as Ni, will promote better results. Other reports also suggest that Fe and stainless steel are ideal electrodes to produce CNT[55]. The central hypothesis of the unstable result on Stainless Steel is that stainless steel responds better at higher temperatures (773 ºC – 873 ºC) and has higher external potential (4V – 6V), and poorly responds outside of those parameters values compare to NiCr, which has a more stable response.

XRD was used to detect impurities and carbon structure in the soot, and crystalline size was calculated from XRD data. The crystalline in this research indicates the thickness of the wall in the MWCNT cases. The relation of wall thickness to Bragg's law is detailed in previous research[31]. The XRD result of varied temperatures (Figure 36 and Table 15) indicates that higher temperatures result in a thicker wall of MWCNT, which is also supported by the diameter

distribution of MWCNT in Figure 39 increasing with the temperature increase. The XRD result of varied External-potential (Figure 41 and Table 19) shows that a higher value of potential external results in smaller wall thickness similar pattern is also shown in diameter distribution (Figure 44). The XRD result of varied Variance CO_2 Flowrate (Figure 46 and Table 23) shows that the MWCNT wall thickness pattern is undefined. The diameters distribution in Figure 50 also supports this undefined pattern. The XRD result of varied Cathodes is shown in figure 53 and table 27, resulting in the Cu cathode being the thickest wall of MWCNT while Stainless steel produces the smallest MWCNT wall. The sequence base on wall thickness was Cu>Galv> Ni>NiCr>SS.

773 ºC can be considered the optimised temperature since a technical issue in lower temperature occurs, which is unmelted lithium carbonate. It is possible since the temperature control has a ~ 5 ºC work range from the temperature target. Therefore, in the Electrodeposition at the lowest temperature (723 ºC), the Li_2CO_3 fluctuated and was not always in the liquid phase.

Further increase in temperature is also counterproductive. Higher working temperature (823-923 ºC) results in a lower growth rate and MWCNT yield than 723 ºC. It has been reported in previous research and is strongly believed to be caused by two factors. The first one is the lower density value of molten salt as a result of temperature increase[148]. Although higher temperatures increase the conductivity value of molten salt, the lower density will counteract the conductivity gain. Secondly, the counter-Ion gets close together due to liquid expansion in higher temperatures. High temperature is indeed linked to increased ion velocity, which will increase conductivity in general, but the extended temperature will cause counter ions even closer.

5V external potential results in the highest growth rate and MWCNT yield, while further increasing external potential causes growth rate and MWCNT yield to decrease. Some research reported this decrease due to current instability[82]. A higher growth rate and MWCNT

yield are achieved by increasing external potential from 2V to 5V. Higher external voltage increases the energy used in the electrodeposition and can be translated to the increasing potential energy of electrodeposition and more carbon deposit growth and yield[114][148]. Excessive external potential (6V) results in decreased performance due to current instability. The current instability is causing CO_3^{2-} unstable reduction, as studied in the previous report[82]. Reduction instability will interrupt the indirect reaction of CO_2 conversion to C (equation 5-9). Therefore the CNT growth is declined. Figure 44 SEM result shows denser CNT accompanied by lower wall thickness (Table 19) of MWCNT in the higher external voltage. The energy achieved in higher external potential will make carbon close to each other, resulting in denser and lower wall thickness phenomena[115].

The highest flow rate result is the highest growth rate and MWCNT yield, but it triggered the current efficiency decline. The decline is due to excessive CO_2, which is not converted into Carbon in the process. MWCNT wall thickness (Figure 46 and Table 23) and diameters distribution (Figure 50) pattern is undefined. The interaction plot (Figure 34) also shows a complex relationship between CO_2 flow rates to other parameters. A possible explanation for this complex is changing the amount of CO_2 in the system, creating a wide range of wall thickness and diameter distribution ranging from 40 nm to 140 nm. The reaction of the CO_2 conversion will change depending on the availability of CO_2 and whether it is a direct or direct reaction (equation 2-9).

Sixty minutes of Electrodeposition resulting the highest growth rate and MWCNT yield compared to longer electrodeposition time. Longer electrodeposition time tends to produce carbon debris rather than MWCNT. Figure 62 shows that longer electrodeposition times have an enormous gap between carbon growth rate and MWCNT yield, indicating that the system produces more carbon than MWCNT. The carbon debris phenomenon was also reported in previous research[57], [82]. MWCNT wall thickness (Figure 58 and Table 31) and diameters distribution (Figure 61) are undefined. Longer electrodeposition time allows the creation of a

broader range of MWCNT wall thickness and diameters; therefore, the measurement is varied. However, the difference in wall thickness is ~1 nm, which can be neglected, and it can be assumed that both CO2 flow rates and time parameters are not affecting CNT's diameter and wall thickness.

The highest growth rate and MWCNT yield were also achieved using NiCr and SS cathode with sequence Cu<Ni<Galv<SS<NiCr. This result is in line with the previous theory that metal alloys and mixtures were essential to promote Carbon growth and MWCNT yield[56][98][57]. Cu gains the lowest carbon growth, and MWCNT yield does not provide the metal initiator. Similar to Cu, Ni also does provide a metal initiator but creates more metal growth nucleation. While Galvanized steel provides Zn as an initiator, the system lacks metal growth nuclei compere to NiCr and SS. The thickest MWCNT wall and largest diameter were achieved in Cu cathode with a uniquely short and straight shape compared to other results. The absence of the metal initiator and the low amount of metal nuclei might be causing this morphology. The SS cathode produces the highest purity in this experiment with 92.32% however higher Carbon growth and MWCNT growth is achived with NiCr cathode.

4.6 Conclusions

The Taguchi experiment is designed to optimise the parameter value of the Electoredopsition method, while one factor at a time is designed to investigate the dynamics of CNT properties on each variable. The optimised parameter's values are 773 °C temperature, 5 V external potential, 185 ml/min CO_2 flowrates, NiCr cathode, and 60 minutes synthesis time. These combined experiment methods resulted in a notable trend for each parameter.

The optimum value from the L25 Orthogonal Arrays Taguchi method of each parameter are temperature = 773 ºC; external potential = 5V; CO_2 Flowrate = 185 ml/min; Electrodeposition time = 60 min, and; cathode = NiCr with a high carbon growth rate (1.787 g cm^{-2} h^{-1}) and

MWCNT yield (1.76 g cm^{-2} h^{-1}) in atmospheric pressure. Furthermore, solid evidence of Raman features indicates the presence of MWCNT.

Taguchi and OFAT show a performance drop from 773 °C to higher temperatures. Specifically, in OFAT, the sloping trend of both the carbon growth rate and MWCNT yield was noticeable. The CNT was detected and confirmed by Raman analysis from XRD and FTIR results. Possibly, this pattern is due to the expansion of molten salt counteracting conductivity gain. Furthermore, the Counter-ion complicates the synthesis process.

The external potential is limited to 5 V before Electrodeposition experiences adverse effects on the carbon growth rate and MWCNT yield. Higher growth rate and yield were achieved When the external potential value changed from 2 V to 5 V. However, further increase in external value will reduce the growth rate and yield. Increasing external potential from 2V to 5V, increasing Carbon growth rate from 0.894 to 1.787 $gr.cm^{-2}.hour^{-1}$. While 6V produces a 1.599 $gr.cm^{-2}.hour^{-1}$ growth rate. The reduction of carbon growth rate can be caused by current instability occurring on external potential higher than 5.5 V. The MWCNT yield also follows a similar pattern with the highest value of 1.76 1.787 $gr.cm^{-2}.hour^{-1}$ at 5V.

CO_2 flow rate has a positive effect on the result. Increasing the value from 5 ml/min to 185 ml/min also increases growth rate and yield. However, from a current efficiency standpoint, the higher flow rate (185ml/min) resulted in a lower value. Longer deposition time negatively affects the Electrodeposition result. The total deposit of carbon is higher in a longer deposit time. However, the growth rate is decreasing, and the MWCNT yield result shows a further noticeable pattern.

Two Cathode materials that resulted in a high growth rate are NiCr and SS. Although NiCr has a higher growth rate and yield, SS purity is slightly better. NiCr produces a slightly higher MWCNT yield (1.76 $gr.cm^{-2}.hour^{-}1$) with a bigger diameter (65 nm)of MWCNT. Stainless steel fabricates a slightly lower Electrodeposition rate with better purity (92.32%) and smaller MWCNT (60 nm average diameter distribution).

Chapter 5 – Discussion and Conclusion

5.1 Discussion

This study presents Electrodeposition as an alternative to produce CNT. This study started with several essential backgrounds. The notable one is a significant gap between the supply and demand of CNT in the market resulting in the high price of the commodity. The high price of CNT leads to less price to performance value and, most importantly, the visibility of research. Therefore, the need for a new approach to producing CNT is necessary.

With the essential background in mind, the literature review is conducted. The comparison of Arc discharge, Laser ablation, Chemical Vapour Deposition and Electrodeposition method divulge the advantages and disadvantages of each method. The distinctive advantages of Electrodeposition are unnecessary catalyst preparation which leads to an uncomplex setup and potentially reduces the cost of CNT production. Other advantages, such as the possibility of large-scale production and flexibility to produce SWCNT and SWCNT, make Electrodeposition appealing. Furthermore, this method uses atmospheric CO_2, which is abundant in availability. However, carbon footprint research is necessary to prove that Electrodeposition can reduce greenhouse emissions.

Despite its advantages, Electrodeposition needs to address challenges. The first one is the inconsistency of CNT appearance in the end product of Electrodeposition. Another challenge is the Impartial study of Electrodeposition. Both of these challenges were related to Electrodeposition. Furthermore, there were opportunities to improve the growth rate and yield of CNT by optimising parameters.

Three further studies were conducted to address the challenges and utilise opportunities. The first is a Molecular Dynamics study to set a base expectation of the parameter's behaviour. MD simulation result shows that increasing temperature, external potential, carbon atom number, and time parameters will increase the rate of carbon-to-carbon bonds. While comparing Cu and

Ni as Cathode results in a higher rate of carbon-to-carbon bonds using Ni as Cathode. The carbon-to-carbon bonds created in the MD simulation are affected by the total energy in the system. Therefore, parameters that increase the total energy component (kinetic and potential energy) will increase the carbon-to-carbon bonds. Temperature directly affects kinetic energy while external potential, carbon atom, and cathode atom type effecting potential energy.

The following study was Electrodeposition optimation with the Taguchi method. The result of Taguchi's experiments is optimised parameters; the highest carbon growth rate is achieved with 773 ºC temperature, 5 V external potential, 185 ml/min, 60 minutes synthesis time, and NiCr Cathode. However, it needs to be considered that SS resulted in a higher quality of CNT.

The last study was the OFAT experiment investigating CNT properties for each variable. The OFAT experiment was designed to investigate further characterisation using optimised parameters from the Taguchi experiment. From XRD, we can gain information on impurities that remained in the end product. FTIR was used to identify the functional group, Raman analysis to identify CNT carbonization, EDX to determine carbon purities, and SEM to analyse the produced soot morphology.

Comparing the MD simulation results and experiment results, there were differences. In the temperature parameters. The resulting pattern is different. MD simulation shows that higher temperatures will create higher carbon-carbon bond rates. In comparison, both experiments resulted in slope patterns for temperatures above 773 ºC. Several factors cause this different pattern. First, an increase in temperature leads to a lower density value counteracting the conductivity gained from the temperature changes[148]. Second, the increase in temperature is directly linked to the increase in ion velocity, increasing the conductivity in general. However, the effect of temperature increases also liquid expansion. As a result, the counter-ions get closed together[149][150]. Both phenomena result in higher temperatures increasing molten salt conductivity, but this does not mean producing more carbon or CNT[80]. Molecular dynamics simulation fails to capture this phenomenon due to the limitation of the force field

used in the MD. The Force field that presents lithium carbonate is non-existent at the moment. However, the result of MD was still useful for predicting a basic pattern of the temperature behaviour based on theoretical.

Other differences between MD simulation and experiment are the contributions of parameters. In the MD, the most significant contributor is the Carbon number, while in the experiment, the lowest was CO_2; it seems to be the opposite result and can be caused by several factors. The first one is, as mentioned in section 3.4, the simulation carbon number is high compared to typical electrodeposition resulting in a higher response followed by high contribution. Although in the experiment, the highest CO_2 flow (185 ml/min) was also considered high in the typical electrodeposition, it contributed lower than other parameters because of the second factor. The second factor is that in simulation, Carbon stock was in carbon atom form, while in the experiment, carbon was in the CO_2 form. Carbon atoms will react directly, while in the experiment, the excess CO_2 can be released into the gas outlet. Another factor that needs to be considered is that MD's main objectives are to establish a base expectation of the parameters; therefore, CNT, which includes SWCNT and MWCNT, is not considered in the simulation. Only the carbon-carbon bond created in the system was examined, while the CNT was examined thoroughly in the experiment.

In terms of External potential noticeable decline in the growth rate and MWCNT yield occurs in the highest external potential (6V). The decline is due to the current instability appearance, which is reported to start to occur at 5.5 V[82]. CO_2 Flowrate has a positive effect on carbon growth rate and MWCNT yield. However, it must be considered that a higher CO_2 flow rate results in lower current efficiency.

On the contrary, a longer Electrodeposition time results in a lower growth rate and MWCNT yield. In longer deposition times, excessive carbon deposits and debris were found. Furthermore, the current efficiency also shows a drop pattern. The highest growth rate and

MWCNT yield were also achieved using NiCr and SS cathode. These are supported by the previous research that mixture metal is essential to promote CNT synthesis[98][56].

Comparing the carbon growth rate this research achieved, which is 1.787 g cm^{-2} h^{-1}, is high from previous research, which is typical ~0.1 g cm^{-2} h^{-1}[80]. However, previous research also reported a higher growth rate with 600 m^2 g^{-1}[82]. This indicates that the research is producing an acceptably high carbon growth rate. However, neither research did find CNT in their end product. Comparing the purity assessment, which can be up to 90%[57] OFAT experiment shows that using NiCr cathode results in 88.27% purity. Although higher purity can be achieved using SS cathode (92.32%), the growth rate and MWCNT yield is decreasing. Higher quality of SWCNT is achieved in previous research[55] with the addition of catalyst preparation, which in this research cannot be achieved. However, this research aims to maintain the uncomplex nature of Electrodeposition without catalyst preparation. Therefore it can be concluded that this research can produce a high yield (1.76 g cm^{-2} h^{-1}) MWCNT product with maintaining the uncomplex nature of the method.

5.1.1 Limitation of the research

First, the limitation of the MD force field needed to be addressed. Despite the current MD capturing fundamental kinetic and potential energy theories, the lack of capturing molten salt behaviour and cathode metals option makes different results with experiment counterpart.

Second, Predicting CNT's metal initiation and nuclei growth is not possible now, especially with the electrodeposition method. Adding external potential and molten salt characteristics is complicated, and the method to accommodate it still does not exist.

Third, the TEM analysis is not used in this research because SEM is adequate to measure outer diameter and XRD to measure the wall thickness of MWCNT. However, TEM will have more accuracy in analysing the morphology of MWCNT.

Fourth, The restriction of financial resources resulted in the limitation of tests and analyses conducted. In the Molecular Dynamics simulation approach, the running time of the simulation approaches six days of each run. The total time to run the simulation is approximately three months (does not consider the error during the run time) if using a single personal computer. The solution options to these situations are hiring an expert to improve the program efficiency and renting simulation computers. The financial restriction only allows for a later option: two simulation computers. The Taguchi method's experiment is restricted to only EDX analysis and one Raman analysis. One Factor at Time (OFAT) experiment method does not include Transmission Electron Microscopy (TEM) and Thermogravimetric analysis (TGA) for the same reason.

Fifth, time and equipment availability are impacted during the pandemic situation. During the Covid-19 pandemic, access to the laboratory was limited. For example, the SEM-EDX and XRD test is only limited to use by laboratory staff without the researcher's presence, resulting in miscommunication during data collection and the need for recollection, which is time-consuming. Third-party equipment is also not available to use during the pandemic situation.

5.1.2 Future work

Better work can be proposed for CNT production, such as adding electrodes and catalyst treatment and preparation. The possibility of other CO_2 utilities also can be explored better for future work. Some tests and experiments have been left for the future due to financial resources and time restrictions (i.e. program script optimisation in Molecular Dynamics simulation, Transmission Electron Microscopy (TEM) and Thermogravimetric analysis (TGA) in the experiment). These will help deeper analysis which is not captured in this study.

Following this Electrodeposition study, future work could conduct several ideas:

1. Research electrode and catalyst preparation to better control the CNT chirality and diameters. Catalyst research can improve the electrodeposition method but needs to be conducted carefully since adding a catalyst will increase electrodeposition complexity. There is also a possibility that the result is subdued by other methods such as Laser ablation and CVD, which also typically need catalyst preparation.
2. Research on the electrolyte in the electrodeposition will improve the optimization of electrodeposition. The current research indicates that combinations of electrolytes potentially positively affect the Electrodeposition method.
3. The utilisation of CO_2 needs to be explored further. Current use of CO2 such as Enhanced Oil Recovery, Carbonate beverage, Refrigerant, Decaffeination agent, and other mineral carbonation will promote further CO_2 atmospheric reduction.
4. The utilisation of MWCNT research will enhance the end product of electrodeposition value. The current utilisation of MWCNT is comprehensive, including polymers, solar cells, batteries, transistors, and many others. Finding a suitable application for MWCNT, which is produced in this research (typically ~18 nm wall thickness and 70 nm diameter), will increase the MWCNT value.
5. Considering the presence of molten salt in the simulation approach and counter-ion behaviour will improve the result accuracy. The molecular dynamics script optimisation will help reduce the simulation time.
6. Further analysis using TEM and TGA will improve the accuracy of the experiment.
7. Further development of force field which captures molten salt behaviour will support the metal initiation and metal nuclei process of CNT growth

5.2 Conclusion

The Electrodeposition method used in this study has the advantage of a cheaper CNT production cost than other methods. Besides, the process is relatively simple, making this method have good potential for producing CNT. The Electrodeposition studied in this study are temperature, electrodes, carbon source, external potential, and Electrodeposition time. Each variable influences the growth rate and the shape of the CNT. The conclusions that can be drawn from this research are as follows:

1	a)	A new approach to CNT production, such as Electrodeposition, is necessary due to the need for an uncomplex protocol method. MWCNT synthesis using Electrodeposition is advantageous to use due to its simple setup. Furthermore, this method can be done using atmospheric CO_2 conditions.
	b)	More work is needed to optimise the parameters to improve the end product quantity and quality of the Electrodeposition method because there are still questionable effects on the end product due to partial research and in conjunction with the parameters.
2	a)	The parameters base expectation of Electrodeposition can be achieved with MD simulation, which is more carbon-carbon bond created with the increased value of each parameter.
	b)	A validation study shows that total energy in the simulation system increases with the parameter value increase, which supports parameters base expectation.
3		The optimum value from L25 Orthogonal Arrays Taguchi method of each parameters are temperature = 773 ºC; external potential = 5V; CO_2 Flowrate = 185 ml/min; Electrodeposition time = 60 min and; cathode = NiCr in term of carbon production.
4	a)	Electrodeposition is an alternative uncomplex method to produce CNT with a high carbon growth rate (1.787 g cm^{-2} h^{-1}) and MWCNT yield (1.76 g cm^{-2} h^{-1}) in

		atmospheric pressure. Compared with previous work, the result is higher with solid evidence of Raman features indicating the presence of MWCNT.
	b)	XRD examines phase identification of cathodic products and MWCNT wall thickness. All of the XRD results show that (002) miller indices are present, which indicates the carbon deposition occurred in all scenarios presented in this work. Higher temperature and external voltage increase MWCNT wall thickness while increasing CO2 flow rate, and extended electrodeposition time does not.
	c)	The functional element in the end product was characterised using FTIR analysis. CNT primary mode (A2u and E1u) appears in all results except the product of the lowest temperature setting. The wavelength upshifts and downshift also occur in some cases.
	d)	Raman spectroscopy analysis was used to investigate graphitization degree. D, G, and G' features were shown and used as CNT defects and purity assessment. The lowest temperature scenario (723 ºC) indicates CNT synthesis difficulty with the absence of G' and broad D and G band feature in the Raman spectroscopy. Temperature of 773 ºC, External potential of 5V, 185ml/min CO_2 Flowrates, NiCr electrode, 60 minutes synthesis time result in the highest purity 88.27% (IG'/ID = 2.01) and relatively high quality (ID/IG = 0.73).
	e)	SEM-EDX analysis discloses the morphology and composition of the electrodeposition end product and outer diameter. The stainless steel cathode achieved the smallest diameter, followed by nichrome, while the Cu cathode has the biggest and lowest temperature diameter, showing no CNT.
	f)	The temperature of 723 °C has the lowest deposition rate due to the stability of the electrolyte. It is hard to maintain electrolytes in liquid form at 723 °C. At 773 °C, a higher deposition rate and deposition rate value gradually decrease with increasing temperature. Higher temperature also tends to grow larger, thicker wall MWCNT.

	g)	Ni-Ni, Cu-Ni, SS-Ni, NiCr-Ni, and Galvanized-Ni electrodes, were examined. The highest MWCNT yield is obtained using a NiCr-Ni and SS-Ni electrode. However, the residue and the morphology of the CNT made are different. NiCr produces a slightly higher MWCNT yield (1.76 $gr.cm^{-2}.hour^{-}1$) with a bigger diameter (65 nm)of MWCNT. Stainless steel fabricates a slightly lower Electrodeposition rate with better purity (92.32%) and smaller MWCNT (60 nm average diameter distribution).
	h)	The optimum external potential is 5V for the CNT deposition rate. Increasing external potential from 2V to 5V, increasing Carbon growth rate from 0.894 to 1.787 $gr.cm^{-2}.hour^{-1}$. While 6V produces a 1.599 $gr.cm^{-2}.hour^{-1}$ growth rate. The reduction of carbon growth rate can be caused by current instability occurring on external potential higher than 5.5 V. The MWCNT yield also follows a similar pattern with the highest value of 1.76 1.787 $gr.cm^{-2}.hour^{-1}$ at 5V.
	i)	The optimum CO_2 flow rate is 185 ml/min. 140 ml/min flow rate producing slightly lower purity (83.03%) compare to 185 ml/min (83.03%). This trend continues until the smallest value of CO2 flow rate (5 ml/min) with 76.20% purity.
	j)	The longer Electrodeposition process results in a lower deposition rate, and the optimum time is 60 minutes. A longer electrodeposition time produces a higher total carbon mass than a short one. However, the carbon weight (wt%) decreases, and MWCNT purity decreases even further. The lowest MWCNT purity is 0.48% at 180 minutes of electrodeposition time.

References

[1] S. Iijima, “Helical microtubules of graphitic carbon,” *Nature*, vol. 354, pp. 56–58, 1991, doi: 10.1038/354056a0.

[2] V. G. Chilkuri, S. Evangelisti, T. Leininger, and A. Monari, “The Electronic Structure of Short Carbon Nanotubes: The Effects of Correlation,” *Adv. Condens. Matter Phys.*, vol. 2015, 2015, doi: 10.1155/2015/475890.

[3] M. V. Kharlamova, “Electronic properties of pristine and modified single-walled carbon nanotubes,” *Uspekhi Fiz. Nauk*, vol. 183, no. 11, pp. 1145–1174, 2013, doi: 10.3367/UFNr.0183.201311a.1145.

[4] D. Tasis, N. Tagmatarchis, A. Bianco, and M. Prato, “Chemistry of carbon nanotubes,” *Chem. Rev.*, vol. 106, no. 3, pp. 1105–1136, 2006, doi: 10.1021/cr050569o.

[5] D. R. Dreyer, S. Park, C. W. Bielawski, and R. S. Ruoff, “The chemistry of graphene oxide,” *Chem. Soc. Rev.*, vol. 39, no. 1, pp. 228–240, 2010, doi: 10.1039/b917103g.

[6] H. Kataura *et al.*, “Optical properties of single-wall carbon nanotubes,” *Synth. Met.*, vol. 103, no. 1–3, pp. 2555–2558, 1999, doi: 10.1016/S0379-6779(98)00278-1.

[7] S. Kruss, A. J. Hilmer, J. Zhang, N. F. Reuel, B. Mu, and M. S. Strano, “Carbon nanotubes as optical biomedical sensors,” *Adv. Drug Deliv. Rev.*, vol. 65, no. 15, pp. 1933–1950, 2013, doi: 10.1016/j.addr.2013.07.015.

[8] B. Arash, Q. Wang, and V. K. Varadan, “Mechanical properties of carbon nanotube/polymer composites,” *Sci. Rep.*, vol. 4, pp. 1–8, 2014, doi: 10.1038/srep06479.

[9] J. Chen, B. Liu, X. Gao, and D. Xu, “A review of the interfacial characteristics of polymer nanocomposites containing carbon nanotubes,” *RSC Adv.*, vol. 8, no. 49, pp. 28048–28085, 2018, doi: 10.1039/c8ra04205e.

[10] W. Winarto, D. Priadi, N. Sofyan, and A. Wicaksono, “Wear Resistance and Surface Hardness of Carbon Nanotube Reinforced Alumina Matrix Nanocomposite by Cold Sprayed Process,” *Procedia Eng.*, vol. 170, pp. 108–112, 2017, doi: 10.1016/j.proeng.2017.03.020.

[11] L. Kong, C. Wang, X. Yin, X. Fan, W. Wang, and J. Huang, “Electromagnetic wave absorption properties of a carbon nanotube modified by a tetrapyridinoporphyrazine interface layer,” *J. Mater. Chem. C*, vol. 5, no. 30, pp. 7479–7488, 2017, doi: 10.1039/c7tc02701j.

[12] B. Kumanek and D. Janas, “Thermal conductivity of carbon nanotube networks: a review,” *J. Mater. Sci.*, vol. 54, no. 10, pp. 7397–7427, 2019, doi: 10.1007/s10853-019-03368-0.

[13] Z. Han and A. Fina, “Thermal conductivity of carbon nanotubes and their polymer nanocomposites: A review,” *Prog. Polym. Sci.*, vol. 36, no. 7, pp. 914–944, 2011, doi: 10.1016/j.progpolymsci.2010.11.004.

[14] Y. Usui, H. Haniu, S. Tsuruoka, and N. Saito, “Medicinal chemistry Carbon Nanotubes Innovate on Medical Technology,” *Med. Chem. (Los. Angeles).*, vol. 2, pp. 1–6, 2012, doi: 10.4172/2161-0444.

[15] L. Yang, L. Zhang, and T. J. Webster, “Carbon nanostructures for orthopedic medical applications,” *Nanomedicine*, vol. 6, pp. 1231–1244, 2011, doi: 10.2217/nnm.11.107.

[16] M. C. Paiva and J. A. Covas, “Carbon Nanofibres and Nanotubes for Composite Applications,” in *Springer Science+Business Media, Singapore*, S. Rana and R. Fangueiro, Eds. Singapore: Springer Singapore, 2016, pp. 231–260.

[17] J. R. Sanchez-Valencia *et al.*, “Controlled synthesis of single-chirality carbon nanotubes,” *Nature*, vol. 512, no. 1, pp. 61–64, 2014, doi: 10.1038/nature13607.

[18] F. Yang *et al.*, “Chirality-specific growth of single-walled carbon nanotubes on solid alloy catalysts,” *Nature*, vol. 510, no. 7506, pp. 522–524, 2014, doi: 10.1038/nature13434.

[19] MATT DAVENPORT, “Much Ado About Small Things,” *Chem. Eng. News Arch.*, vol. 93, no. 23, pp. 10–15, Jun. 2015, doi: 10.1021/cen-09323-cover.

[20] M. Johnson *et al.*, “Carbon nanotube wools made directly from CO2by molten electrolysis: Value driven pathways to carbon dioxide greenhouse gas mitigation,” *Mater. Today Energy*, vol. 5, pp. 230–236, 2017, doi: 10.1016/j.mtener.2017.07.003.

[21] F. Wu, Z. Zhou, S. Temizel-Sekeryan, R. Ghamkhar, and A. L. Hicks, “Assessing the environmental impact and payback of carbon nanotube supported CO2 capture technologies using LCA methodology,” *J. Clean. Prod.*, vol. 270, p. 122465, 2020, doi: 10.1016/j.jclepro.2020.122465.

[22] R. Das, Z. Shahnavaz, M. E. Ali, M. M. Islam, and S. B. Abd Hamid, “Can We Optimize Arc Discharge and Laser Ablation for Well-Controlled Carbon Nanotube Synthesis?,” *Nanoscale Res. Lett.*, vol. 11, no. 1, 2016, doi: 10.1186/s11671-016-1730-0.

[23] N. Saifuddin, A. Z. Raziah, and A. R. Junizah, “Carbon Nanotubes : A Review on Structure and Their Interaction with Proteins,” vol. 2013, 2013.

[24] I. Jeon, Y. Matsuo, and S. Maruyama, “Single-Walled Carbon Nanotubes in Solar Cells,” *Top. Curr. Chem.*, vol. 376, no. 1, pp. 1–28, 2018, doi: 10.1007/s41061-017-0181-0.

[25] P. C. Eklund, J. M. Holden, and R. A. Jishi, “Vibrational modes of carbon nanotubes; Spectroscopy and theory,” *Carbon N. Y.*, vol. 33, no. 7, pp. 959–972, 1995, doi: 10.1016/0008-6223(95)00035-C.

[26] J. Kastner *et al.*, “Resonance Raman and infrared spectroscopy of carbon nanotubes,” *Chem. Phys. Lett.*, vol. 221, no. 1–2, pp. 53–58, 1994, doi: 10.1016/0009-2614(94)87015-2.

[27] U. Kuhlmann, H. Jantoljak, N. Pfänder, C. Journet, P. Bernier, and C. Thomsen, “Infrared reflectance of single-walled carbon nanotubes,” *Synth. Met.*, vol. 103, no. 1–3, pp. 2506–2507, 1999, doi: 10.1016/S0379-6779(98)01077-7.

[28] H. Kuzmany, B. Burger, A. Thess, and R. E. Smalley, “Vibrational spectra of single wall carbon nanotubes,” *Carbon N. Y.*, vol. 36, no. 5–6, pp. 709–712, 1998, doi: 10.1016/S0008-6223(98)00071-2.

[29] A. Misra, P. K. Tyagi, P. Rai, and D. S. Misra, “FTIR spectroscopy of multiwalled

carbon nanotubes: A simple approach to study the nitrogen doping," *J. Nanosci. Nanotechnol.*, vol. 7, no. 6, pp. 1820–1823, 2007, doi: 10.1166/jnn.2007.723.

[30] S. Sahebian, S. M. Zebarjad, J. vahdati Khaki, and A. Lazzeri, "A study on the dependence of structure of multi-walled carbon nanotubes on acid treatment," *J. Nanostructure Chem.*, vol. 5, no. 3, pp. 287–293, 2015, doi: 10.1007/s40097-015-0160-3.

[31] J. P. Tessonnier *et al.*, "Analysis of the structure and chemical properties of some commercial carbon nanostructures," *Carbon N. Y.*, vol. 47, no. 7, pp. 1779–1798, 2009, doi: 10.1016/j.carbon.2009.02.032.

[32] F. Habeb Abdulrazzak, A. Fadel Alkiam, and F. Hasan Hussein, "Behavior of X-Ray Analysis of Carbon Nanotubes," *Perspect. Carbon Nanotub.*, no. July, 2019, doi: 10.5772/intechopen.85156.

[33] T. Belin and F. Epron, "Characterization methods of carbon nanotubes: A review," *Mater. Sci. Eng. B Solid-State Mater. Adv. Technol.*, vol. 119, no. 2, pp. 105–118, 2005, doi: 10.1016/j.mseb.2005.02.046.

[34] A. Jorio, "Raman Spectroscopy in Graphene-Based Systems: Prototypes for Nanoscience and Nanometrology," *ISRN Nanotechnol.*, vol. 2012, no. 2, pp. 1–16, 2012, doi: 10.5402/2012/234216.

[35] R. A. DiLeo, B. J. Landi, and R. P. Raffaelle, "Purity assessment of multiwalled carbon nanotubes by Raman spectroscopy," *J. Appl. Phys.*, vol. 101, no. 6, 2007, doi: 10.1063/1.2712152.

[36] R. DiLeo, B. Landi, and R. Raffaelle, "Application of the G'/D raman ratio for purity assessment of multi-walled carbon nanotubes," *Mater. Res. Soc. Symp. Proc.*, vol. 1018, pp. 49–54, 2007, doi: 10.1557/proc-1018-ee05-11.

[37] C. Lamprecht, J. T. Huzil, and S. S. Sensors, "Pharmaceutical characterization of solid and dispersed carbon nanotubes as nanoexcipients," no. May 2014, 2012, doi: 10.2147/IJN.S27442.

[38] R. Herrera-Basurto, Á. I. López-Lorente, and M. Valcárcel, "Scanning electron microscopy of carbon nanotubes dispersed in ionic liquid: Solvent influence study," *Microchem. J.*, vol. 122, pp. 137–143, 2015, doi: 10.1016/j.microc.2015.04.012.

[39] Y. Lin, F. Lu, Y. Tu, and Z. Ren, "Glucose Biosensors Based on Carbon Nanotube Nanoelectrode Ensembles," *Nano Lett.*, vol. 4, no. 2, pp. 191–195, 2004, doi: 10.1021/nl0347233.

[40] F. C. Vicentini, B. C. Janegitz, C. M. A. Brett, and O. Fatibello-Filho, "Tyrosinase biosensor based on a glassy carbon electrode modified with multi-walled carbon nanotubes and 1-butyl-3-methylimidazolium chloride within a dihexadecylphosphate film," *Sensors Actuators, B Chem.*, vol. 188, pp. 1101–1108, 2013, doi: 10.1016/j.snb.2013.07.109.

[41] R. Alshehri, A. M. Ilyas, A. Hasan, A. Arnaout, F. Ahmed, and A. Memic, "Carbon Nanotubes in Biomedical Applications: Factors, Mechanisms, and Remedies of Toxicity," *J. Med. Chem.*, vol. 59, no. 18, pp. 8149–8167, 2016, doi: 10.1021/acs.jmedchem.5b01770.

[42] A. Pietroiusti *et al.*, "Low doses of pristine and oxidized single-wall carbon nanotubes affect mammalian embryonic development," *ACS Nano*, vol. 5, no. 6, pp. 4624–4633, 2011, doi: 10.1021/nn200372g.

[43] S. T. Yang *et al.*, “Biodistribution of pristine single-walled carbon nanotubes in vivo,” *J. Phys. Chem. C*, vol. 111, no. 48, pp. 17761–17764, 2007, doi: 10.1021/jp070712c.

[44] L. Yongfeng, T. Kaneko, J. Kong, and R. Hatakeyama, “Photoswitching in azafullerene encapsulated single-walled carbon nanotube FET devices,” *J. Am. Chem. Soc.*, vol. 131, no. 10, pp. 3412–3413, 2009, doi: 10.1021/ja810086g.

[45] N. D. Cox, J. E. Rossi, and B. J. Landi, “Carbon nanotube metal matrix composites for solar cell electrodes,” in *2015 IEEE 42nd Photovoltaic Specialist Conference (PVSC)*, Jun. 2015, pp. 1–4, doi: 10.1109/PVSC.2015.7355867.

[46] F. Wang *et al.*, “Considerably improved photovoltaic performance of carbon nanotube-based solar cells using metal oxide layers,” *Nat. Commun.*, vol. 6, pp. 1–7, 2015, doi: 10.1038/ncomms7305.

[47] C. W. Chen, M. H. Lee, and S. J. Clark, “Band gap modification of single-walled carbon nanotube and boron nitride nanotube under a transverse electric field,” *Nanotechnology*, vol. 15, no. 12, pp. 1837–1843, 2004, doi: 10.1088/0957-4484/15/12/025.

[48] C. Klinger, Y. Patel, and H. W. C. Postma, “Carbon nanotube solar cells,” *PLoS One*, vol. 7, no. 5, pp. 1–9, 2012, doi: 10.1371/journal.pone.0037806.

[49] S. D. Dutta, D. K. Patel, and K.-T. Lim, *Carbon nanotube-based nanohybrids for agricultural and biological applications*, no. March. 2020.

[50] A. M. DeRosa, K. Greco, S. Rajamani, and B. Sitharaman, “Recent patents on single-walled carbon nanotubes for biomedical imaging, drug delivery and tissue regeneration,” *Recent Pat. Biomed. Eng.*, vol. 3, no. 2, pp. 86–94, 2010, doi: 10.2174/1874764711003020086.

[51] A. Eatemadi *et al.*, “Carbon nanotubes: Properties, synthesis, purification, and medical applications,” *Nanoscale Res. Lett.*, vol. 9, no. 1, pp. 1–13, 2014, doi: 10.1186/1556-276X-9-393.

[52] E. Dervishi *et al.*, “Carbon nanotubes: Synthesis, properties, and applications,” *Particulate Science and Technology*. 2009, doi: 10.1080/02726350902775962.

[53] N. Bagotia and D. Sharma, “Review on CNTs and graphene based polycarbonate nanocomposites,” no. September, pp. 1–54, 2019, [Online]. Available: file:///C:/Users/nishu.goyal/Desktop/978-620-0-21547-5.pdf.

[54] C. Journet and P. Bernier, “Production of carbon nanotubes,” *Appl. Phys. A Mater. Sci. Process.*, vol. 67, no. 1, pp. 1–9, 1998, doi: 10.1007/s003390050731.

[55] A. Douglas, R. Carter, M. Li, and C. L. Pint, “Toward Small-Diameter Carbon Nanotubes Synthesized from Captured Carbon Dioxide: Critical Role of Catalyst Coarsening,” *ACS Appl. Mater. Interfaces*, vol. 10, no. 22, pp. 19010–19018, 2018, doi: 10.1021/acsami.8b02834.

[56] J. Ren, F.-F. Li, J. Lau, L. González-Urbina, and S. Licht, “One-Pot Synthesis of Carbon Nanofibers from CO_2,” *Nano Lett.*, vol. 15, no. 9, pp. 6142–6148, 2015, doi: 10.1021/acs.nanolett.5b02427.

[57] S. Arcaro, F. A. Berutti, A. K. Alves, and C. P. Bergmann, “Applied Surface Science MWCNTs produced by electrolysis of molten carbonate : Characteristics of the cathodic products grown on galvanized steel and nickel chrome electrodes,” *Appl. Surf. Sci.*, vol. 466, no. April 2018, pp. 367–374, 2019, doi: 10.1016/j.apsusc.2018.10.055.

[58] T. Okada, T. Kaneko, and R. Hatakeyama, “Conversion of toluene into carbon nanotubes using arc discharge plasmas in solution,” *Thin Solid Films*, vol. 515, no. 9, pp. 4262–4265, 2007, doi: 10.1016/j.tsf.2006.02.067.

[59] M. V. Antisari, R. Marazzi, and R. Krsmanovic, “Synthesis of multiwall carbon nanotubes by electric arc discharge in liquid environments,” *Carbon N. Y.*, vol. 41, no. 12, pp. 2393–2401, 2003, doi: 10.1016/S0008-6223(03)00297-5.

[60] X. Lin *et al.*, “Large scale synthesis of single-shell carbon nanotubes,” vol. 181, no. May 2014, pp. 8–11, 2005, doi: 10.1063/1.111525.

[61] Z. Shi *et al.*, “Mass-production of single-wall carbon nanotubes by arc discharge method,” *Carbon N. Y.*, vol. 37, no. 9, pp. 1449–1453, 1999, doi: 10.1016/S0008-6223(99)00007-X.

[62] T. Guo, P. Nikolaev, A. Thess, D. T. Colbert, and R. E. Smalley, “Catalytic growth of single-walled manotubes by laser vaporization,” *Chem. Phys. Lett.*, vol. 243, no. 1–2, pp. 49–54, 1995, doi: 10.1016/0009-2614(95)00825-O.

[63] M. Yudasaka, R. Yamada, N. Sensui, T. Wilkins, T. Ichihashi, and S. Iijima, “Mechanism of the effect of NiCo, Ni and Co catalysts on the yield of single-wall carbon nanotubes formed by pulsed Nd:YAG laser ablation,” *J. Phys. Chem. B*, vol. 103, no. 30, pp. 6224–6229, 1999, doi: 10.1021/jp9908451.

[64] W. K. Maser *et al.*, “Production of high-density single-walled nanotube material by a simple laser-ablation method,” *Chem. Phys. Lett.*, vol. 292, no. 4–6, pp. 587–593, 1998, doi: 10.1016/S0009-2614(98)00776-3.

[65] T. Guo, P. Nikolaev, A. G. Rinzler, D. Tomanek, D. T. Colbert, and R. E. Smalley, “Self-assembly of tubular fullerenes,” *J. Phys. Chem.*, vol. 99, no. 27, pp. 10694–10697, 1995, doi: 10.1021/j100027a002.

[66] R. Yuge, K. Toyama, T. Ichihashi, T. Ohkawa, Y. Aoki, and T. Manako, “Characterization and field emission properties of multi-walled carbon nanotubes with fine crystallinity prepared by CO 2 laser ablation,” *Appl. Surf. Sci.*, vol. 258, no. 18, pp. 6958–6962, 2012, doi: 10.1016/j.apsusc.2012.03.143.

[67] M. Kusaba and Y. Tsunawaki, “Production of single-wall carbon nanotubes by a XeCl excimer laser ablation,” *Thin Solid Films*, vol. 506–507, pp. 255–258, 2006, doi: 10.1016/j.tsf.2005.08.037.

[68] V. Le Borgne, B. Aïssa, M. Mohamedi, Y. A. Kim, M. Endo, and M. A. El Khakani, “Pulsed KrF-laser synthesis of single-wall-carbon-nanotubes: Effects of catalyst content and furnace temperature on their nanostructure and photoluminescence properties,” *J. Nanoparticle Res.*, vol. 13, no. 11, pp. 5759–5767, 2011, doi: 10.1007/s11051-011-0409-9.

[69] A. Jedrzejewska *et al.*, “A systematic and comparative study of binary metal catalysts for carbon nanotube fabrication using CVD and laser evaporation,” *Fullerenes Nanotub. Carbon Nanostructures*, vol. 21, no. 4, pp. 273–285, 2013, doi: 10.1080/1536383X.2011.613540.

[70] H. Dai, A. G. Rinzler, P. Nikolaev, A. Thess, D. T. Colbert, and R. E. Smalley, “Single-wall nanotubes produced by metal-catalyzed disproportionation of carbon monoxide,” *Chem. Phys. Lett.*, vol. 260, no. 3–4, pp. 471–475, 1996, doi: 10.1016/0009-2614(96)00862-7.

[71] R. T. K. Baker, “Catalytic growth of carbon filaments,” *Carbon N. Y.*, vol. 27, no. 3, pp.

315–323, Jan. 1989, doi: 10.1016/0008-6223(89)90062-6.

[72] M. Su, B. Zheng, and J. Liu, “A scalable CVD method for the synthesis of single-walled carbon nanotubes with high catalyst productivity,” *Chem. Phys. Lett.*, vol. 322, no. 5, pp. 321–326, 2000, doi: 10.1016/S0009-2614(00)00422-X.

[73] Y. V Shubin, L. I. Yudanova, and L. G. Bulusheva, “Growth of Carbon Nanotubes via Chemical Vapor Deposition on Co Catalyst Nanoparticles Dispersed in CaO,” vol. 44, no. 3, pp. 213–218, 2008, doi: 10.1134/S0020168508030011.

[74] P. Nikolaev *et al.*, “Gas-phase catalytic growth of single-walled carbon nanotubes from carbon monoxide,” *Chem. Phys. Lett.*, vol. 313, no. 1–2, pp. 91–97, 1999, doi: Doi 10.1016/S0009-2614(99)01029-5.

[75] M. D. Ingram, B. Baron, and G. J. Janz, “The electrolytic deposition of carbon from fused carbonates,” *Electrochim. Acta*, vol. 11, no. 11, pp. 1629–1639, 1966, doi: 10.1016/0013-4686(66)80076-2.

[76] J. Ren and S. Licht, “Tracking airborne CO2mitigation and low cost transformation into valuable carbon nanotubes,” *Sci. Rep.*, vol. 6, no. June, 2016, doi: 10.1038/srep27760.

[77] S. Licht, A. Douglas, J. Ren, R. Carter, M. Lefler, and C. L. Pint, “Carbon nanotubes produced from ambient carbon dioxide for environmentally sustainable lithium-ion and sodium-ion battery anodes,” *ACS Cent. Sci.*, vol. 2, no. 3, pp. 162–168, 2016, doi: 10.1021/acscentsci.5b00400.

[78] S. Licht, “Efficient solar-driven synthesis, carbon capture, and desalinization, STEP: Solar thermal electrochemical production of fuels, metals, bleach,” *Adv. Mater.*, vol. 23, no. 47, pp. 5592–5612, 2011, doi: 10.1002/adma.201103198.

[79] A. T. Dimitrov, “STUDY OF MOLTEN Li 2 CO 3 ELECTROLYSIS AS A METHOD FOR PRODUCTION OF CARBON NANOTUBES,” *Maced. J. Chem. Chem. Eng.*, vol. 28, no. 1, pp. 111–118, 2009.

[80] H. V. Ijije, C. Sun, and G. Z. Chen, “Indirect electrochemical reduction of carbon dioxide to carbon nanopowders in molten alkali carbonates: Process variables and product properties,” *Carbon N. Y.*, vol. 73, pp. 163–174, 2014, doi: 10.1016/j.carbon.2014.02.052.

[81] X. Qiao, H. Li, W. Zhao, and D. Li, “Effects of deposition temperature on electrodeposition of zinc-nickel alloy coatings,” *Electrochim. Acta*, vol. 89, pp. 771–777, 2013, doi: 10.1016/j.electacta.2012.11.006.

[82] D. Tang, H. Yin, X. Mao, W. Xiao, and D. H. Wang, “Effects of applied voltage and temperature on the electrochemical production of carbon powders from CO2 in molten salt with an inert anode,” *Electrochim. Acta*, vol. 114, pp. 567–573, 2013, doi: 10.1016/j.electacta.2013.10.109.

[83] J. Ren, M. Johnson, R. Singhal, and J. Licht, “Transformation of the greenhouse gas CO2 by molten electrolysis into a wide controlled selection of carbon nanotubes,” *J. CO2 Util.*, vol. 18, pp. 335–344, 2017, doi: 10.1016/j.jcou.2017.02.005.

[84] A. Douglas, N. Muralidharan, R. Carter, and C. L. Pint, “Sustainable Capture and Conversion of Carbon Dioxide into Valuable Multiwalled Carbon Nanotubes Using Metal Scrap Materials,” *ACS Sustain. Chem. Eng.*, vol. 5, no. 8, pp. 7104–7110, 2017, doi: 10.1021/acssuschemeng.7b01314.

[85] H. V Ijije, R. C. Lawrence, and G. Z. Chen, “Carbon electrodeposition in molten salts:

Electrode reactions and applications," *RSC Advances*, vol. 4, no. 67. Royal Society of Chemistry, pp. 35808–35817, 2014, doi: 10.1039/c4ra04629c.

[86] H. V Ijije *et al.*, "Electro-deposition and re-oxidation of carbon in carbonate-containing molten salts," *Faraday Discuss.*, vol. 172, pp. 105–116, 2014, doi: 10.1039/c4fd00046c.

[87] L. Hu *et al.*, "Direct Conversion of Greenhouse Gas CO2 into Graphene via Molten Salts Electrolysis," *ChemSusChem*, vol. 9, no. 6, pp. 588–594, 2016, doi: 10.1002/cssc.201501591.

[88] S. Tebriani, "Analisa Pengaruh Tegangan Terhadap Hasil Elektrodeposisi Pada Lapisan Tipis Magnetite Menggunakan Arus Continue Direct Current," vol. 4, pp. 555–560, 2018.

[89] M. Gao, B. Deng, Z. Chen, M. Tao, and D. Wang, "Cathodic reaction kinetics for CO2 capture and utilization in molten carbonates at mild temperatures," *Electrochem. commun.*, vol. 88, no. January, pp. 79–82, 2018, doi: 10.1016/j.elecom.2018.02.003.

[90] M. G. Fontana, "Corrosion engineering. Third edition.," 1986.

[91] C. T. Lin and K. L. Lin, "Effects of current density and deposition time on electrical resistivity of electroplated Cu layers," *J. Mater. Sci. Mater. Electron.*, vol. 15, no. 11, pp. 757–762, 2004, doi: 10.1023/B:JMSE.0000043425.91103.da.

[92] A. T. Dimitrov, "THE ELECTROLYTIC DEPOSITION OF CARBON FROM MOLTEN Li 2 CO 3," pp. 338–343, 2003.

[93] S. Sigit, G. Widodo, B. Wasito, K. T. Basuki, and F. Fahrunissa, "Effect of Current, Time, Feed and Cathode Type on Electroplating Process of Uranium Solution," *Urania J. Ilm. Daur Bahan Bakar Nukl.*, vol. 23, no. 1, pp. 11–22, 2017, doi: 10.17146/urania.2017.23.1.3155.

[94] Gunawan, A. Haris, H. Widiyandari, and D. S. Widodo, "Effect of potentials and electric charges for copper and indium depositions to the photocurrent responses of CuInS2 thin films fabricated by stack electrodeposition followed by sulfurization," *IOP Conf. Ser. Mater. Sci. Eng.*, vol. 349, no. 1, 2018, doi: 10.1088/1757-899X/349/1/012074.

[95] P. M. Hannula *et al.*, "Carbon nanotube-copper composites by electrodeposition on carbon nanotube fibers," *Carbon N. Y.*, vol. 107, pp. 281–287, 2016, doi: 10.1016/j.carbon.2016.06.008.

[96] Z. Fan and W. Xiao, "Electrochemical Splitting of Methane in Molten Salts To Produce Hydrogen," *Angew. Chemie - Int. Ed.*, vol. 60, no. 14, pp. 7664–7668, 2021, doi: 10.1002/anie.202017243.

[97] J. Singh and D. W. Dhar, "Overview of carbon capture technology: Microalgal biorefinery concept and state-of-the-art," *Front. Mar. Sci.*, vol. 6, no. FEB, pp. 1–9, 2019, doi: 10.3389/fmars.2019.00029.

[98] J. Ren, J. Lau, M. Lefler, and S. Licht, "The Minimum Electrolytic Energy Needed To Convert Carbon Dioxide to Carbon by Electrolysis in Carbonate Melts," *J. Phys. Chem. C*, vol. 119, no. 41, pp. 23342–23349, Oct. 2015, doi: 10.1021/acs.jpcc.5b07026.

[99] M. Chen, Y. C. Kao, H. W. Yu, S. C. Lu, and H. S. Koo, "Influence of CO2 and N2 on the growth of carbon nanotubes by using thermal chemical vapor deposition," *Thin Solid Films*, vol. 516, no. 2–4, pp. 277–283, 2007, doi: 10.1016/j.tsf.2007.07.211.

[100] J. Polanski, “Chemoinformatics,” no. January 2007, 2017.

[101] M. S. FRIEDRICHS *et al.*, “Accelerating Molecular Dynamic Simulation on Graphics Processing Units,” *J. Comput. Chem.*, vol. 30, no. 10, pp. 1545–1614, 2009, doi: 10.1002/jcc.

[102] A. F. Voter, “Hyperdynamics: Accelerated Molecular Dynamics of Infrequent Events Arthur,” *Phys. Rev. Lett.*, vol. 78, no. 20, pp. 3908–3911, 1997, doi: 10.1016/S1385-8947(99)00055-8.

[103] C. C. Hsu, M. J. Buehler, and A. Tarakanova, “The Order-Disorder Continuum: Linking Predictions of Protein Structure and Disorder through Molecular Simulation,” *Sci. Rep.*, vol. 10, no. 1, p. 2068, 2020, doi: 10.1038/s41598-020-58868-w.

[104] M. A. L. Eriksson, J. Pitera, and P. A. Kollman, “Prediction of the binding free energies of new TIBO-like HIV-1 reverse transcriptase inhibitors using a combination of PROFEC, PB/SA, CMC/MD, and free energy calculations,” *J. Med. Chem.*, vol. 42, no. 5, pp. 868–881, 1999, doi: 10.1021/jm980277y.

[105] S. Hug, “Classical molecular dynamics in a nutshell,” *Methods Mol. Biol.*, vol. 924, pp. 127–152, 2013, doi: 10.1007/978-1-62703-17-5_6.

[106] S. J. Plimpton and B. A. Hendrickson, “Parallel Molecular Dynamics With the Embedded Atom Method,” *MRS Proc.*, vol. 291, p. 37, Jan. 1992, doi: 10.1557/PROC-291-37.

[107] M. S. Daw, S. M. Foiles, and M. I. Baskes, “The embedded-atom method: a review of theory and applications,” *Mater. Sci. Reports*, vol. 9, no. 7–8, pp. 251–310, Mar. 1993, doi: 10.1016/0920-2307(93)90001-U.

[108] S. M. Foiles, M. I. Baskes, C. F. Melius, and M. S. Daw, “Calculation of hydrogen dissociation pathways on nickel using the embedded atom method,” *J. Less Common Met.*, vol. 130, pp. 465–473, Mar. 1987, doi: 10.1016/0022-5088(87)90144-5.

[109] T. Treeratanaphitak, M. D. Pritzker, and N. M. Abukhdeir, “Kinetic monte carlo simulation of electrodeposition using the embedded-atom method,” *Electrochim. Acta*, vol. 121, pp. 407–414, 2014, doi: 10.1016/j.electacta.2013.12.166.

[110] Y. Shibuta and S. Maruyama, “Molecular dynamics simulation of formation process of single-walled carbon nanotubes by CCVD method,” *Chem. Phys. Lett.*, vol. 382, no. 3–4, pp. 381–386, 2003, doi: 10.1016/j.cplett.2003.10.080.

[111] J. Behler and M. Parrinello, “Generalized Neural-Network Representation of High-Dimensional Potential-Energy Surfaces,” *Phys. Rev. Lett.*, vol. 98, no. 14, p. 146401, Apr. 2007, doi: 10.1103/PhysRevLett.98.146401.

[112] H. M. Aktulga, J. C. Fogarty, S. A. Pandit, and A. Y. Grama, “Parallel reactive molecular dynamics: Numerical methods and algorithmic techniques,” *Parallel Comput.*, vol. 38, no. 4–5, pp. 245–259, 2012, doi: 10.1016/j.parco.2011.08.005.

[113] H. M. Aktulga, S. A. Pandit, A. C. T. Van Duin, and A. Y. Grama, “Reactive molecular dynamics: Numerical methods and algorithmic techniques,” *SIAM J. Sci. Comput.*, vol. 34, no. 1, 2012, doi: 10.1137/100808599.

[114] N. Onofrio and A. Strachan, “Voltage equilibration for reactive atomistic simulations of electrochemical processes,” *J. Chem. Phys.*, vol. 143, no. 5, 2015, doi: 10.1063/1.4927562.

[115] A. C. T. Van Duin, S. Dasgupta, F. Lorant, and W. A. Goddard, “ReaxFF: A reactive force field for hydrocarbons,” *J. Phys. Chem. A*, vol. 105, no. 41, pp. 9396–9409, 2001, doi: 10.1021/jp004368u.

[116] N. Onofrio and A. Strachan, “Voltage equilibration for reactive atomistic simulations of electrochemical processes,” *J. Chem. Phys.*, vol. 143, no. 5, 2015, doi: 10.1063/1.4927562.

[117] K. D. Nielson, A. C. T. Van Duin, J. Oxgaard, W. Q. Deng, and W. A. Goddard, “Development of the ReaxFF reactive force field for describing transition metal catalyzed reactions, with application to the initial stages of the catalytic formation of carbon nanotubes,” *J. Phys. Chem. A*, vol. 109, no. 3, pp. 493–499, 2005, doi: 10.1021/jp046244d.

[118] A. Stukowski, “Visualization and analysis of atomistic simulation data with OVITO-the Open Visualization Tool,” *Model. Simul. Mater. Sci. Eng.*, vol. 18, no. 1, 2010, doi: 10.1088/0965-0393/18/1/015012.

[119] S. Nose, “A molecular dynamics method for simulations in the canonical ensemble,” *Mol. Phys.*, vol. 52, no. 2, pp. 255–268, 1984, doi: 10.1080/00268970110089l0.

[120] T. P. Senftle *et al.*, “The ReaxFF reactive force-field: Development, applications and future directions,” *npj Comput. Mater.*, vol. 2, no. September 2015, 2016, doi: 10.1038/npjcompumats.2015.11.

[121] N. Onofrio, D. Guzman, and A. Strachan, “Atomic origin of ultrafast resistance switching in nanoscale electrometallization cells,” *Nat. Mater.*, vol. 14, no. 4, pp. 440–446, 2015, doi: 10.1038/nmat4221.

[122] N. C. Fei, N. M. Mehat, and S. Kamaruddin, “Practical Applications of Taguchi Method for Optimization of Processing Parameters for Plastic Injection Moulding: A Retrospective Review,” *ISRN Ind. Eng.*, vol. 2013, p. 462174, 2013, doi: 10.1155/2013/462174.

[123] H. Hanaei, A. Fakhru’L-Razi, D. R. A. Biak, I. S. Ahamad, and F. Danafar, “Effects of synthesis reaction temperature, deposition time and catalyst on yield of carbon nanotubes,” *Asian J. Chem.*, vol. 24, no. 6, pp. 2407–2414, 2012.

[124] A. C. T. Van Duin, S. Dasgupta, F. Lorant, and W. A. Goddard, “ReaxFF: A reactive force field for hydrocarbons,” *J. Phys. Chem. A*, vol. 105, no. 41, pp. 9396–9409, 2001, doi: 10.1021/jp004368u.

[125] N. Onofrio and A. Strachan, “Voltage equilibration for reactive atomistic simulations of electrochemical processes,” *J. Chem. Phys.*, vol. 143, no. 5, 2015, doi: 10.1063/1.4927562.

[126] H. Yin *et al.*, “Capture and electrochemical conversion of CO2 to value-added carbon and oxygen by molten salt electrolysis,” *Energy Environ. Sci.*, vol. 6, no. 5, 2013, doi: 10.1039/c3ee24132g.

[127] A. Douglas, R. Carter, N. Muralidharan, L. Oakes, and C. L. Pint, “Iron catalyzed growth of crystalline multi-walled carbon nanotubes from ambient carbon dioxide mediated by molten carbonates,” *Carbon N. Y.*, vol. 116, pp. 572–578, 2017, doi: 10.1016/j.carbon.2017.02.032.

[128] A. G. Rinzler *et al.*, “Large-scale purification of single-wall carbon nanotubes: Process, product, and characterization,” *Appl. Phys. A Mater. Sci. Process.*, vol. 67, no. 1, pp. 29–37, 1998, doi: 10.1007/s003390050734.

[129] B. P. Singh, S. Samal, S. Nayak, S. M. Majhi, L. Besra, and S. Bhattacharjee, “The production of a multi-walled carbon nanotube/hexamethylene diisocyanate nanocomposite coating on copper by electrophoretic deposition,” *Surf. Coatings Technol.*, vol. 206, no. 6, pp. 1319–1326, 2011, doi: 10.1016/j.surfcoat.2011.08.054.

[130] A. Grzechnik, P. Bouvier, and L. Farina, “High-pressure structure of Li2CO3,” *J. Solid State Chem.*, vol. 173, no. 1, pp. 13–19, 2003, doi: 10.1016/S0022-4596(03)00053-7.

[131] W. Linert, “Aromaticity of Carbon Nanotubes †,” pp. 887–890, 2007.

[132] B. P. Vinayan, R. Nagar, V. Raman, N. Rajalakshmi, K. S. Dhathathreyan, and S. Ramaprabhu, “Synthesis of graphene-multiwalled carbon nanotubes hybrid nanostructure by strengthened electrostatic interaction and its lithium ion battery application,” *J. Mater. Chem.*, vol. 22, no. 19, pp. 9949–9956, 2012, doi: 10.1039/c2jm16294f.

[133] R. Saito, M. Hofmann, G. Dresselhaus, A. Jorio, and M. S. Dresselhaus, “Raman spectroscopy of graphene and carbon nanotubes,” *Adv. Phys.*, vol. 60, no. 3, pp. 413–550, 2011, doi: 10.1080/00018732.2011.582251.

[134] H. Hiura, T. W. Ebbesen, K. Tanigaki, and H. Takahashi, “Raman studies of carbon nanotubes,” *Chem. Phys. Lett.*, vol. 202, no. 6, pp. 509–512, 1993, doi: 10.1016/0009-2614(93)90040-8.

[135] H. Yin *et al.*, “Capture and electrochemical conversion of CO2 to value-added carbon and oxygen by molten salt electrolysis,” *Energy Environ. Sci.*, vol. 6, no. 6, pp. 1538–1545, 2013, doi: 10.1039/c3ee24132g.

[136] M. Flygare and K. Svensson, “Quantifying crystallinity in carbon nanotubes and its influence on mechanical behaviour,” *Mater. Today Commun.*, vol. 18, no. November 2018, pp. 39–45, 2019, doi: 10.1016/j.mtcomm.2018.11.003.

[137] C. Branca *et al.*, “Structural and vibrational properties of carbon nanotubes by TEM and infrared spectroscopy,” *Diam. Relat. Mater.*, vol. 13, no. 4–8, pp. 1249–1253, 2004, doi: 10.1016/j.diamond.2003.11.059.

[138] O. Dubay and G. Kresse, “Accurate density functional calculations for the phonon dispersion relations of graphite layer and carbon nanotubes,” *Phys. Rev. B - Condens. Matter Mater. Phys.*, vol. 67, no. 3, pp. 1–13, 2003, doi: 10.1103/PhysRevB.67.035401.

[139] J. Bantignies *et al.*, “Infrared-active phonons in carbon nanotubes To cite this version : HAL Id : hal-00514943,” 2017.

[140] K. Le Van *et al.*, “Electrochemical formation of carbon nano-powders with various porosities in molten alkali carbonates,” *Electrochim. Acta*, vol. 54, no. 19, pp. 4566–4573, 2009, doi: 10.1016/j.electacta.2009.03.049.

[141] R. Y. S. Zampiva, C. G. Kaufmann Junior, J. S. Pinto, P. C. Panta, A. K. Alves, and C. P. Bergmann, “3D CNT macrostructure synthesis catalyzed by MgFe 2 O 4 nanoparticles—A study of surface area and spinel inversion influence,” *Appl. Surf. Sci.*, vol. 422, pp. 321–330, 2017, doi: 10.1016/j.apsusc.2017.06.020.

[142] A. M. Rao *et al.*, “Diameter-selective Raman scattering from vibrational modes in carbon nanotubes,” *Science (80-.).*, vol. 275, no. 5297, pp. 187–190, 1997, doi: 10.1126/science.275.5297.187.

[143] M. S. Dresselhaus, G. Dresselhaus, A. Jorio, A. G. Souza Filho, and R. Saito, “Raman spectroscopy on isolated single wall carbon nanotubes,” *Carbon N. Y.*, vol. 40, no. 12,

pp. 2043–2061, 2002, doi: 10.1016/S0008-6223(02)00066-0.

[144] J. M. Benoit, J. P. Buisson, O. Chauvet, C. Godon, and S. Lefrant, “Low-frequency Raman studies of multiwalled carbon nanotubes: Experiments and theory,” *Phys. Rev. B - Condens. Matter Mater. Phys.*, vol. 66, no. 7, pp. 1–4, 2002, doi: 10.1103/PhysRevB.66.073417.

[145] A. Douglas and C. L. Pint, “Review—Electrochemical Growth of Carbon Nanotubes and Graphene from Ambient Carbon Dioxide: Synergy with Conventional Gas-Phase Growth Mechanisms,” *ECS J. Solid State Sci. Technol.*, vol. 6, no. 6, pp. M3084–M3089, 2017, doi: 10.1149/2.0131706jss.

[146] M. Kumar and Y. Ando, “Chemical Vapor Deposition of Carbon Nanotubes: A Review on Growth Mechanism and Mass Production,” *J. Nanosci. Nanotechnol.*, vol. 10, no. 6, pp. 3739–3758, 2010, doi: 10.1166/jnn.2010.2939.

[147] A. V. Radhamani, H. C. Lau, and S. Ramakrishna, “CNT-reinforced metal and steel nanocomposites: A comprehensive assessment of progress and future directions,” *Compos. Part A Appl. Sci. Manuf.*, vol. 114, no. August, pp. 170–187, 2018, doi: 10.1016/j.compositesa.2018.08.010.

[148] M. M. Walz and D. van der Spoel, “Microscopic origins of conductivity in molten salts unraveled by computer simulations,” *Commun. Chem.*, vol. 4, no. 1, pp. 1–10, 2021, doi: 10.1038/s42004-020-00446-2.

[149] M. M. Walz and D. Van Der Spoel, “Molten alkali halides-temperature dependence of structure, dynamics and thermodynamics,” *Phys. Chem. Chem. Phys.*, vol. 21, no. 34, pp. 18516–18524, 2019, doi: 10.1039/c9cp03603b.

[150] M. M. Walz and D. Van Der Spoel, “Direct Link between Structure, Dynamics, and Thermodynamics in Molten Salts,” *J. Phys. Chem. C*, vol. 123, no. 42, pp. 25596–25602, 2019, doi: 10.1021/acs.jpcc.9b07756.

[151] F. Habeb Abdulrazzak, A. Fadel Alkiam, and F. Hasan Hussein, “Behavior of X-Ray Analysis of Carbon Nanotubes,” *Perspect. Carbon Nanotub.*, pp. 1–16, 2019, doi: 10.5772/intechopen.85156.

[152] T. W. Ebbesen, “Large-scale syntesis of carbon nanotube,” *Lett. to Nat.*, vol. 358, pp. 220–222, 1992.

[153] S. Iijima and T. Ichihashi, “Single-shell carbon nanotubes of 1-nm diameter,” *Nature*, vol. 363, pp. 603–605, 1993.

[154] D. S. Bethune *et al.*, “Cobalt-catalysed growth of carbon nanotubes with single-atomic-layer walls,” *Nature*, vol. 363, no. 6430, pp. 605–607, 1993, doi: 10.1038/363605a0.

[155] A. Loiseau and H. Pascard, “Synthesis of long carbon nanotubes filled with Se, S, Sb and Ge by the arc method,” *Chem. Phys. Lett.*, vol. 256, no. 3, pp. 246–252, 1996, doi: 10.1016/0009-2614(96)00459-9.

[156] C. Journet *et al.*, “Large-scale production of single-walled carbon nanotubes by the electric-arc technique,” *Nature*, vol. 388, no. 6644, pp. 756–758, 1997, doi: 10.1038/41972.

[157] M. E. Itkis *et al.*, “Optimization of the Ni-Y catalyst composition in bulk electric arc synthesis of single-walled carbon nanotubes by use of near-infrared spectroscopy,” *J. Phys. Chem. B*, vol. 108, no. 34, pp. 12770–12775, 2004, doi: 10.1021/jp0487307.

[158] M. Yao *et al.*, “Synthesis of single-wall carbon nanotubes and long nanotube ribbons with Ho/Ni as catalyst by arc discharge,” *Carbon N. Y.*, vol. 43, no. 14, pp. 2894–2901, 2005, doi: 10.1016/j.carbon.2005.05.019.

[159] X. Sun, W. Bao, Y. Lv, J. Deng, and X. Wang, “Synthesis of high quality single-walled carbon nanotubes by arc discharge method in large scale,” *Mater. Lett.*, vol. 61, no. 18, pp. 3956–3958, 2007, doi: 10.1016/j.matlet.2006.12.070.

[160] M. Jahanshahi, J. Raoof, and R. Jabari Seresht, “Voltage effects on the production of nanocarbons by a unique arc-discharge set-up in solution,” *J. Exp. Nanosci.*, vol. 4, no. 4, pp. 331–339, 2009, doi: 10.1080/17458080903071796.

[161] P. Hou, C. Liu, Y. Tong, S. Xu, M. Liu, and H. Cheng, “Purification of single-walled carbon nanotubes synthesized by the hydrogen arc-discharge method,” pp. 2526–2529, 2001.

[162] M. I. Mohammad, A. a. Moosa, J. H. Potgieter, and M. K. Ismael, “Carbon Nanotubes Synthesis via Arc Discharge with a Yttria Catalyst,” *ISRN Nanomater.*, vol. 2013, pp. 1–7, 2013, doi: 10.1155/2013/785160.

[163] L. Fang *et al.*, “Effect of adding W to Fe catalyst on the synthesis of SWCNTs by arc discharge,” *Phys. E Low-Dimensional Syst. Nanostructures*, vol. 50, pp. 116–121, 2013, doi: 10.1016/j.physe.2013.03.005.

[164] H. Dai, J. H. Hafner, A. G. Rinzler, D. T. Colbert, and R. E. Smalley, “Nanotubes as nanoprobes in scanning probe microscopy,” *Nature*, vol. 384, no. 6605, pp. 147–150, 1996, doi: 10.1038/384147a0.

[165] A. M. Cassell, J. A. Raymakers, J. Kong, and H. Dai, “Large Scale CVD Synthesis of Single-Walled Carbon Nanotubes,” *J. Phys. Chem. B*, vol. 103, no. 31, pp. 6484–6492, 1999, doi: 10.1021/jp990957s.

[166] P. Nikolaev *et al.*, “Gas-phase catalytic growth of single-walled carbon nanotubes from carbon monoxide,” *Chem. Phys. Lett.*, vol. 313, no. 1–2, pp. 91–97, 1999, doi: 10.1016/S0009-2614(99)01029-5.

[167] E. Flahaut, A. Govindaraj, A. Peigney, C. Laurent, A. Rousset, and C. N. R. Rao, “Synthesis of single-walled carbon nanotubes using binary (Fe, Co, Ni) alloy nanoparticles prepared in situ by the reduction of oxide solid solutions,” *Chem. Phys. Lett.*, vol. 300, no. 1–2, pp. 236–242, 1999, doi: 10.1016/S0009-2614(98)01304-9.

[168] J. L. Bahr, J. Yang, D. V Kosynkin, M. J. Bronikowski, R. E. Smalley, and J. M. Tour, “Functionalization of Carbon Nanotubes by Electrochemical Reduction of Aryl Diazonium Salts : A Bucky Paper Electrode,” no. 14, pp. 6536–6542, 2001.

[169] T. E. Shigeo Maruyama*, Erik Einarsson, Yoichi Murakami, “Growth process of vertically aligned single-walled carbon nanotubes,” pp. 1–10, 2005.

[170] R. Xiang, E. Einarsson, Y. Murakami, J. Shiomi, S. Chiashi, and Z. Tang, “Diameter Modulation of Vertically Aligned Single-Walled Carbon Nanotubes,” pp. 1–25.

[171] A. Thess *et al.*, “Crystalline Ropes of Metallic Carbon Nanotubes,” *Science (80-.).*, vol. 273, no. 5274, pp. 483–487, Jul. 1996, doi: 10.1126/science.273.5274.483.

[172] D. Laplaze, P. Bernier, W. K. Maser, G. Flamant, T. Guillard, and A. Loiseau, “Carbon nanotubes: The solar approach,” *Carbon N. Y.*, vol. 36, no. 5–6, pp. 685–688, 1998, doi: 10.1016/S0008-6223(98)00025-6.

[173] E. Muñoz *et al.*, “Single-walled carbon nanotubes produced by cw CO2-laser ablation: study of parameters important for their formation,” *Appl. Phys. A*, vol. 70, no. 2, pp. 145–151, 2000, doi: 10.1007/s003390050026.

[174] A. P. Bolshakov *et al.*, “A novel CW laser-powder method of carbon single-wall nanotubes production,” *Diam. Relat. Mater.*, vol. 11, no. 3–6, pp. 927–930, 2002.

[175] N. Braidy, M. A. El Khakani, and G. A. Botton, “Single-wall carbon nanotubes synthesis by means of UV laser vaporization,” *Chem. Phys. Lett.*, vol. 354, no. 1, pp. 88–92, 2002, doi: https://doi.org/10.1016/S0009-2614(02)00110-0.

[176] T. Ikegami, F. Nakanishi, M. Uchiyama, and K. Ebihara, “Optical measurement in carbon nanotubes formation by pulsed laser ablation,” *Thin Solid Films*, vol. 457, no. 1, pp. 7–11, 2004, doi: 10.1016/j.tsf.2003.12.033.

[177] L. L. Lebel, B. Aissa, M. A. El Khakani, and D. Therriault, “Preparation and mechanical characterization of laser ablated single-walled carbon-nanotubes/polyurethane nanocomposite microbeams,” *Compos. Sci. Technol.*, vol. 70, no. 3, pp. 518–524, 2010, doi: https://doi.org/10.1016/j.compscitech.2009.12.004.

Appendix 1 – Input script

```
units          real
atom_style     full
boundary       p p s

read_data      100.data

pair_style     reax/c NULL checkqeq yes
pair_coeff     * * ../../lammps-stable/lammps/potentials/reaxff.cnt Ni C
```

```
group           Ni type 1
group           C type 2

mass            1 58.6934
mass            2 12.0107

fix         6 all qeq/reax 1 0.0 9.0 1.0e-10 reax/c

#boundary conditions regions
region          boundatas block 0 12 0 12 0 12 units lattice
group           electhi region boundatas
region          boundbawah block 0 12 36 48 0 12 units lattice
group           electlo region boundbawah

dump 1 all atom 1000 output/equilibrium.1100-1100.lammpstrj
log output/equilibrium.1100-1100.log

thermo          100
thermo_style custom step etotal temp bonds pe ke evdwl press pxx pyy pzz pxy pxz pyz lx ly
lz

minimize        1e-35 1e-25 2000 5000

#initialize the property
fix             0 all property/atom d_locpot d_lap
compute         0 all property/atom d_locpot d_lap

#initialize local electrochemical potential
set             type 1 d_locpot 0.0

fix             1 all nvt temp 1073.0 1073.0 100.0
fix             2 all qeq/shielded 1 10.0 1.0e-6 1000 param.qeq
fix             3 Ni echemdid 1 k 6.0 rc 4.0 norm 0.629967 nelec 10 electhi electlo volt 4.0
```

```
fix             4 all reax/c/bonds 1000 bonds.reaxc
fix             5 C reax/c/bonds 1000 bondsC.reaxc
restart 10000 input/equilibrium.1100-1100.restart

run 50000
```

Appendix 2 - lithium carbonate reaction

The reaction below is a reaction to find out how much CO_2 is needed to convert Li_2O back into Li_2CO_3at 40 grams of lithium carbonate.

$Li_2O + CO_2 = Li_2CO_3$ Equation 19

Li_2O = mass Li_2 + mass O Equation 20

= 13.882 gr + 16 gr

= 29.882 gr

CO_2 = mass C + mass O_2 Equation 21

= 12 gr + 32 gr

= 44 gr

Total mass Li_2CO_3 = 73.882 gr

Calculate the mass fraction from Li_2O and CO_2 :

Mass fraction Li_2O = $\frac{29.882 \text{ gr}}{73.882 \text{ gr}}$

= 0.404

Mass fraction CO_2 = $\frac{44 \text{ gr}}{73.882 \text{ gr}}$

= 0.595

Mass fraction CO_2 × 40 gr = 23.82 gr

The amount of carbon produced in the reaction using 40 grams of lithium carbonate is 4,722 grams. At the same time, the need for CO_2 in this condition is 23.82 gr.

The reaction rate of 40 grams of lithium carbonate in 60 minutes can be calculated by:

v = $-\frac{1}{a} \times \frac{[A]}{dt}$

decsription :

v = reaction rate

a = reaction coefficient

[A] = substances involved in the reaction

dt = time

then the reaction rate at 40 gr lithium carbonate

$Li_2CO_3 - C + 3Li_2O$ Equation 22

$\mathrm{Li_2CO_3}$ = 0.541 mol (initial)

$\mathrm{C + 3Li_2O}$ = 0.744 mol (final)

[A] = (initial) – (final)

= 0.541 – 0.744

= - 0.203 mol

v = -1× $\frac{-0.203}{60\ minutes}$

= 0.00338 mol/minutes

= 3.4 × 10-3 mol/minutes

Appendix 3 - Fourier Transform Infrared (FTIR)

Fourier Transform Infrared (FTIR) is a type of infrared spectroscopy that is commonly used in CNT characterization. This analysis setup is described in Figure 64. Fourier's theory states that mathematical functions (x, y-axis) can accurately display sin and cos waves. Therefore, FTIR changes the time function into a wavelength function utilising this theory.

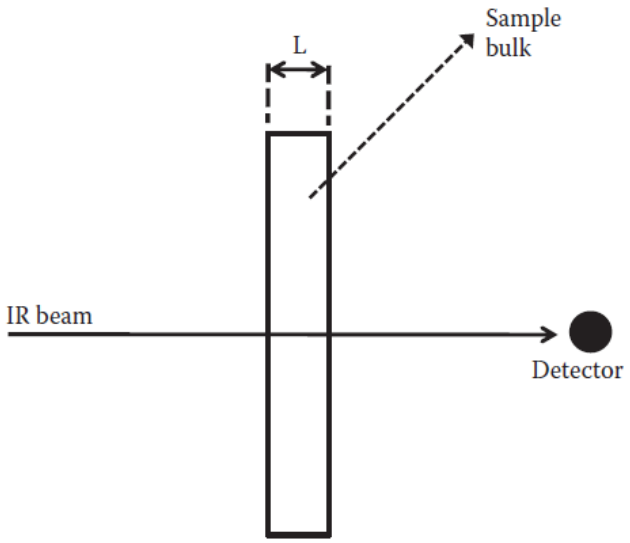

Figure 64 Infrared spectroscopy

There are two types of presentation of FTIR data, first based on absorbance and second based on % transmittance. The equation used to determine the absorbance spectrum uses the following equation:

$$A = \log(I_0/I)$$

A = Absorbance

I_0 = intensity in the background spectrum

I = Intensity in the sample spectrum

The following equation can be used to find the concentration of a molecule:

$$A = \varepsilon . l . c$$

A = Absorbance

ε = Absorbptivity

l = Pathlength

c = Concentration

The following equation can be used to determine the per % transmittance:

$$\%T = 100 \text{ x } (\frac{I}{I_0})$$

%T = per cent transmittance

I_0 = intensity in the background spectrum

I = intensity in the sample spectrum

Appendix 4 - X-Rays Diffraction (XRD)

X-Rays Diffraction (XRD) is a non-destructive test that uses X-rays with an energy of 100 eV to 10 MeV. This test is generally used to measure the average distance between layers, and

the arrangement of atoms, determine the orientation of a single crystal or grain and analyze the crystal structure. Size, shape and internal stress measurement of the crystalline area and quantifying the interlayer distance and composition of the sample also the robust capabilities of these tests. Bragg's law is used to find the interlayer distance:

$$2\,d'\sin\theta = n\lambda$$

d' = spacing of the crystal layer

$\sin\theta$ = the angle between the scatter and plane incident ray (incident angle)

n = integer

λ = wavelength

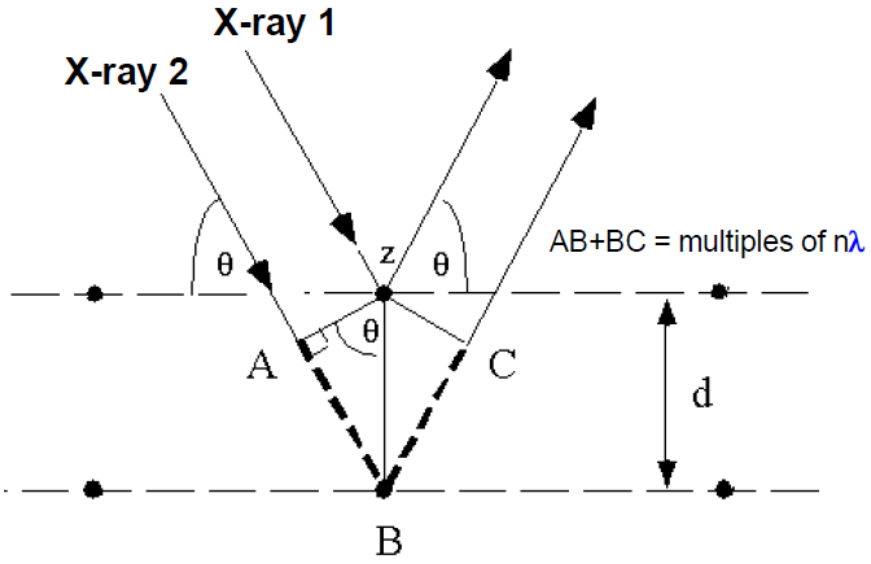

Figure 65 XRD process to calculate interlayer spacing

XRD analysis method was used to describe the morphology and structure of CNTs at different angles (Figure 65).

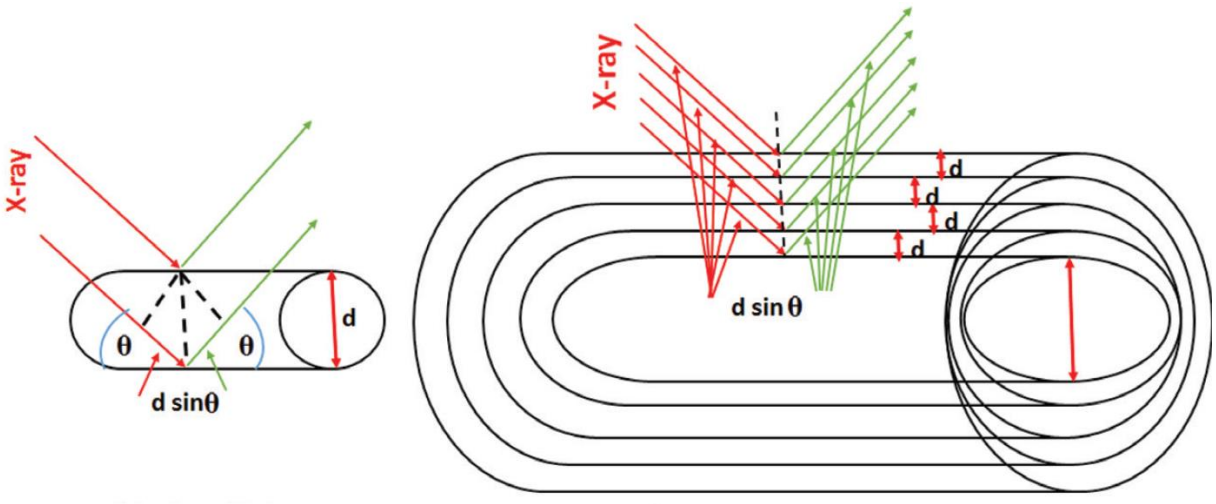

Figure 66 [151] Effect of a multilayer with XRD diffraction

Appendix 5 - Raman spectroscopy

The relation between RMB and the diameter of nanotubes describes as follows:

$$\omega RBM = \frac{A}{d} + B$$

Where d is the diameter of SWCNT, A and B are parameters determined experimentally. Parameter A is related to graphite dispersion, and parameter B is related to frequency shift caused by van der Waals force.

Appendix 6 - Scanning Electron Microscopy (SEM)

Scanning Electron Microscopy (SEM) is a test that uses an electron microscope that produces an image of a sample by scanning the surface using a focused electron beam to determine the resulting sample's microstructure morphology and chemical composition. Image formation in SEM depends on the signal gain resulting from the electron beam and specimen interaction. These interactions can be divided into two main categories: elastic interactions and inelastic interactions. The simplified explanation of these interactions is whether electron beam energy is transferred to the sample or not. Elastic interaction happens when no energy is transferred,

while inelastic interaction is the opposite. From these interactions, the result is a signal which can be processed into an image.

Appendix 7 - Electrochemistry in Electrodeposition

Electrochemistry is a branch of science that studies the phenomenon of electric flow and chemical reactions. This field of study is the basic concept of Electrodeposition. Whether the chemical reaction occurs spontaneously or not depends on Gibbs Free Energy (∆G). Spontaneous or non-spontaneous response conditions differentiate electrochemical processes into two electrochemical cells: voltaic and electrochemical cells. In the electrochemical process, there are reduction and oxidation reactions. The reduction is a process where there is an addition of electrons in an electrochemical process. At the same time, oxidation is a process with a reduction in electrons in an electrochemical process. Both reduction and oxidation reactions occur in one chemical reaction, but the half-reaction method is often used to facilitate calculation and identification.

Gibbs free energy, or free energy for short (∆G), is a system measuring a chemical process's spontaneity and the energy used from or needed to add to that process. Based on free energy, electrochemistry can be divided into two types. These types are voltaic cells and electrolytic cells. A voltaic cell is an electrochemical cell condition with ∆G <0. This gives rise to a spontaneous reaction that results in excess energy. Meanwhile, the electrolytic cell is an electrochemical condition with ∆G> 0. This condition gives rise to a non-spontaneous response in which external energy is required for a chemical reaction to occur. Figure 67 shows the two processes. (∆G) can be determined by the equation:

$$\Delta G = \Delta H - T\Delta S \qquad \text{Equation 23}$$

G = Gibbs Free Energy

H = enthalpy

T = temperature

S = entropy

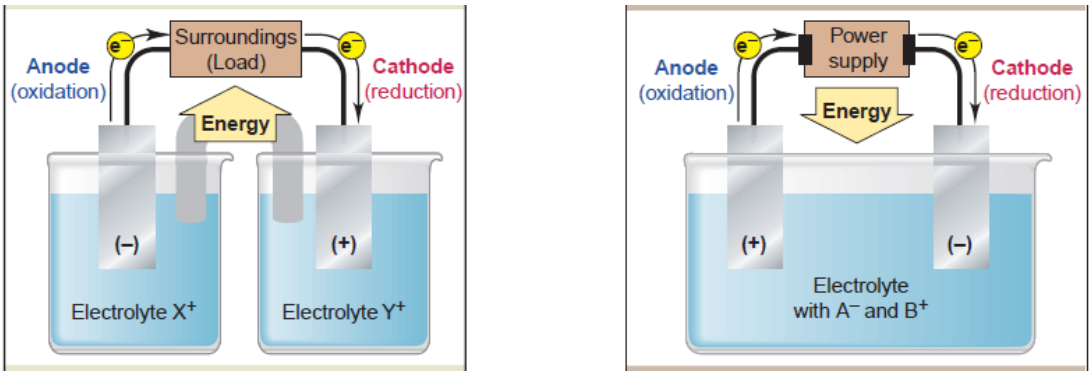

Figure 67 Voltaic cell dan Electrolityc cell

The reduction reaction, which is the addition of electrons, occurs at the cathode (-), and oxidation, namely the reduction of electrons, appears at the anode (+). The identification of reduction and oxidation reactions can use the half-reaction method.

$$X \rightarrow X^+ + e^- \qquad \text{Equation 24}$$

$$e^- + Y^+ \rightarrow Y \qquad \text{Equation 25}$$

$$X + Y^+ \rightarrow X^+ + Y;\ \Delta G < 0 \qquad \text{Equation 26}$$

$$A^- \rightarrow A + e^- \qquad \text{Equation 27}$$

$$e^- + B^+ \rightarrow B \qquad \text{Equation 28}$$

$$A^- + B^+ \rightarrow A + B;\ \Delta G > 0 \qquad \text{Equation 29}$$

Equation (24) - (26) is the reaction in the voltaic cell, while equation (27) - (29) is the reaction in the electrolytic cell. The oxidation reaction is shown in equations (24) and (27), while the reduction reaction is shown in equations (25) and (29).

In determining the spontaneous reaction under standard conditions using the E° calculation (electrode potential), it also needs to be taken into account that if $E^{\circ} > 0$, then the reaction occurs spontaneously. Meanwhile, if the value of $E^{\circ} < 0$, then the reaction is not spontaneous. E° calculation uses the following equation:

$$\mathrm{Eo} = E^{o}{}_{Cathod} - E^{o}{}_{anode} \qquad \text{Equation 30}$$

The process of getting the potential of an electrode uses a comparison method against the reference standard half cell, namely the hydrogen electrode. Table 34 shows the example of the standard potential value at 25 $^{\circ}$C.

Table 34 Standard potential on metals

Metal	Standard potential, E_0 (V)
Li	-3.05
Al	-1.66
Zn	-0.76
Cr	-0.74
Fe	-0.44
Ni	-0.28
H	0.00
Cu	0.34
Pt	1.20
Au	1.50

The electrochemical process investigation involving electrochemical kinetics commonly uses the Butler-Volmer equation as one of the fundamental relationships. This equation describes the relationship between the electrical current through an electrode and the voltage difference between the electrode and electrolyte in a simple, unimolecular redox reaction.

$$i = i_o \left[e^{\frac{-\alpha F \eta}{RT}} - e^{\frac{(1-\alpha) F \eta}{RT}} \right] \qquad \text{Equation 31}$$

Where: i = current, i_0 = exchange current, R = molar gas constant , F = Faraday's constant,α = transfer coefficient, T = absolute temperature and η = overpotential.

Appendix 8 - Research on CNT Production using Arc Discharge Method

Year—author	Arc current, voltage, synthesis time	Environment, pressure	Type of CNTs, diameter, yield
1991—Iijima [1]		Argon/Helium, 100 torr	MWNT, 5–20 nm
1992—Ebbesen and Ajayan [152]	100 A, 18 V	Helium, 500 torr	CNT, 2–20 nm
1993—Iijima et al. [153]	200 A, 20 V	10 torr methane and 40 torr argon	CNT, 0.75–13 nm
1993—Bethune et al. [154]	95–105 A	Helium, 100–500 Torr	SWCNT, 20 nm
1996—Loiseau and Pascard [155]	100–110 A, 30–45 min	Helium, 0.6 bar	CNT
1997—Journet et al. [156]	100 A, 2 min	Helium, 500 torr	MWNT, 1 nm
1999—Shi et al. [61]	40 A, ~ 120 min	Helium, 1520 Torr	MWNT, 115 mg/min
2004—Itkis et al.[157]	90 A, 60–90 min	Helium, 680 Torr	SWNT, 5–15 g
2005—Yao et al. [158]	a 90 A, 5–10 min	Helium, 600 Torr	SWNT, 10–30 nm, 0.6–1 g
2007—Sun et al. [159]	70–100 A, 10 min	Hydrogen–argon, 200 Torr	SWNT, 0.8 g
2009—Jahanshahi et al. [160]		LiCl	MWNT/SWNT, 7.7 mg/min
2011—Hou et al. [161]	150 A, 3 min	Hydrogen, 200 Torr	SWNT, 1 g
2013—Mohammad et al. [162]	75–95 A, 5 min	Hydrogen–argon, 150 Torr	CNTs, 34–44 mg
2013—Fang et al. [163]	80 A, 10 min	Hydrogen–argon, 200 Torr	SWNT, 10–30 nm, 100–200 mg

Appendix 9 - Research on CNT Production using CVD Method

Year—author	Carbon source	Environment, Pressure, flow rate, time	Temperature	Catalyst, the support material	Type of CNTs, diameter, length	Yield
1996- Hongjie Dai et al. [164]	Carbon monoxide	100 Torr, 1200 sccm, 1 hour	1200 °C	Molybdenum (few nanometer size)	SWNT, 1-5 nm, 100 nm	-
1999- Alan M. Cassell et al. [165]	Methane	1.27 atm ,6000 cm3/min, 30 min	900 °C	Fe–Mo bimetallic; Fe2(SO4)3/Al2O3 (5 g)	SWNT, 2-50 nm,	42 wt. %/ g (1.5 g) catalyst yield after 45 min of CH4 CVD
1999- Pavel Nikolaev et al [166]	Carbon monoxide, Fe(CO)5	1–10 atm,	800 - 1200 °C	Fe/Quartz	SWNT 0.7 nm, 1 μ	44% the weight of the catalysts , 1,38 mg/h
1999- E. Flahaut et al. [167]	CH4	H2	1070 °C	Co or Ni	SWNTs, 0.8–5	-
2000- Ming Su et al. [72]	Methane	Ar/H2, 1000 sccm, 30 min	850 °C - 1000 °C	Co or Ni	MWNT, 1 nm	200% the weight of the catalysts
2001- Michael J. Bronikowski et al [168]	Carbon monoxide, Fe(CO)5	30–50 atm,	900–1100 °C	Fe/Quartz	SWNT	450 mg/h
2002 - Shigeo Maruyama et al [169]	alcohol, methanol	Ar, 200 sccm	550-600 °C	Fe, Co, zeolite	SWNT	-
2009 - Rong Xiang et al [170]	ethanol	Ar/H2, 40 kPa	800 °C	Co/Mo	SWNTs	-

Appendix 10 - Research on CNT Production using Laser Ablation Method

Target material	Metal catalyst (%)	Inert gas	Pressure (Torr)	Furnace/oven temp. (°C)	Laser properties (laser vaporization pulse)				Major observation	Refs
					Type	Oscillation wavelength (nm)	Heat (mJ/pulse)	Spot diameter (mm)		
Graphite rod	–	Ar	500	1200 900 200	Nd:YAG	532	250	3 and 6	MWCNTs of length 300 nm are obtained with 4–24 layers. Yields depend on the following temp.: (a) At 1200 °C, defect-free MWCNTs are obtained; (b) At 900 °C, number of defects is increased; and (c) At 200 °C, no MWCNTs are synthesized	[65]
Metal-graphite rod	Co (1) Cu (0.6) Nb (0.6) Ni (0.6) Pt (0.2) Co:Ni (0.6/0.6) Co:Pt (0.6/0.2) Co: Cu (0.6/0.5) Ni/Pt (0.6/0.2)	Ar	500	1200	Nd:YAG	532	300	6–7	SWCNT are obtained with increasing temp up to 1200 °C. Yields obtained in an order of (a) Ni > Co > Pt, (b) Co/Ni > Co/Pt > Ni/Pt > Co/Cu. For Cu and Nb: no SWCNTs are secured	[62]
Metal-graphite rod	Ni-Co (1.2)	Ar	500	1200	Nd:YAG	532 1064	250 300	5-7	>70% SWCNTs are secured with uniform diameter in the form of rope. One rope contains from 100 to 500 SWCNTs	[171]

Metal-graphite rod	Co/Ni (1)	Ar	500	200	Nd:YAG	532	490	6	When the flow tube is 2.5 cm in diameter, Web-like SWCNT deposit is retained When the tube dimension is increased by ~5 cm in diameter, 50 vol% of SWNCT is obtained When 2.5 cm in diameter quartz tube coaxial and 5 cm tube extending are installed, 60 to 90 vol% SWCNT is acquired 1 g/day SWCNTs are accomplished	[128]
Metal-graphite rod	Ni (2) Co (2) Fe (2) Y (0.5) Ni/Y (4.2/1, 2/0.5, 1/0.25, 0.6/0.6, 0.5/0.1) Ni/Co (4.2/1, 2/2, 2/0.5, 1/0.25, 0.6/0.6, 0.5/0.13,0.4/0.4) Ni/Fe (4.2/1, 2/0.5, 0.6/0.6)	Ar	400	No Furnace is used	CO_2 250 W	-	-	-	The soot contains large amounts of clean bundles of SWCNT (diameter 20 nm and lengths >1 μm) SWCNTs of 80 vol% are synthesized at a rate of 50 mg/h Ni/Y or Ni/Co showed rubbery web-like SWCNT soot	[64]
Graphite + catalysts powder	Co Ni Y (2)	Ar	187–337	-	Solar energy (2000 W)	-	-	-	Parallel and bundled SWCNTs are obtained	[172]
Metal-graphite rod	Ni (2) Co (2) Y (0.5) Fe (2) Ni/Co (4.2/1, 2/ 2, 0.5/ 1, 0.6/0.6, 0.5/0.1) Ni/Y (4.2/1, 2/ 0.5, 1/0.25, 0.6/ 0.6, 0.5/0.1)	Ar N2 He	400	-	CO_2 12000 W	-	-	0.16	SWCNTs of diameter 1.4 nm are self-organized into a 20 nm bundle. Maximum yield was noticed with Ni/Y and Ni/Co catalysts. Cw-CO_2 laser ablation is an easy and environment	[173]

	Ni/Fe (4.2/1, 2/ 0.5, 0.6/0.6) Co/Y (2/0.5) Ni/La (2/0.5)								favorable method for the growth of high-quality SWCNT	
Metal-graphite rod	Co and Ni (2.5)	Ar N2	750	1100 °C	CO_2 2100 W	-		-	20–40% SWCNT with mean diameter of 1.2–1.3 nm are obtained	[174]
Metal-graphite rod	Co–Ni (0.6)	Ar	500	25–1150	UV	248	-	-	SWCNTs with 15–20 nm in diameter are secured. Yield is lower at lower temp. Repetition rate of 30 to 150 Hz leads to a higher yield and larger bundles	[175]
Metal-graphite rod	Ni (1) Co (1)	Ar N2	600	7726	Nd:YAG	532	240	-	N2 atmosphere produces more bundled than those of Ar ambience	[176]
Metal-graphite rod	Co Ni (1.2)	Ar	750	999 1099 1199 1349	UV	308	58	-	SWCNTs are formed with diameter 1.2∼1.7 nm and length >2 μm. The highest yields at 1349 °C	[67]
Metal-graphite rod	Co Ni	Ar	500	1100	UV	248	-	-	SWCNT deposit of diameter 1.2 nm is secured	[177]
Metal-graphite rod	Co/Ni	Ar	500	900 1000 1150	UV	248	-	-	SWCNT of diameter 1.2 nm and length 10 μm aggregate into bundles containing 2–40 nanotubes. Optimal catalyst concentration of 1.2% synthesis high-quality SWCNT Increasing the furnace temperature increases diameters	[68]

Appendix 11 - Ni cathode EDX result

Microanalysis Report

Prepared for: *LSUMP 916*

Prepared by: *Laboratorium Sentral FMIPA UM*

10/14/2020

B746

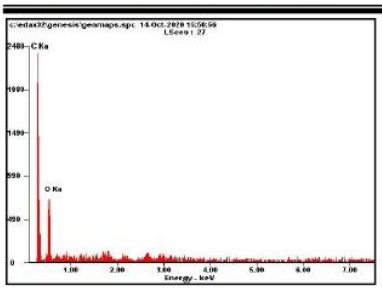

Element	Wt%	At%
CK	61.79	68.29
OK	38.21	31.71
Matrix	Correction	ZAF

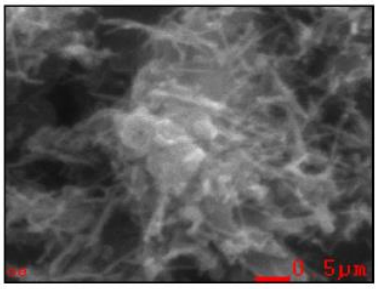

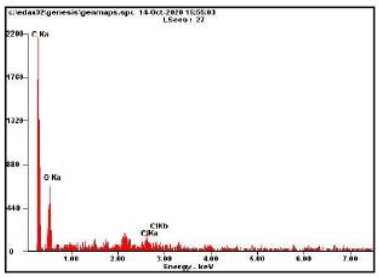

Element	Wt%	At%
CK	60.60	67.68
OK	37.84	31.73
ClK	01.56	00.59
Matrix	Correction	ZAF

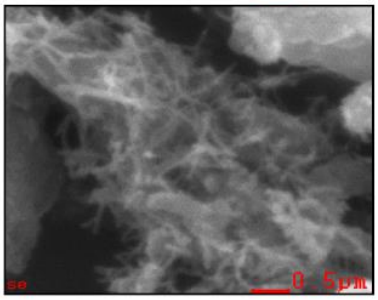

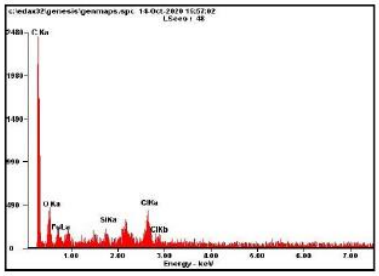

Element	Wt%	At%
CK	69.65	76.76
OK	25.97	21.49
SiK	01.15	00.54
ClK	03.23	01.21
Matrix	Correction	ZAF

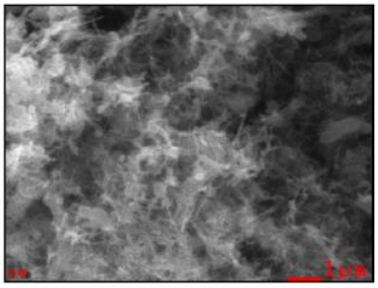

Figure 68 Ni cathode EDX result

The EDX result for Ni cathode in the OFAT experiment (section 4.3.4) has an anomaly where the MWCNT result is higher than the carbon growth rate. It was caused by the range of EDX results we received. As shown in Figure 68, the result ranges from 60.60% to 69.65%. We choose the middle value of 61.79% resulting in the anomaly result. However, if the highest value (69.65%) is chosen, the growth rate is higher than the MWCNT yield.